PERMANENT MAGNET MULTIPHASE MACHINE MODELING AND CONTROL FOR MV WIND ENERGY APPLICATIONS

MIKEL ZABALETA MAEZTU

A thesis submitted in partial fulfilment of the requirements of Liverpool John Moores University for the degree of Doctor of Philosophy

This research programme was carried out in collaboration with Ingeteam Power Technology S.A.

March 2018

ABSTRACT

Due to the rapid development of the power electronics in the second half of the twentieth century, a significant research effort has been put into the modelling of electrical machines to provide mathematical models for control purposes. As the power electronics isolate the machine from the grid, the number of phases on both sides no longer needs to be the same, thus allowing for use of multiphase machines. Several studies have shown that multiphase machines can yield lower torque ripple, provide higher torque per phase current, and that they can continue to operate with one or more faulty phases, thus increasing the robustness of the power stage. This, amongst other benefits, has led to increased interest in multiphase machine employment for critical applications, such as more-electric aircraft, electrical propulsion systems for ships and offshore wind, etc.

Amongst the different multiphase machine constructions, the multiple three-phase winding structure with isolated neutral points is of special interest. It can be operated using multiple three-phase converters, so that almost no modification of hardware is needed. Furthermore, with high power machines (above the 5 MW class), several converters in parallel should be used when increased availability is desired. This is where multiple three-phase winding machines show an additional benefit, galvanic isolation between the windings. By connecting one three-phase converter to each of the three-phase windings of the machine, the increased availability of paralleling converters is obtained while the problem of the circulating current between paralleled converters is practically eliminated thanks to said galvanic isolation.

The control schemes of three-phase machines should not be directly applied to multiple three-phase winding machines, since these show internal cross couplings between the different three-phase windings that may affect dynamic performance. To examine the behaviour and design control schemes for multiple three-phase winding machines, modelling approaches based on vector space decomposition, multiple *dq* modelling approach and a novel approach, specifically developed in this thesis for the independent power flow control in individual three-phase windings, are studied. It is demonstrated that, by including appropriate decoupling terms in the traditional three-phase control structure, a completely decoupled operation can be obtained in all the three-phase windings in the machine when control scheme is based on the multiple *dq* modelling approach. With this control approach, the control of these machines is accomplished using control structures and model transformations familiar to those skilled in the art of the three-phase machines. For six-phase machines the existing transformations are sufficient for all control purposes, while the novel transformation becomes a useful tool when there are three or more three-phase windings.

The influence of a low switching to fundamental frequency ratio on behaviour of the controlled object is also covered in this work. This has a great impact on the modelling of current control loops, especially when using the synchronously rotating reference frame in variable fundamental frequency applications, such as motor drives. The precise modelling of the actual control loops is of vital importance since it allows development of faithful control tuning techniques. With these, the regulator parameters, which ensure certain specified dynamic performance of the loops, are obtained and their behaviour can be precisely described and predicted by simulations. The machine's parameter identification has also been approached in this work; accurate parameter knowledge is of essential importance to ensure the correct match between experimental and simulation results. All the experimental work has been done using a 150 kW permanent magnet synchronous generator in six-phase configuration with two three-phase winding placed spatially in phase.

Unequal power sharing between different three-phase windings is studied further, including the simultaneous operation of one winding in motoring and the other in generation for a six-phase machine. This particular mode of operation has been found as very useful in development of a novel testing method for the machines with multiple three-phase windings, of synthetic loading type, which is fully verified by experimentation. A corresponding theoretical/simulation work has been performed for a nine-phase (triple three-phase) machine.

ACKNOWLEDGEMENT

First and foremost, I would like to acknowledge the Board of Directors of Ingeteam's Windpower Department for giving me the opportunity to develop this project by providing me with the financial support needed, and for the confidence in me which is one of the best rewards one can have.

When back in 2011 I accepted to take the challenge of doing a PhD while working, I was definitively not aware of what it really implied. Long nights, working overtime and, what may be the worst, having difficulties to fully disconnect from the electrical machine's stuff are some exemplary situations I had to overcome along the course of these studies.

Added to the inherent difficulties of doing a part-time PhD, this study also included the factor of the physical distance between me (most of the time working in Pamplona) and my supervising team (placed in Liverpool). Fortunately, I was tutored and supervised by Prof. Emil Levi and Dr. Martin Jones who made huge efforts to make me feel supported. From them, I take the strictness, the precision and the consistency required in the academic world, which is something I lacked after 10 years in industry.

On the other side, I would like to express my sincere gratitude to the Ingeteam's windpower MV team for their incredible work during these years and for their ability to work with a somehow part-time leader. Special mention to Iñigo Garin, Guillermo Nuñez and Eduardo Burguete for their support in migrating the control code to the CCU and for the help in the experimental testbench, and to Igor Larrazabal for his commitment with this project and for the confidence in me.

I would like to express my gratitude to my parents Rita and Jose for their invaluable advices and guidance along my life path and for continuously pushing me towards the PhD completion. My sister Ane also receives a special mention here for showing me that there are other arts and abilities outside engineering.

Last but not least, I would like to express my endless gratitude to my beloved wife Maitane for always being beside me showing me her love, support and confidence, and to my little princesses Naia and Nagore for giving me reasons for waking up every morning with a smile and for showing me what really important in life is.

CONTENTS

CHAPTER 4 MODELLING OF MULTIPHASE MACHINES WITH MULTIPLE THREE-PHASE WINDINGS

LIST OF PRINCIPAL SYMBOLS

ψ_{PM}	Permanent magnet's magnetic flux [Vs]
n	Number of phases
kt	Scaling factor applied to the transformation from the natural to the stationary reference frame.
k	Number of three-phase systems
θ_r	Angular position of the rotor expressed in electrical radians [rad]
ω_r	Speed of the rotor expressed in electrical radians per second [rad/s]
σ	Angular displacement between the reference phases of different three-phase systems expressed in electrical radians [rad]
L_{ls}	Stator's phase leakage inductance
$L_{\alpha\alpha}$	Stator's self inductance in the α-axis (stationary reference frame)
$L_{\beta\beta}$	Stator's self inductance in the β-axis (stationary reference frame)
$L_{\alpha\beta}$	Stator's mutual inductance between the α- and the β-axes (stationary reference frame)
L_{md}	Stator's self inductance in the d-axis on a per phase base (rotating reference frame)
L_{mq}	Stator's self inductance in the q-axis on a per phase base (rotating reference frame)
$[a]$	Sub-matrix of the speed-EMF term
$[b]$	Sub-matrix of the speed-EMF term
$[A]$	States matrix in a state space representation
$[B]$	Inputs matrix in a state space representation
$[C]$	Outputs matrix in a state space representation
x_{dk}	Magnitude x (v for voltages, i for currents, Ψ for fluxes) of the k three-phase system referred to the d-axis
x_{qk}	Magnitude x (v for voltages, i for currents, Ψ for fluxes) of the k three-phase system referred to the q-axis
g_{dii}	Term reflecting the influence of the input on the d-axis of the three-phase system i in the output on the d-axis of said three-phase system according to the multiple dq approach.
g_{qii}	Term reflecting the influence of the input on the q-axis of the three-phase system i in the output on the q-axis of said three-phase system according to the multiple dq approach.
g_{dij}	Term reflecting the influence of the input on the d-axis of the three-phase system j in the output on the d-axis of the three-phase system i according to the multiple dq approach.
g_{qij}	Term reflecting the influence of the input on the q-axis of the three-phase system j in the output on the q-axis of the three-phase system i according to the multiple dq approach.
$[K_{dq}]$	d-q axes decoupling matrix according to the multiple dq approach.
$[K_{st}]$	Stator-stator decoupling matrix according to the multiple dq approach.
$[K_{in}]$	Inputs decoupling matrix according to the multiple dq approach.
I_s	Stator's current amplitude (peak value)
α_c	Angle between the stator's current vector and the permanent magnet's flux vector.
p	Pole pairs of the machine.
$\Re_m$	Magnetic reluctance [$\frac{A \cdot turn}{V \cdot s}$]
$[X_s]_{abc}$	Column vector of the stator's magnitude X (V for voltages, i for currents, Ψ for fluxes, R for resistances, L for inductances) expressed in the natural reference frame.
$[T]$	Generic transformation matrix

$[X_s]_t$	Column vector of the variable X (v for voltages, i for currents, $\varPsi$ for fluxes) or square matrix representing the variable X (R for resistances, L for inductances) expressed in a stationary reference frame.
$[X_s]_{t+r}$	Column vector of the variable X (v for voltages, i for currents, $\varPsi$ for fluxes) or square matrix representing the variable X (R for resistances, L for inductances) expressed in a rotating reference frame.
T_s	Sampling time for discrete controllers
T_{sw}	Converter switching period
T_d	Delay time in a control loop

LIST OF USED ABBREVIATIONS

3L-NPC	Three level neutral point clamped topology
BW	Bandwidth of a control loop
CCU	Converter control unit
DDQ	Double dq
DSP	Digital signal processor
DTC	Direct torque control
EMF	Electromotive force
FFT	Fast Fourier transformation
FOC	Field-oriented control
FPGA	Field programmable gate array
GSC	Grid side converter
IGBT	Insulated gate bipolar transistor
IGCT	Integrated gate-commutated thyristor
MMF	Magnetomotive force
MPDTC	Model predictive direct torque control
MPC	Model predictive control
MQE	Minimum quadratic error
MSC	Machine side converter
MSS	Minimum the settling time (time to reach the steady state)
MV	Medium voltage
NPC	Neutral point clamped
PC	Predictive controller
PI	Proportional and integral controller
PIc	Complex proportional and integral controller
PMSM	Permanent magnet synchronous machine
PM	Phase margin of a control loop
PR	Proportional and resonant controller
PTF	Probability to fail
PWM	Pulse width modulation
SCIM	Squirrel cage induction machine
SM	Synchronous machine
SRF	Synchronously rotating reference frame
SV-PWM	Space vector pulse width modulation
THD	Total harmonic distortion
VSC	Voltage source converter
VSD	Vector space decomposition
WECS	Wind energy conversion system

CHAPTER 1

Introduction

1.1 Preliminary considerations

Wind energy has appeared during the last decade or so as the main alternative electric energy source. It is of renewable nature and widely available worldwide, although the patterns are unpredictable and this imposes certain problems for the electric power system control. Utilisation of wind energy requires wind turbines, towers, electric generators, and power electronic converters for interfacing the generator to the grid. Various solutions are possible, depending on the wind farm location (onshore or offshore), power rating of the individual generators, and the power electronic converter assembly used to connect the generator to the grid. While so-called doubly-fed induction generators currently dominate the market and are widely used for onshore wind farms, it is expected that the main machine for the remote offshore farms will be either squirrel-cage induction machine (SCIM) or synchronous machine (SM) with fully rated power electronic converter connected directly to the stator winding (Zhang et al., 2013). The machine-side converter (MSC) can be in principle either uncontrollable, i.e. a diode rectifier (applicable only in the case of synchronous machines) or a fully controllable pulse-width modulated (PWM) voltage source converter (VSC) (for both machine types). The solution of interest in this project is a wind energy conversion system (WECS) consisting of a permanent magnet synchronous machine (PMSM) with a fully controllable PWM VSC.

During the last two decades, very demanding environmental agreements, signed by developed countries (especially European), have led to a fast development and exponential increase in the number of installations of wind turbines all across the continent. This rapid pace of development has led to the erection of a wind turbine wherever feasible in terms of wind availability and has left no good enough onshore sites for newly designed wind turbines. The unpredictable regulatory framework in most of the countries has favoured that the wind turbine manufacturers and operators focused more on extending the lifetime and capabilities of the existing wind turbines rather than substituting them by newly-designed and more efficient ones. As a consequence of this, the authorities laid their eyes on the sea where better wind conditions are to be expected, thus increasing the potential energy harvest. Additionally, being willing to increase the predictability of the energy production, the European governments boosted pilot projects to develop offshore windfarms and encouraged wind turbine manufacturers to develop new models specifically aimed for offshore conditions. In offshore windfarms, the cost of the wind turbine drops below 30% of the overall cost (Irena, 2012), leading to the current trend of increasing the power rating of the wind turbine as much as feasible. This increase in power and the increase in the maintenance costs derived from offshore sites have led to multiple redundancy requirements across the offshore wind turbines especially affecting the power converter and the control equipment.

Nowadays, the top-level electrical machines manufacturers have deep experience and knowledge in designing and manufacturing electrical machines to be used in conjunction with electronic drives. This has led to a minor impact on wind turbines availability related to machine's stator insulation breakdown issues [(Tavner, 2011) and (ReliaWind, 2013)]. These failure modes are the only ones whose effects can be minimized by means of special winding arrangements. Failures in the power converter devices are much more likely to happen as these devices are normally subjected to strong thermal cycles and overloads. All this raises the interest in providing the power converter with means to remain in operation after a failure in any of its power devices.

In the traditional three-phase machines and converters, a failure in any of the phases automatically leads to the wind turbine being taken out of service and an immediate maintenance scheduling is required to restore the operation. In offshore applications such an immediate access to the

plant is unacceptable, requiring that the wind turbine has as much fault tolerance built in as possible. This has increased the interest in multiphase machines and drives as they inherently include this fault tolerant capability. In a multiphase machine (with phase number greater than 3), when a phase is disconnected, it is still possible to obtain a quasi-circular trajectory of the machine's flux thus allowing to keep operating the machine with a rotating field and constant (but reduced) average torque. This increases the availability of multiphase drives in comparison to traditional three-phase ones, in which a single failure requires that the machine is taken out of service.

With currently available power electronic devices, the power range of a single three-phase power converter is limited well below the power ratings foreseen for offshore wind turbines. This makes it necessary to use several power converters in parallel. By connecting each of these converters to one three-phase winding in the stator of the machine, a multiphase conversion system is obtained allowing to exploit its fault tolerance. The degree of independence of the converters strongly depends on the machine's stator winding design, and the pros and cons of several machine's constructions will be analysed. One solution is to design the machine with multiple three-phase windings (with isolated neutrals); the number of three-phase windings is made equal to the number of three-phase converters that will be used as paralleled converters. The galvanic isolation between converters is automatically obtained in this way, thus reducing the interaction between them and facilitating their parallelisation. At the grid side, one can envisage two alternatives regarding the dc bus, the first one where all three-phase machine-side converters are paralleled to the same dc link and there is a single three-phase converter at the grid side; and the second one where each of the three-phase converters has its own independent dc bus.

The manufacturing of machines with multiple three-phase windings does not present a great problem because, internally, almost all the high power machines are wound with several three-phase systems; but, in the terminal box, all these stator windings are hard-paralleled. The concept is illustrated in Fig. 1.1, where two individual phases (bottom) are hard-paralleled into one phase in the terminal box (top).
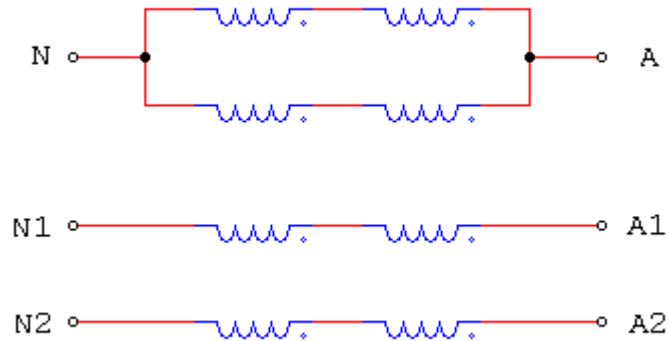
Fig. 1.1 A machine with two three-phase stator windings hard paralleled (top) and electrically independent (bottom). Only phase A is shown.

In this work, the focus will be placed on converter and generator sets using multiple three-phase winding permanent magnet synchronous machines with and without spatial phase displacement between them. This is so as these types of machines require no special design and manufacturing means and can be sourced from almost any electrical machine manufacturer. This is a key factor in windpower business as special proprietary solutions are not adequate for the globalised playground and wind turbine manufacturers do not usually accept solutions that tie them to single-source suppliers.

1.2   Aim and objectives

The overall aim of the project is to realise a novel hardware and software solution for offshore wind based electricity generation, using a multiple three-phase PMSM and multiple three-phase power

converters in parallel. The solution should provide increased availability in terms of energy production with a trade-off between system complexity and redundancy. The achievement of the aim will require, as the first step, original contributions in the areas of mathematical modelling of six-, nine- and twelve-phase asymmetrical machines. This is so since the existing methods of model transformation do not specifically focus on power sharing amongst the different three-phase systems in the machine. For this purpose, new specific model transformations are to be introduced so that a more intuitive power sharing between the three-phase systems is achieved. Additionally from the machine modelling step, deep knowledge of the machine's internal interactions will be acquired leading to contributions on cross-coupling decoupling techniques.

The targeted power electronic conversion stage is to be a back-to-back-topology formed by several three-phase three-level NPC converters in parallel (ideally one three-phase converter per three-phase system in the machine). The intention is to use low (< 10 times) switching to fundamental frequency ratio, this being commensurate with the target generator power rating. This will require original contributions in the design and modelling of the control algorithm. New control structures for the machine-side converter are to be proposed including the decoupling terms previously obtained from the machine modelling step. These novel control structures will be needed to deal with the desired current sharing between three-phase systems in both static and dynamic conditions. Needless to say, that the controller structure should be kept as simple as possible and should assure good performance under the aforementioned low switching to fundamental frequency ratio. Ideally, the novel control structures for multiple three-phase machines should try to approximate the control of the multiphase machine to that of its three-phase counterpart as much as possible so that field engineers do not require extensive new knowledge.

The main objectives of this work, which will enable achievement of the stated aim, are as follows:

(i)   To review the literature regarding modelling of multiphase machines, control schemes and techniques for multiphase machines in normal operation and under faulty conditions. Special emphasis will be placed on the permanent magnet synchronous machine with a low switching frequency converter.

(ii)   To develop a convenient set of new mathematical transformations, suitable for use in conjunction with machines with multiple three-phase windings, that will enable independent power flow control through each three-phase winding. The study will focus on six- and nine-phase machines.

(iii) Using the developed transformations, to formulate suitable control algorithms for the PMSM that will enable precise control of both steady state and dynamic operation on per winding basis. The focus will be on low switching frequency PWM techniques and on discrete-time algorithms.

(iv)   To examine the performance of the devised control schemes using simulation. Extensive use of Matlab/Simulink will be required at this stage as numerous simulations will be performed.

(v)   To develop power sharing algorithms for multiple three-phase winding machines using various model transformation approaches.

(vi)   To build an experimental rig and test the hardware and the developed algorithms using laboratory prototype.

1.3   Thesis structure

The thesis is organised as follows:

Chapter 2 provides a comprehensive literature review regarding multiphase conversion systems and it consists of in essence four independent surveys. Firstly, the multiphase machine configurations are surveyed highlighting the different winding arrangements that have been proposed. This is followed by surveys of the different machine transformations and generating system configurations already published. The last survey is focused on the existing fault-tolerant control strategies applied to multiphase machine and converter sets.

Chapter 3 is devoted to the mathematical transformations for multiphase machine models. Existing approaches to the model transformation are addressed first, with emphasis placed on the vector space decomposition approach and the multiple dq circuit approach. A novel transformation,

specifically aimed for multiple three-phase winding machines, is then developed, with the idea of facilitating the control of current sharing between the different three-phase systems. The last part of this chapter establishes a correlation between the different transformations focusing on the physical interpretation of the transformed variables, the representation of operational asymmetries and the harmonic mapping.

Chapter 4 begins with a brief introduction about the electromagnetic modelling applied to rotating machines. The models for dual and triple three-phase permanent magnet machines following the multiple *dq*, the VSD and novel approaches are then derived. Once the models are obtained, a decoupling procedure by means of a state-feedback decoupling is presented, yielding a set of fully decoupled equations.

Chapter 5 focuses mainly on the current controllers for multiple three-phase machines. The current loops are described in detail and an analytical tuning procedure is developed to obtain the PI parameters yielding certain desired dynamic response. The dynamic response obtained from the tuning procedure is firstly compared with that from the simulation model and later with the one obtained from the experimental testbench in order to validate the algorithm output.

Chapter 6 shows how with a fully decoupled model (as the one obtained in Chapter 4), different power sharing amongst the three-phase systems can be easily obtained. Examples of power sharing situations for dual and triple three-phase windings machines are presented for the three modelling approaches mentioned above.

Finally, the thesis concludes with a summary of the results obtained in each chapter, and the plans for the future work in Chapter 7.

Following the main chapters, five appendices are included to provide clearer insight into certain aspects. In the Appendix 1, the source code of a script in Matlab is provided, which generates the inductance matrix of any multiple three-phase system machine in the natural (phase variable) domain. In the Appendix 2, the source code of a Matlab script, which generates the transformation matrix related to the above mentioned novel transformation, is given. It is applicable to any *n*-phase machine, provided that *n* is an integer multiple of three. Appendix 3 shows the cross-coupling decoupling terms for six-, nine- and twelve-phase machines in both stationary and rotating frames. Appendix 4 describes the tuning procedure for a PI controller following the bandwidth and phase margin approach. Finally Appendix 5 gathers the output of the current regulator's tuning algorithm for an exemplary machine.

1.4   Original contributions of the thesis

In Chapter 3, after a detailed analysis of the available multiphase machine's transformations, a novel one is proposed especially focusing on the power sharing between the different three-phase systems in the machine. This transformation yielded the following publications (Zabaleta et al., 2016a) and (Zabaleta et al., 2016b). Additionally, the novel transformation proposed is also studied in (Zoric et al., 2017).

Chapter 4 develops the mathematical models of six- and nine-phase permanent magnets machines in both stationary and rotating frames. It obtains the state-space representation of the machines and develops a cross-coupling decoupling strategy that yields a fully decoupled model. This decoupling is very suitable for control purposes since it transforms the original machine's model into several (depends on the machine's number of phases) mutually independent first order systems. The decoupling strategy proposed is disclosed in (Zabaleta et al., 2017a).

In Chapter 5, the detailed modelling of the current loops is performed, including all the non-idealities present in industrial applications. After the detailed modelling, a tuning algorithm is developed to obtain the PI parameters of the current regulators following some dynamic response optimization criteria. The current regulator model and the tuning algorithm description are covered in (Zabaleta et al., 2017a). Additionally, a procedure to identify the machine's parameters, given the dynamic response of the current loops, is also derived and its validity demonstrated with the machine acquired for the experimental testbench (Zabaleta et al., 2017b).

Chapter 6 demonstrates the suitability of the above mentioned decoupling strategy for the current control of dual and triple three-phase permanent magnet machines. It shows how the current in

each three-phase winding can be controlled completely independently from the others, even allowing to operate some of them as motors while the others are generating (Zabaleta et al., 2018a). This operational scenario can yield huge savings in terms of investment and operational cost on the machine's (and/or converter) testbench (Zabaleta et al., 2018b). This is so since a machine (and/or converter) full-load test can be carried out with barely half the components required in traditional testing layouts.

CHAPTER 2

Literature review

2.1 Introduction

In this chapter, a detailed review of the state-of-the-art in multiphase machines modelling and control is presented. For the sake of completeness, this chapter begins with a brief historical introduction, which is then followed by four specific sections. Section 2.2 deals with the different multiphase machine's constructive configurations with special focus on multiple three-phase winding arrangements. Section 2.3 focuses on the different transformations for multiphase machines available in the existing literature. Section 2.4 reviews the state-of-the-art with regard to different configurations that use multiphase machines as generating units in conjunction with multiphase power converters. Finally, section 2.5 describes the state-of-the-art in the area of control strategies when a failure in one or more phases occurs.

Since the victory of the ac over the dc in the so-called "War of Currents" (Wolf, 2012), a three-phase distribution system has been adopted as the standard all over the world, leading to the massive study and use of three-phase machines. In the late 1960s, the inverter-fed ac drives were in an incipient stage with only slow switching power devices available. A six-step mode was the unique possibility, resulting in low frequency torque ripple whose lowest harmonic frequency is directly related to the number of phases (Levi, 2008). As the inverter isolates the machine from the grid, any number of phases can be used in the machine, independently of the grid's. Ward and Härer in (Ward and Härer, 1969) performed some experiments on a five-phase induction motor driven by a five-phase inverter concluding that the amplitude of the torque ripple is reduced by two thirds in comparison to an equivalent three-phase machine. Work in (Terrien and Benkhoris, 1999) reached a similar conclusion when using an asymmetrical six-phase machine with 30º shifted stator windings. This improvement in torque ripple has been historically seen as the main advantage of multiphase machines, but nowadays it is not as important thanks to the use of fast switching power devices in voltage source converters (VSC) which has greatly reduced the inverter harmonic voltages and thus, the torque harmonics (Levi, 2008).

Over the recent years, extensive research on multiphase machines applied to electric vehicles, aerospace and ship propulsion has brought out some other benefits of the multiphase machines (Khan et al., 2008) and drives (Bojoi, 2002) such as:

i) The phase currents in a multiphase machine are reduced (compared to those in an equivalent three-phase machine) allowing to match them with the power devices capabilities.
ii) Multiphase machines and drives can continue to operate with one or more faulty phase, which increases overall reliability.
iii) The harmonic content of the dc-link current is reduced allowing the use of smaller capacitance (especially in 180 degrees conduction mode).
iv) Smoother torque waveform is obtained when operating in 180 degrees conduction mode.

2.2 Multiphase machine configurations

Disregarding the excitation principle of the machine (whether it is synchronous or induction), multiphase machines can be classified basically according to two design features:

i) The phase coil distribution along the stator slots, which determines if the machine is a concentrated winding machine, a sinusoidally distributed winding machine or a modular design machine (Levi, 2008). This defines whether the magnetomotive force (MMF) distribution along the airgap is quasi-trapezoidal (in concentrated winding and in modular design) or it is

sinusoidally distributed (in sinusoidally distributed winding case). The three previously mentioned phase winding arrangements are shown in Fig. 2.1. In the configuration (a), the phase windings are distributed across several stator slots producing a staircase-shaped MMF which approximates a sinusoidal shape as the number of stator slots per phase increases. In configuration (b), all the phase windings are arranged in the same stator slot, resulting in a trapezoidally-shaped MMF as a consequence of the proximity of the phase windings. In (c), a modular construction is shown characterized by the fact that the phase winding is wound around a salient pole of the stator resulting in a square-shaped MMF. This construction allows implementing multiple three-phase system in the same stator, minimizing the mutual coupling between them and increasing the reliability as the machine could be operated even in the event of a winding short-circuit (Barcaro et al., 2010).

(a)   (b)   (c)
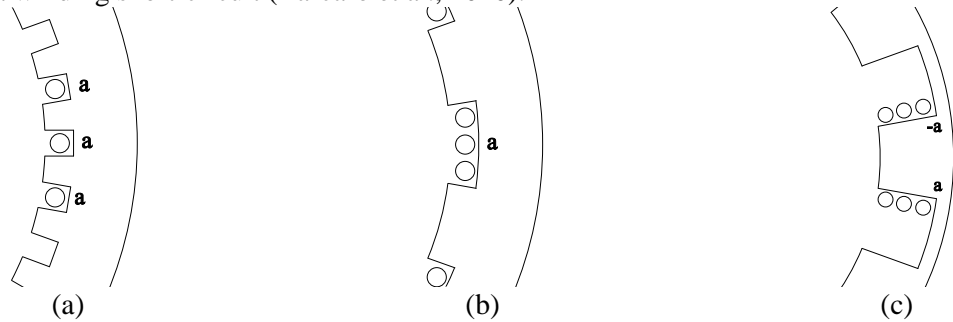
Fig. 2.1 Possible phase coils arrangements: (a) single-layer distributed winding for sinusoidal MMF, (b) concentrated winding and (c) modular design winding.

ii) The phase shift between two consecutive phase windings and the neutral points connection which defines the stator winding configuration. In general, two constructions are possible, as shown in Fig. 2.2 (an example of a six-phase machine). In this figure, the configuration (a) consists of two three-phase systems with isolated neutrals and an angular displacement (σ) between the first phases of the two systems. This configuration is usually referred to as a split-phase machine or asymmetrical six-phase machine (Levi et al., 2007). The angular displacement between the first phases of the three-phase windings in this type of machine is usually set to 0 or π/n electrical degrees (where n is the number of phases) and the neutrals are kept independent. In the configuration (b), usually referred to as symmetrical six-phase machine, a displacement of $2 \cdot \pi/n$ electrical degrees is between any two consecutive phases. All the phases can share a common neutral, as shown in the figure, or two neutral points could be used again. A different connection of the phases in a symmetrical six-phase machine (leading to triple H-bridge inverter supply of pairs of phases connected in series) is described in (Nabi et al., 2011) to reduce the number of independent currents.

(a)   (b)
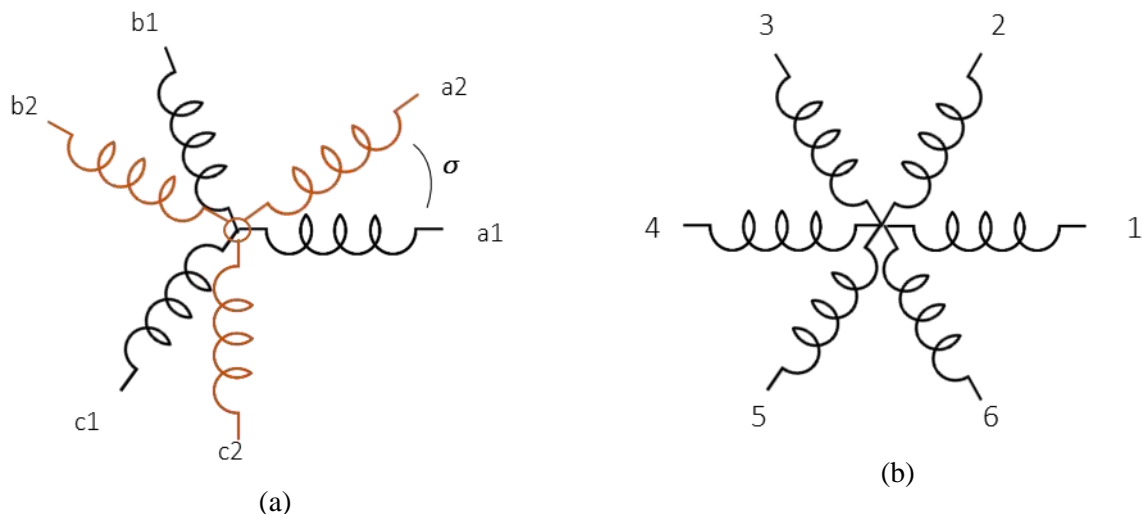
Fig. 2.2 Stator winding configuration alternatives for a six-phase system: (a) is a split-phase configuration; (b) is a symmetrical configuration.

The focus in this research work will be mainly placed on asymmetrical machines (Fig. 2.2(a)) with different angular displacements. The stator windings will be sinusoidally distributed as in Fig. 2.1(a), since these are the most frequently used ones in industrial applications nowadays; modular design as in Fig. 2.1(c) will also be addressed due to its benefits in terms of fault tolerance and in terms of manufacturing in the case of large diameter machines such are those commonly used in direct drive wind-applications (Siemens, 2012).

A huge body of published work has focused on analysing the consequences of the different available displacement angles between consecutive phases and the neutral connection in multiple three-phase system machines. A model for a dual three-phase induction machine (30º shift between the two three-phase windings) is developed in (Zhao and Lipo, 1995) using the so-called vector space decomposition (VSD) approach. In the resulting model the main low-order odd harmonics (5th and 7th) are mapped into the non-flux/torque producing subspace. The same conclusion is arrived at in (Hadiouche et al., 2000). This behaviour improves the machine's torque waveform (since the first lowest possible harmonic in the torque ripple now becomes the 12th). However, a new control problem now arises, as a traditionally wound machine, with distributed and short-pitched windings, provides very low impedance in the non-flux/torque producing subspace (a recirculating path between the different three-phase systems), so that high current values may appear if the converter (or the machine) induces a voltage at any of those frequencies (Hadiouche et al., 2004). Additionally, the machine's construction directly affects the voltage capability of the converter (Dujic et al., 2010). Dujic analyses different multiphase stator arrangements and how these affect the dc voltage utilisation of the VSC in the linear modulation range. It is shown that symmetrical and single neutral arrangements lead to lower dc bus utilization, with the maximum modulation index being only 1 for windings with 6, 12, 18 ... phases.

As a solution for the above-mentioned recirculating path issue, great research effort has been devoted to analysing different phase coil distributions for multiple three-phase systems machines, aiming to minimize the interaction between them [(Xu and Ye, 1995), (Hadiouche et al., 2004), (Barcaro et al., 2010), (Mese et al., 2012) and (Wang et al., 2013)]. In (Xu and Ye, 1995), the addition of magnetic rings across the end windings of the stator is proposed to reduce the 5th and 7th current harmonics recirculation in a 30º shifted dual three-phase stator induction machine. The same concept is addressed by means of an external filter in (Wang et al., 2013), which, resembling the targeted machine's stator construction, selectively introduces additional impedance in the recirculating path. A different approach to the same problem is followed in (Hadiouche et al., 2004) where a thorough theoretical analysis has been performed to obtain the key factors influencing the mutual leakage coupling between two three-phase stator windings, concluding that the coil pitch and the slot shape are the main factors that affect the impedance of the recirculating path. With this approach, a stator structure that maximises the impedance of the recirculating path can be obtained without the addition of further components. Barcaro in (Barcaro et al., 2010) analyses different coil arrangements along the stator slots to minimize the influence of a stator phase short circuit over the healthy phases. It is stated that when one or more phases are short-circuited, the unbalanced radial force in the rotor grows substantially due to the loss of symmetry. In (Mese et al., 2012) different stator winding patterns are compared aiming at obtaining the minimum coupling between the two three-phase sets and concluding that, with concentrated windings and precise location of the coils in the stator periphery, enough magnetic isolation can be obtained to operate the machine with low torque ripple when one three-phase system is operating as a motor and the other as a generator.

2.3   Multiphase machine model transformations

As will be further demonstrated in Chapter 3, the set of equations that describe the behaviour of multiphase machines in the natural reference frame, in terms of phase parameters and variables, is characterised with substantial cross-couplings between the different equations and with numerous time-varying coefficients, so that the model is a set of non-linear differential equations with time-varying coefficients (Levi, 2011a). This presents unnecessary difficulties in simulations and the model is of no use when it comes down to the control of the system as all the equations are cross-coupled. Hence, as is the case with the three-phase machines, the model in terms of phase variables (for

multiphase machines) is also transformed into some fictitious variables. The purpose of the transformations is that the set of equations gets simplified (minimizing the cross-couplings) and that the time dependency of the coefficients gets eliminated.

The basics behind the transformations rely on the fact that the initial set of equations of a multiphase machine can be rearranged in the form of the equations of (*n*-1)/2 (when *n* is an odd number) mutually independent submachines (Vizireanu et al., 2005). In this manner, controlling each of the submachines becomes simple and controlling all of them leads to control of the original multiphase machine. This is also just an alternative interpretation of the so-called Vector Space Decomposition (VSD) approach to the modelling described in (Zhao and Lipo, 1995).

A substantial body of work has been published with regard to the different transformation matrices for multiphase machines. There are several reasons for having different transformations within the electrical machine modelling field as each transformation may provide different benefits that will satisfy different application's requirements. These may include:

i)   Diagonalization and constant values in the inductance matrix, which facilitates the control tasks,
ii) Different harmonic mapping to facilitate elimination of undesirable current harmonics,
iii) Easiness of analysis of the model in terms of transformed variables,
iv) Facilitation of certain control tasks by using transformed variables.

Consider for example a multi-motor drive system composed of a number of multiphase machines, connected in an opportune manner in series, and of a single multiphase supply source. For series-connected multi-machine drive applications, one of the machines is controlled using one specific fundamental frequency, while the others are controlled using different fundamental frequencies, one per additional non-flux/torque producing planes. It is thus interesting to have each frequency component mapped into a single additional plane (i.e. non-flux/torque producing subspace) so that it can be easily controlled to a desired value. Jones in (Jones et al., 2005) and Malvar in (Malvar et al., 2014) show how, with phase transposition between the series-connected machines, different mapping of the frequency components is obtained for each machine and so independent control of two (or more, depending on the phase number) machines can be obtained with only one converter. For this type of application, a transformation that maps each frequency component uniquely into a single subspace is preferred, because this simplifies the control.

2.3.1   Multiple *dq* circuit modelling approach

A straightforward transformation directly derived from that of three-phase machines can be applied to multiphase machines with a number of phases *n*= 3*k, k* = 2, 3, 4, …. In these machines, the multi-dimensional *n*-domain can be divided into *k* three-dimensional domains each of which can be modelled as a three-phase machine. These *k* three-phase machines can be transformed into *k* stationary reference frames (flux/torque producing subspaces) by using trigonometric relations. This approach focuses on the flux/torque producing subspace in which the electromechanical conversion is represented, and "masks" in it the information about the other non-flux/torque producing subspaces which have information about mutual interactions between the different three-phase systems that do not produce electromechanical energy transfer. This implies that all the information about the machine is shown in the flux/torque producing subspace, leading to a lack of clarity in the information that may be completely unacceptable.

In (Nelson and Krause, 1974) a dual three-phase induction machine (with 30º shift) is modelled by constructing a transformation matrix for the six-phase machine by means of individual three-phase transformation matrixes. The same problem is solved in (Lipo, 1980) by applying the three-phase Clark's transformation to each of the two three-phase systems. In this particular machine, the double *d-q* approach cannot explain why the low order odd harmonics in the stator currents (5th and 7th primarily) reach high amplitudes when the output voltage waveform of the converter introduces them with rather small amplitudes. Another disadvantage of this modelling approach is that in the multi-star machines, there appear mutual couplings between the different three-phase systems which are difficult to fully compensate; hence, the dynamic response becomes compromised [(Kallio et al., 2013) and (Hu

et al., 2014)]. To overcome this last difficulty, Kallio introduces an additional transformation (a simple rows and columns rearrangement), after the transformation into the multiple *dq* variables, that leads to a full diagonalization of the inductance matrix.

To the best of the author's knowledge, (Tessarolo et al., 2013a) and (Tessarolo et al., 2013b) are the only published works in which the multiple *dq* approach has been applied to asymmetrical machines with $n > 6$ (nine- and twelve-phase machines) to obtain the equivalent circuit and its parameters. In this work, this approach shows that when $k > 2$, the *d-q* axes of each three-phase systems are no longer de-coupled, as a coupling of the stator leakage flux (mutual leakage inductances) appears. The existence of these mutual leakage inductances does not manifest itself unless the currents in the different three-phase systems are different in amplitudes (different load sharing).

2.3.2   Vector space decomposition approach

The VSD approach transforms the original *n*-dimensional space (with *n* being the number of phases) into a set of $(n-1)/2$ (when *n* is an odd number) mutually orthogonal two-dimensional subspaces (Zhao and Lipo, 1995). With this, the machine's model can be easily described by the set of decoupled subspaces. The procedure to obtain the transformation matrix depends on the machine's configuration, more specifically on whether it is a symmetrical or an asymmetrical multiphase machine (Levi et al., 2007), but the basis of the transformation is the same for both cases. Given the configuration of the machine, symmetrical or asymmetrical, the transformation matrix form will also depend on the number of isolated neutral points. With this approach, the multi-dimensional domain is not "masked" at all; in fact, it is divided into different subspaces each of which may reflect different aspects of the machine depending on the transformation matrix applied.

It is of vital importance to select adequate subspaces so that the behaviour of the machine is decoupled as much as possible. For this reason, one of the subspaces will always be chosen within the cross-sectional plane of the machine. This subspace (the flux/torque producing) will gather the information about the fluxes that do really cross the air-gap and concatenate stator and rotor, thus leading to the torque production. The additional $(n-4)/2$ (or $(n-3)/2$ for *n*= odd) (Levi et al., 2007) subspaces (non-flux/torque producing) and a zero-sequence subspace (z_1-z_2) should be defined with mutual orthogonal relations to guarantee that no cross-coupling occurs between subspaces (Zhao and Lipo, 1995):

In (Che et al., 2014a), a detailed analysis of the VSD approach and a comparison with the double *d-q* approach is performed in the case of an asymmetrical six-phase machine, concluding that the currents in the non-flux/torque producing subspace can be physically interpreted as recirculating currents between the two three-phase systems of the machine. From this, it can also be deduced that the asymmetries between the three-phase systems will be represented in the non-flux/torque producing subspace as fundamental frequency components with different sequences depending on the nature of the asymmetry. Che analyses the three types of asymmetry that can be found in the operation of a dual stator machine and how these map into the different subspaces.

2.3.3   Other approaches

Figueroa in (Figueroa et al., 2006) presents a simplified calculation of the transformed variables, for the case of symmetrical multiphase machines with any number of phases, by introducing two intermediate transformation matrices whose inverses can be easily calculated. In this case, the transformation matrix can be obtained by multiplying a complex permutation matrix P with a Fortescue transformation matrix F (commonly referred to as symmetrical components transformation (White and Woodson, 1959)). The main limitation of this approach is that it can only be used for machines with a phase displacement of $2 \cdot \pi/n$ (so-called symmetrical), thus leaving all the asymmetrical machines (whose phase displacement is π/n) out of this approach and therefore lacking generality. To overcome this limitation, Tessarolo in (Tessarolo, 2011) proposes to apply at first a geometrical transformation which maps the original multiphase machine into a so-called conventional *n*-phase arrangement with a

phase displacement of π/n and then apply a transformation matrix to treat this conventional n-phase winding arrangement. The transformation matrix for such arrangement can be obtained similarly as that in 2.3.2 but care has to be taken since the phase displacement is π/n instead of $2 \cdot \pi/n$ as in the symmetrical $2n$-phase machine used in 2.3.2.

In (Tani et al., 2013), a slightly different approach to that of the above mentioned transformations is used to model an asymmetrical twelve-phase machine configured as a quadruple three-phase system. This introduces four mutually orthogonal four-dimensional space vectors that cope with all the degrees of freedom of the machine's model. One of the space vectors maps the information about the cross-sectional plane of the machine thus mapping the torque- and flux-related components, while the other three map information about the current sharing among the four three-phase systems. Similarly, in (Kestelyn et al., 2009), a different point of view is taken, as the original multiphase machine is divided into a principal machine (which produces all of the torque in machines with sinusoidal MMF distribution) and several auxiliaries (which do not produce torque when the winding yields sinusoidal MMF). This transforms the control of the original multiphase machine into control of several magnetically independent two-phase fictitious machines and thus simplifies it. Analysing in detail these two approaches, it can be seen that in these two cases each of the space vectors in (Tani et al., 2013) and each of the fictitious machines in (Kestelyn et al., 2009) are contained in each of the subspaces defined in the VSD theory (section 2.3.2), so similar results are to be expected.

2.4 Multiphase generator system configurations

Nowadays the power of an electrical machine that can be used in wind energy generation is limited by the available maximum power rating of the power converter. With the power electronic components available at present, the maximum power rating of a three-phase converter for wind power applications is around 8 MVA (using medium voltage devices and three-level converter topologies) (ABB, 2013). In order to improve the fault tolerance for critical applications (such as in offshore wind turbines), the idea of modularity becomes very interesting since it prevents the application from fully going out of service when a failure in the converter occurs. This means that it may be interesting to use two paralleled 4 MVA converters instead of a single 8 MVA converter [(Geyer and Schröder, 2010) and (Zabaleta, 2014)]. When paralleling power converters, it is always recommendable to introduce galvanic isolation (or magnetically coupled reactors) between them. This prevents the formation of undesired loops for circulating current flow between the converters and simplifies the control and modulation techniques.

Among the available synchronous machine types, the three-phase permanent magnet synchronous machine (PMSM) with fully rated converter arrangement has become the trendy choice (Lawson, 2012) and it has gained a significant market share of the installed wind energy conversion capacity. This is mainly due to the advancement in production of magnets with superior magnetic properties and certain stabilization in the price of the magnets (Widmer et al., 2015). PMSMs are compact in size and light in weight, as well as highly efficient (as rotor excitation is provided by magnets) making them attractive especially for offshore wind application where part-load efficiency is a key factor. But an offshore wind energy system has to be not only lightweight and efficient, but also reliable. Most of the failures in wind turbines are known to have electrical or electronic origin, and the impact on the overall energy harvest is higher than that from the failures with mechanical origin (ReliaWind, 2013). These statistics enhance the necessity for fault-tolerant operation in the electrical system. If the conversion system is of a three-phase type, it is a fact that a failure in one of the phases leads to a full shut-down of the wind turbine, thus directly affecting the energy produced. To increase the energy production, multiphase systems (i.e. machine-converter structures with more than three phases) can be used, as these provide better means for fault-tolerant operation, as described in (Zhao and Lipo, 1996) and (Che et al., 2013).

One solution to increase the fault tolerance of the conversion stage is to design the machine with multiple three-phase windings. The number of three-phase windings is made equal to the number of three-phase converters that will be used as paralleled converters (in the example given previously this is two three-phase windings and two converters of 4.5 MVA each). A schematic of one possible configuration of such a system is given in Fig. 2.3, where the PMSM is connected to the grid by means

of several paralleled conversion lines, connected in a back-to-back configuration. The galvanic isolation between converters is automatically obtained in this way, thus reducing the interaction between them and facilitating their parallelisation. At the grid side, in addition to the solution of Fig. 2.3, a solution where all of the conversion lines share the same dc link can also be conceived (Fig. 2.4).
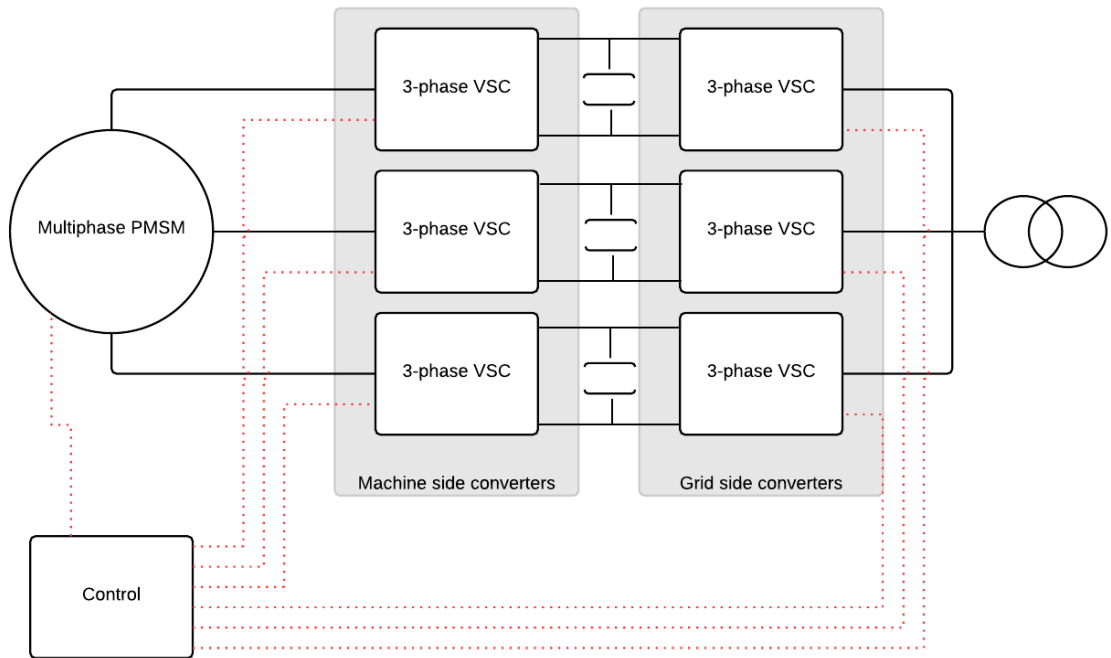
Fig. 2.3 Schematic representation of a back-to-back conversion system with three independent stages.
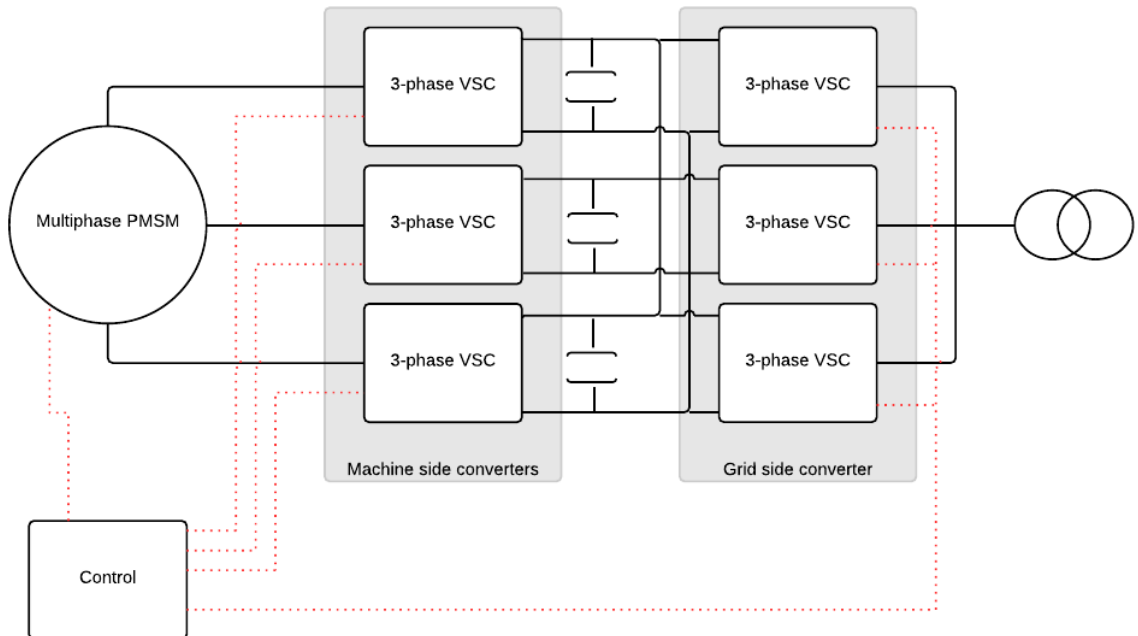
Fig. 2.4 Schematic representation of back-to-back conversion system with three stages with common dc bus.

Multiple three-phase system machines present several advantages over traditional three-phase machines, for example, between the different three-phase systems a galvanic isolation is inherently introduced (if neutrals are kept independent) thus providing the best scenario to parallel power converters. Another advantage is that the short-circuit current (and hence the short-circuit torque peak

as well) is reduced, as only one of the three-phase systems may be short-circuited thus allowing to reduce the mechanical requirements in the drivetrain.

As noted in conjunction with Fig. 2.3 and Fig. 2.4, this research targets back-to-back voltage source power stage configurations with multiphase PMSM, aimed at being used mainly in wind turbines rated above 5 MW. For such high power applications, the power stage configuration is likely to be a three-level topology based on medium voltage semiconductors (for reaching 3.3 kV of the line-to-line stator voltage). The medium voltage semiconductors require low switching frequencies (below 1 kHz) because the switching losses of the semiconductors increase with their rated blocking voltage and with switching frequency (Filsecker et al., 2013) and (Bauer et al., 2014).

2.4.1   Various back-to-back connection topologies

Different multiphase generation systems can be found in the literature; the most frequently met solutions have in common that they are based on machines with multiple three-phase windings. The main differences between them can usually be found in the machine-side converter (MSC) topology. Several research efforts have been based on uncontrollable rectifiers, as in (Jordan and Apsley, 2011) for aircraft applications, and in (Di Gerlando et al., 2012) in relation to a wind energy conversion system (WECS). This topology provides a simple MSC with high robustness and efficiency, but high low-frequency harmonic currents appear in the machine windings increasing the losses within the machine. Furthermore, uncontrolled rectifiers do not allow to properly control the machine to obtain maximum torque and lead to non-optimal operating points. This is especially noticeable at higher loads, where the unity power factor imposed by the uncontrollable rectifiers under-excites excessively the machine, thus reducing dramatically its torque capability unless the machine has been constructed with an increased volume of magnet material (Monajemy, 2000). Jordan in (Jordan and Apsley, 2011) highlights that increasing the number of phases in the machine leads to a reduction in the torque ripple and in the damper losses, but also points out that there is an upper limit for the number of phases before the commutation time of the diodes (this depends on the commutation inductance seen by them) exceeds its on-time. Work carried out in (Di Gerlando et al., 2012) focuses on different rectifying solutions based on three-phase diode systems, where a modular machine with four three-phase systems (two systems shifted 30º from the other two) is connected in various ways. The influence on torque ripple and current harmonics is analysed. The arrangements taking advantage of the 30º shift by transforming the output of two three-phase rectifiers into a twelve-pulse system are advantageous from the torque ripple and the current harmonics point of view.

Work presented in (Xiang-Jun et al., 2012) suggests a more complicated conversion stage, by introducing Vienna rectifiers as machine-side converters (MSC) (instead of uncontrollable diode rectifiers) and three-level neutral point clamped (3L-NPC) converter as the grid-side converter (GSC) to control a quadruple three-phase PMSM. This solution provides more sinusoidal stator currents (than in the case of uncontrollable rectifiers), but it still lacks the ability to modify the power factor of the machine as the Vienna rectifiers are limited to close to unity power factor (Kolar and Zach, 1994). A comparison between an uncontrolled rectifier and a Vienna rectifier for wind-power application is presented in (Nikouei, 2013) concluding that higher power can be extracted with a Vienna rectifier, but higher dc-bus voltage is required, increasing the voltage blocking requirement for the GSC. Another disadvantage of the Vienna rectifier is highlighted in (Radomski, 2005) where it is demonstrated that there is an inter-relation between the dc-bus voltage and the phase displacement between the ac voltage and current, thus not allowing to independently control active and reactive powers when the dc-bus voltage is fixed.

By using fully controllable rectifiers in the MSC, the complexity of the conversion stage is increased (and so is its probability-to-fail (PTF)), but the extra degree of freedom in the control allows to optimally operate the machine and reduce its losses due to stator current harmonics. For example, the control of a dual three-phase PMSM for wind energy conversion was presented in (Sheng-Nian et al., 2011), where the two sets of three-phase windings are controlled independently by using two independent VSCs. A single control unit is used for both three-phase systems and a current harmonic

reduction is claimed; however, details of neither the control algorithm nor the modulation strategy have been provided.

The requirement of being able to operate the different three-phase systems at different load levels introduces the necessity to use independent conversion lines for each of the systems. Work carried out in (Duran et al., 2011) introduces a conversion stage integrating two two-level VSCs on the machine side (one connected to each of the three-phase systems) with a single 3L-NPC grid-side converter. Each of the machine-side converters is connected to each of the dc half-voltage buses of the 3L-NPC converter. Gonzalez in (Gonzalez et al., 2014) proposes a power stage similar to this one but with two paralleled VSCs in each stator winding, and performs an optimisation analysis to obtain the maximum torque with one VSC failed. This optimal strategy leads to an unbalanced power output between the two three-phase windings, thus unbalancing the voltage of the dc half-voltage buses and creating a problem for the grid-side converter (GSC) modulator. In a similar way, Estay in (Estay et al., 2012) proposes a similar conversion stage with a couple of two-level diode rectifiers on the machine-side connected to each of the dc buses of a single 3L-NPC converter through dc/dc boost converters. These solutions provide a conversion stage with a minimum number of devices, so a reduction of the failure rate might be expected; however the severity of the failures may be increased as the solutions do not allow operation under faulty conditions. In all these cases, as each of the machine-side converters are connected to each of the dc half-voltage buses in the grid-side converter, equal power sharing between them might be required to keep the voltage in both dc half-voltage buses balanced and allow a normal operation of the GSC.

2.4.2   Machine-side converter control

Depending on the final multiphase machine's construction, the control structure may be different to adapt it to the special requirements of each machine's type, but the basics of the controllers are pretty much the same as those applicable to three-phase machines.

The simplest control structure for an ac electrical machine may be the so-called open-loop scalar control (or V/f control) which represents the most popular scheme for low-performance induction machine drives (Stulrajter et al., 2007). This basically imposes the voltage at the machine's terminals with the frequency required to make the rotor turn at, approximately, the desired speed and the amplitude of the voltage is obtained by keeping V/f ratio fixed at the rated value thus, theoretically, keeping the machine's flux at its rated value. The application of this structure to a PMSM requires including a damping strategy in the control algorithm to reduce rotor oscillations when a torque change occurs. This strategy consists of introducing a feedback signal from the high frequency torque oscillations in the speed command (Brock and Pajchrowski, 2011) and (Agarlita et al., 2013). This is so because this machine has, intrinsically, very low damping in the rotor body as no physical damping circuit exists. This leads to a parasitic damping mainly due to eddy currents and mechanical losses, which is not sufficient to provide proper dampened response. The main benefits of this control approach are the simplicity, no requirement for knowledge of any machine parameter, and there is no regulator to be tuned. On the other hand, the main drawback is that, as it is a fully open-loop strategy, it does not provide precise control of any of the machine's variables. This is of especial concern during transient conditions and it could lead to an overcurrent trip in the VSC if a steep torque change is demanded.

The most widely used control method to control both torque and flux in three-phase electrical machines is the so-called field-oriented control (FOC), which is an indirect method as it controls the final variables (torque and flux) by means of the machine's currents. Amongst all the possible current regulators, the dual PI controller (one PI for d- and one for q-axis) in a synchronously rotating frame (SRF) is the preferred choice (Novotny and Lipo, 2000). This reference frame introduces a coupling between both axes (a machine's speed dependant complex pole) that strongly affects the performance of the loops (Briz et al., 2000). The classical approach to reduce the axes cross-coupling in the SRF consists in modifying the plant poles by means of a state feedback. If the state feedback is exactly performed, it removes the imaginary part of the plant pole, leaving the plant as an *RL* load. Other approach to compensate the cross-couplings is to use complex PI (PIc) in the SRF as in (Briz et al.,

1999). This controller, instead of altering the plant's transfer function, has a modified structure that inherently cancels the complex pole of the plant, again leaving it as a simple *RL* load. When the machine's parameters are known accurately, these two types of controllers behave in terms of command tracking in a similar manner (Yepes et al., 2014), but when parameter estimation errors appear, the behaviour slightly differs with some low frequency (at the fundamental frequency) oscillations appearing in the closed loop response of PIc, usually resulting in an unacceptable performance (Harnefors and Nee, 1998). The theory behind this complex modelling approach is described in general terms in (Martin, 2004) and with reference to electrical systems in (Harnefors, 2007), with several examples that facilitate the comprehension. This approach unifies both *d* and *q* axis behaviour into a single complex transfer function that fully represents the cross-couplings, so a complex controller can be tuned taking into account the interaction of both axes.

A different approach to reduce the machine's cross-couplings may be to use a stationary reference frame control. If the control is performed in the stationary reference frame, the control scheme may be quite different from the traditional structure that relies on the SRF. To begin with, the variables will be with sinusoidal variation in time, so standard PI controllers do not lead to the zero steady state error as the gain value is limited by the actual delays in the control loop (Holmes et al., 2009). This can be easily solved with the use of resonant controllers (PR), dynamically tuned at the fundamental frequency (a PR is a controller formed by the addition of two terms, a proportional and a resonant integrator). As it is stated in (Yepes, 2011), the proportional constant of the PR controller directly affects the stability (and the dynamic performance) of the closed loop, so it should be chosen with special care. In his dissertation, Yepes provides a precise analysis of resonant controllers with transition from the continuous domain to the equivalents in the digital domain; also, different discretization methods are compared in terms of implementation complexity, frequency shift, etc. In (Rodriguez et al., 2012) a procedure for tuning a second-order generalized integrator (SOGI)-type resonant controller (among other types) is presented and its good performance has been demonstrated. The use of resonant regulators has been widely studied for fixed fundamental frequency (or nearly fixed) applications such as grid-side converters (Zmood et al., 2001) and (Guillaud et al., 2007), but there is not much research performed in relation to applications with variable fundamental frequencies, such as for example machine-side converters with wide speed variations (Yepes et al., 2012). In order to guarantee that the desired dynamic response and stability requirements are fulfilled in all the operating points (at different fundamental frequencies), dynamic variation of the regulator's parameters might be necessary.

Several applications of FOC to multiphase machines have been described, such as for example in (Bojoi et al., 2002) for the case of an asymmetrical six-phase machine, where an independent SRF current regulator for each three-phase systems is proposed; similarly, in (Hua et al., 2006) independent SRF current regulators are used to control a quadruple three-phase synchronous machine using a FOC referred to the air-gap flux vector (so-called MT reference frame). Work in (Vukosavic et al., 2005) presents a FOC for a symmetrical six-phase machine following the VSD approach and including current regulators in the stationary frame. In (Levi, 2011b), a review of the FOC for electrical machines (including multiphase machines) is available focusing exclusively on the control structure itself, assuming the presence of speed sensor and perfect knowledge of the machine's parameters.

Generally, FOC provides excellent steady-state behaviour with low ripple amplitudes in both torque and flux (Chikhi et al., 2010) and good transient behaviour (very good when a speed sensor is provided (Garcia et al., 2006)). It normally involves constant switching frequency fixed by the PWM carrier guaranteeing its determinism and facilitating the filtering. On the downside, FOC requires precise information about the rotor position as it relies on coordinate transformations that include it, so position/speed sensor is recommendable; this however reduces the robustness of the drive. To eliminate this drawback, a lot of research has been published about sensor-less speed estimation methods for both induction and PMSM. Work in (Kubota and Matsuse, 1994) and (Ha and Sul, 1999) focuses on the induction machine, consisting basically in introducing higher-than-fundamental frequency signals and obtaining information about the rotor speed and the rotor resistance. For the case of PMSM, two different techniques have been described (Corley and Lorenz, 1998), such as reconstructing the back electromotive force (EMF) of the machine in (Wu and Slemon, 1990), and

again injecting high-frequency currents and taking advantage of the inductance spatial variation due to the inherent rotor saliency (Kulkarni and Ehsani, 1992).

Decoupling between torque and flux control and the current regulators' tuning depend on machine's parameters such as inductances (Garcia et al., 2006), so the effective performance may vary as the machine's inductances become saturated or there exist errors in the estimations. Another minor disadvantage is the relatively high computational burden required by FOC algorithms, which limits the minimum sampling period and requires high-performance digital signal processors (DSP) capable of processing trigonometric functions. Thanks to the advances in microprocessors, this is nowadays not a problem anymore.

An evolution of the traditional, PI controller based, FOC is the substitution of the PI regulators by a predictive controller (PC) to perform the current regulation (Le-Huy et al., 1991) and (Kukrer, 1996). Work in (Le-Huy et al., 1991) proposes a PC, in the stationary frame, that calculates the voltage vector that would, theoretically, obtain a zero current error. This voltage vector is synthetized combining two of the VSC available voltage vectors similarly as in the space-vector modulation. To minimize the effect of parameter estimation inaccuracies, an integral compensation of the current error is introduced in parallel. Kukrer analyses the effect of the computational delay on the performance of the predictive controller and its effects on the estimation techniques. It concludes that these controllers require high-order prediction laws which impose a high computational burden.

An alternative way of controlling electric machine's torque and flux is the use of direct torque control (DTC), firstly described in (Takahashi and Noguchi, 1986) and in (Depenbrock, 1988) for the use in induction machines. This method relies on the fast dynamics of the stator's flux and its direct dependency on the instantaneous stator's voltage (provided by the status of the power converter switches, usually termed switching state). By means of the proper selection of the converter switching state, the stator's flux is modified both in amplitude and in speed (angular position) obtaining a very fast control of the magnitude of the stator's flux and the torque. The switching state choice is typically made every 25 µs (ABB, 2011) and it is selected from a predesigned look-up table with both torque and flux error entries to keep both magnitudes within their hysteresis bands. The amplitudes of the hysteresis bands determine both the ripple amplitude of the controlled variables (torque and stator's flux) and the effective switching frequency of the power devices, so usually a trade-off between the current harmonics (due to stator's flux hysteresis band) and the maximum switching frequency (mainly dependant on the torque hysteresis band) should be found (Casadei et al., 1994). This means that if the torque ripple needs to be reduced, the amplitudes of the hysteresis bands will also need to be reduced but the switching frequency will increase (increasing the power device losses). Work in (Zhong and Rahman, 1997) may be one of the first applications of the direct torque control method to a permanent magnet machine where the base equations for torque and flux control are obtained. An important result from this work is that the DTC for PMSM with rotor saliency can only be applied if a certain condition regarding the stator's and rotor's flux is satisfied at all times. This condition requires setting up of the stator flux amplitude below a certain magnitude, depending on the rotor flux and machine's inductances; this is so to obtain a positive torque derivative with positive torque angle derivatives in the whole operating range. Luukko in (Luukko, 2000) highlights the importance of limiting the torque below the stability limit of a synchronous machine. This is especially important because machine parameter deviations could lead to torque angle estimation errors that may force the machine beyond the stability margin, leading to unstable operation as further increases in the torque angle would reduce the actual torque (Zhong and Rahman, 1997).

DTC has been applied to symmetrical multiphase machines (Toliyat and Xu, 2000) and (Kestelyn et al., 2005) where an improvement in the control of the stator's flux and torque is highlighted thanks to the increase in the number of the available voltage vectors that allows a higher flexibility in selecting the inverter switching states (Mythili and Thyagarajah, 2005). The approach followed by Kestelyn divides the originally complex DTC control in a five-phase machine into two classical DTC controls, one for each of the two sub-machines, thus simplifying the control structure and enabling independent control of the torque and flux contribution from the so-called auxiliary machine. Research has also been done to apply a DTC to an asymmetrical multiphase machine, e.g. (Bojoi et al., 2005), where a predictive DTC is used by means of deadbeat controllers to estimate the torque and flux in the next step allowing to keep fixed switching frequency and reduce the current's

distortion due to low-order harmonics. In the case of multiphase machines, special care needs to be taken, especially if non-fixed switching frequency DTC is used (Bojoi et al., 2006), because generation of low-order harmonics may produce highly distorted currents due to the low impedance in the non-flux/torque producing subspaces (Hatua and Ranganathan, 2005).

DTC is, as a control method in its basic hysteresis band based form, very well suited to control of three-phase machines, since it is inherently a two-variable control method. As far as the multiphase machines are concerned, the generic hysteresis form of the DTC is only appropriate for concentrated winding machines, since only one voltage space vector is applied in a switching period. In machines with sinusoidal MMF this leads to high low-order harmonic currents in the non-flux/torque producing plane(s) and, since there is no current control, an increase in the losses in the machine. Hence the successful applications of the DTC to multiphase machines normally relate to the concentrated winding machines, with a very few solutions developed so far for multiphase machines with sinusoidal MMF. Notable exceptions are the DTC for a sinusoidal MMF five-phase machine described in (Gao and Parsa, 2007) and in (Gao et al., 2010) and the DTC for an asymmetrical six-phase machine described in (Hatua and Ranganathan, 2005) and in (Hoang et al., 2015). In the former, a modified look-up table is proposed to minimize the non-flux/torque producing components. This is achieved by taking advantage of the fact that medium voltage vectors have the opposite direction in the non-flux/torque producing subspace, than the direction is of the corresponding large (and short) ones. The corresponding large (short) voltage vector is the one which has the same direction in the flux/torque producing subspace. This means that from the flux/torque regulation point of view, these corresponding voltage vectors can be considered as redundant; but in the non-flux/torque producing subspace, these corresponding voltage vectors are antagonists. Work in (Gao et al., 2010) combines corresponding medium and large voltage vectors (and medium and short ones) to create virtual voltage vectors which inherently cancel the non-flux/torque producing components. This work focuses on the demagnetization effect produced by the application of the virtual voltage vectors that has the greatest influence on the torque. This issue is of especial concern when the main flux of the machine is near the boundaries of a sector and the speed is low. To overcome this demagnetization, Gao proposes the use of virtual voltage vectors with lower influence on torque (providing slightly slower torque dynamics) under these circumstances by using different look-up tables depending on the actual speed of the machine. In the case of asymmetrical machines, (Hatua and Ranganathan, 2005) analyse different control strategies for a six-phase machine according to the way the stator's flux is controlled. The conclusion is that controlling each three-phase stator's flux magnitude individually is the best option to reduce the dc drift tendency. Additionally, by making use of individual switching tables for each of the three-phase systems and increasing the complexity (by using higher level and number of hysteresis controllers), a reduced torque ripple can be obtained compared to that of a three-phase machine, while keeping the value of low order current harmonics negligible. Work in (Hoang et al., 2015) focuses on trying to keep at zero, on average, the flux in the non-flux/torque producing subspace so that a reduction in the current harmonics is obtained. For this, Hoang proposes to use not only the largest voltage vectors but also the second largest (which have opposite direction in the non-flux/torque producing subspace). Depending on the instantaneous position of the non-flux/torque producing subspace flux vector, the largest voltage vector, or the second largest is used.

DTC strategy outperforms FOC in terms of the transient behaviour, as it can obtain excellent torque response times in the range of few milliseconds (Casadei et al., 2013). It does not require information about the position of the rotor and is therefore inherently sensorless (however, speed/position information will be needed for closed loop speed/position control) and the only machine's parameter required is the stator resistance (no inductances needed). The downside is that the steady-state behaviour is worse than that of the FOC, as higher torque and flux ripples appear, the switching frequency is variable and dependent on the operating point, and the torque response is highly speed-dependant (Casadei et al., 2013). To overcome these drawbacks, several modifications to the basic DTC structure have been proposed (Vyncke et al., 2006), some of them by using modified switching tables as in (Li et al., 2002), (Ozcira and Bekiroglu, 2011) and in (Lang et al., 2006). Work in (Sutikno et al., 2011) achieves quasi-constant switching frequency by modifying the torque controller structure with the inclusion of two triangular carriers and two comparators. Another proposal is the hybrid of FOC and DTC, consisting in including a modulator to provide constant switching

frequency [(Swierczynski and Kazmierkowski, 2002) and (Limei and Yanping, 2007)]. Another difficulty in actual implementations of the DTC is the necessity for an accurate estimation of the stator's flux vector. This is especially noticeable at low speeds when fundamental frequency tends towards zero (Bausch et al., 1994). The estimation techniques can be generally divided into three commonly used approaches:

i)   One relies on the integration of the stator's voltage equation, which is very sensitive to dc offsets in measurements (especially at low speeds), so different modified integrators have been proposed [(Hu and Wu, 1998) and (Stojic, 2012)]. However, a limitation at low-speed operation arises as the modified integrators introduce an unacceptable phase lag at low fundamental frequencies. An option to remove the above mentioned limitation is to estimate the offset and compensate it (Holtz and Quan, 2003), allowing to use a pure integrator without a dynamical limitation.

ii) The second strategy relies on the machine's current model, which requires the knowledge of the machine's inductances [(Tajima and Hori, 1993) and (Zhen and Xu, 1998)]. This approach is very parameter sensitive and can lead to unacceptable errors, especially at high-load operation when saturation effects are more prominent. The current model approach can be used at low-speed low-load operation and one can switch to the voltage model approach at higher speeds and loads, as proposed in [(Umeno et al., 1990), (Jansen and Lorenz, 1994) and (Chouhan and Chandra Jain, 2011)].

iii) The third approach relies on the observer theory (Peterson, 1996). It uses the state-space model of the machine (with certain modifications on the inputs) to estimate all the state-variables (so-called identity observer) or only a subset of them (so-called reduced observer (Luenberger, 1979)).

An evolution of the DTC strategies is the so-called model predictive direct torque control (MPDTC). This strategy replaces the DTC's pre-designed switching table by a solver that computes a cost-function for each of the available voltage vectors, at each sampling time. After this, the voltage vector that minimizes the above-mentioned cost-function is selected. This evolution claims a reduction in the switching frequency while maintaining the same ripple and dynamic performance as traditional DTC (ABB, 2013). An excellent comparison between FOC, DTC and MPDTC control strategies is performed in (Geyer, 2010) and in (Geyer, 2011) for the application in three-phase medium voltage converter-fed drives. The conclusion is that predictive strategies outperform the traditional ones only if the prediction horizon is relatively long (30-100 time steps); this as the downside, imposes a very high computational burden.

A leap forward in the predictive control field is the use of the so-called model predictive control (MPC) whose background theory is described in (Papafotiou et al., 2004) and in (Geyer et al., 2009). It generally consists of performing the following steps:

i)   Estimating the target variable values along a predefined prediction horizon considering all the available VSC voltage vectors.

ii) Selecting those voltage vectors that lead to feasible target variable's values at the end of the prediction horizon or points in the right direction for all time-steps within the prediction horizon.

iii) Evaluating a cost function for each of the feasible voltage vectors.

iv) Selecting the VSC voltage vector that minimizes the cost function.

Depending on how the cost function is defined, different dynamic behaviour and switching frequencies can be obtained. One of the simplest cost functions (the current error value) is used in (Rodriguez et al., 2007) where the good dynamic behaviour of the controller is demonstrated. In (Ramirez et al., 2010), an interesting combination between MPC and hysteresis current controllers is presented. It introduces an additional step to those above mentioned as it performs extrapolations of the trajectories until the hysteresis band restriction is violated (in any of the target variables) to account for the predicted switching frequency of each of them. The selected VSC voltage vector is the one that minimizes the predicted switching frequency. Work in (Kouro et al., 2009) provides a thorough review of the MPC possibilities to control power converters. This highlights the perfect match between the power converter control and the MPC theory and the flexibility of the latter to take into account the converter non-idealities.

MPC is perfectly suited for controlling multiphase machines as the cost function can include as many variables as desired, so complete control of all the subspaces can be achieved. Previous work has mainly focused on the dual three-phase machine with isolated neutrals as in (Barrero et al., 2009a), (Barrero et al., 2009b), (Gregor et al., 2010) and (Barrero et al., 2011). The main difficulty in applying MPC to multiphase machines is the high number of available voltage vectors which increases the computational cost exponentially with the number of phases (Barrero et al., 2009a). This work analyses the effect of considering a reduced subset of voltage vectors (only the large ones) on the control performance. It concludes that the computational cost reduction obtained compensates the minor performance degradation. In (Barrero et al., 2009b), a modified MPC is applied to an asymmetrical six-phase machine. The novelty resides in the application of a combination of two voltage vectors (one large and one zero) in each switching period resulting in a better approximation of the required voltage vector. The selection of the fraction of time (in terms of the switching period) that each of the two voltage vectors will be applied is performed to obtain a minimal tracking error along the switching period. In (Gregor et al., 2010), a combination of MPC and a modulator stage is presented. The selected voltage vector from the predictive stage is fed as the input to a space-vector PWM (SV-PWM) modulator which ensures constant switching frequency and allows zeroing the voltage components in the non-flux/torque producing subspace. In (Barrero et al., 2011), a combination of the last two previously mentioned strategies is presented introducing the addition of the zero vector into the SV-PWM. The application of MPC to five-phase symmetrical machines is described in (Lim et al., 2014) where a cost function including current errors in both flux/torque and non-flux/torque producing subspaces is used. By modifying the weight on the non-flux/torque producing subspace current error, sinusoidal currents can be obtained in a five-phase sinusoidally wound induction machine. This work also demonstrates that the use of the small voltage vectors is unnecessary as the same performance is obtained without them, so a reduction in the computational burden of the MPC is possible without performance degradation. In fact, the optimal subset of voltage vectors from the current ripple point of view is the one considering large, medium and zero vectors.

The requirement to keep switching frequencies at low values introduces difficulties in the control of the machine's currents, since the non-idealities of the converter become more detrimental for the performance as the switching frequency is decreased, which especially affects FOC strategies. In particular, the current controllers tend to perform unsatisfactorily due to inaccuracies in the dynamic model of the machine's cross-couplings (Holtz et al., 2004). The sampling and computation delays also become much more significant as the sampling frequency decreases, introducing additional phase lags in the regulation loops, thus decreasing the phase margin and affecting the stability (Buso and Mattavelli, 2006). Work in (Kim et al., 2010) presents a comparison of the different current regulators usually applied to electrical machines operating at low sampling-to-fundamental frequency ratios, suggesting the use of direct design methods in the discrete time domain (instead of discretizing a continuous controller) to avoid performance degradation as the fundamental frequency increases. Modelling of the current control loops for high power converters with low sampling ratios is presented, using complex transfer functions in (Shen et al., 2012). Shen extends the negative frequency axis of the frequency response diagram obtaining a positive and a negative bandwidth that can explain the poor dynamic performance (and even the instability) of the current loops.

A large body of work has been published about different control schemes applicable to asymmetrical multiphase machines, with main differences stemming primarily from the modelling approach (whether it is a VSD or a multiple dq approach). The straightforward approach based on a three-phase machine theory is followed in (Bojoi et al., 2005), where it is shown that it is possible to supply a dual three-phase induction machine (with windings shifted by 30º) from converters with independent control and with different load sharing between them by means of a current distribution strategy. Reference currents for both three-phase stator windings are generated and applied to the current regulators of each three-phase winding. Similarly, work in (Karttunen et al., 2012) introduces a dual-star synchronous machine fed by two independent VSCs and implements independent three-phase vector control for each of them. The main problem of these strategies is that having independent current regulators for each three-phase winding yields a complex control structure, since the stator-stator cross-couplings need to be taken into account and compensated for to provide adequate transient response. Work in (De Camillis et al., 2001) proposes the use of state-space modelling approach for a

dual star asynchronous machine to construct a current controller structure that fully decouples the flux/torque producing subspaces in both three-phase systems.

Another rather significant body of the research work has focused on control structures that help compensating the operating unbalances that can appear in a multi-star winding machine. These unbalances can lead to different currents flowing along the different three-phase systems, but also it can happen that the currents within one (or more) of the three-phase systems might not be balanced. In (Zhao and Lipo, 1995), the VSD approach is followed and a control scheme, that forces to zero the non-flux/torque producing subspace voltages (no closed-loop current control), is presented relying on the perfect symmetry of the machine and the converter to avoid current flowing in the non-flux/torque producing subspace. In reality, machines present structural unbalances and converters have non-idealities that are translated into fundamental frequency current flowing in the non-flux/torque producing subspace; these will be reflected as current asymmetries between the different three-phase systems. Work in (Bojoi et al., 2003) presents two alternative control structures to cancel the effects of the unbalances. One is based on the multiple *dq* approach and basically consists in regulating each three-phase system currents independently. The other one is based on the VSD approach and it includes a compensation branch to cope with the unbalances between the different three-phase systems. In both cases, additional current regulators are required to guarantee balanced operation. Following the VSD theory, work in (Che et al., 2014a) presents a comparison of different current control schemes for a dual three-phase induction machine concluding that, to guarantee a balanced operation within both three-phase systems under any circumstance, a dual-PI controller, i.e. two PI controllers (one in the positive and the other in the negative sequence reference frame) per non-flux/torque producing axis, is required. An alternative to this that also leads to balanced operation is presented in (Bojoi et al., 2006), where a thorough analysis of PR controller for dual three-phase machine current control purposes is presented. The use of this type of controllers is suggested for both the flux/torque producing and the non-flux/torque producing subspaces of the six-phase machine. Only a small body of the published research work has focused explicitly on the current sharing between the different three-phase systems. In (Grandi et al., 2011), a power sharing strategy is provided for a six-phase open-end winding machine fed by four three-phase converters. This proves that, with an appropriate control algorithm, the total motor power can be shared among the four independent dc buses.

In the case of symmetrical multiphase machines, a great research effort has been focused on motoring applications where the maximum torque obtainable from a machine is the key interest. This has led to numerous publications analysing odd phase number concentrated winding machines in which some odd low-order harmonics can be used to increase the torque capabilities of the machines (Levi et al., 2007). Work in (Lipo and Wang, 1984) showed that an improvement in the machine's performance, when driven by a converter, is obtained when the stator is wound in a concentrated way and quasi-rectangular voltage waveforms are applied, leading to a better utilization of the iron core and to an increase in the peak of the fundamental component of the air-gap flux, thus increasing the torque capability of the machine. In (Toliyat et al., 1991a), the analytical calculation of the mutual inductances in a three-phase machine wound with concentrated windings is performed, showing a trapezoidally-shaped interaction. In (Toliyat et al., 1991b), a five-phase induction motor with concentrated windings is modelled and it is concluded that by injecting a third-harmonic current, an improvement in the flux distribution and the output torque is obtained. Work in (Xu et al., 2001) deals with the vectorial control of a five-phase induction motor with concentrated windings, concluding that it can be considered as two independent machines, one at fundamental frequency and the other at the third harmonic frequency, both requiring their respective torque and flux controllers. Similar conclusions have been addressed in (Parsa and Toliyat, 2005) for a five-phase permanent magnet synchronous machine wound with concentrated windings.

Another widely studied application of sinusoidally-distributed winding symmetrical multiphase machines is the series connection of several machines (Levi et al., 2004b) driven by a single VSC as described in (Levi et al., 2004a), (Jones et al., 2005) and in (Malvar et al., 2014). By means of proper phase transpositions and making use of additional degrees of freedom in multiphase machines, different planes can be used to independently control torque and flux of the different series-connected machines. This yields a reduction of the number of inverter legs required, although this can also be seen as a certain disadvantage as the fault tolerance regarding the VSC is reduced. Another feature of

such arrangements is that they intrinsically introduce additional impedance (the flux/torque producing subspace impedance of one of the other machines) in the non-flux/torque producing subspaces of each of the serial-connected machines thus almost eliminating the undesired current circulation within them and simplifying the modulation. Additionally, the control of all the serial-connected machines can be accomplished by means of a single DSP reducing the number of control electronic components required. On the downside, some disadvantages can be highlighted such as the increased losses in the machine windings as the summation of the currents of all the machines circulates through the stator windings. An increased dc bus voltage is therefore required due to the additional voltage drops within the series-connected machines and an increased bandwidth is needed to control successfully such a set of the series-connected machines.

Modulation techniques for multiphase machines have also been extensively investigated, since now additional degrees of freedom appear, when compared to a three-phase case. The aim of these techniques is usually to keep unexcited the non-flux/torque producing subspaces on average during the switching period (Dujic et al., 2007). In this work, a space vector modulation for a symmetrical nine-phase load is analysed and implemented guaranteeing that the average voltage applied in all the non-flux/torque producing subspaces is zero, thus avoiding the generation of undesired low-order harmonics. Work in (Jones et al., 2012) presents a review of the available solutions for the modulation of multiphase multi-level converters with a special focus on five- and seven-phase machines. A similar work has been done in (Duran et al., 2007) where a review of the different possibilities for selecting the active vectors is presented. In (Zhao and Lipo, 1995), a modulation technique for an asymmetrical six-phase machine is proposed to minimize the current harmonic flow in the non-flux/torque producing subspace. This is accomplished by using the four active vectors, positioned at the outermost polygon of the flux/torque producing subspace and adjacent to the reference voltage, and one of the zero vectors. By using such technique, it can be demonstrated that the average volt-seconds in the non-flux/torque producing subspace can be kept at zero during every switching period. In addition to this, the instantaneous excitation of the non-flux/torque producing subspace is minimized as the projections of the active vectors used are the minimum possible. A procedure to automate the selection of the vectors in a five-phase machine is proposed in (Gataric, 2000) and in (Duran and Levi, 2006). In both cases, the closest vectors to the reference are selected, but the main difference is that in (Gataric, 2000), two large vectors and two medium vectors are taken into account, while in (Duran and Levi, 2006) three medium vectors and one large are used. In (Iqbal and Levi, 2006), a survey of different modulation strategies for a five-phase machine is presented, proposing two alternative methods to reach the maximum output voltage while using medium and large active vectors at all times. This provides the minimum THD in the flux/torque producing subspace and at the same time allows to cancel any excitation in the non-flux/torque producing subspace.

2.4.3   Grid-side converter control

The GSC in back-to-back arrangements is usually in charge of keeping the dc bus voltage controlled at a certain level and, in case of 3L-NPC converters, its functions also include the balancing of the dc bus neutral point voltage. Nowadays, in wind turbine applications, practically 100% of the available turbines include VSC on the grid side, mainly because of their fast response and means for independent control of active and reactive power (Teodorescu et al., 2011). These are key features when fulfilment of the grid-codes is a must.

A lot of work has been done in relation to the control of a grid-connected VSC. Different reference frames, such as SRF (Shen et al., 2012) or stationary reference frame (Holmes et al., 2009), different current controllers, such as PI, PIc (Briz et al., 2000), PR (Yepes, 2011), dead-beat (Buso et al., 2000), hysteresis (Kale and Ozdemir, 2004), etc., and different control approaches, such as voltage oriented control, model predictive control (Shen, 2013), direct power control (Escobar et al., 2003), etc. can be found in the literature. A thorough review and comparison of the different current control schemes for grid-connected VSC is presented in (Limongi et al., 2009).

A huge body of research work has also been published about different modulation techniques that can be applied to a grid-connected VSC. Of especial interest are those related to 3L-NPC

converters because in this type of converters, the modulation plays an important role in terms of balancing the dc bus neutral point voltage (Alonso, 2005). Furthermore, the low ratios between the sampling and the fundamental frequency (as noted in section 2.4) introduce additional control difficulties and complicate the fulfilment of the grid-codes in terms of harmonic emissions that may inevitably require a combined design of the grid-side filter and the GSC modulation (Zabaleta et al., 2016).

2.5   Fault-tolerant control

A constant-amplitude rotating MMF can be produced with at least two independent currents (Clarke, 1943). This means that a multiphase machine (with $n > 3$) can still produce a rotating MMF even with one (or more, depending on the value of n) of its phases in open-circuit. This is one of the actual benefits derived from the use of multiphase machines because three-phase machines cannot produce rotating MMF with a single open-circuited phase. This is so as the currents along the other two phases are no longer independent and therefore cannot produce a constant-amplitude rotating MMF. To overcome this issue, some research has been focused on providing the three-phase machine with the ability to produce two independent currents when a phase is opened as in (Wallmark et al., 2007). A fourth converter leg is connected for this purpose to the machine's neutral, allowing to independently control the current of any two phases, and thus, producing constant-amplitude rotating MMF when one of the three phases is opened.

In a wind turbine conversion stage, the power converter is responsible for the 13% of the failures (resulting in a contribution to the downtime of 18%) as concluded from the surveys performed in [(Spinato et al., 2009) and (Wilkinson, 2011)]. The higher probability failures within the power converters are usually those related to the power electronic devices (IGBTs or IGCTs and driver circuitry) and to the converter control unit (CCU) as depicted in [(Birk and Andresen, 2007) and (Yang et al., 2011)]. The effects of the failures related to the CCU and other low-voltage auxiliaries can be easily mitigated by means of oversizing and/or redundancy with a negligible increase of the converter cost. The failures related to power electronics require especial care as these have been found to be a frequent root cause of fire (Anjar et al., 2011). Introducing some additional diagnosis capabilities and isolation devices, a phase leg of a converter could be safely left open-circuited after a failure in any of its power electronic devices while the other phase legs are in operation. With this add-on, an improvement in the availability and in the energy production could be obtained with the use of multiphase machines and converters as these can keep operation with one (or more) open-circuited phase(s).

The idea behind fault-tolerant strategies in multiphase machines is to continue generating a constant-amplitude rotating MMF by means of the currents in the (at least) three healthy phases (Levi, 2008). This can be achieved by applying different strategies depending on the machine's construction. For example, in the case of several three-phase systems with isolated neutrals, after a failure in one phase it is possible to take out of service the whole three-phase system in which the faulty phase is, and operation can continue with the other healthy three-phase systems as it is described in (Mantero et al., 1999) and in (Ben Ammar and Sami, 2008). The main benefit of this strategy is that the control algorithm needs to be only slightly modified (principally the generation of the controller set-points and feed-forward terms) for the operation after a failure (Ben Ammar and Sami, 2008). The drawback is that this technique strongly de-rates the capability of the drive after a failure as it disconnects one entire three-phase system, thus unnecessarily reducing the number of operational phases, and so, the available torque. In the case of a single neutral point for all the phases, after a fault, it is no longer required to disconnect three phases as a whole; instead, disconnecting only the faulty one is possible, thus keeping the number of operational phases at a maximum at all times. It should be noted that, to produce a constant-amplitude rotating MMF with a set of non-uniformly spatially distributed windings, the currents through those windings will inevitably need to be unbalanced in amplitudes (Levi, 2008). Hence a phase will conduct a higher current value thus setting the limit in terms of available torque. This unbalanced operation will establish fundamental frequency currents in the non-flux/torque producing subspaces, which may be controlled to optimize the unbalance, minimizing the current amplitude differences between the healthy phases (Fu and Lipo, 1994). Depending on the current limits

in the VSC and in the machine's phase windings, even rated torque could be available during the faulty operation if it is acceptable to continuously operate at a current level $n/(n\text{-}f)$ [pu], where f is the number of faulty phases (Levi, 2008) in the case of symmetrical machines.

With the evolution of the more-electric aircraft, and mainly due to high reliability required (PTF less than 1×10^{-9} per flight hour), several investigations have been performed aiming at highlighting the electrical machine requirements to reach these reliability figures, e.g. (Jordan, 2013) and (Mohammadpour, 2014). Both works share in common the necessity of using a multiphase machine with independent phases (modular design), supplied by phase-modular converters.

Modelling of multiphase machines with structural unbalances (due to an open-circuited phase) has been deeply analysed for different types of machines. In (Zhao and Lipo, 1996), a model for a six-phase induction machine with one open-circuited phase is presented and a procedure to control the healthy phase currents in a similar way as in the case of no fault (so-called double-plane current regulation) is proposed. This procedure tries to minimize the currents in the non-flux/torque producing subspaces to obtain maximum efficiency. This is accomplished by constructing a new transformation matrix for the case of post-fault operation. Similarly, for the case of a five-phase machine, Guzman in (Guzman et al., 2012) states that using the pre-fault transformation during the operation with one faulty phase leads to pulsating terms at twice the fundamental frequency in the back-EMF terms making the control of the currents difficult. This result has also been addressed in (Kianinezhad et al., 2008) for the case of a symmetrical six-phase machine and a specific flux/torque producing subspace current set-point strategy was proposed to minimize the torque oscillations.

Another way to overcome this problem is by using new post-fault specific transformation that allows keeping all the equations with time-invariant terms (Guzman et al., 2012). Work in (Zarri et al., 2011) presents a review of the consequences of manufacturing- and fault-created unbalances within the different windings in an odd phase number induction machine, concluding that these are represented as currents in the non-flux/torque producing subspaces whose analysis may be useful to detect the source of the unbalance. Che in (Che et al., 2014b) presents a thorough analysis of the post-fault operation strategies for a six-phase asymmetrical machine with one and two isolated neutral points, concluding that the same transformation matrix as in the case of healthy phases can be used, and only minor control modifications (mainly current set-point calculations and enabling of certain current controllers) are required to obtain a smooth torque waveform. In (Meinguet et al., 2012), a procedure to detect a failure in a phase of a five-phase PMSM (or its associated VSC) is presented by analysing the unbalances in the phase currents and their frequencies by means of evaluation of different proposed fault indices.

Other solution to obtain smooth post-fault operation can be the use of fuzzy logic controllers (FLC) within the FOC structure. By this, the FLC takes care of the different configurations that can be present in the machine, thus acting as the torque and flux controller. Additionally, FLC are also introduced in the current control loops to deal with the effect of the loss of one (or more) stator phase(s) on the electrical parameters of the machine's model (Betin et al., 2014). Work in (Fnaiech et al., 2010) introduces a comparison between a FOC based on traditional PI controllers and based on FLC, when one and two phases are open-circuited in a six-phase induction machine. It can be seen how with PI based controllers an oscillation in steady state occurs when a phase is open-circuited whereas in FLC it does not. This is due to the change in the model (both in the electric and in the mechanical) that implies the loss of a phase, which the PI based controllers cannot fully compensate for, producing a worsened behaviour compared to that of the healthy condition.

Different approaches exist to achieve the fault-tolerant operation, as is evident from the given survey. They principally differ with respect to the use of the modified/original machine model and modified/original decoupling transformation in post-fault operation.

2.6 Summary

In this chapter, a review of the state-of-the-art in the area of multiphase machines is reported, with the emphasis placed on the aspects related to modelling and control. Special focus has been put on the transformations usually applied to multiphase machines, seeking to highlight the main differences between them and their limitations. As multiphase machine control structures might be directly derived

from those in existence for three-phase ones, a thorough review of the different available control structures already applied to three-phase machines has been provided.

Most of the research about multiphase machines has focused on motoring applications where the induction machine is the major player due to its ruggedness and controllability. Only a small part of the published work is focused on PMSM working as a generator.

An aspect that has not been fully covered by the published research work is the effect of the low ratio between the sampling and the fundamental frequency that it is known to strongly affect the performance of the control loops as the machine speed varies. An analysis of the different available control schemes will be performed and their performance and complexity will be compared.

CHAPTER 3

Model transformations

3.1 Introduction

In this chapter, a thorough review of the model transformations for multiphase machines will be provided. The first part of the chapter is an introduction into the background and purpose of the model transformations, which is then followed by five particular sections. Section 3.2 develops the model of a permanent magnet machine with multiple three-phase systems in the original reference frame, which will highlight the necessity for the transformations. Sections 3.3 and 3.4 describe the VSD transformation and the multiple dq transformation approaches, respectively. Section 3.5 will cover other transformations already described in the literature. Next, section 3.6 presents transformations developed during the work on this project. Finally, section 3.7 provides a comparison between the multiple dq, the VSD and the novel transformation regarding the behaviour with regard to different non-idealities that may arise during operation.

Historically, the purpose of the model transformation in ac rotating machines has been to obtain a new set of equations, usually fewer in number and less complex in nature, representing the machine's behaviour exactly as the original equations. As a consequence of the less complex nature, the transformed equations usually lead to an easier understanding of the model. Initially applied to three-phase machines, the model transformation basically consists in referring the equations to a new reference frame constituted by three mutually orthogonal axes. Two of them are placed on the cross-sectional plane of the machine and are usually referred to as α-β or d-q. These axes represent the electromagnetic energy transfer across the airgap and constitute the so-called flux/torque producing subspace (α-β subspace herein after). The third axis, usually denoted as 0, represents the zero-sequence components (Park, 1929) and is seldom used, as, normally, the neutral point of the ac rotating machines is left isolated.

With the advancement in power electronics and control devices, the electrical machine transformations have been used to develop transformed model of the ac machines as similar as possible to that of an independently excited dc machine. In this machine, there is one current that controls the flux magnitude while the other one controls the torque, without any interaction between them. This is the ideal behaviour from the control point of view, as it can provide independent control of both flux and torque values and is the basic idea behind FOC.

In multiphase machines, the basic idea of the model transformations is kept the same but, due to the increase in the dimension of the system, it introduces additional degrees of freedom. There is again an α-β subspace representing the electromagnetic energy transfer across the airgap, but there appear additional, mutually orthogonal, subspaces whose components do not contribute to the energy transfer. These subspaces have been previously referred to as non-flux/torque producing subspaces and will be referred to as x-y subspaces further on. The existence of the x-y subspaces introduces additional complications in the control as the currents in them do not give any benefit, but they may need to be controlled to avoid additional losses in the machine and the converter.

The original results of the work described in this chapter have been published in (Zabaleta et al., 2016a) and in (Zabaleta et al., 2016b).

3.2 PMSM model in the natural domain

In the following, the equations describing the behaviour of a multiple three-phase system permanent magnet synchronous machine will be obtained for the natural reference frame (such a model is also called phase variable model). The following assumptions are made:

i)   There are no rotor windings,
ii) The effects of magnetic saturations are neglected,
iii) The leakage inductance is constant and equal in all phases,
iv) No leakage coupling between phases is considered,
v)   The stator windings will be sinusoidally distributed so that only the fundamental harmonic is of concern in terms of MMF,
vi) The permanent magnet's flux is considered constant under all the operating conditions,
vii) Space harmonics in the air-gap field due to rotor saliency are considered up to the second-order harmonic.

The relation between the electric and the magnetic sub-systems, which also includes representation of the behaviour of any magnetically coupled windings, is established as

$$v = r \cdot i + \frac{d\psi}{dt} \tag{3.1}$$

Applying this law to all the windings in the stator of an n-phase machine, the following equations are obtained for the stator phases:

$$v_a = r_a \cdot i_a + \frac{d\psi_a}{dt}$$

$$v_b = r_b \cdot i_b + \frac{d\psi_b}{dt}$$

$$.$$
$$.$$
$$.$$
$$\tag{3.2}$$

$$v_n = r_n \cdot i_n + \frac{d\psi_n}{dt}$$

This set of equations can be expressed in matrix form as

$$[V_s] = [R_s] \cdot [I_s] + \frac{d[\Psi_s]}{dt} \tag{3.3}$$

The magnetic equations of a machine establish the relationship between the magnetic flux produced by one winding and its effects on the others. It is convenient to refer the MMF of all the windings to a rotating frame fixed to the rotor as shown in Fig. 3.1 for a six-phase machine. This is so because the rotor is usually the main element responsible for the anisotropy in the magnetic circuit, usually having two clearly differentiable directions for each pole pair (typically referred to as d and q).
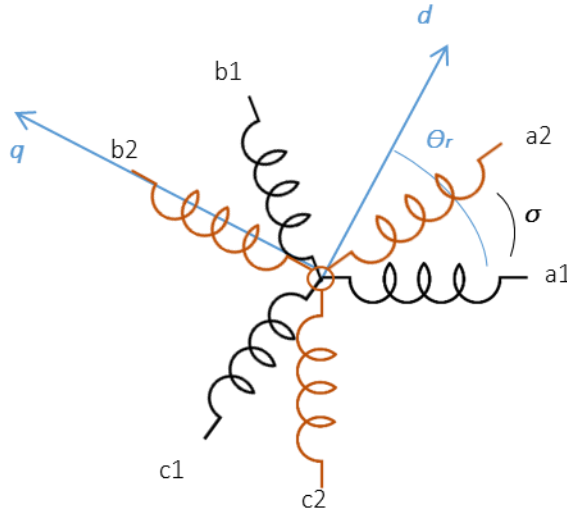

Fig. 3.1 Stator winding projections in a rotating reference frame.

With simple trigonometry, the following projections can be obtained, where F_{aid} is the MMF of the winding a_i projected on the d axis,

$$F_{aid} = F_{ai} \cdot cos(\theta_r - (i-1) \cdot \sigma)$$

$$F_{aiq} = -F_{ai} \cdot sin(\theta_r - (i-1) \cdot \sigma)$$

$$F_{bid} = F_{bi} \cdot cos\left(\theta_r - \frac{2 \cdot \pi}{3} - (i-1) \cdot \sigma\right)$$

$$F_{biq} = -F_{bi} \cdot sin\left(\theta_r - \frac{2 \cdot \pi}{3} - (i-1) \cdot \sigma\right) \tag{3.4}$$

$$F_{cid} = F_{ci} \cdot cos\left(\theta_r - \frac{4 \cdot \pi}{3} - (i-1) \cdot \sigma\right)$$

$$F_{ciq} = -F_{ci} \cdot sin\left(\theta_r - \frac{4 \cdot \pi}{3} - (i-1) \cdot \sigma\right)$$

and i varies from 1 to k; it denotes the sequential number of the three-phase system under analysis. In equation (3.4), σ is the electrical phase shift between the different three-phase systems in the stator and θ_r is the electrical angle between the rotor's reference north pole and the stator's reference phase (a_1 in Fig. 3.1). Again with the use of trigonometry, the projections of the rotating frame components on the different stator windings can be obtained as

$$F_{d|ai} = F_d \cdot cos(\theta_r - (i-1) \cdot \sigma)$$

$$F_{q|ai} = -F_q \cdot sin(\theta_r - (i-1) \cdot \sigma)$$

$$F_{d|bi} = F_d \cdot cos\left(\theta_r - \frac{2 \cdot \pi}{3} - (i-1) \cdot \sigma\right)$$

$$F_{q|bi} = -F_q \cdot sin\left(\theta_r - \frac{2 \cdot \pi}{3} - (i-1) \cdot \sigma\right) \tag{3.5}$$

$$F_{d|ci} = F_d \cdot cos\left(\theta_r - \frac{4 \cdot \pi}{3} - (i-1) \cdot \sigma\right)$$

$$F_{q|ci} = -F_q \cdot sin\left(\theta_r - \frac{4 \cdot \pi}{3} - (i-1) \cdot \sigma\right)$$

where $F_{d|ai}$ is the projection of the d-axis components on the stator winding a_i.

3.2.1   Stator self-inductances

The self-inductance represents the effect that a current through a winding has on the magnetic flux seen by it. In the case of the phase a_1 in Fig. 3.1,

$$\psi_{ma1} = N_{eq\_s} \cdot \frac{F_{a1}}{\mathfrak{R}_{ma1}} = N_{eq\_s} \cdot \left(\emptyset_{a1d}\Big|_{\substack{proj \\ a1\ axis}} + \emptyset_{a1q}\Big|_{\substack{proj \\ a1\ axis}}\right)$$

$$= N_{eq\_s} \cdot \left(\frac{F_{a1d}}{\mathfrak{R}_{md}} \cdot cos(\theta_r) - \frac{F_{a1q}}{\mathfrak{R}_{mq}} \cdot sin(\theta_r)\right) \tag{3.6}$$

where $\emptyset_{ma1}$ is the magnetic flux generated by phase a_1; N_{eq_s} is the equivalent number of turns of the stator phases (taking into account the pitch and distribution factors); F_{a1} is the MMF generated by the phase a_1; $\mathfrak{R}_{ma1}$ is the instantaneous magnetic reluctance along the direction of the phase a_1 magnetic axis; $\mathfrak{R}_{md}$ and $\mathfrak{R}_{mq}$ are the magnetic reluctances in the d and q axes, respectively, and θ_r is the angular position of the rotor with respect to the magnetic axis of the stator phase $a1$.

The magnetic permeances in the d and q directions (P_d and P_q) are defined as the inverses of the magnetic reluctances in each direction. Substituting the magnetomotive forces (F_{a1d} and F_{a1q}) firstly

by their expression in terms of F_{a1} (equation (3.4)) and afterwards the latter by their expressions in terms of i_{a1} leads to:

$$\psi_{ma1} = N_{eq\_s}{}^2 \cdot \left(P_d \cdot cos^2(\theta_r) + P_q \cdot sin^2(\theta_r) \right) \cdot i_{a1} \tag{3.7}$$

Having in mind the following trigonometric relationships:

$$sin^2(A) + cos^2(A) = 1$$

$$cos^2(A) = \frac{1 + cos(2 \cdot A)}{2} \tag{3.8}$$

the relation between the magnetic flux and the current creating it is obtained,

$$\psi_{ma1} = N_{eq\_s}{}^2 \cdot \left(\frac{P_d + P_q}{2} + \frac{P_d - P_q}{2} \cdot cos(2 \cdot \theta_r) \right) \cdot i_{a1} \tag{3.9}$$

The self-inductance of the phase a_1 can be easily obtained now by applying the definition of inductance as the ratio between the magnetic flux of a winding and the current required to create it,

$$L_{ma1} = \frac{\psi_{ma1}}{i_{a1}} = N_{eq\_s}{}^2 \cdot \left(\frac{P_d + P_q}{2} + \frac{P_d - P_q}{2} \cdot cos(2 \cdot \theta_r) \right) \tag{3.10}$$

Defining the rotating frame inductances

$$L_{md} = N_{eq\_s}{}^2 \cdot P_d$$

$$L_{mq} = N_{eq\_s}{}^2 \cdot P_q \tag{3.11}$$

as per (3.11), the self-inductance of the different stator windings can be expressed,

$$L_{mai} = \frac{L_{md} + L_{mq}}{2} + \frac{L_{md} - L_{mq}}{2} \cdot cos(2 \cdot \theta_r - 2 \cdot (i-1) \cdot \sigma)$$

$$L_{mbi} = \frac{L_{md} + L_{mq}}{2} + \frac{L_{md} - L_{mq}}{2} \cdot cos\left(2 \cdot \theta_r - \frac{4 \cdot \pi}{3} - 2 \cdot (i-1) \cdot \sigma\right) \tag{3.12}$$

$$L_{mci} = \frac{L_{md} + L_{mq}}{2} + \frac{L_{md} - L_{mq}}{2} \cdot cos\left(2 \cdot \theta_r - \frac{2 \cdot \pi}{3} - 2 \cdot (i-1) \cdot \sigma\right)$$

where i stands again for the stator's three-phase winding number (1, 2, 3 … k).

The definition of the rotating frame inductances shown in (3.11) differs from the typically adopted for three phases machines where these are defined as

$$L_{md} = \frac{3}{2} \cdot N_{eq\_s}{}^2 \cdot P_d$$

$$L_{mq} = \frac{3}{2} \cdot N_{eq\_s}{}^2 \cdot P_q \tag{3.13}$$

In multiple three-phase machines, the rotating frame inductances as in (3.11) can be obtained scaling down those of any of its three-phase systems with 2/3.

3.2.2   Mutual inductances

Proceeding in a similar way as in 3.2.1, the general expression for the mutual inductance between any two phases, in different three-phase systems, with the same index (a, b, or c) can be given as:

$$L_{aiaj} = \frac{L_{md} + L_{mq}}{2} \cdot cos((i-j) \cdot \sigma) + \frac{L_{md} - L_{mq}}{2} \cdot cos(2 \cdot \theta_r - (i+j-2) \cdot \sigma) \tag{3.14}$$

$$L_{bibj} = \frac{L_{md} + L_{mq}}{2} \cdot cos((i-j) \cdot \sigma) + \frac{L_{md} - L_{mq}}{2} \cdot cos\left(2 \cdot \theta_r - \frac{4 \cdot \pi}{3} - (i+j-2) \cdot \sigma\right)$$

$$L_{cicj} = \frac{L_{md} + L_{mq}}{2} \cdot cos((i-j) \cdot \sigma) + \frac{L_{md} - L_{mq}}{2} \cdot cos\left(2 \cdot \theta_r - \frac{2 \cdot \pi}{3} - (i+j-2) \cdot \sigma\right)$$

Similarly, mutual inductances between any two phases, in different three-phase systems, with the different index result in the form:

$$L_{aibj} = \frac{L_{md} + L_{mq}}{2} \cdot cos\left(\frac{2 \cdot \pi}{3} - (i-j) \cdot \sigma\right) + \frac{L_{md} - L_{mq}}{2} \cdot cos\left(2 \cdot \theta_r - \frac{2 \cdot \pi}{3} - (i+j-2) \cdot \sigma\right)$$

$$L_{biaj} = \frac{L_{md} + L_{mq}}{2} \cdot cos\left(\frac{2 \cdot \pi}{3} + (i-j) \cdot \sigma\right) + \frac{L_{md} - L_{mq}}{2} \cdot cos\left(2 \cdot \theta_r - \frac{2 \cdot \pi}{3} - (i+j-2) \cdot \sigma\right)$$

$$L_{aicj} = \frac{L_{md} + L_{mq}}{2} \cdot cos\left(\frac{2 \cdot \pi}{3} + (i-j) \cdot \sigma\right) + \frac{L_{md} - L_{mq}}{2} \cdot cos\left(2 \cdot \theta_r - \frac{4 \cdot \pi}{3} - (i+j-2) \cdot \sigma\right)$$

$$L_{ciaj} = \frac{L_{md} + L_{mq}}{2} \cdot cos\left(\frac{2 \cdot \pi}{3} - (i-j) \cdot \sigma\right) + \frac{L_{md} - L_{mq}}{2} \cdot cos\left(2 \cdot \theta_r - \frac{4 \cdot \pi}{3} - (i+j-2) \cdot \sigma\right)$$

$$L_{bicj} = \frac{L_{md} + L_{mq}}{2} \cdot cos\left(\frac{2 \cdot \pi}{3} - (i-j) \cdot \sigma\right) + \frac{L_{md} - L_{mq}}{2} \cdot cos(2 \cdot \theta_r - (i+j-2) \cdot \sigma)$$

$$L_{cibj} = \frac{L_{md} + L_{mq}}{2} \cdot cos\left(\frac{2 \cdot \pi}{3} + (i-j) \cdot \sigma\right) + \frac{L_{md} - L_{mq}}{2} \cdot cos(2 \cdot \theta_r - (i+j-2) \cdot \sigma)$$

(3.15)

3.2.3   Stator inductance matrix

With the previously calculated inductances, the inductance matrix of the stator windings can be constructed as:

$$
\begin{aligned}
&L_{ss}\\
&= \begin{bmatrix}
L_{ls} + L_{ma1} & L_{a1b1} & L_{a1c1} & \cdot & \cdot & L_{a1ak} & L_{a1bk} & L_{a1ck} \\
L_{b1a1} & L_{ls} + L_{mb1} & L_{b1c1} & \cdot & \cdot & L_{b1ak} & L_{b1bk} & L_{b1ck} \\
L_{c1a1} & L_{c1b1} & L_{ls} + L_{mc1} & \cdot & \cdot & L_{c1ak} & L_{c1bk} & L_{c1ck} \\
\cdot & \cdot & \cdot & \cdot & \cdot & \cdot & \cdot & \cdot \\
\cdot & \cdot & \cdot & \cdot & \cdot & \cdot & \cdot & \cdot \\
L_{aka1} & L_{akb1} & L_{akc1} & \cdot & \cdot & L_{ls} + L_{mak} & L_{akbk} & L_{akck} \\
L_{bka1} & L_{bkb1} & L_{bkc1} & \cdot & \cdot & L_{bkak} & L_{ls} + L_{mbk} & L_{bkck} \\
L_{cka1} & L_{ckb1} & L_{ckc1} & \cdot & \cdot & L_{ckak} & L_{ckbk} & L_{ls} + L_{mck}
\end{bmatrix}
\end{aligned}
$$

(3.16)

By inspecting the inductance matrix, it can be seen how the stator inductances (both the self and the mutual) depend on the rotor position in the case of anisotropy within the magnetic circuit ($L_{md} \neq L_{mq}$). This dependency on the rotor position makes it complicated to simulate a model in this natural reference frame as the inductance matrix would be changing at each simulation step as the rotor rotates. This difficulty can be overcome with the use of transformations that are the result of generalizing those for the three-phase machines. A script to construct the inductance matrix for an *n*-phase machine in Matlab ® is included in Appendix 1.

With this matrix, the magnetic equation of the machine can be expressed as:

$$[\Psi_s] = [L_{ss}(\theta_r)] \cdot [I_s] + [\Psi_{PM}]$$

(3.17)

where

$$[\Psi_s] = \begin{bmatrix} \Psi_{a1} \\ \Psi_{b1} \\ \Psi_{c1} \\ . \\ . \\ . \\ \Psi_{ak} \\ \Psi_{bk} \\ \Psi_{ck} \end{bmatrix} \qquad [I_s] = \begin{bmatrix} i_{a1} \\ i_{b1} \\ i_{c1} \\ . \\ . \\ . \\ i_{ak} \\ i_{bk} \\ i_{ck} \end{bmatrix}$$

$$[\Psi_{PM}] = \begin{bmatrix} \psi_{PM}\big|_{\substack{proj \\ axis\ a1}} \\ \psi_{PM}\big|_{\substack{proj \\ axis\ b1}} \\ \psi_{PM}\big|_{\substack{proj \\ axis\ c1}} \\ . \\ . \\ . \\ \psi_{PM}\big|_{\substack{proj \\ axis\ ak}} \\ \psi_{PM}\big|_{\substack{proj \\ axis\ bk}} \\ \psi_{PM}\big|_{\substack{proj \\ axis\ ck}} \end{bmatrix} = \begin{bmatrix} \psi_{PM} \cdot cos(\theta_r) \\ \psi_{PM} \cdot cos\left(\theta_r - \dfrac{2 \cdot \pi}{3}\right) \\ \psi_{PM} \cdot cos\left(\theta_r - \dfrac{4 \cdot \pi}{3}\right) \\ . \\ . \\ . \\ \psi_{PM} \cdot cos(\theta_r - (k-1)\cdot\sigma) \\ \psi_{PM} \cdot cos\left(\theta_r - \dfrac{2 \cdot \pi}{3} - (k-1)\cdot\sigma\right) \\ \psi_{PM} \cdot cos\left(\theta_r - \dfrac{4 \cdot \pi}{3} - (k-1)\cdot\sigma\right) \end{bmatrix} \qquad \textbf{(3.18)}$$

3.3   Vector space decomposition transformation

As it has been described in section 2.3.2, the VSD transformation consists of transforming the original multiphase machine into several, mutually orthogonal, two-phase machines. The transformation is given with:

$$\left[X_{\alpha\beta x1y1..z}\right] = [C_{VSD}] \cdot [X_{abc...k}] \qquad \textbf{(3.19)}$$

In general, there is a slight difference in the matrix structure depending on whether the number of phases is odd or even, but it can be constructed in a similar way.

3.3.1   Symmetrical machines

For symmetrical multiphase machines, the transformation matrix is straightforward to obtain once the number of phases has been defined. The construction method basically consists of the following steps leading to the transformation matrices shown in (Rockhill and Lipo, 2009) and in (Levi et al., 2007):

i)   Draw the polygon with the same number of sides as the number of phases with the reference phase (numbered 1) placed in the horizontal line to the right. Each vertex will correspond to each of the consecutive phases of the machine in a counter clockwise sense (Fig. 3.2).

ii) Assign to each vertex the trigonometric factors of its projections to the horizontal and the vertical axes that define the centre point of the polygon. The factors of the projections onto the horizontal axis will constitute the first row of the transformation matrix while the projections onto the vertical axis will form the second row.

iii) The following $(n$-$4)/2$ (or $(n$-$3)/2$ for n = odd) set of rows are the result of copying the first set of rows and substituting the phase shift angle (σ) by 2σ for the second set of rows, 3σ for the third set and so on…

iv) The last set of rows represents the zero-sequence component(s).
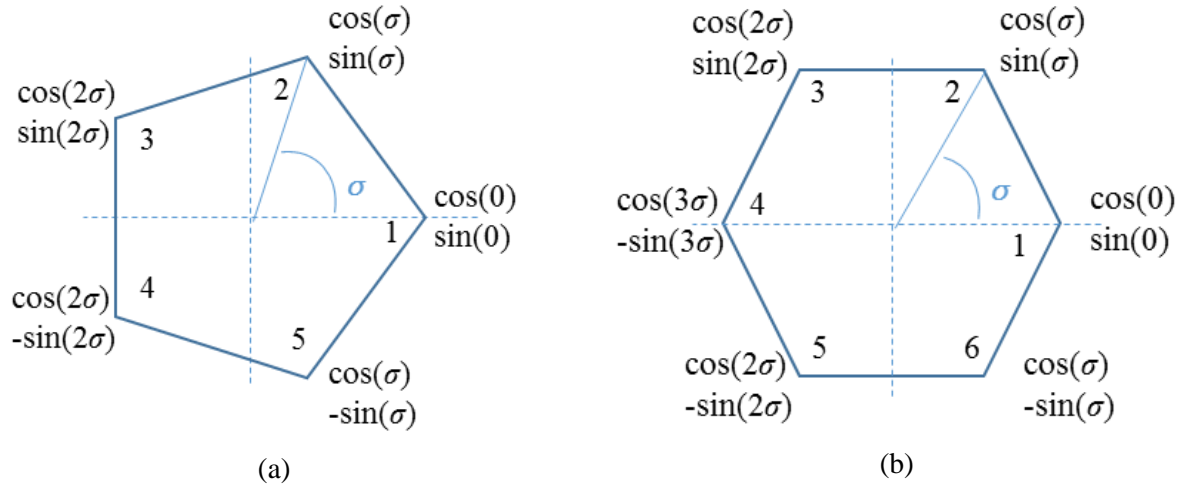
Fig. 3.2 Transformation matrix construction for a five-phase (a) and a six-phase (b) machine.

Applying the above described method to a symmetrical six-phase machine, the transformation matrix, considering the constant amplitude transformation, is obtained as shown in (3.20), where each row represents one of the following axes:

i)   The row 1 in (3.20) represents the α axis
ii) The row 2 in (3.20) represents the β axis
iii) The row 3 in (3.20) represents the x axis
iv) The row 4 in (3.20) represents the y axis
v)   The row 5 and 6 in (3.20) represents the $z1$ and $z2$ axes respectively

$$C_{VSD\_symm} = k_6 \cdot \begin{bmatrix} 1 & 1/2 & -1/2 & -1 & -1/2 & 1/2 \\ 0 & \sqrt{3}/2 & \sqrt{3}/2 & 0 & -\sqrt{3}/2 & -\sqrt{3}/2 \\ 1 & -1/2 & -1/2 & 1 & -1/2 & -1/2 \\ 0 & \sqrt{3}/2 & -\sqrt{3}/2 & 0 & \sqrt{3}/2 & -\sqrt{3}/2 \\ c_6 & -c_6 & c_6 & -c_6 & c_6 & -c_6 \\ c_6 & c_6 & c_6 & c_6 & c_6 & c_6 \end{bmatrix} \qquad (3.20)$$

where k_6 is the constant that determines the relationship between the power in the original and the transformed models and c_6 determines the amplitude of the zero sequence components in the transformed model.

3.3.2   Asymmetrical machines

In the case of asymmetrical machines, the procedure to construct the transformation matrix involves additional steps to the previously defined in section 3.3.1. An asymmetrical machine can be considered as the so-called semi-2n-phase machine (Tessarolo, 2009) and its transformation matrix can be obtained from that of a symmetrical 2n-phase machine by eliminating the columns representing the variables in the negative windings and the rows that become zeroed (Abbas et al., 1984).
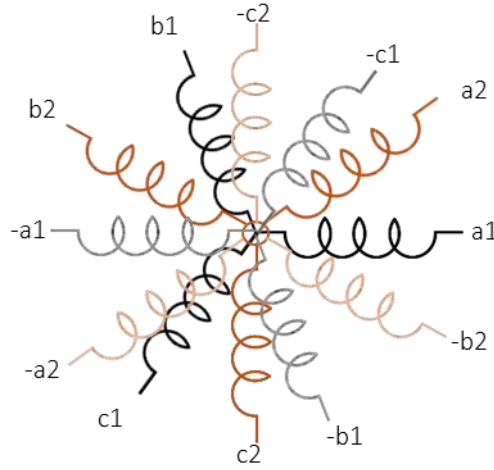
Fig. 3.3 Asymmetrical six-phase machine (solid lines) and the additional phases of the equivalent symmetrical twelve-phase machine (faded lines).

Following the above mentioned procedure of row and columns elimination (axes to be eliminated are shown in Fig. 3.3 with dashed lines), the transformation matrix for a six-phase asymmetrical machine is obtained as (the phase variables are again arranged as $a1$, $b1$, $c1$, $a2$, $b2$, $c2$):

$$
C_{VSD\_asymm} = k_6
\cdot
\begin{bmatrix}
1 & cos(2 \cdot \pi/3) & cos(4 \cdot \pi/3) & cos(\sigma) & cos(\sigma + 2 \cdot \pi/3) & cos(\sigma + 4 \cdot \pi/3) \\
0 & sin(2 \cdot \pi/3) & sin(4 \cdot \pi/3) & sin(\sigma) & sin(\sigma + 2 \cdot \pi/3) & sin(\sigma + 4 \cdot \pi/3) \\
1 & cos(10 \cdot \pi/3) & cos(20 \cdot \pi/3) & cos(5 \cdot \sigma) & cos(5 \cdot (\sigma + 2 \cdot \pi/3)) & cos(5 \cdot (\sigma + 4 \cdot \pi/3)) \\
0 & sin(10 \cdot \pi/3) & sin(20 \cdot \pi/3) & sin(5 \cdot \sigma) & sin(5 \cdot (\sigma + 2 \cdot \pi/3)) & sin(5 \cdot (\sigma + 4 \cdot \pi/3)) \\
c_6 & c_6 \cdot cos(6 \cdot \pi/3) & c_6 \cdot cos(12 \cdot \pi/3) & c_6 \cdot cos(3 \cdot \sigma) & c_6 \cdot cos(3 \cdot (\sigma + 2 \cdot \pi/3)) & c_6 \cdot cos(3 \cdot (\sigma + 4 \cdot \pi/3)) \\
0 & c_6 \cdot sin(6 \cdot \pi/3) & c_6 \cdot sin(12 \cdot \pi/3) & c_6 \cdot sin(3 \cdot \sigma) & c_6 \cdot sin(3 \cdot (\sigma + 2 \cdot \pi/3)) & c_6 \cdot sin(3 \cdot (\sigma + 4 \cdot \pi/3))
\end{bmatrix}
\tag{3.21}
$$

For the particular case of the shift angle being equal to 0º,

$$
C_{VSD_{asymm_{0}º}} = k_6 \cdot
\begin{bmatrix}
1 & -1/2 & -1/2 & 1 & -1/2 & -1/2 \\
0 & \sqrt{3}/2 & -\sqrt{3}/2 & 0 & \sqrt{3}/2 & -\sqrt{3}/2 \\
1 & -1/2 & -1/2 & 1 & -1/2 & -1/2 \\
0 & -\sqrt{3}/2 & \sqrt{3}/2 & 0 & -\sqrt{3}/2 & \sqrt{3}/2 \\
c_6 & c_6 & c_6 & 0 & 0 & 0 \\
0 & 0 & 0 & c_6 & c_6 & c_6
\end{bmatrix}
\tag{3.22}
$$

the matrix in (3.22) is obtained. In this matrix, it can be seen that the α-β (first two rows) and the x-y (third and fourth rows) subspaces are exactly the same with the only difference in the changed sign in the second and fourth row. This implies that they gather the same information so one pair of them can be considered as redundant.

For the case of 30º shift angle,

$$
C_{VSD_{asymm_{30}º}} = k_6 \cdot
\begin{bmatrix}
1 & -1/2 & -1/2 & \sqrt{3}/2 & -\sqrt{3}/2 & 0 \\
0 & \sqrt{3}/2 & -\sqrt{3}/2 & 1/2 & 1/2 & -1 \\
1 & -1/2 & -1/2 & -\sqrt{3}/2 & \sqrt{3}/2 & 0 \\
0 & -\sqrt{3}/2 & \sqrt{3}/2 & 1/2 & 1/2 & -1 \\
c_6 & c_6 & c_6 & 0 & 0 & 0 \\
0 & 0 & 0 & c_6 & c_6 & c_6
\end{bmatrix}
\tag{3.23}
$$

the matrix in (3.23) is obtained.

3.4 Multiple *dq* circuit transformation

The multiple *dq* transformation consists of applying the well-known three-phase machine transformations to each of the three-phase systems in the stator. The transformation is given with

$$\left[X_{\alpha1\beta101\ldots\alpha k\beta k0k}\right] = \left[C_{Mdq}\right] \cdot \left[X_{a1b1c1\ldots akbkck}\right] \tag{3.24}$$

In the following, whenever a transformation matrix for a multiple three-phase machine is described, the phase variables arrangement will be assumed as already stipulated, i.e.,

$$X_{a1b1c1a2b2c2} = \begin{bmatrix} a1 \\ b1 \\ c1 \\ a2 \\ b2 \\ c2 \end{bmatrix} \tag{3.25}$$

The transformation matrix for the case of a six-phase machine with an arbitrary shift angle (σ) between the three-phase systems can be written as follows,

$$C_{Ddq} = k_3 \cdot \begin{bmatrix} 1 & -1/2 & -1/2 & 0 & 0 & 0 \\ 0 & \sqrt{3}/2 & -\sqrt{3}/2 & 0 & 0 & 0 \\ c_3 & c_3 & c_3 & 0 & 0 & 0 \\ 0 & 0 & 0 & \cos(\sigma) & \cos(2\cdot\pi/3+\sigma) & \cos(4\cdot\pi/3+\sigma) \\ 0 & 0 & 0 & \sin(\sigma) & \sin(2\cdot\pi/3+\sigma) & \sin(4\cdot\pi/3+\sigma) \\ 0 & 0 & 0 & c_3 & c_3 & c_3 \end{bmatrix} \tag{3.26}$$

where k_3 is the constant that determines the relationship between the power in the original and the transformed models and c_3 determines the amplitude of the zero sequence components in the transformed model.

It can be seen how in each row, the non-zero coefficients affect only the phase variables of one of the three-phase systems, so that the transformation can be separated into two independent three-phase transformations. Corresponding rows have the following meaning:

i)   The row 1 in (3.26) represents the $\alpha1$ axis
ii) The row 2 in (3.26) represents the $\beta1$ axis
iii) The row 3 in (3.26) represents the 01 axis
iv) The row 4 in (3.26) represents the $\alpha2$ axis
v)   The row 5 in (3.26) represents the $\beta2$ axis
vi) The row 6 in (3.26) represents the 02 axis

Extending this transformation to a nine-phase machine gives the following matrix:

$$C_{Tdq} = k_3 \cdot \begin{bmatrix} 1 & -1/2 & -1/2 & 0 & 0 & 0 & 0 & 0 & 0 \\ 0 & \sqrt{3}/2 & -\sqrt{3}/2 & 0 & 0 & 0 & 0 & 0 & 0 \\ c_3 & c_3 & c_3 & 0 & 0 & 0 & 0 & 0 & 0 \\ 0 & 0 & 0 & \cos(\sigma) & \cos(2\cdot\pi/3+\sigma) & \cos(4\cdot\pi/3+\sigma) & 0 & 0 & 0 \\ 0 & 0 & 0 & \sin(\sigma) & \sin(2\cdot\pi/3+\sigma) & \sin(4\cdot\pi/3+\sigma) & 0 & 0 & 0 \\ 0 & 0 & 0 & c_3 & c_3 & c_3 & 0 & 0 & 0 \\ 0 & 0 & 0 & 0 & 0 & 0 & \cos(2\cdot\sigma) & \cos(2\cdot\pi/3+2\cdot\sigma) & \cos(4\cdot\pi/3+2\cdot\sigma) \\ 0 & 0 & 0 & 0 & 0 & 0 & \sin(2\cdot\sigma) & \sin(2\cdot\pi/3+2\cdot\sigma) & \sin(4\cdot\pi/3+2\cdot\sigma) \\ 0 & 0 & 0 & 0 & 0 & 0 & c_3 & c_3 & c_3 \end{bmatrix} \tag{3.27}$$

3.5 Other transformations

As it has been described in section 2.3.3, Figueroa proposed a general method to obtain the transformation matrix in the case of symmetrical machines leading to the following transformation matrix for the case of a symmetrical six-phase machine:

$$C_{Figueroa} = k_6 \cdot \begin{bmatrix} c_6 & c_6 & c_6 & c_6 & c_6 & c_6 \\ 1 & 1/2 & -1/2 & -1 & -1/2 & 1/2 \\ 1 & -1/2 & -1/2 & 1 & -1/2 & -1/2 \\ c_6 & -c_6 & c_6 & -c_6 & c_6 & -c_6 \\ 0 & -\sqrt{3}/2 & \sqrt{3}/2 & 0 & -\sqrt{3}/2 & \sqrt{3}/2 \\ 0 & \sqrt{3}/2 & \sqrt{3}/2 & 0 & -\sqrt{3}/2 & -\sqrt{3}/2 \end{bmatrix} \qquad \textbf{(3.28)}$$

By comparing the matrix in (3.28) with the one obtained in (3.20), the following relations can be observed, leading to the conclusion that both transformations are equivalent but with the sequences inverted in the *x-y* subspace:

i)   The row 1 in (3.28) coincides with the row 6 in (3.20)   -> axis $z2$

ii)   The row 2 in (3.28) coincides with the row 1 in (3.20)   -> axis α

iii) The row 3 in (3.28) coincides with the row 3 in (3.20)   -> axis x

iv) The row 4 in (3.28) coincides with the row 5 in (3.20)   -> axis $z1$

v)   The row 5 in (3.28) coincides with the row 4 in (3.20) with opposite sign -> axis $-y$

vi) The row 6 in (3.28) coincides with the row 2 in (3.20)   -> axis β

To generalize this approach to any kind of machine (symmetrical or asymmetrical), Tessarolo proposed the use of a geometrical transformation. The geometrical transformation refers the phases of the original six-phase machine (shown in Fig. 3.4a), to those of a conventionally arranged one (Fig. 3.4b).

(a)   (b)
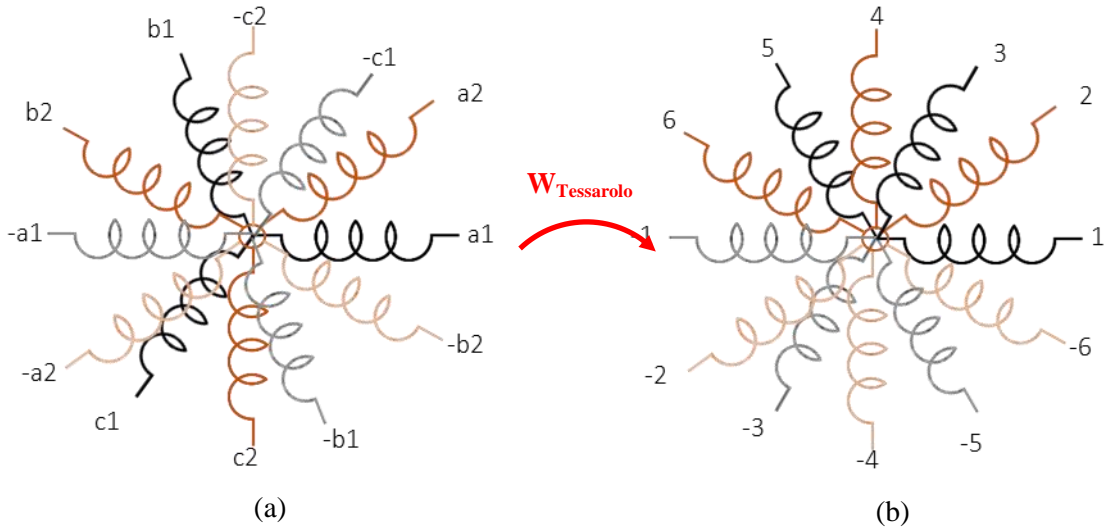
Fig. 3.4 Transformation of an asymmetrical six-phase machine arrangement (a) into a conventional six-phase arrangement (b) with a phase displacement of π/n.

When the phase variables are arranged as shown in (3.25), the geometrical transformation is a row permutation,

$$W_{Tessarolo} = \begin{bmatrix} 1 & 0 & 0 & 0 & 0 & 0 \\ 0 & 0 & 0 & 1 & 0 & 0 \\ 0 & 0 & -1 & 0 & 0 & 0 \\ 0 & 0 & 0 & 0 & 0 & -1 \\ 0 & 1 & 0 & 0 & 0 & 0 \\ 0 & 0 & 0 & 0 & 1 & 0 \end{bmatrix} \qquad \textbf{(3.29)}$$

Applying both matrices $W_{Tessarolo}$ and the matrix C for a symmetrical six-phase machine (3.20), the resultant transformation matrix for an asymmetrical six-phase machine is obtained as

$$C_{Tessarolo\_asymm} = k_6 \cdot \begin{bmatrix} 1 & -1/2 & -1/2 & \sqrt{3}/2 & -\sqrt{3}/2 & 0 \\ 0 & \sqrt{3}/2 & -\sqrt{3}/2 & 1/2 & 1/2 & -1 \\ c_6 & c_6 & c_6 & 0 & 0 & 0 \\ 0 & 0 & 0 & c_6 & c_6 & c_6 \\ 1 & -1/2 & -1/2 & -\sqrt{3}/2 & \sqrt{3}/2 & 0 \\ 0 & -\sqrt{3}/2 & \sqrt{3}/2 & 1/2 & 1/2 & -1 \end{bmatrix} \qquad \textbf{(3.30)}$$

Comparing the matrix in (3.30) with that in (3.22), it can be clearly seen that the differences are just due to row permutations.

3.6 Novel transformation

The basic idea behind a transformation is to obtain an inductance matrix with constant coefficients, and diagonal in form. This makes it easier to tune the regulators as constant inductance values are obtained and furthermore, if the matrix is diagonal, independent regulation in each axis is possible reducing the cross-couplings to only parasitic components such as leakage coupling (Hadiouche et al., 2000). Additionally, the transformation should not incur any loss of information of the system that would not permit to reconstruct the original waveforms.

To those above mentioned requirements for a transformation, some others can be added as follows:

i) During balanced operation, the fundamental frequency projections in all the non-flux/torque producing subspaces should be zero. This condition facilitates the correction of unbalances that may appear in the operation.

ii) A physical interpretation for each non-flux/torque producing subspace should be provided to facilitate the control task.

As will be seen in section 3.7.3, no physical interpretation can be assigned to the x-y subspaces for machines with more than two three-phase systems with the available transformations. To overcome this limitation, a novel transformation is proposed especially focusing on facilitating the load sharing between all the three-phase systems in the machine. For this purpose, a main subspace will be defined which will gather information about the electromagnetic energy conversion within the entire machine (correspondent to the α-β subspace in VSD transformation). Additionally to this, $k-1$ auxiliary subspaces will also be defined gathering information about the relationship between each of the three-phase systems and the reference one. These will be referred to as auxiliary subspaces $1i$ with i varying from 2 to k. In general, the three-phase system number 1 will be taken as the reference. All the other three-phase systems will be compared with the reference so that all the information about the machine state in the auxiliary subspaces is gathered with regard to the three-phase system number 1. It can be easily deduced that the auxiliary subspaces will not be mutually orthogonal as they all share the information about the reference three-phase system but, as will be further demonstrated, this is not really a problem.

Following the above mentioned requirements, a transformation matrix can be constructed for a machine with k three-phase systems and n-phases as follows:

- Axis α: reflects the summation of the projections in α of all the three-phase systems
- Axis β: reflects the summation of the projections in β of all the three-phase systems
- Axis α_{12}: reflects the difference in the projections in α of the systems number 1 and 2
- Axis β_{12}: reflects the difference in the projections in β of the systems number 1 and 2

    …

- Axis α_{1k}: reflects the difference in the projections in α of the systems number 1 and k
- Axis β_{1k}: reflects the difference in the projections in β of the systems number 1 and k
- Axis z_{12}: reflects the difference in the projections in 0 of the systems number 1 and 2

    .

- Axis z_{1k}: reflects the difference in the projections in 0 of the systems number 1 and k
- Axis z_n: reflects the summation of the projections in 0 of all the three-phase systems.

Following the procedure described above, the general form of the transformation matrix is the following:

$$
\begin{bmatrix}
\alpha_1 & \alpha_2 & \alpha_3 & \alpha_4 & \alpha_5 & \alpha_6 & \alpha_7 & \alpha_8 & \alpha_9 & . & . & . & \alpha_{n-2} & \alpha_{n-1} & \alpha_n \\
\beta_1 & \beta_2 & \beta_3 & \beta_4 & \beta_5 & \beta_6 & \beta_7 & \beta_8 & \beta_9 & . & . & . & \beta_{n-2} & \beta_{n-1} & \beta_n \\
\alpha_1 & \alpha_2 & \alpha_3 & -\alpha_4 & -\alpha_5 & -\alpha_6 & 0 & 0 & 0 & . & . & . & 0 & 0 & 0 \\
\beta_1 & \beta_2 & \beta_3 & -\beta_4 & -\beta_5 & -\beta_6 & 0 & 0 & 0 & . & . & . & 0 & 0 & 0 \\
\alpha_1 & \alpha_2 & \alpha_3 & 0 & 0 & 0 & -\alpha_7 & -\alpha_8 & -\alpha_9 & 0 & . & . & 0 & 0 & 0 \\
\beta_1 & \beta_2 & \beta_3 & 0 & 0 & 0 & -\beta_7 & -\beta_8 & -\beta_9 & 0 & . & . & 0 & 0 & 0 \\
. & . & . & . & . & . & . & . & . & . & . & . & . & . & . \\
. & . & . & . & . & . & . & . & . & . & . & . & . & . & . \\
. & . & . & . & . & . & . & . & . & . & . & . & . & . & . \\
\alpha_1 & \alpha_2 & \alpha_3 & 0 & 0 & 0 & 0 & 0 & 0 & . & . & . & -\alpha_{n-2} & -\alpha_{n-1} & -\alpha_n \\
\beta_1 & \beta_2 & \beta_3 & 0 & 0 & 0 & 0 & 0 & 0 & . & . & . & -\beta_{n-2} & -\beta_{n-1} & -\beta_n \\
c & c & c & -c & -c & -c & 0 & 0 & 0 & . & . & . & 0 & 0 & 0 \\
c & c & c & 0 & 0 & 0 & -c & -c & -c & 0 & . & . & 0 & 0 & 0 \\
. & . & . & . & . & . & . & . & . & . & . & . & . & . & . \\
c & c & c & 0 & 0 & 0 & 0 & 0 & 0 & . & . & . & -c & -c & -c \\
c & c & c & c & c & c & c & c & c & . & . & . & c & c & c
\end{bmatrix}
\tag{3.31}
$$

where α_1, α_2,… α_n and β_1, β_2,… β_n are the coefficients of the first and second rows of the VSD transformation respectively, and c determines the amplitude of the zero sequence components in the transformed model. With a transformation matrix such as the one shown in (3.31), not only a clear interpretation of the auxiliary subspaces is provided, but also a zero projection in all auxiliary subspaces under balanced conditions is achieved.

3.6.1   Application to a six-phase machine

With the procedure described above, the following transformation matrix can be constructed for a six-phase machine with an arbitrary phase shift σ,

$$
C = k_6 \cdot
\begin{bmatrix}
1 & cos(2\cdot\pi/3) & cos(4\cdot\pi/3) & cos(\sigma) & cos(2\cdot\pi/3+\sigma) & cos(4\cdot\pi/3+\sigma) \\
0 & sin(2\cdot\pi/3) & sin(4\cdot\pi/3) & sin(\sigma) & sin(2\cdot\pi/3+\sigma) & sin(4\cdot\pi/3+\sigma) \\
1 & cos(2\cdot\pi/3) & cos(4\cdot\pi/3) & -cos(\sigma) & -cos(2\cdot\pi/3+\sigma) & -cos(4\cdot\pi/3+\sigma) \\
0 & sin(2\cdot\pi/3) & sin(4\cdot\pi/3) & -sin(\sigma) & -sin(2\cdot\pi/3+\sigma) & -sin(4\cdot\pi/3+\sigma) \\
c & c & c & -c & -c & -c \\
c & c & c & c & c & c
\end{bmatrix}
\tag{3.32}
$$

where k_6 is the constant that determines the relationship between the power in the original and the transformed models and c determines the amplitude of the zero sequence components in the transformed model.

In what follows the following notation is used: variables obtained after application of the transformation (3.32) are denoted as α, β for the main subspace and α_{12} and β_{12} for the auxiliary, while variables after subsequent rotational transformation are labelled as d, q, d_{12} and q_{12}. The other symbols used α_1, β_1, α_2, β_2, d_1, q_1, d_2, q_2, stand for the corresponding variables that are obtained after multiple dq transformation.

Translating the listed requirements into equations, and applying some maths to isolate the currents in each of the three-phase systems (those obtained after multiple dq transformation), the following relations are obtained:

$$i_{\alpha 1} = \frac{i_\alpha + i_{\alpha 12}}{2}$$

$$i_{\beta 1} = \frac{i_\beta - i_{\beta 12}}{2}$$

$$i_{\alpha 2} = \frac{i_\alpha - i_{\alpha 12}}{2} \tag{3.33}$$

$$i_{\beta 2} = \frac{i_\beta + i_{\beta 12}}{2}$$

Applying the transformation to the rotating reference frame to the equations in (3.33),

$$i_{dj} = i_{\alpha j} \cdot cos(\theta) + i_{\beta j} \cdot sin(\theta)$$
$$i_{qj} = -i_{\alpha j} \cdot sin(\theta) + i_{\beta j} \cdot cos(\theta) \tag{3.34}$$

where i_{dj} and i_{qj} are the projections of the currents of the jth three-phase system onto a synchronously rotating frame (herein after d-axis and q-axis currents), the following results:

$$i_{d1} = \frac{1}{2} \cdot (i_d + i_{d12})$$

$$i_{q1} = \frac{1}{2} \cdot (i_q + i_{q12})$$

$$i_{d2} = \frac{1}{2} \cdot (i_d - i_{d12}) \tag{3.35}$$

$$i_{q2} = \frac{1}{2} \cdot (i_q - i_{q12})$$

Defining certain current-sharing coefficients (k_d and k_q) that determine the fraction of the overall machine current (in d and q axes, respectively) that will be taken by each three-phase system,

$$i_{d1} = k_d \cdot i_d$$
$$i_{q1} = k_q \cdot i_q$$
$$i_{d2} = i_d - i_{d1} \tag{3.36}$$
$$i_{q2} = i_q - i_{q1}$$

and substituting them in the equations in (3.35), the values for the currents in the auxiliary subspace 12, to obtain the desired current sharing, can be calculated as

$$i_{d12} = (2 \cdot k_d - 1) \cdot i_d$$
$$i_{q12} = (2 \cdot k_q - 1) \cdot i_q \tag{3.37}$$

3.6.2   Application to a nine-phase machine

A similar procedure can be followed to construct the transformation matrix for a nine-phase asymmetrical machine as the one shown in Fig. 3.5. This machine is constituted by three three-phase windings spatially shifted by an angle σ one from the other, and the three neutral points are kept independent.
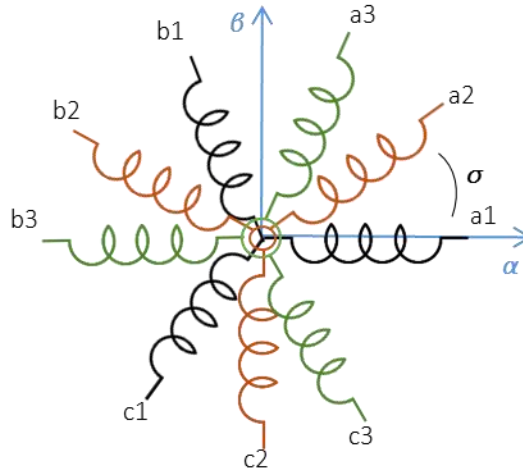
Fig. 3.5 Asymmetrical nine-phase machine: winding distribution.

In this case, the following transformation matrix can be constructed for a nine-phase machine,

$$
C = k_9 \cdot \begin{bmatrix}
1 & \cos(2\cdot\pi/3) & \cos(4\cdot\pi/3) & \cos(\sigma) & \cos(2\cdot\pi/3+\sigma) & \cos(4\cdot\pi/3+\sigma) & \cos(2\cdot\sigma) & \cos(2\cdot\pi/3+2\cdot\sigma) & \cos(4\cdot\pi/3+2\cdot\sigma) \\
0 & \sin(2\cdot\pi/3) & \sin(4\cdot\pi/3) & \sin(\sigma) & \sin(2\cdot\pi/3+\sigma) & \sin(4\cdot\pi/3+\sigma) & \sin(2\cdot\sigma) & \sin(2\cdot\pi/3+2\cdot\sigma) & \sin(4\cdot\pi/3+2\cdot\sigma) \\
1 & \cos(2\cdot\pi/3) & \cos(4\cdot\pi/3) & -\cos(\sigma) & -\cos(2\cdot\pi/3+\sigma) & -\cos(4\cdot\pi/3+\sigma) & 0 & 0 & 0 \\
0 & \sin(2\cdot\pi/3) & \sin(4\cdot\pi/3) & -\sin(\sigma) & -\sin(2\cdot\pi/3+\sigma) & -\sin(4\cdot\pi/3+\sigma) & 0 & 0 & 0 \\
1 & \cos(2\cdot\pi/3) & \cos(4\cdot\pi/3) & 0 & 0 & 0 & -\cos(2\cdot\sigma) & -\cos(2\cdot\pi/3+2\cdot\sigma) & -\cos(4\cdot\pi/3+2\cdot\sigma) \\
0 & \sin(2\cdot\pi/3) & \sin(4\cdot\pi/3) & 0 & 0 & 0 & -\sin(2\cdot\sigma) & -\sin(2\cdot\pi/3+2\cdot\sigma) & -\sin(4\cdot\pi/3+2\cdot\sigma) \\
c & c & c & -c & -c & -c & 0 & 0 & 0 \\
c & c & c & 0 & 0 & 0 & -c & -c & -c \\
c & c & c & c & c & c & c & c & c
\end{bmatrix}
\qquad \textbf{(3.38)}
$$

It can be demonstrated that a transformation matrix like the one shown in (3.38) provides constant inductance coefficients and diagonal inductance matrix (after applying Park's rotational transformation to the α-β subspace) so the condition to facilitate the tuning of the controllers is satisfied. Additionally, during balanced operation, the fundamental frequency components in all the auxiliary subspaces are zeroed. This, in conjunction with the clear physical meaning of each auxiliary subspace, facilitates the identification and correction of the unbalances that may appear during operation.

In what follows, the following notation is used: variables obtained after application of the transformation (3.38) are denoted as α, β for the main subspace and α_{12}, β_{12}, α_{13}, β_{13} for the auxiliary subspaces, while variables after subsequent rotational transformation are labelled as d, q, d_{12}, q_{12}, d_{13} and q_{13}. The other symbols used $\alpha_1, \beta_1, \alpha_2, \beta_2, \alpha_3, \beta_3, d_1, q_1, d_2, q_2$, and d_3, q_3 stand for the corresponding variables that are obtained after multiple dq transformation.

Translating the requirements into equations, and applying some maths to isolate the currents in each of the three-phase systems (those obtained after multiple dq transformation), the relationships

$$
i_{\alpha 1} = \frac{i_\alpha - i_{\alpha 12} - i_{\alpha 13}}{3}
$$

$$
i_{\beta 1} = \frac{i_\beta - i_{\beta 12} - i_{\beta 13}}{3}
$$

$$
i_{\alpha 2} = \frac{i_\alpha - 2\cdot i_{\alpha 12} + i_{\alpha 13}}{3}
$$

$$
i_{\beta 2} = \frac{i_\beta - 2\cdot i_{\beta 12} + i_{\beta 13}}{3}
\qquad \textbf{(3.39)}
$$

$$
i_{\alpha 3} = \frac{i_\alpha + i_{\alpha 12} - 2\cdot i_{\alpha 13}}{3}
$$

$$
i_{\beta 3} = \frac{i_\beta + i_{\beta 12} - 2\cdot i_{\beta 13}}{3}
$$

are obtained. Applying the transformation to the rotating reference frame (3.34) to the equations in (3.39), results in

$$i_{d1} = \frac{1}{3} \cdot (i_d - i_{d12} - i_{d13})$$

$$i_{q1} = \frac{1}{3} \cdot (i_q - i_{q12} - i_{q13})$$

$$i_{d2} = \frac{1}{3} \cdot (i_d - 2 \cdot i_{d12} + i_{d13})$$

$$i_{q2} = \frac{1}{3} \cdot (i_q - 2 \cdot i_{q12} + i_{q13})$$
$$\tag{3.40}$$

$$i_{d3} = \frac{1}{3} \cdot (i_d + i_{d12} - 2 \cdot i_{d13})$$

$$i_{q3} = \frac{1}{3} \cdot (i_q + i_{q12} - 2 \cdot i_{q13})$$

Defining the current-sharing coefficients similarly as in 3.6.1,

$$i_{d1} = k_{d1} \cdot i_d$$

$$i_{q1} = k_{q1} \cdot i_q$$

$$i_{d2} = k_{d2} \cdot i_d$$

$$i_{q2} = k_{q2} \cdot i_q \tag{3.41}$$

$$i_{d3} = i_d - i_{d1} - i_{d2}$$

$$i_{q3} = i_q - i_{q1} - i_{q2}$$

and substituting them in the equations in (3.40), the values for the currents in the auxiliary subspaces can be calculated to obtain the desired current sharing:

$$i_{d12} = (k_{d1} - k_{d2}) \cdot i_d$$

$$i_{q12} = (k_{q1} - k_{q2}) \cdot i_q$$
$$\tag{3.42}$$

$$i_{d13} = (2 \cdot k_{d1} + k_{d2} - 1) \cdot i_d$$

$$i_{q13} = (2 \cdot k_{q1} + k_{q2} - 1) \cdot i_q$$

It has to be noted that in a machine with k three-phase systems, when controlling the main subspace (α-β), only k-1 of the three-phase systems can be controlled independently, so only $2 \cdot (k$-1) current sharing coefficients will be needed. Obtaining these current values for machines with higher number of phases is rather straightforward and is shown in Appendix 2 for twelve- and fifteen-phase machines.

3.7   Correlation between different transformations

Along this chapter, a thorough analysis of the different transformations will be performed, focusing on three main aspects which are:
  i)   the physical interpretation of the subspaces,
  ii) how the different operational asymmetries are represented and
  iii) how the different time-harmonics are mapped.
        To obtain the physical interpretation of the different subspaces, the different transformations will be compared to that of a three-phase machine applied to each of the k three-phase systems. With this, a correlation between the projections on the different subspaces and those from the three-phase transformation will be sought.

The different asymmetries that may appear during operation of a multiphase machine will be defined and applied to each of the transformations to see how these affect the projections in the different subspaces.

For the analysis of harmonic mapping, an *n*-phase voltage source supply will be formulated to include the typical low-, medium- and high-order harmonics (up to the third side-band around the switching frequency) usually present in a power converter with sinusoidal PWM and dead time. For the sake of simplicity, a switching frequency of 1 kHz has been set, fundamental frequency is fixed at 50 Hz, and all the harmonics will have amplitude equal to 1 p.u. (Fig. 3.6).
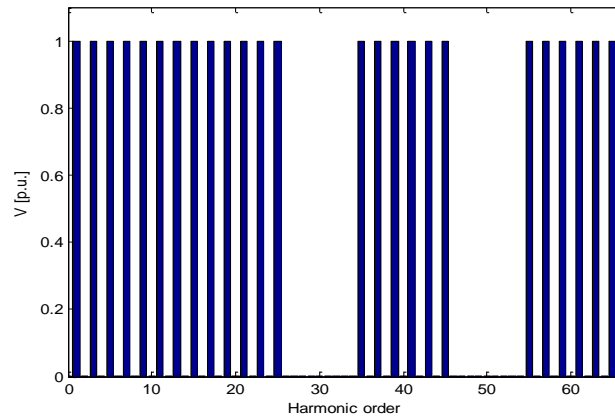
Fig. 3.6 Harmonic spectrum of the voltage source.

To study the asymmetries and the harmonic mapping, a Simulink model has been created as shown in Fig. 3.7. It receives the desired input voltages from a Matlab's script and executes the desired transformation from a code written in C. The transformation's code requires the voltages and the fundamental frequency (to perform the *d-q* transformation) and outputs the transformed voltages and also the voltages with the transformation and inverse transformation applied (to verify that the transformation and inverse transformation have been correctly coded). Within the Matlab's script, the waveform of the voltage of each of the phases can be generated with any harmonic content and with any kind of asymmetry.

The results shown in these sections are covered in (Zabaleta et al., 2016a) for the case of six-phase machines and in (Zabaleta et al., 2016b) for the nine-phase case.
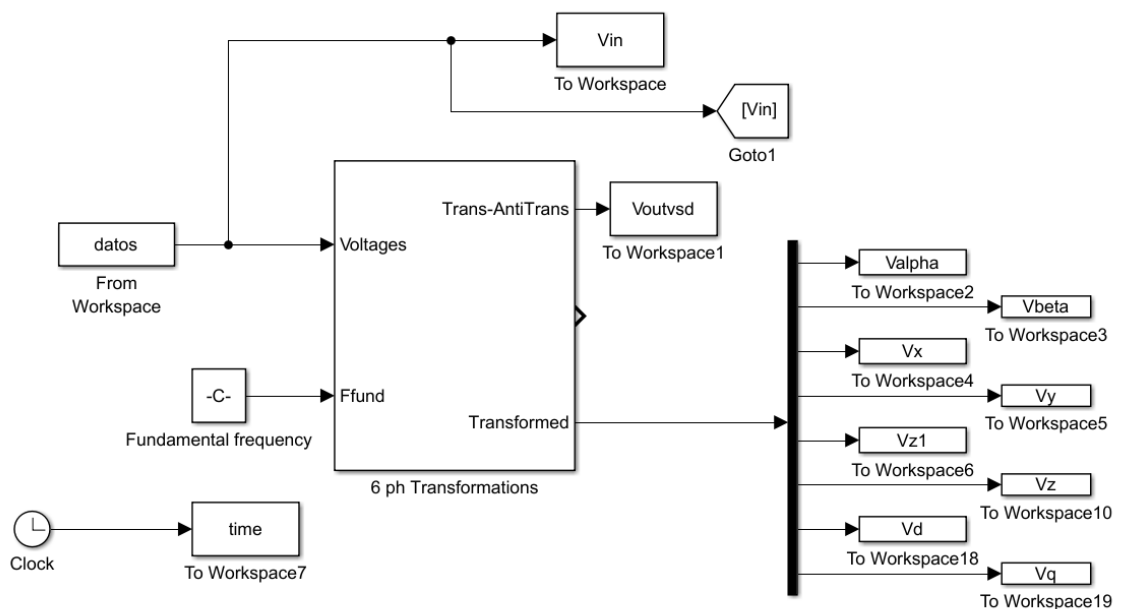
Fig. 3.7 Simulink model to analyse asymmetries and harmonic mapping in a six-phase machine.

3.7.1   Six-phase machine with double *d-q* transformation

In six-phase machines, three different phase shifting angles can be typically found; these are 0, 30 and 60º as seen in Fig. 3.8.

(a)

(b)

(c)
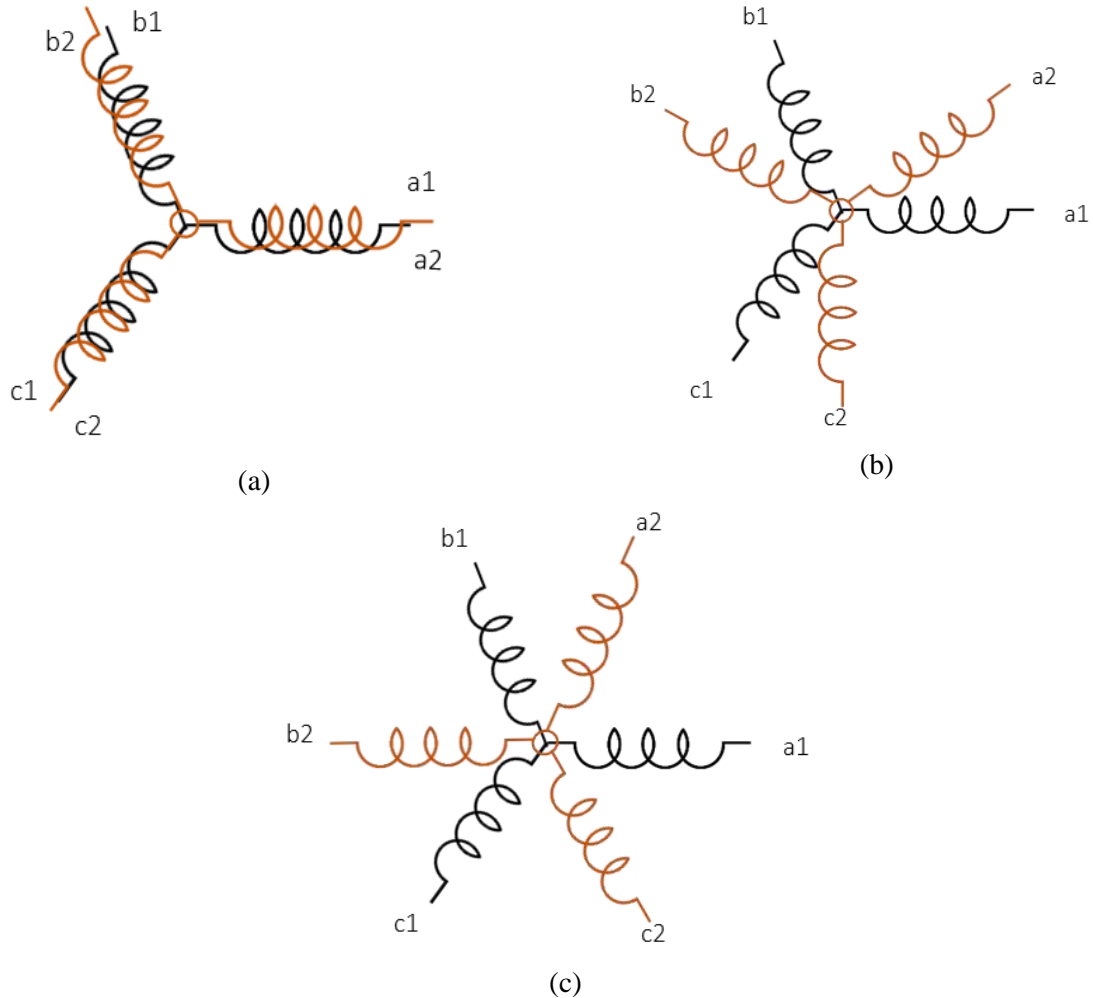
Fig. 3.8 Winding layouts for a six-phase machine: (a) 0º shift, (b) 30º shift and (c) 60º shift.

As can be seen in Fig. 3.8 (c), the configuration with 60º shift can be arranged in a similar manner as the 0º shift by just reversing the polarity of the second three-phase system phases (a2, b2 and c2). With this change, the phase a2 coincides with the phase b1, the phase b2 with the c1 and the phase c2 with a1; hence, similar results are to be expected with both configurations. Thus, only six-phase machines with 0º and 30º shift will be studied.

As noted already, an asymmetrical six-phase machine consists of two three-phase systems, spatially shifted by 30º, wound around a single stator core (see Fig. 3.8 (b)). The spatial shift between the three-phase systems introduces the corresponding time-shift in the waveforms of the induced voltages as can be seen in Fig. 3.9.
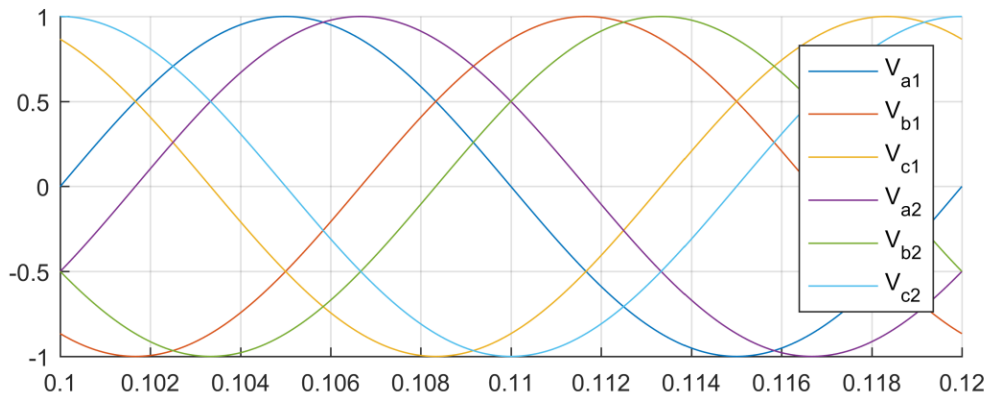
Fig. 3.9 Voltage waveforms of a six-phase machine with 30º shift.

3.7.1.1   Physical interpretation of the subspaces

Obtaining the physical interpretation of the *x-y* subspace is of vital importance as these subspaces should be taken into account in the regulation strategy to optimally control the machine. This is of special concern in machines with sinusoidal MMF as high low-order harmonic currents may flow along the stator windings if no care is taken regarding the *x-y* subspaces (see 2.3.1). Additionally, the *x-y* subspaces also gather the information about the current sharing between the different three-phase systems (in multiple three-phase systems machines), so the physical interpretation is vital in applications where different current sharing is required.

Applying the double *d-q* transformation, an independent approach to each of the three-phase systems is implicitly assumed, yielding results similar to those obtained considering two independent three-phase machines. The consequence of such approach is that it generates two parallel three-dimensional subspaces to which the information of each of the three-phase systems is mapped. As it was mentioned in 2.3.1, this approach cannot isolate the mutual interaction between the three-phase systems so it becomes very complicated to properly compensate for such coupling. This can be easily understood by means of Fig. 3.10. This represents how the double *d-q* approach treats the six-phase machine as two three-phase machines leaving the mutual interactions outside the approach.
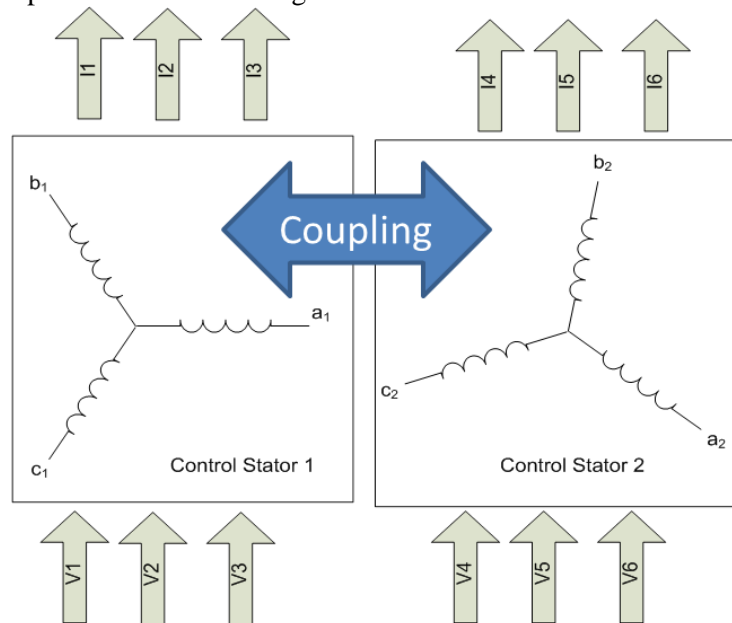
Fig. 3.10 Double d-q modelling approach.

3.7.1.2   Representation of asymmetries

Voltage supply is assumed to contain only the fundamental component. In general, three asymmetries can be found when operating an asymmetrical multiphase machine,

i)   CASE 1: Both three-phase systems are balanced but with different amplitudes (number 1 at 1 p.u. and number 2 at 0.9 p.u.)

ii)   CASE 2: Both three-phase systems are equally unbalanced (the phases c_i at 0.9 and the rest at 1 p.u.)

iii)   CASE 3: Three-phase system number 1 is balanced and the other unbalanced (two phases at 0.9 p.u.)

With this approach, as each of the three-phase systems are considered as independent, each of the subspaces will only reflect the asymmetries affecting its related three-phase system. As it can be seen in Fig. 3.11, each subspace reflects only the asymmetries affecting its related three-phase system, thus ignoring what happens in the other one.

(a)　　　　　　　　　　　(b)

(c)
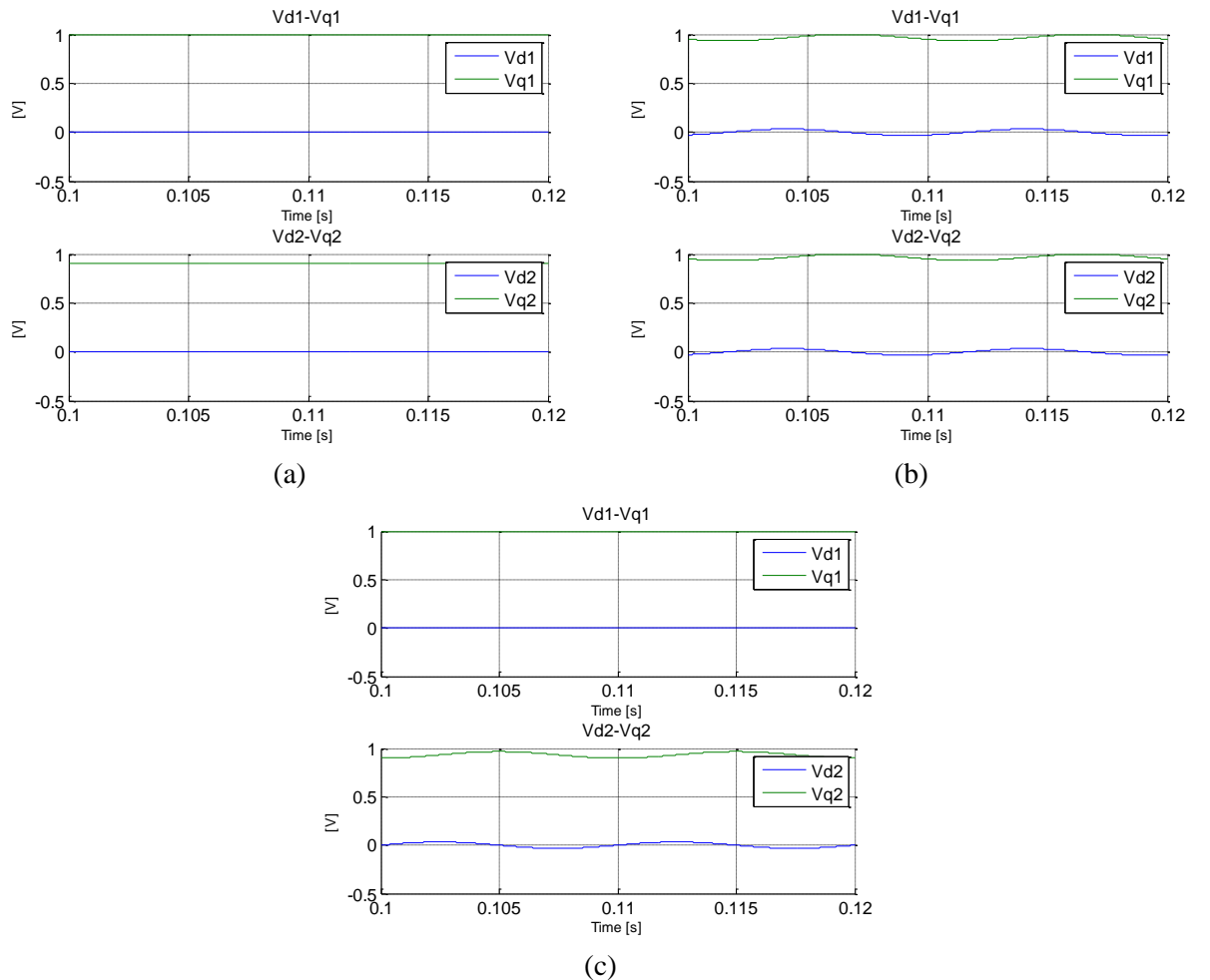
Fig. 3.11 Projections on d1-q1 (upper) and d2-q2 (lower) subspaces (double d-q transformation) for different asymmetries: (a) CASE 1, (b) CASE 2 and (c) for CASE 3.

3.7.1.3   Harmonic mapping

As it has been mentioned in 3.7, a voltage source including certain harmonics will be used to demonstrate the mapping of each harmonic. In the upper part of Fig. 3.12, the Fast Fourier Transformation (FFT) has been applied to the voltage from the source. The following figures are the FFT of the projections on the $\alpha1$-$\beta1$, $\alpha2$-$\beta2$ and $z1$-$z2$ subspaces, respectively.

In Fig. 3.12, it can be seen that the spectrum in the two subspaces $\alpha1$-$\beta1$, $\alpha2$-$\beta2$ (i.e. $d1$-$q1$ and $d2$-$q2$) is the same from the point of view of harmonic mapping, certifying the fact that the two are parallel.
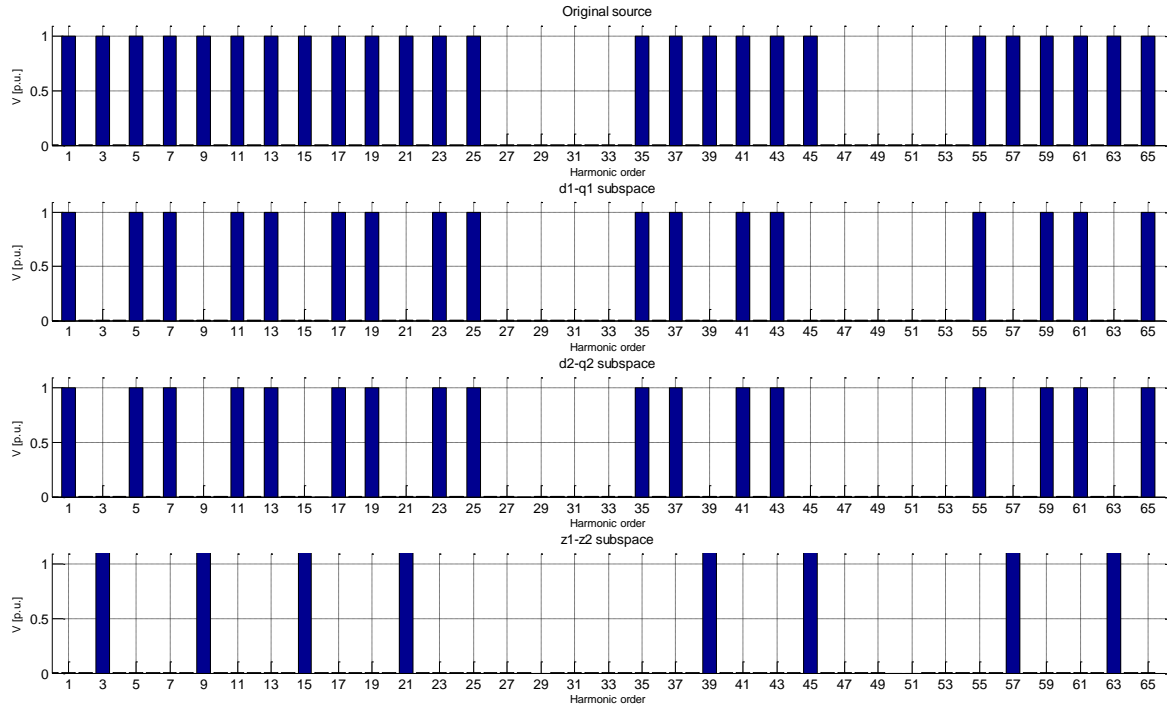
Fig. 3.12 Harmonic mapping using double d-q transformation.

3.7.2   Six-phase machine with VSD

It can be easily demonstrated that, in the case of a six-phase machine with 30º shift, the transformation matrices of both the VSD and the novel approach are almost exactly equal. This can be easily seen when comparing matrices in equations (3.23) and (3.32). The only difference comes from the sign of the $y1$ axis coefficients regarding the second three-phase system. This reverses the sequence of the projections in the $x1$-$y1$ subspace, but does not alter the physical meaning and harmonic mapping. Knowing this, all the conclusions obtained from the analysis within this section are fully applicable to the novel transformation.

Along this chapter, the VSD transformation described in (Levi et al., 2007) and defined in (3.22) will be considered to transform the input voltages.

3.7.2.1   Physical interpretation of the subspaces

A meaningful interpretation can be easily obtained by simply comparing the matrices in (3.23) and in (3.26). From equation (3.23), the relations between the original and the transformed variables can be obtained for the case of the VSD transformation and a 30º shift,

$$i_\alpha = k_6 \cdot \left(i_{a1} - 0.5 \cdot (i_{b1} + i_{c1}) + 0.866 \cdot (i_{a2} - i_{b2})\right)$$

$$i_\beta = k_6 \cdot (0.866 \cdot (i_{b1} - i_{c1}) + 0.5 \cdot (i_{a2} + i_{b2}) - i_{c2})$$

$$i_x = k_6 \cdot \left(i_{a1} - 0.5 \cdot (i_{b1} + i_{c1}) - 0.866 \cdot (i_{a2} - i_{b2})\right)$$

$$i_y = k_6 \cdot (-0.866 \cdot (i_{b1} - i_{c1}) + 0.5 \cdot (i_{a2} + i_{b2}) - i_{c2})$$

$$i_{z1} = k_6 \cdot c_6 \cdot (i_{a1} + i_{b1} + i_{c1} + i_{a2} + i_{b2} + i_{c2})$$

$$i_{z2} = k_6 \cdot c_6 \cdot \left(i_{a1} + i_{b1} + i_{c1} - (i_{a2} + i_{b2} + i_{c2})\right)$$

(3.43)

Doing the same with (3.26),

$$i_{\alpha 1} = k_3 \cdot \left(i_{a1} - 0.5 \cdot (i_{b1} + i_{c1})\right)$$

$$i_{\beta 1} = k_3 \cdot \left(0.866 \cdot (i_{b1} - i_{c1})\right)$$

$$i_{01} = k_3 \cdot (i_{a1} + i_{b1} + i_{c1})$$

$$i_{\alpha 2} = k_3 \cdot \left(0.866 \cdot (i_{a2} - i_{b2})\right)$$

$$i_{\beta 2} = k_3 \cdot (0.5 \cdot (i_{a2} + i_{b2}) - i_{c2})$$

$$i_{02} = k_3 \cdot (i_{a2} + i_{b2} + i_{c2})$$

(3.44)

The relation for the case of double *d-q* transformation is obtained. Now, combining equations (3.43) and (3.44),

$$i_\alpha = \frac{k_6}{k_3} \cdot (i_{\alpha 1} + i_{\alpha 2})$$

$$i_\beta = \frac{k_6}{k_3} \cdot (i_{\beta 1} + i_{\beta 2})$$

$$i_x = \frac{k_6}{k_3} \cdot (i_{\alpha 1} - i_{\alpha 2})$$

$$i_y = \frac{k_6}{k_3} \cdot (-i_{\beta 1} + i_{\beta 2})$$

$$i_{z1} = \frac{k_6 \cdot c_6}{k_3 \cdot c_3} \cdot (i_{01} + i_{02})$$

$$i_{z2} = \frac{k_6 \cdot c_6}{k_3 \cdot c_3} \cdot (i_{01} - i_{02})$$

(3.45)

the equalities shown in (3.45) are obtained leading to the following conclusions:

i) The α axis in VSD is proportional to the summation of $\alpha 1$ and $\alpha 2$

ii) The β axis in VSD is proportional to the summation of $\beta 1$ and $\beta 2$

iii) The x axis in VSD is proportional to the difference of $\alpha 1$ and $\alpha 2$

iv) The y axis in VSD is proportional to the difference of $\beta 2$ and $\beta 1$

v)   The $z1$ axis in VSD is proportional to the summation of 01 and 02

vi) The $z2$ axis in VSD is proportional to the difference of 01 and 02

3.7.2.2   Representation of asymmetries

The same asymmetries previously defined in 3.7.1.2 will be applied in this case. Each of these asymmetries will translate into the *x-y* subspace in a different manner as can be seen in Fig. 3.13. In Fig. 3.13a and b, the projections for the asymmetry defined in CASE 1 and 2 are shown where it can be seen that both axes have the same amplitude implying a circular trajectory along the *x-y* subspace. This means that there is only one sequence present in the projections; but, comparing both figures, it can be easily seen that they have opposite rotational directions when represented as space vectors, which agrees with the results in (Che et al., 2014a). On the contrary, in Fig. 3.13c, it can be seen how the projections have different amplitudes meaning that both sequences are present at the same time. It can also be seen in Fig. 3.13 that depending on the type of the asymmetry, the *α-β* (*d-q* for ease of analysis) subspace may be slightly altered, thus affecting the torque and flux waveforms.

(a)   (b)

(c)
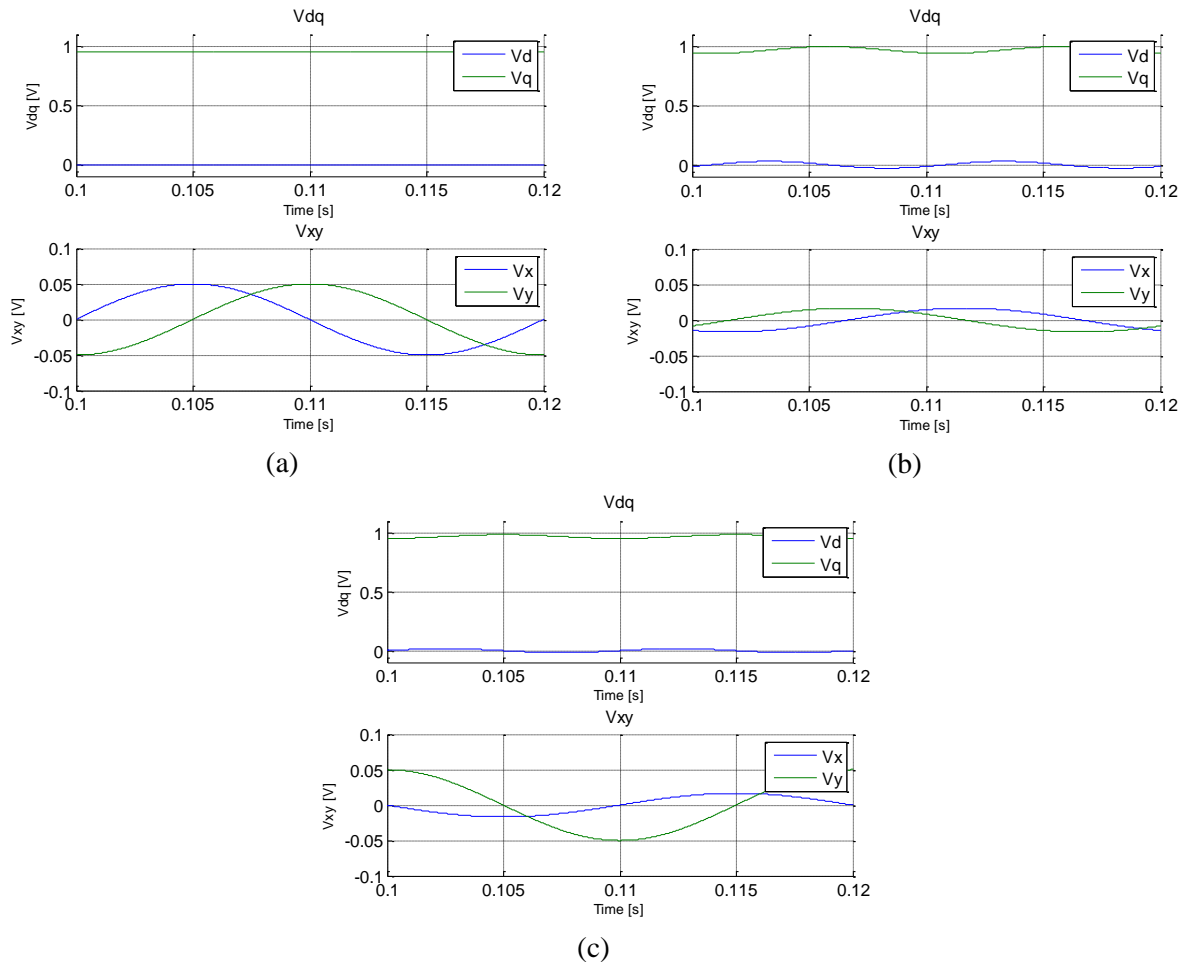
Fig. 3.13 Projections in d-q (upper) and x-y (lower) subspaces (VSD transformation) for different asymmetries: (a) CASE 1, (b) CASE 2 and (c) for CASE 3.

From these results, a conclusion for the next chapter can be obtained: it can be deduced that if different current sharing between the three-phase systems of the machine is required, some fundamental-frequency currents will need to be controlled in the *x-y* subspaces.

3.7.2.3   Harmonic mapping

As it has been mentioned in 3.7, a voltage source including certain harmonics will be used to demonstrate the mapping of each harmonic. In the top part of Fig. 3.14, the voltage of the source is given to which the Fast Fourier Transformation (FFT) has been applied. The subsequent plots are the FFT of the projections in the α-β, x-y and $z1$-$z2$ subspace, respectively.

In Fig. 3.14, it can be seen how the 5th and 7th harmonics are not mapped into the α-β subspace (meaning a lack of effect on the electromechanical energy conversion). On the contrary, they are mapped exclusively in the x-y subspace where the VSD approach establishes a path with only the stator resistance and leakage inductance as impedances (Zhao and Lipo, 1995). This can explain the circulation of high low-order harmonic currents reported in the literature review as the stator resistance and leakage inductance are usually kept as low as possible to increase machine's performance.

Depending on the actual phase shift between the two three-phase systems, the harmonics will be mapped into different subspaces. In the Table 3.1, the mapping of the odd-order harmonics up to the 65th is shown. The following general mapping rules would apply in the case of 30º shift:

i)   In the α-β subspace, odd harmonics with $i = 12 \cdot m \pm 1$ ($m = 1,2,3....$) are mapped.

ii) In the x-y subspace, odd harmonics with $i = 6 \cdot m \pm 1$ ($m = 1,3,5....$) are mapped.

iii) In the $z1$ and $z2$ axes, all the triplen harmonics are mapped.
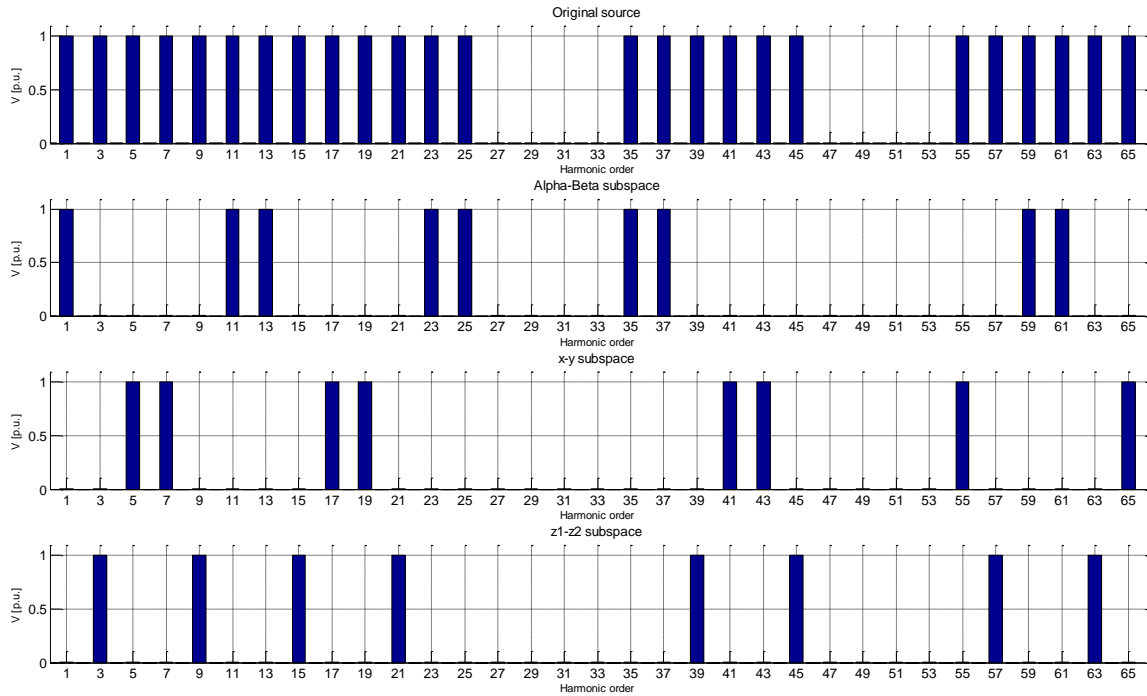
Fig. 3.14 Harmonic mapping using VSD transformation.

Table 3.1 Harmonic mapping for a 30º phase shift between three-phase systems using VSD transformation.

Subspace α-β	1,11,13,23,25,35,37,47,49,59,61
Subspace x-y	5,7,17,19,29,31,41,43,53,55,65
Axes $z1$-$z2$	3,9,15,21,27,33,39,45,51,57,63

From Table 3.1, it can be seen how each harmonic is mapped exclusively into only one subspace. This makes it very easy to control any harmonic as only its corresponding subspace should be focused on.

3.7.3   Nine-phase machine with VSD

A nine-phase asymmetrical machine has three three-phase systems wound on a single stator core, as shown in Fig. 3.5. Again, a spatial shift between the three-phase systems is usually provided leading to the corresponding time-shift in the voltages (shown in Fig. 3.15).
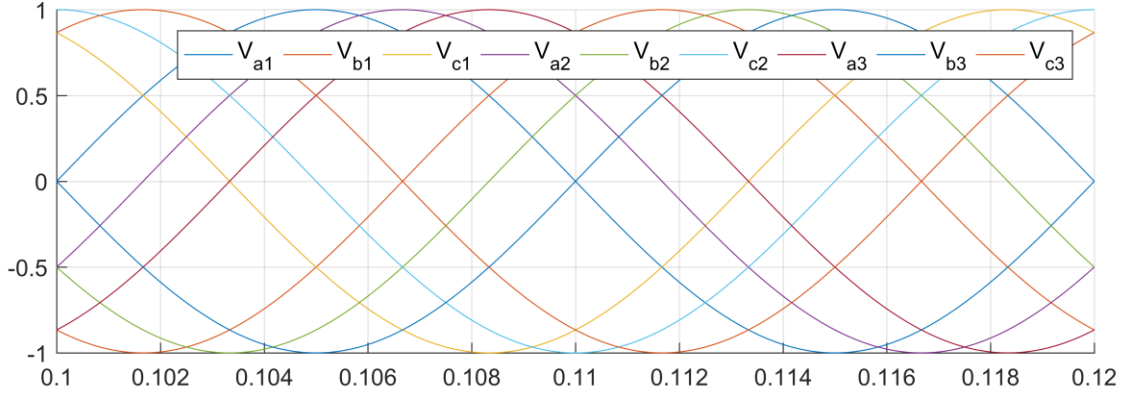
Fig. 3.15 Voltage waveforms of a nine-phase machine with 20º shift.

In this section, the VSD transformation described in (Levi, 2011a) will be considered to transform the input voltages.

3.7.3.1   Physical interpretation of the subspaces

In the case of a nine-phase machine with independent neutral points, two *x-y* subspaces and three zero sequence axes will appear. These will be referred to as $x1$-$y1$, $x2$-$y2$ and $z1$, $z2$ and $z3$ respectively.

Applying the transformation, the equations

$$i_\alpha = k_9 \cdot (i_{a1} - 0.5 \cdot (i_{b1} + i_{c1}) + 0.939 \cdot i_{a2} - 0.766 \cdot i_{b2} - 0.174 \cdot i_{c2} + 0.766 \cdot i_{a3} - 0.939 \cdot i_{b3} + 0.174 \cdot i_{c3})$$

$$i_\beta = k_9 \cdot (0.866 \cdot (i_{b1} - i_{c1}) + 0.342 \cdot i_{a2} + 0.643 \cdot i_{b2} - 0.985 \cdot i_{c2} + 0.643 \cdot i_{a3} + 0.342 \cdot i_{b3} - 0.985 \cdot i_{c3})$$

$$i_{x1} = k_9 \cdot (i_{a1} - 0.5 \cdot (i_{b1} + i_{c1}) - 0.174 \cdot i_{a2} + 0.939 \cdot i_{b2} - 0.766 \cdot i_{c2} - 0.939 \cdot i_{a3} + 0.174 \cdot i_{b3} + 0.766 \cdot i_{c3})$$

$$i_{y1} = k_9 \cdot (-0.866 \cdot (i_{b1} - i_{c1}) + 0.985 \cdot i_{a2} - 0.342 \cdot i_{b2} - 0.643 \cdot i_{c2} - 0.342 \cdot i_{a3} + 0.985 \cdot i_{b3} - 0.643 \cdot i_{c3})$$

$$i_{x2} = k_9 \cdot (i_{a1} - 0.5 \cdot (i_{b1} + i_{c1}) - 0.766 \cdot i_{a2} - 0.174 \cdot i_{b2} + 0.939 \cdot i_{c2} + 0.174 \cdot i_{a3} + 0.766 \cdot i_{b3} - 0.939 \cdot i_{c3})$$

$$i_{y2} = k_9 \cdot (0.866 \cdot (i_{b1} - i_{c1}) + 0.643 \cdot i_{a2} - 0.985 \cdot i_{b2} + 0.342 \cdot i_{c2} - 0.985 \cdot i_{a3} + 0.643 \cdot i_{b3} + 0.342 \cdot i_{c3})$$

$$i_{z1} = k_9 \cdot c_9 \cdot (i_{a1} + i_{b1} + i_{c1})$$

$$i_{z2} = k_9 \cdot c_9 \cdot (i_{a2} + i_{b2} + i_{c2})$$

$$i_{z3} = k_9 \cdot c_9 \cdot (i_{a3} + i_{b3} + i_{c3})$$

(3.46)

are obtained for the case of a machine with a phase displacement (σ) of 20 electrical degrees and three independent neutral points. Using the multiple *dq* approach,

$$i_{\alpha1} = k_3 \cdot \left(i_{a1} - 0.5 \cdot (i_{b1} + i_{c1}) \right)$$

$$i_{\beta1} = k_3 \cdot \left(0.866 \cdot (i_{b1} - i_{c1}) \right)$$

$$i_{01} = k_3 \cdot c_3 \cdot (i_{a1} + i_{b1} + i_{c1})$$

$$i_{\alpha2} = k_3 \cdot (0.939 \cdot i_{a2} - 0.766 \cdot i_{b2} - 0.174 \cdot i_{c2})$$

$$i_{\beta2} = k_3 \cdot (0.342 \cdot i_{a2} + 0.643 \cdot i_{b2} - 0.985 \cdot i_{c2})$$

$$i_{02} = k_3 \cdot c_3 \cdot (i_{a2} + i_{b2} + i_{c2})$$

(3.47)

$$i_{\alpha 3} = k_3 \cdot (0.766 \cdot i_{a3} - 0.939 \cdot i_{b3} + 0.174 \cdot i_{c3})$$

$$i_{\beta 3} = k_3 \cdot (0.643 \cdot i_{a3} + 0.342 \cdot i_{b3} - 0.985 \cdot i_{c3})$$

$$i_{03} = k_3 \cdot c_3 \cdot (i_{a3} + i_{b3} + i_{c3})$$

the equations in (3.47) are obtained. Combining equations (3.46) and (3.47), the equalities

$$i_\alpha = \frac{k_9}{k_3} \cdot (i_{\alpha 1} + i_{\alpha 2} + i_{\alpha 3})$$

$$i_\beta = \frac{k_9}{k_3} \cdot (i_{\beta 1} + i_{\beta 2} + i_{\beta 3})$$

$$i_{z1} = \frac{k_9 \cdot c_9}{k_3 \cdot c_3} \cdot (i_{01}) \tag{3.48}$$

$$i_{z2} = \frac{k_9 \cdot c_9}{k_3 \cdot c_3} \cdot (i_{02})$$

$$i_{z3} = \frac{k_9 \cdot c_9}{k_3 \cdot c_3} \cdot (i_{03})$$

are obtained, leading to the following conclusions:

i)   The α axis in VSD is proportional to the summation of $\alpha 1$, $\alpha 2$ and $\alpha 3$

ii) The β axis in VSD is proportional to the summation of $\beta 1$, $\beta 2$ and $\beta 3$

iii) The $z1$, $z2$ and $z3$ axes in VSD is proportional to 01, 02 and 03 respectively

No relationship between x-y subspaces and αi-βi can be obtained; so, it can be deduced that no physical meaning of the x-y subspaces can be arrived at when using the VSD transformation, agreeing with (Rockhill and Lipo, 2009).

3.7.3.2   Representation of asymmetries

As it has been demonstrated in 3.7.3.1, no clear physical meaning for all the x-y subspaces can be derived when using VSD transformation. Work in (Rockhill and Lipo, 2009) confirms this statement as it concludes that asymmetries produce projections in more than one xi-yi subspace, thus not providing clear information about them.

In this case, the considered asymmetries that can be found when operating an asymmetrical multiphase machine are defined as:

i)   CASE 1: The three three-phase systems are balanced but with different amplitudes (1 p.u. for the number 1 and 0.9 p.u. for the other two), Fig. 3.16(a).

ii) CASE 2: The three three-phase systems are equally unbalanced (the phases c_i at 0.9 and the rest at 1 p.u.), Fig. 3.16(b).

iii) CASE 3: One three-phase system is balanced and the other two unbalanced (three-phase system number 1 balanced at 1 p.u. and the other two with phases b_i and c_i at 0.9 p.u.), Fig. 3.16(c).

(a)   (b)

(c)
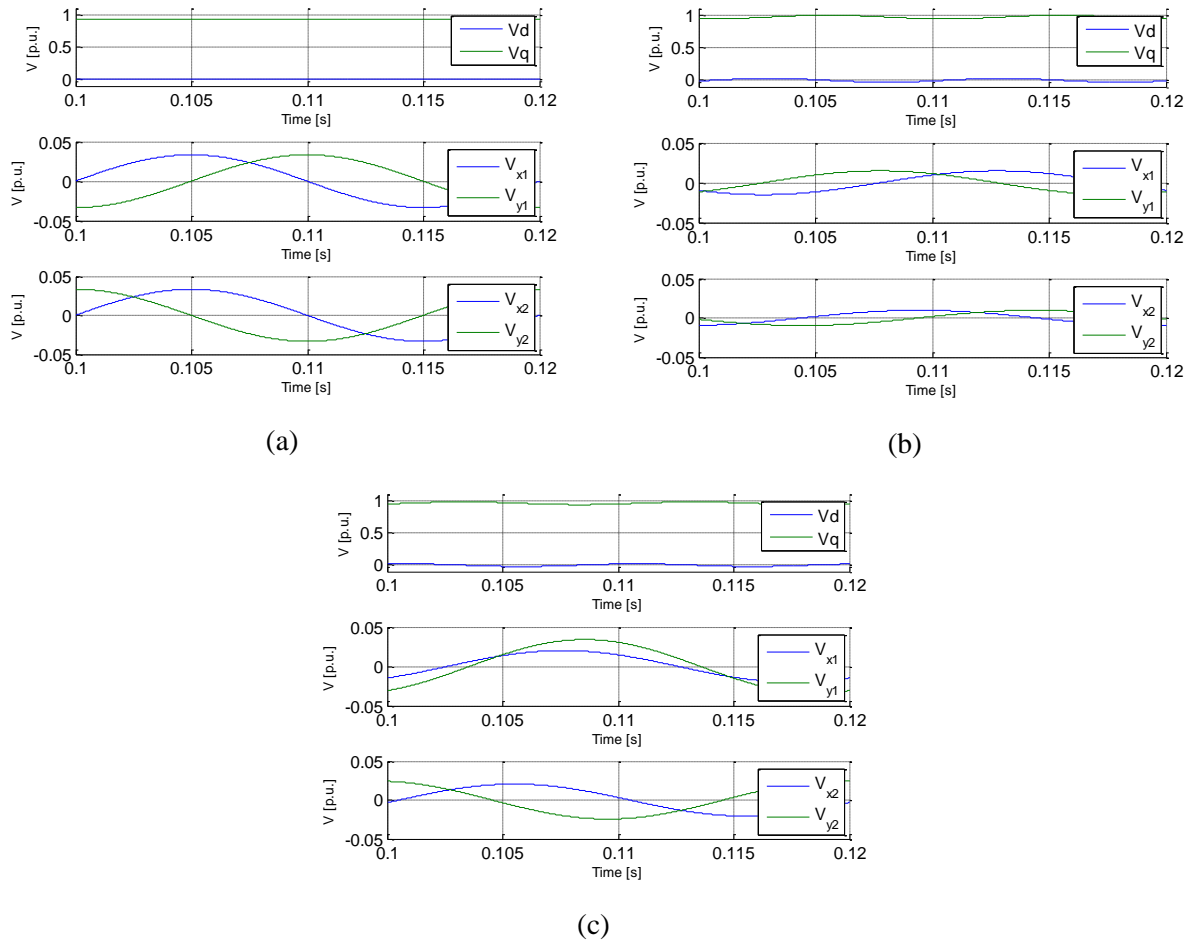
Fig. 3.16 Projections into xi-yi subspaces (VSD transformation) for different asymmetries: (a) CASE 1, (b) CASE 2 and (c) CASE 3.

To compare with the novel transformation, some particular asymmetry cases will be simulated to highlight the differences between two transformations. The first particular case will affect only the three-phase system number 2, having voltages of the said three-phase system phases at 0.9 p.u. (Fig. 3.17(a)). Similarly, the second particular case will affect only the three-phase system number 3 with the same situation as in the previous case (Fig. 3.17 (b)). The last case will affect the three-phase system number 1 (Fig. 3.17 (c)). In the three situations shown in Fig. 3.17, the three-phase systems not explicitly mentioned are balanced at 1 p.u.

It can be seen from Fig. 3.17 that any type of asymmetry, even when it affects only one of the three-phase systems, will have projections in both $x1$-$y1$ and $x2$-$y2$ subspaces. The plots in Fig. 3.16 and Fig. 3.17 agree with the results in (Rockhill and Lipo, 2009) and demonstrate that any kind of asymmetry will have projections in both x-y subspaces in the case of a nine-phase machine transformed using VSD transformation.

(a)   (b)

(c)
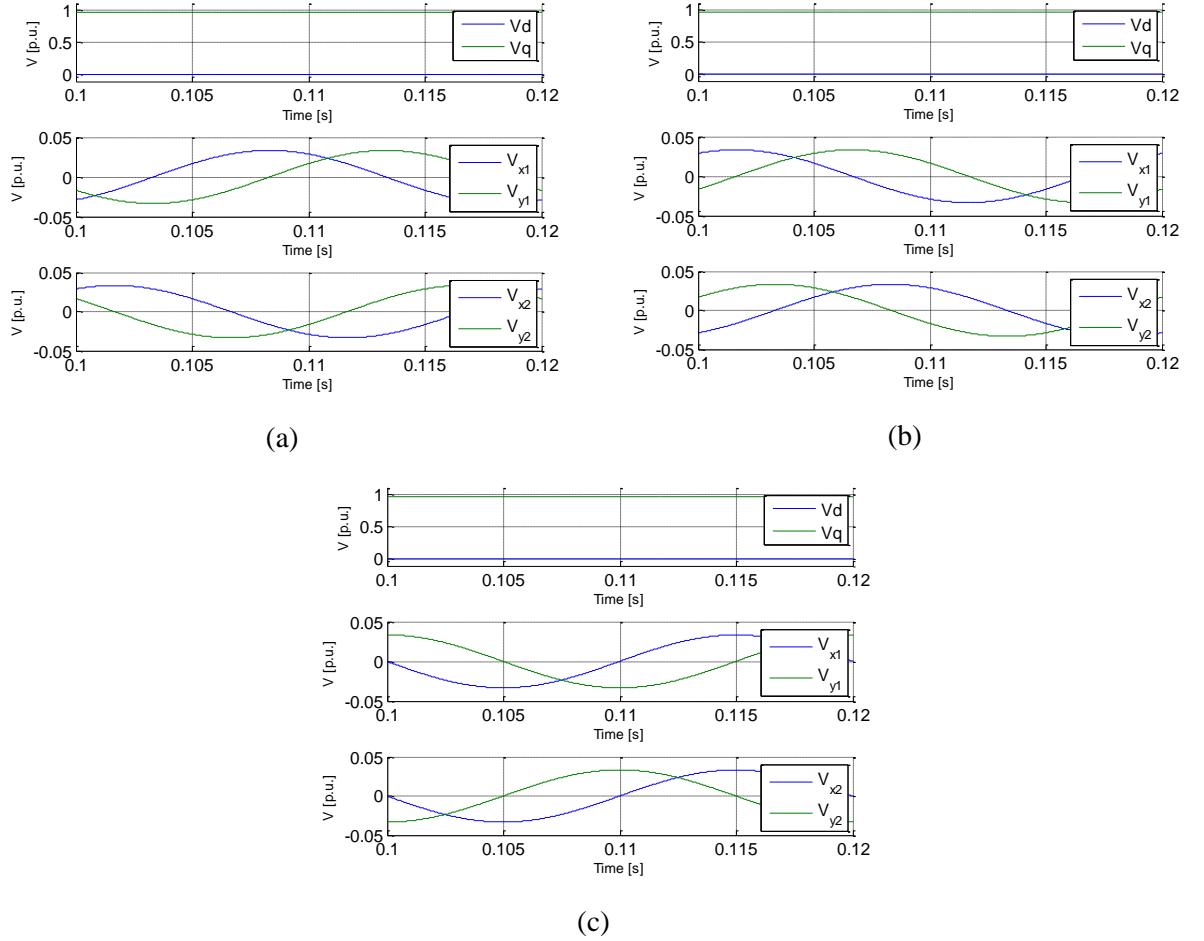
Fig. 3.17 Projections into xi-yi subspaces (VSD transformation) when (a) the three-phase system number 2 is balanced at 0.9 p.u., (b) the three-phase system number 3 is balanced at 0.9 p.u. and (c) the three-phase system number 1 is balanced at 0.9 p.u.

3.7.3.3   Harmonic mapping

Using the voltage source described in 3.7 and applying the VSD transformation, the harmonic mapping shown in Fig. 3.18 is obtained. In this figure, the $z1$, $z2$ and $z3$ axes have been omitted for the sake of legibility. From this figure, it can be seen how each harmonic is uniquely mapped into only one subspace. This result is obvious as this transformation generates mutually orthogonal subspaces, so no harmonic can have projections in more than one subspace.

In the Table 3.2, the mapping of the odd-order harmonics up to the 65th is shown. The following general mapping rules would apply in the case of 20º shift:

i)   In the α-β subspace, odd harmonics with $i = 18 \cdot m \pm 1$ (m=1,2,3….) are mapped.

ii) In the $x1$-$y1$ subspace, odd harmonics with $i = 9 \cdot m \pm 4$ (m=1,3,5….) are mapped.

iii) In the $x2$-$y2$ subspace, odd harmonics with $i = 9 \cdot m \pm 2$ (m=1,3,5….) are mapped.

iv) In the $z1$, $z2$ and $z3$ axes, all the triplen harmonics are mapped.
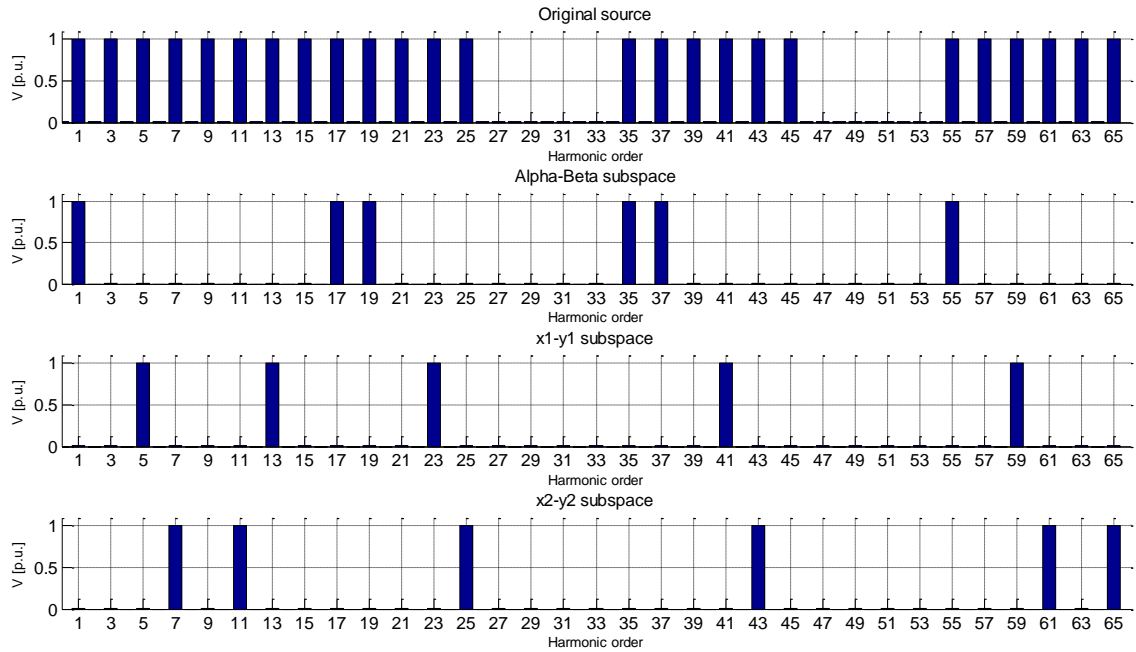
Fig. 3.18 Harmonic mapping using VSD transformation for the case of 20º shift.

Table 3.2 Harmonic mapping for a 20º phase shift using VSD transformation.

Subspace d-q	1,17,19,35,37,53,55
Subspace $x1$-$y1$	5,13,23,31,41,49,59
Subspace $x2$-$y2$	7,11,25,29,43,47,61,65
z1, z2 and z3	3,9,15,21,27,33,39,45,51,57,63

In the case of a symmetrical nine-phase machine (with 40º shift), the harmonic mapping is exactly the same as for the asymmetrical one (changing the order of the auxiliary subspaces $x1$-$y1$ and $x2$-$y2$) as can be seen in Fig. 3.19. Hence no difference in the behaviour in terms of torque ripple is to be expected between them.

In these cases, the VSD approach maps each harmonic into only one subspace facilitating its regulation or cancellation in case it is required. This feature makes this transformation appropriate whenever the control or cancellation of certain harmonics is required such as in multi-machine drives, symmetrical multiphase machines and trapezoidal MMF machines with low-order harmonic injection. Additionally, it will be perfectly applicable to sinusoidal MMF asymmetrical machines when cancellation of low-order harmonics is required. Another application for this transformation may be its use to determine which harmonics impact on the torque and flux waveform given a windings shift angle.
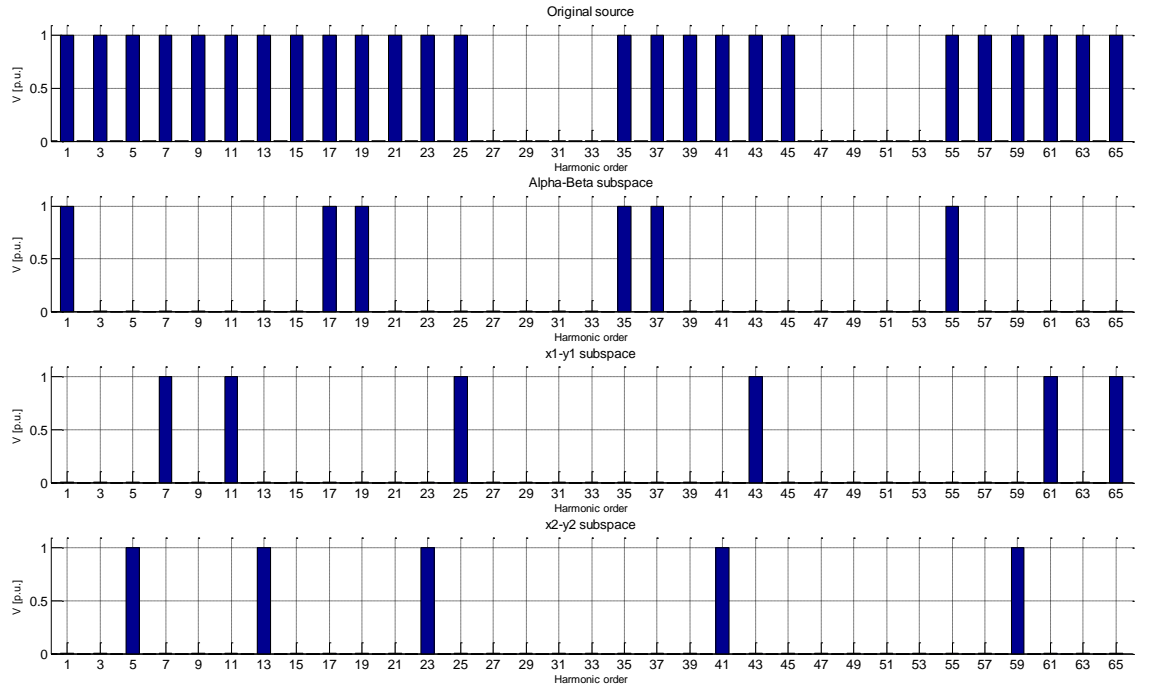
Fig. 3.19 Harmonic mapping using VSD transformation for the case of 40º shift.

3.7.4   Nine-phase machine with novel transformation

Along this chapter, the transformation described in section 3.6.2 will be used in the same scenario as that previously defined in 3.7.3.

3.7.4.1   Physical interpretation of the subspaces

As it has been described in 3.6, this transformation is based on assigning a physical interpretation to each of the *x-y* subspaces. For the case of a nine-phase machine, the following applies:

-    Axis α: reflects the summation in α in all the three-phase systems

-    Axis β: reflects the summation in β in all the three-phase systems

-    Axis α_{1i}: reflects the difference in α between the three-phase system number 1 and i (i= 2, 3)

-    Axis β_{1i}: reflects the difference in β between the three-phase system number 1 and i (i= 2, 3)

-    Axis z_{1i}: reflects the difference in 0 between the three-phase system number 1 and i

-    Axis z_9: reflects the summation in 0 in all the three-phase systems.

3.7.4.2   Representation of asymmetries

Using the same definitions for asymmetries as in 3.7.3.2, the projections in the different subspaces when applying the novel transformation are shown in Fig. 3.20. Comparing these with those obtained applying the VSD transformation (Fig. 3.16), it can be seen that, although different, they are quite similar in the fact that any kind of asymmetry will be mapped into both *x*1-*y*1 and *x*2-*y*2 subspaces.

(a)   (b)

(c)
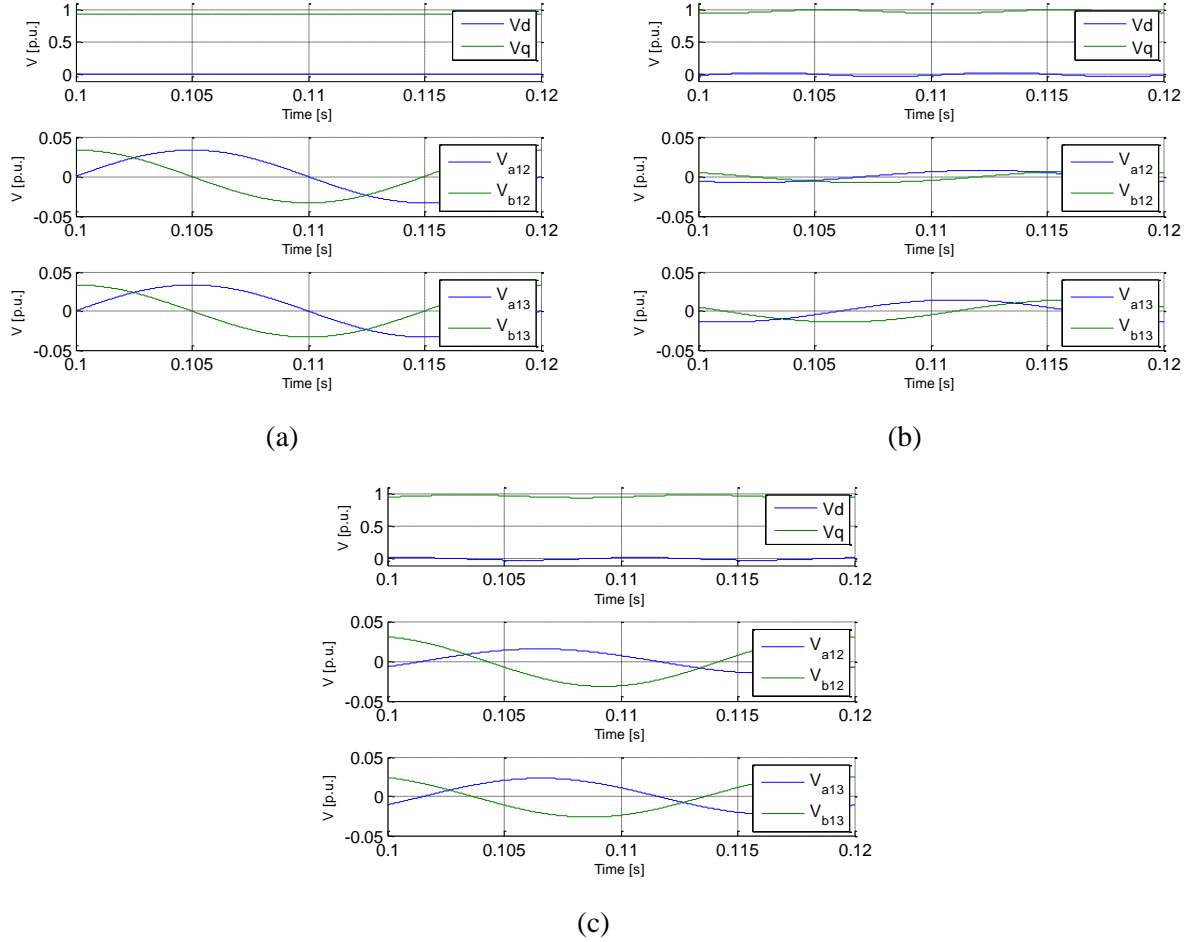
Fig. 3.20 Projections into the auxiliary subspaces for different asymmetries: (a) CASE 1, (b) CASE 2 and (c) CASE 3.

The particularity of this transformation comes from the fact that one of the three-phase systems is taken as a reference, so differences in the projections of certain types of asymmetries are to be expected. The difference comes when the asymmetry affects only one of the three-phase systems. For example, if the asymmetry affects only the three-phase system number 2, it will exclusively map into the 12 subspace, as can be seen in Fig. 3.21(a). Similarly, if the asymmetry affects only the three-phase system number 3, this will map exclusively into 13 subspace (Fig. 3.21 (b)). In case that the asymmetry affects the reference three-phase system, it will map into both 12 and 13 subspaces as seen in Fig. 3.21 (c). In the three situations shown in Fig. 3.21, the three-phase systems not explicitly mentioned are balanced at 1 p.u.

(a)   (b)

(c)
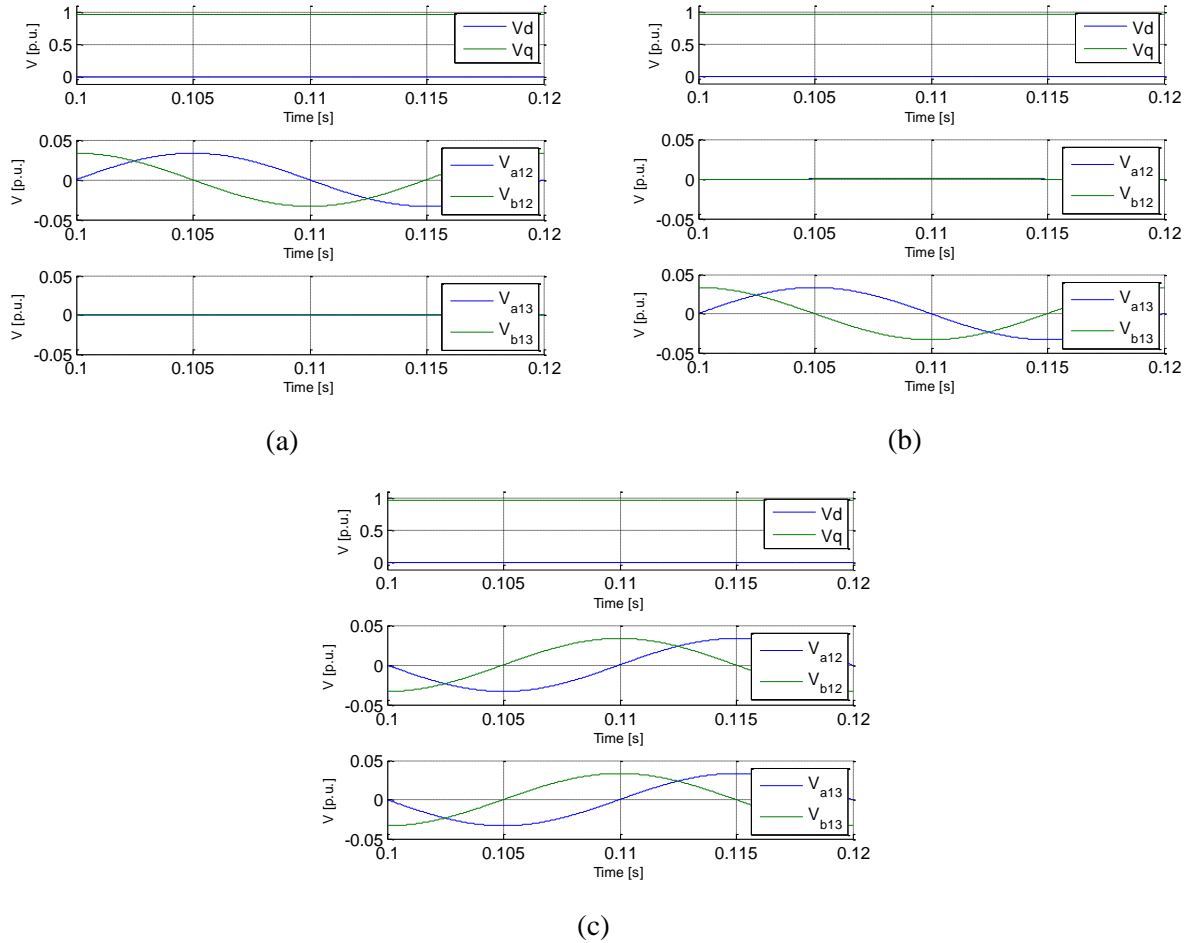
Fig. 3.21 Projections into the auxiliary subspaces when (a) the three-phase system number 2 is balanced at 0.9 p.u., (b) the three-phase system number 3 is balanced at 0.9 p.u. and (c) the three-phase system number 1 (reference) is balanced at 0.9 p.u.

The plots in Fig. 3.21 can be compared with those in Fig. 3.16 as both represent the same situations. It can be seen how with the novel transformation, when the asymmetry affects only one three-phase system, only projections in one of the auxiliary subspaces appear. This characteristic helps identifying the source of the asymmetry as it provides clear information to the control system. This is true only if the asymmetry does not affect the reference three-phase system, because in this case, the projections appear in both auxiliary subspaces (Fig. 3.21 (c)).

3.7.4.3   Harmonic mapping

As the auxiliary subspaces obtained with this transformation are not mutually orthogonal, there will not be a unique mapping for each harmonic. This means that certain harmonics will be mapped into more than one auxiliary subspace. In Fig. 3.22, the harmonic's mapping with the novel transformation is shown. It can be seen how in terms of harmonic mapping, both auxiliary 12 and auxiliary 13 subspaces are having identical spectra, gathering components from all non-torque and flux producing harmonics.
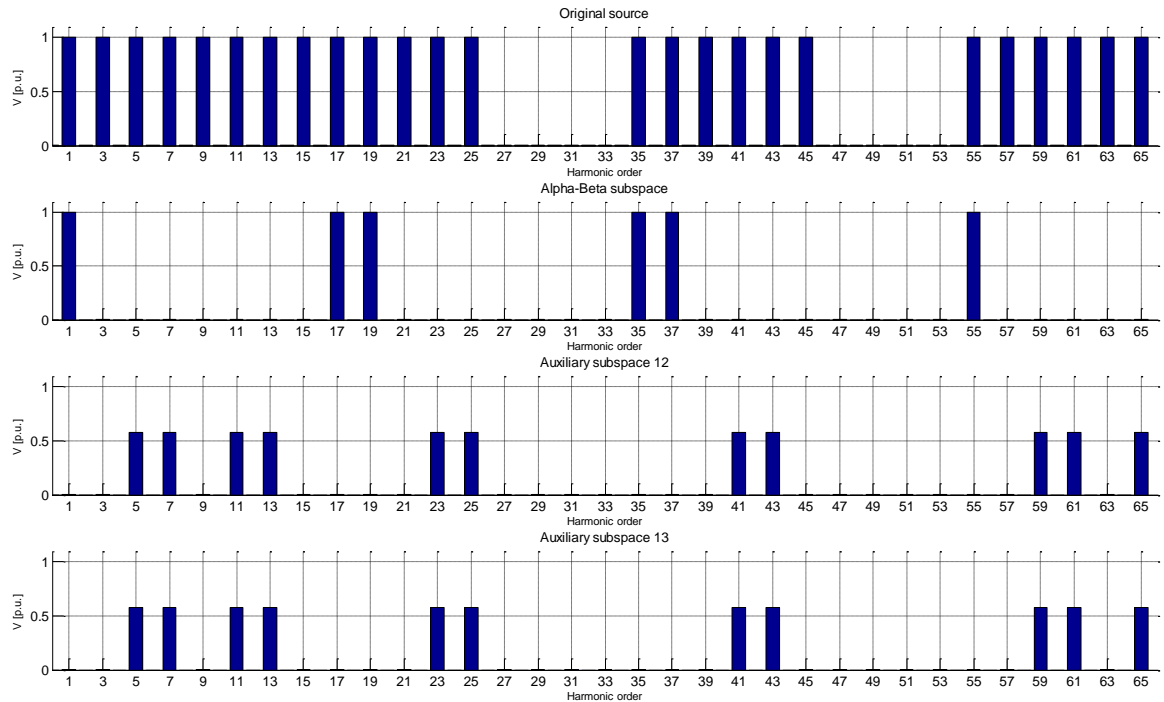
Fig. 3.22 Harmonic mapping using the novel transformation.

An important observation from Fig. 3.22 is that the amplitudes of the harmonics in the subspaces *x-y* are different (lower) than the originals introduced by the source (1 p.u.). On the contrary, in Fig. 3.18, it could be seen how the 5th harmonic projection in the subspace *x*1-*y*1 of the VSD transformation had the same amplitude as introduced by the source. This issue can be easily explained with the help of Fig. 3.23 which represents a simplification of the nine-dimensional subspace into a two-dimensional one for the ease of visualization. As the 5th harmonic has the same amplitude in the *x-y* subspace as the original source harmonic (for VSD transformation), it means that the harmonic is fully contained within said subspace. If a different, non-orthogonal, subspace is used (as is the case in the novel transformation), the projections of said 5th harmonic will be somehow lower than the original one and these will depend on the relative angle between two subspaces. This can be easily seen in a two-dimensional space such as the one shown in Fig. 3.23, but in a nine-dimensional space it is not so obvious even though the basic principle yields the same.
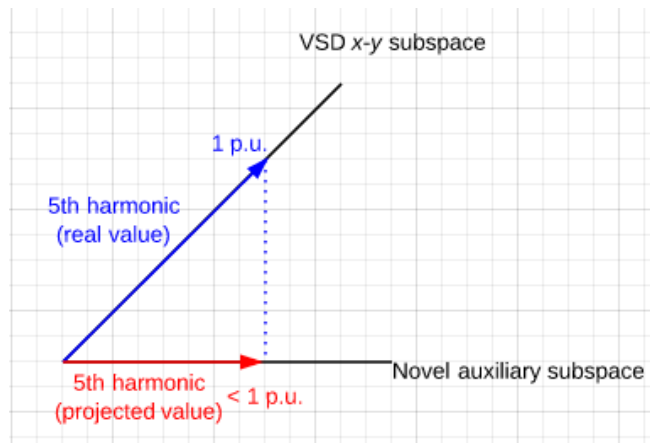
Fig. 3.23 Harmonic mapping using the novel transformation.

To obtain the relationship between the original amplitudes of the harmonics (represented in the VSD transformation), and the ones yielded by the novel transformation, it is necessary to perform the dot product of the different vectors within the transformation matrices,

$$C_{VSD} \cdot (C_{Novel})^T$$

$$= \begin{bmatrix}
4.5 & 0 & 0 & 0 & 0 & 0 & 0 & 0 & 0 \\
0 & 4.5 & 0 & 0 & 0 & 0 & 0 & 0 & 0 \\
0 & 0 & 2.25 & -1.299 & 2.25 & 1.299 & 0 & 0 & 0 \\
0 & 0 & -1.299 & -2.25 & 1.299 & -2.25 & 0 & 0 & 0 \\
0 & 0 & 2.25 & 1.299 & 2.25 & -1.299 & 0 & 0 & 0 \\
0 & 0 & -1.299 & 2.25 & 1.299 & 2.25 & 0 & 0 & 0 \\
0 & 0 & 0 & 0 & 0 & 0 & 6.75 & 6.75 & 6.75 \\
0 & 0 & 0 & 0 & 0 & 0 & -6.75 & 0 & 6.75 \\
0 & 0 & 0 & 0 & 0 & 0 & 0 & -6.75 & 6.75
\end{bmatrix}$$

(3.49)

yielding the matrix shown in (3.49) where the multiplying factor k has been taken as unity for simplicity. In this matrix, the row i represent the dot product of the vector i from the VSD transformation with the subsequent vectors from the novel transformation. Regarding the first two rows, it can be seen that the α and β vectors are orthogonal to all the other vectors as the non-diagonal elements are zero. The third row represents the dot product of the $x1$ axis of the VSD transformation, and special attention should be paid to columns three and four as these represent the dot product with the $\alpha12$ and $\beta12$ axes of the novel transformation, respectively. Obtaining the modulus of the projections of the axis $x1$ of the VSD on the $\alpha12$-$\beta12$ novel subspace,

$$\left| x1_{VSD_{proj}aux12} \right| = \sqrt{2.25^2 + 1.299^2} = 2.598$$

(3.50)

and dividing it by the squared Euclidean norm (which is the equivalent of the modulus for multidimensional vectors) of the $x1$ axis of the VSD,

$$SF_{VSD_{x1-y1}-Novel_{x1-y1}} = \frac{2.598}{4.5} = 0.577$$

(3.51)

leads to the attainment of the scaling factor between the $x1$-$y1$ subspace from VSD and the $\alpha12$-$\beta12$ of the novel transformation (3.51) which clearly coincides with the results in Fig. 3.22. With the observation of the 5th and 6th rows of the matrix in (3.49) it can be easily demonstrated that the same scaling factor applies between $x2$-$y2$ and the $\alpha13$-$\beta13$ subspaces.

In the Table 3.3, the mapping of the odd-order harmonics up to the 65th is shown. The following general mapping rules would apply in the case of 20º shift:

    i)   In the α-β subspace, odd harmonics with $i = 18 \cdot m \pm 1$ ($m = 1,2,3....$) are mapped.

    ii) In the $x1$-$y1$ and $x2$-$y2$ subspaces, odd harmonics with $i = 9 \cdot m \pm 2$ and $9 \cdot m \pm 4$ ($m = 1,3,5....$) are mapped.

    iii) In the $z12$, $z13$ and $z9$ axes, all the triplen harmonics are mapped.

Table 3.3 Harmonic mapping for a 20º phase shift between three-phase systems using the novel transformation.

Subspace d-q	1,17,19,35,37
Subspace $\alpha12$-$\beta12$	5,7,11,13,23,25,29,31,41,43,47,49,59,61,65
Subspace $\alpha13$-$\beta13$	5,7,11,13,23,25,29,31,41,43,47,49,59,61,65
$z12$, $z13$ and $z9$ axes	3,9,15,21,27,33,39,45,51,57,63

3.8 Summary

Along this chapter, a demonstration of the necessity of the transformations for multiphase machines has been provided together with a brief description and a method to obtain the already available transformation matrices. A further detailed analysis of the existing transformations yields the conclusion that no physical interpretation for the x-y subspaces can be obtained for machines with more than six phases. This fact enormously complicates the operation if unbalanced current sharing between

the three-phase systems of said machines is required. This is so because it is necessary to generate non-zero current setpoints in the *x-y* subspaces to operate a machine with different current sharing between the three-phase systems. By using the existing VSD transformation, the generation of such non-zero current setpoints to obtain a desired unbalanced current sharing is not obvious due to the lack of physical meaning of the *x-y* subspaces, and may impose a high computational burden (Tani et al., 2013).

Focusing on assigning physical interpretation to the *x-y* subspaces, a novel transformation has been proposed that easily allows operating an asymmetrical machine with different current sharing amongst its three-phase systems. To fully characterise the implications of the novel transformation, a correlation between the VSD and multiple *dq* transformation has been established regarding the harmonic mapping and the representation of asymmetries. The novel transformation has been applied to a six- and to a nine-phase asymmetrical machine but the extension to twelve- or fifteen-phase machines is straightforward. A script in Matlab ® to build the transformation matrix for any *n*-phase machine has been included in Appendix 2.

The novel transformation provides an easier unbalanced current sharing strategy thanks to the physical interpretation of its auxiliary subspaces. Additionally, it provides clearer information about operational unbalances within the three-phase systems under certain conditions. The only drawback that can be related to the novel transformation is the fact that it does not provide a unique harmonic mapping so it may not be appropriate for applications where a harmonic control is required.

CHAPTER 4

Modelling of multiphase machines with multiple three-phase windings

4.1 Introduction

In general, the modelling of a multiphase machine is very similar to that of a three-phase machine, with the only difference in the dimension of the domain. To start with, the equation of the stator's voltages in the natural domain can be expressed as

$$[v_s]_{abc} = [R_s]_{abc} \cdot [i_s]_{abc} + \frac{d[\Psi_s]_{abc}}{dt} \qquad (4.1)$$

where the dimensions of the voltage ($[v_s]_{abc}$), current ($[i_s]_{abc}$) and flux vectors ($[\Psi_s]_{abc}$) are nx1 and the resistance matrix ($[R_s]$) is nxn and diagonal in form.

To apply a generic transformation matrix $[T]$ to the equation (4.1), both sides of the equation can be pre-multiplied by it without altering the equality. Hence

$$[T] \cdot [v_s]_{abc} = [T] \cdot [R_s]_{abc} \cdot [i_s]_{abc} + [T] \cdot \frac{d[\Psi_s]_{abc}}{dt} \qquad (4.2)$$

is completely equivalent to (4.1). Next, the reversibility principle of the transformation matrix is applied to (4.2),

$$[T] \cdot [X]_{abc} = [X]_t$$
$$[X]_{abc} = [T]^{-1} \cdot [X]_t \qquad (4.3)$$

where $[X]_t$ is the vector of transformed variables. The voltage equation is then fully transformed into the new reference frame defined by the transformation $[T]$ as

$$[v_s]_t = [T] \cdot [R_s]_{abc} \cdot [T]^{-1} \cdot [i_s]_t + [T] \cdot \frac{d([T]^{-1} \cdot [\Psi_s]_t)}{dt} \qquad (4.4)$$

In equation (4.4), the right-most term includes the derivative of a product of matrices, so special care should be taken when developing it. In the case of transformations to stationary reference frames, the transformation matrix $[T]$ has constant coefficients, so it can be taken out of the derivative term, thus simplifying the voltage equation to

$$[v_s]_t = [T] \cdot [R_s]_{abc} \cdot [T]^{-1} \cdot [i_s]_t + \frac{d([\Psi_s]_t)}{dt} \qquad (4.5)$$

Here, special care needs to be taken with the derivative of the stator's flux as the inductance matrix in the stationary reference frame may not be constant and so, it should be differentiated. On the contrary, if the transformation refers to a rotating frame, the resultant inductance matrix is constant but the coefficients in $[T]$ will no longer be constant so the derivative of the product of matrices still has to be determined,

$$[v_s]_{t+r} = [T] \cdot [R_s]_{abc} \cdot [T]^{-1} \cdot [i_s]_{t+r} + [T] \cdot \frac{d([T]^{-1})}{dt} \cdot [\Psi_s]_{t+r} + \frac{d([\Psi_s]_{t+r})}{dt} \qquad (4.6)$$

yielding the equation shown above. The term involving the derivative of the inverse of the transformation matrix is usually referred to as 'speed-EMF' while the term with the derivative of the transformed flux is usually referred to as 'transformer-EMF' (Watson and Arrillaga, 2003).

Following the same procedure, the equation of the fluxes in the natural domain

$$[\Psi_s]_{abc} = [L_s]_{abc} \cdot [i_s]_{abc} + [\Psi_{PM}]_{abc} \qquad (4.7)$$

should also be transformed, where $[L_s]_{abc}$ represents the stator's inductance matrix and $[\Psi_{PM}]_{abc}$ the flux provided by the permanent magnets. Pre-multiplying both sides of equation (4.7) with the transformation matrix $[T]$ and applying the relations shown in (4.3), the transformed equation of fluxes is obtained as

$$[\Psi_s]_t = [T] \cdot [L_s]_{abc} \cdot [T]^{-1} \cdot [i_s]_t + [T] \cdot [\Psi_{PM}]_{abc}$$

(4.8)

which is applicable to transformations into both stationary and rotating reference frames.

As was mentioned in Chapter 3, the main target of a transformation is to obtain a diagonal inductance matrix with constant coefficients. This means that the transformed inductance matrix $[T] \cdot [L_s]_{abc} \cdot [T]^{-1}$ in (4.8) should satisfy said requirements.

From the equations above, the terms

$$[R_s]_t = [T] \cdot [R_s] \cdot [T]^{-1} = [R_s] \qquad\qquad [L_s]_t = [T] \cdot [L_s]_{abc} \cdot [T]^{-1}$$

$$[\Psi_{PM}]_t = [T] \cdot [\Psi_{PM}]_{abc} \qquad [Speed - EMF] = [T] \cdot \frac{d([T]^{-1})}{dt} \cdot [\Psi_s]_{t+r}$$

(4.9)

need to be calculated. It can be easily demonstrated that the application of a matrix and its inverse to a diagonal matrix (such as $[R_s]$), yields the same matrix $[R_s]$, so only the transformed inductance matrix $[L_s]_t$ and the transformed permanent magnet's flux vector $[\Psi_{PM}]_t$ remain unknown.

In what follows, all the transformations applied following the multiple *dq* approach are considered with the scaling factor (k_t) equal to 2/3 and the zero-sequence factor (*c*) equal to 1 unless explicitly stated. On the other hand, when VSD or the novel approach is followed, the scaling factor (k_t) will be equal to 2/*n* and the zero-sequence factor (*c*) equal to 1 unless explicitly stated. Here *n* stands for the number of phases.

4.2 Modelling of permanent magnet machines with multiple three-phase windings

4.2.1 Dual three-phase machines

4.2.1.1 Models resulting from multiple *dq* approach

The multiple *dq* transformation consists in applying the well-known three-phase transformation to each of the three-phase systems within the stator of the machine. The transformation matrices for a six-phase machine are given by (3.26). Substituting in equations (4.4) and in (4.8) the generic transformation matrix $[T]$ by C_{Ddq} (3.26), the transformed equations for a six-phase machine are obtained. Calculating the unknown terms (4.9) for a six-phase machine,

$$[L_s]_t = \begin{bmatrix} L_{ls} + L_{\alpha\alpha} & L_{\alpha\beta} & 0 & L_{\alpha\alpha} & L_{\alpha\beta} & 0 \\ L_{\alpha\beta} & L_{ls} + L_{\beta\beta} & 0 & L_{\alpha\beta} & L_{\beta\beta} & 0 \\ 0 & 0 & L_{ls} & 0 & 0 & 0 \\ L_{\alpha\alpha} & L_{\alpha\beta} & 0 & L_{ls} + L_{\alpha\alpha} & L_{\alpha\beta} & 0 \\ L_{\alpha\beta} & L_{\beta\beta} & 0 & L_{\alpha\beta} & L_{ls} + L_{\beta\beta} & 0 \\ 0 & 0 & 0 & 0 & 0 & L_{ls} \end{bmatrix}$$

(4.10)

$$[\Psi_{PM}]_t = \psi_{PM} \cdot [cos(\theta_r) \quad sin(\theta_r) \quad 0 \quad cos(\theta_r) \quad sin(\theta_r) \quad 0]^T$$

where the superscript T represents the transpose operator, L_{ls} represents the stator's leakage inductance, $L_{\alpha\alpha}$ and $L_{\beta\beta}$ represent the stator's self-inductances in the axes α and β, respectively, and $L_{\alpha\beta}$ represents the mutual inductance between said axes. Their expressions are

$$L_{\alpha\alpha} = \frac{3}{2} \cdot \left(\frac{L_{md} + L_{mq}}{2} + \frac{L_{md} - L_{mq}}{2} \cdot cos(2 \cdot \theta_r) \right)^1 \qquad L_{ss} = 3/2 \cdot \left(\frac{L_{md} + L_{mq}}{2} - \frac{L_{md} - L_{mq}}{2} \cdot cos(2 \cdot \theta_r) \right)$$

$$L_{\alpha\beta} = 3/2 \cdot \left(\frac{L_{md} - L_{mq}}{2} \cdot sin(2 \cdot \theta_r) \right)$$

(4.11)

in which L_{md} and L_{mq} represent the magnetising inductances along the d and q axes [1] defined as in (3.11). Substituting all the terms in equation (4.5) and re-arranging the terms to follow the state-space representation with currents as state variables,

$$\frac{d([i_s]_t)}{dt} = [L_s]_t^{-1} \cdot \left([V_s]_t - [R_s] \cdot [i_s]_t - \frac{d[\Psi_{PM}]_t}{dt} - \frac{d[L_s]_t}{dt} \cdot [i_s]_t \right)$$

(4.12)

the expressions of the equations for each of the axes can be obtained for a six-phase machine in the following form [2]:

$$\frac{di_{\alpha 1}}{dt} = g_{\alpha 1 \alpha 1} \cdot (v_{\alpha 1} - r_s \cdot i_{\alpha 1} + \omega_r \cdot \psi_{PM} \cdot sin(\theta_r) + sal_\alpha) + g_{\alpha\beta} \cdot (v_{\beta 1} - r_s \cdot i_{\beta 1} - \omega_r \cdot \psi_{PM} \cdot cos(\theta_r) + sal_\beta)$$
$$+ g_{\alpha 1 \alpha 2} \cdot (v_{\alpha 2} - r_s \cdot i_{\alpha 2} + \omega_r \cdot \psi_{PM} \cdot sin(\theta_r) + sal_\alpha) + g_{\alpha\beta}$$
$$\cdot (v_{\beta 2} - r_s \cdot i_{\beta 2} - \omega_r \cdot \psi_{PM} \cdot cos(\theta_r) + sal_\beta)$$

$$\frac{di_{\beta 1}}{dt} = g_{\alpha\beta} \cdot (v_{\alpha 1} - r_s \cdot i_{\alpha 1} + \omega_r \cdot \psi_{PM} \cdot sin(\theta_r) + sal_\alpha) + g_{\beta 1 \beta 1} \cdot (v_{\beta 1} - r_s \cdot i_{\beta 1} - \omega_r \cdot \psi_{PM} \cdot cos(\theta_r) + sal_\beta) + g_{\alpha\beta}$$
$$\cdot (v_{\alpha 2} - r_s \cdot i_{\alpha 2} + \omega_r \cdot \psi_{PM} \cdot sin(\theta_r) + sal_\alpha) + g_{\beta 1 \beta 2}$$
$$\cdot (v_{\beta 2} - r_s \cdot i_{\beta 2} - \omega_r \cdot \psi_{PM} \cdot cos(\theta_r) + sal_\beta)$$

$$\frac{di_{\alpha 2}}{dt} = g_{\alpha 2 \alpha 1} \cdot (v_{\alpha 1} - r_s \cdot i_{\alpha 1} + \omega_r \cdot \psi_{PM} \cdot sin(\theta_r) + sal_\alpha) + g_{\alpha\beta} \cdot (v_{\beta 1} - r_s \cdot i_{\beta 1} - \omega_r \cdot \psi_{PM} \cdot cos(\theta_r) + sal_\beta)$$
$$+ g_{\alpha 2 \alpha 2} \cdot (v_{\alpha 2} - r_s \cdot i_{\alpha 2} + \omega_r \cdot \psi_{PM} \cdot sin(\theta_r) + sal_\alpha) + g_{\alpha\beta}$$
$$\cdot (v_{\beta 2} - r_s \cdot i_{\beta 2} - \omega_r \cdot \psi_{PM} \cdot cos(\theta_r) + sal_\beta)$$

(4.13)

$$\frac{di_{\beta 2}}{dt} = g_{\alpha\beta} \cdot (v_{\alpha 1} - r_s \cdot i_{\alpha 1} + \omega_r \cdot \psi_{PM} \cdot sin(\theta_r) + sal_\alpha) + g_{\beta 2 \beta 1} \cdot (v_{\beta 1} - r_s \cdot i_{\beta 1} - \omega_r \cdot \psi_{PM} \cdot cos(\theta_r) + sal_\beta) + g_{\alpha\beta}$$
$$\cdot (v_{\alpha 2} - r_s \cdot i_{\alpha 2} + \omega_r \cdot \psi_{PM} \cdot sin(\theta_r) + sal_\alpha) + g_{\beta 2 \beta 2}$$
$$\cdot (v_{\beta 2} - r_s \cdot i_{\beta 2} - \omega_r \cdot \psi_{PM} \cdot cos(\theta_r) + sal_\beta)$$

$$sal_\alpha = \frac{3}{2} \cdot (L_{md} - L_{mq}) \cdot ((i_{\alpha 1} + i_{\alpha 2}) \cdot sin(2 \cdot \theta_r) - (i_{\beta 1} + i_{\beta 2}) \cdot cos(2 \cdot \theta_r))$$

$$sal_\beta = \frac{-3}{2} \cdot (L_{md} - L_{mq}) \cdot ((i_{\alpha 1} + i_{\alpha 2}) \cdot cos(2 \cdot \theta_r) + (i_{\beta 1} + i_{\beta 2}) \cdot sin(2 \cdot \theta_r))$$

where $v_{\alpha k}$, $v_{\beta k}$ and $i_{\alpha k}$, $i_{\beta k}$ are the α- and β-axis voltages and currents in the three-phase system number k and the coefficients $g_{\alpha\alpha}$ and $g_{\beta\beta}$ can be calculated as

$$g_{\alpha 1 \alpha 1} = g_{\alpha 2 \alpha 2} = \frac{4 \cdot L_{ls}^2 + 9 \cdot L_{ls} \cdot (L_{md} + L_{mq}) + 18 \cdot L_{md} \cdot L_{mq} - 3 \cdot L_{ls} \cdot (L_{md} - L_{mq}) \cdot cos(2 \cdot \theta_r)}{4 \cdot L_{ls} \cdot (L_{ls} + 3 \cdot L_{md}) \cdot (L_{ls} + 3 \cdot L_{mq})}$$

$$g_{\alpha 1 \alpha 2} = g_{\alpha 2 \alpha 1} = \frac{-3 \cdot L_{ls} \cdot (L_{md} + L_{mq}) - 18 \cdot L_{md} \cdot L_{mq} - 3 \cdot L_{ls} \cdot (L_{md} - L_{mq}) \cdot cos(2 \cdot \theta_r)}{4 \cdot L_{ls} \cdot (L_{ls} + 3 \cdot L_{md}) \cdot (L_{ls} + 3 \cdot L_{mq})}$$

$$g_{\alpha\beta} = \frac{-3 \cdot L_{ls} \cdot (L_{md} - L_{mq}) \cdot sin(2 \cdot \theta_r)}{4 \cdot L_{ls} \cdot (L_{ls} + 3 \cdot L_{md}) \cdot (L_{ls} + 3 \cdot L_{mq})}$$

$$g_{\beta 1 \beta 1} = g_{\beta 2 \beta 2} = \frac{4 \cdot L_{ls}^2 + 9 \cdot L_{ls} \cdot (L_{md} + L_{mq}) + 18 \cdot L_{md} \cdot L_{mq} + 3 \cdot L_{ls} \cdot (L_{md} - L_{mq}) \cdot cos(2 \cdot \theta_r)}{4 \cdot L_{ls} \cdot (L_{ls} + 3 \cdot L_{md}) \cdot (L_{ls} + 3 \cdot L_{mq})}$$

$$g_{\beta 1 \beta 2} = g_{\beta 2 \beta 1} = \frac{-3 \cdot L_{ls} \cdot (L_{md} + L_{mq}) - 18 \cdot L_{md} \cdot L_{mq} + 3 \cdot L_{ls} \cdot (L_{md} - L_{mq}) \cdot cos(2 \cdot \theta_r)}{4 \cdot L_{ls} \cdot (L_{ls} + 3 \cdot L_{md}) \cdot (L_{ls} + 3 \cdot L_{mq})}$$

(4.14)[2]

---

[1] The scaling factor 3/2, applied here to the magnetizing inductances (which is not common in the literature), is due to the different definition adopted for the magnetizing inductances in d- and q-axes in Chapter 3.

[2] The expressions of all these terms are written in a DSP-legible C-code style in the Appendix 3. In case of any mismatch between the expressions shown here and in the Appendix, the latter should prevail.

The terms sal_α and sal_β represent the effect of the saliency of the magnetic circuit in the time derivative of the stator's flux.

The $g_{\alpha i \alpha j}$ and $g_{\beta i \beta j}$ coefficients with $i \neq j$ account for the cross-coupling that exists between the different three-phase systems in the machine. Additionally, the $g_{\alpha\beta}$ coefficient represents the cross-coupling of the α-β axes. It can be clearly seen how this coupling is directly proportional to the saliency of the machine (i.e. the difference between the inductances in the d and q axes). These cross-coupling terms make it very difficult to tune the current regulators in both α and β axes as the α-axis current in the three-phase system number one is influenced, through $g_{\alpha 1 \alpha 2}$, by the α-axis voltage ($v_{\alpha 2}$) in the three-phase system number two and through $g_{\alpha\beta}$ by the voltages in β-axis. All this implies that the α-axis and/or the β-axis current in any of the three-phase systems in the machine will be governed by four inputs $v_{\alpha 1}$, $v_{\alpha 2}$, $v_{\beta 1}$ and $v_{\beta 2}$.

By compensating the inputs with the terms related to the flux of the permanent magnets, equation (4.13) is simplified into

$$\frac{di_{\alpha 1}}{dt} = g_{\alpha 1 \alpha 1} \cdot (v_{\alpha 1 c} - r_s \cdot i_{\alpha 1} + sal_\alpha) + g_{\alpha\beta} \cdot (v_{\beta 1 c} - r_s \cdot i_{\beta 1} + sal_\beta) + g_{\alpha 1 \alpha 2} \cdot (v_{\alpha 2 c} - r_s \cdot i_{\alpha 2} + sal_\alpha) + g_{\alpha\beta} \\ \cdot (v_{\beta 2 c} - r_s \cdot i_{\beta 2} + sal_\beta)$$

$$\frac{di_{\beta 1}}{dt} = g_{\alpha\beta} \cdot (v_{\alpha 1 c} - r_s \cdot i_{\alpha 1} + sal_\alpha) + g_{\beta 1 \beta 1} \cdot (v_{\beta 1 c} - r_s \cdot i_{\beta 1} + sal_\beta) + g_{\alpha\beta} \cdot (v_{\alpha 2 c} - r_s \cdot i_{\alpha 2} + sal_\alpha) + g_{\beta 1 \beta 2} \\ \cdot (v_{\beta 2 c} - r_s \cdot i_{\beta 2} + sal_\beta)$$

$$\frac{di_{\alpha 2}}{dt} = g_{\alpha 2 \alpha 1} \cdot (v_{\alpha 1 c} - r_s \cdot i_{\alpha 1} + sal_\alpha) + g_{\alpha\beta} \cdot (v_{\beta 1 c} - r_s \cdot i_{\beta 1} + sal_\beta) + g_{\alpha 2 \alpha 2} \cdot (v_{\alpha 2 c} - r_s \cdot i_{\alpha 2} + sal_\alpha) + g_{\alpha\beta} \\ \cdot (v_{\beta 2 c} - r_s \cdot i_{\beta 2} + sal_\beta)$$

$$\frac{di_{\beta 2}}{dt} = g_{\alpha\beta} \cdot (v_{\alpha 1 c} - r_s \cdot i_{\alpha 1} + sal_\alpha) + g_{\beta 2 \beta 1} \cdot (v_{\beta 1 c} - r_s \cdot i_{\beta 1} + sal_\beta) + g_{\alpha\beta} \cdot (v_{\alpha 2 c} - r_s \cdot i_{\alpha 2} + sal_\alpha) + g_{\beta 2 \beta 2} \\ \cdot (v_{\beta 2 c} - r_s \cdot i_{\beta 2} + sal_\beta)$$

$$(4.15)$$

where $v_{\alpha k c}$ and $v_{\beta k c}$ are the compensated voltages in the α and β axes in the three-phase system number k and their expressions are,

$$v_{\alpha k c} = v_{\alpha k} - \omega_r \cdot \psi_{PM} \cdot sin(\theta_r)$$
$$v_{\beta k c} = v_{\beta k} + \omega_r \cdot \psi_{PM} \cdot cos(\theta_r)$$

$$(4.16)$$

Constructing the matrices of the state-space representation from equation (4.15), while considering the output matrix $[C]$ as equal to an identity matrix, yields:

$$[\dot{X}] = [A] \cdot [X] + [B] \cdot [u] \quad\quad [Y] = [X]$$

$$[X] = [i_{\alpha 1}, i_{\beta 1}, i_{\alpha 2}, i_{\beta 2}]^T \quad [u] = [v_{\alpha 1}, v_{\beta 1}, v_{\alpha 2}, v_{\beta 2}]^T$$

$$[A] = \begin{bmatrix} a_{11} & a_{12} & a_{13} & a_{14} \\ a_{21} & a_{22} & a_{23} & a_{24} \\ a_{13} & a_{14} & a_{11} & a_{12} \\ a_{23} & a_{24} & a_{21} & a_{22} \end{bmatrix}$$

$$[B] = \begin{bmatrix} g_{\alpha 1 \alpha 1} & g_{\alpha\beta} & g_{\alpha 1 \alpha 2} & g_{\alpha\beta} \\ g_{\alpha\beta} & g_{\beta 1 \beta 1} & g_{\alpha\beta} & g_{\beta 1 \beta 2} \\ g_{\alpha 1 \alpha 2} & g_{\alpha\beta} & g_{\alpha 1 \alpha 1} & g_{\alpha\beta} \\ g_{\alpha\beta} & g_{\beta 1 \beta 2} & g_{\alpha\beta} & g_{\beta 1 \beta 1} \end{bmatrix}$$

$$(4.17)$$

and the expressions of the terms in the matrix $[A]$ are

$$a_{11} = -g_{\alpha\beta} \cdot 3 \cdot (L_{md} - L_{mq}) \cdot cos(2 \cdot \theta_r) - g_{\alpha1\alpha1} \cdot \left(r_s - \frac{3}{2} \cdot (L_{md} - L_{mq}) \cdot sin(2 \cdot \theta_r)\right) + g_{\alpha1\alpha2} \cdot \frac{3}{2} \cdot (L_{md} - L_{mq})$$
$$\cdot sin(2 \cdot \theta_r)$$

$$a_{12} = -(g_{\alpha1\alpha1} + g_{\alpha1\alpha2}) \cdot \frac{3}{2} \cdot (L_{md} - L_{mq}) \cdot cos(2 \cdot \theta_r) - g_{\alpha\beta} \cdot (r_s + 3 \cdot (L_{md} - L_{mq}) \cdot sin(2 \cdot \theta_r))$$

$$a_{13} = -g_{\alpha\beta} \cdot 3 \cdot (L_{md} - L_{mq}) \cdot cos(2 \cdot \theta_r) + g_{\alpha1\alpha1} \cdot \frac{3}{2} \cdot (L_{md} - L_{mq}) \cdot sin(2 \cdot \theta_r) - g_{\alpha1\alpha2}$$
$$\cdot \left(r_s - \frac{3}{2} \cdot (L_{md} - L_{mq}) \cdot sin(2 \cdot \theta_r)\right)$$

$$a_{14} = -(g_{\alpha1\alpha1} + g_{\alpha1\alpha2}) \cdot \frac{3}{2} \cdot (L_{md} - L_{mq}) \cdot cos(2 \cdot \theta_r) - g_{\alpha\beta} \cdot (r_s + 3 \cdot (L_{md} - L_{mq}) \cdot sin(2 \cdot \theta_r))$$ **(4.18)**

$$a_{21} = -(g_{\beta1\beta1} + g_{\beta1\beta2}) \cdot \frac{3}{2} \cdot (L_{md} - L_{mq}) \cdot cos(2 \cdot \theta_r) - g_{\alpha\beta} \cdot (r_s - 3 \cdot (L_{md} - L_{mq}) \cdot sin(2 \cdot \theta_r))$$

$$a_{22} = -g_{\alpha\beta} \cdot 3 \cdot (L_{md} - L_{mq}) \cdot cos(2 \cdot \theta_r) - g_{\beta1\beta1} \cdot \left(r_s + \frac{3}{2} \cdot (L_{md} - L_{mq}) \cdot sin(2 \cdot \theta_r)\right) - g_{\beta1\beta2} \cdot \frac{3}{2} \cdot (L_{md} - L_{mq})$$
$$\cdot sin(2 \cdot \theta_r)$$

$$a_{23} = -(g_{\beta1\beta1} + g_{\beta1\beta2}) \cdot \frac{3}{2} \cdot (L_{md} - L_{mq}) \cdot cos(2 \cdot \theta_r) - g_{\alpha\beta} \cdot (r_s - 3 \cdot (L_{md} - L_{mq}) \cdot sin(2 \cdot \theta_r))$$

$$a_{24} = -g_{\alpha\beta} \cdot 3 \cdot (L_{md} - L_{mq}) \cdot cos(2 \cdot \theta_r) - g_{\beta1\beta1} \cdot \frac{3}{2} \cdot (L_{md} - L_{mq}) \cdot sin(2 \cdot \theta_r) - g_{\beta1\beta2}$$
$$\cdot \left(r_s + \frac{3}{2} \cdot (L_{md} - L_{mq}) \cdot sin(2 \cdot \theta_r)\right)$$

The cross-couplings can be clearly seen in both [A] and [B] matrices. The reduction of these cross-couplings can be made progressively following a similar procedure as the one shown in (De Camillis et al., 2001). First, the cross-coupling between the α and β axes should be removed by means of a state feedback added to the inputs of the system, meaning that the new input matrix will be

$$[u_{\alpha\beta}] = [u] + [K_{\alpha\beta}] \cdot [X]$$ **(4.19)**

where $[K_{\alpha\beta}]$ is the state feedback matrix. Introducing the new input matrix in the equation (4.17) and collecting the terms that depend on the state vector $[X]$,

$$[\dot{X}] = ([A] + [B] \cdot [K_{\alpha\beta}]) \cdot [X] + [B] \cdot [u]$$ **(4.20)**

the modified states matrix $[A_{\alpha\beta}]$ is obtained. Aiming at the decoupling between α and β axes, the modified state matrix should look like

$$[A_{\alpha\beta}] = ([A] + [B] \cdot [K_{\alpha\beta}]) = \begin{bmatrix} a_{11} & 0 & a_{13} & 0 \\ 0 & a_{22} & 0 & a_{24} \\ a_{13} & 0 & a_{11} & 0 \\ 0 & a_{24} & 0 & a_{22} \end{bmatrix}$$ **(4.21)**

Manipulating equation (4.21) to isolate the state feedback matrix, one gets

$$[K_{\alpha\beta}] = [B]^{-1} \cdot ([A_{\alpha\beta}] - [A]) = \begin{bmatrix} k_{\alpha\alpha} & k_{\alpha\beta} & k_{\alpha\alpha} & k_{\alpha\beta} \\ k_{\beta\alpha} & k_{\beta\beta} & k_{\beta\alpha} & k_{\beta\beta} \\ k_{\alpha\alpha} & k_{\alpha\beta} & k_{\alpha\alpha} & k_{\alpha\beta} \\ k_{\beta\alpha} & k_{\beta\beta} & k_{\beta\alpha} & k_{\beta\beta} \end{bmatrix}$$ **(4.22)**

provided that the matrix of the inputs [B] is non-singular. With such state feedback, the system now is decoupled in terms of α and β axes but still presents cross-couplings both between the different three-phase systems (terms a_{13} and a_{24} in equation (4.21)) and between the inputs (non-diagonal terms in matrix [B]). The terms in the state feedback matrix can be calculated as

$$k_{\alpha\alpha} = \frac{-2 \cdot g_{\alpha\beta}^2 \cdot (r_s - 3 \cdot (L_{md} - L_{mq}) \cdot sin(2 \cdot \theta_r)) - g_{\alpha\beta} \cdot 3 \cdot (L_{md} - L_{mq}) \cdot (g_{\beta1\beta1} + g_{\beta1\beta2}) \cdot cos(2 \cdot \theta_r)}{-4 \cdot g_{\alpha\beta}^2 + (g_{\alpha1\alpha1} + g_{\alpha1\alpha2}) \cdot (g_{\beta1\beta1} + g_{\beta1\beta2})}$$

$$k_{\beta\beta} = \frac{-2 \cdot g_{\alpha\beta}^2 \cdot (r_s + 3 \cdot (L_{md} - L_{mq}) \cdot sin(2 \cdot \theta_r)) - g_{\alpha\beta} \cdot 3 \cdot (L_{md} - L_{mq}) \cdot (g_{\alpha1\alpha1} + g_{\alpha1\alpha2}) \cdot cos(2 \cdot \theta_r)}{-4 \cdot g_{\alpha\beta}^2 + (g_{\alpha1\alpha1} + g_{\alpha1\alpha2}) \cdot (g_{\beta1\beta1} + g_{\beta1\beta2})}$$

$$k_{\alpha\beta} = \frac{\frac{3}{2} \cdot (g_{\alpha1\alpha1} + g_{\alpha1\alpha2}) \cdot (g_{\beta1\beta1} + g_{\beta1\beta2}) \cdot (L_{md} - L_{mq}) \cdot cos(2 \cdot \theta_r)}{-4 \cdot g_{\alpha\beta}^2 + (g_{\alpha1\alpha1} + g_{\alpha1\alpha2}) \cdot (g_{\beta1\beta1} + g_{\beta1\beta2})} \\ + \frac{g_{\alpha\beta} \cdot (g_{\beta1\beta1} + g_{\beta1\beta2}) \cdot (r_s + 3 \cdot (L_{md} - L_{mq}) \cdot sin(2 \cdot \theta_r))}{-4 \cdot g_{\alpha\beta}^2 + (g_{\alpha1\alpha1} + g_{\alpha1\alpha2}) \cdot (g_{\beta1\beta1} + g_{\beta1\beta2})}$$

$$k_{\beta\alpha} = \frac{\frac{3}{2} \cdot (g_{\alpha1\alpha1} + g_{\alpha1\alpha2}) \cdot (g_{\beta1\beta1} + g_{\beta1\beta2}) \cdot (L_{md} - L_{mq}) \cdot cos(2 \cdot \theta_r)}{-4 \cdot g_{\alpha\beta}^2 + (g_{\alpha1\alpha1} + g_{\alpha1\alpha2}) \cdot (g_{\beta1\beta1} + g_{\beta1\beta2})} \\ + \frac{g_{\alpha\beta} \cdot (g_{\alpha1\alpha1} + g_{\alpha1\alpha2}) \cdot (r_s - 3 \cdot (L_{md} - L_{mq}) \cdot sin(2 \cdot \theta_r))}{-4 \cdot g_{\alpha\beta}^2 + (g_{\alpha1\alpha1} + g_{\alpha1\alpha2}) \cdot (g_{\beta1\beta1} + g_{\beta1\beta2})}$$

(4.23)

Following the same procedure as in the case of the cross-coupling between the α and β axes, an additional state feedback could be defined to remove the cross-couplings between the different three-phase systems as

$$[A_{\alpha\beta st}] = ([A_{\alpha\beta}] + [B] \cdot [K_{st}]) = \begin{bmatrix} a_{11} & 0 & 0 & 0 \\ 0 & a_{22} & 0 & 0 \\ 0 & 0 & a_{11} & 0 \\ 0 & 0 & 0 & a_{22} \end{bmatrix}$$

(4.24)

leading to the following state feedback law:

$$[K_{st}] = [B]^{-1} \cdot ([A_{\alpha\beta st}] - [A_{\alpha\beta}]) = \begin{bmatrix} k_{st1} & k_{st2} & k_{st3} & k_{st2} \\ k_{st4} & k_{st5} & k_{st4} & k_{st6} \\ k_{st3} & k_{st2} & k_{st1} & k_{st2} \\ k_{st4} & k_{st6} & k_{st4} & k_{st5} \end{bmatrix}$$

(4.25)

which eliminates the cross-couplings between the different three-phase systems in the machine. Calculating the terms of the decoupling matrix in (4.25),

$$k_{st1} = \frac{-2 \cdot g_{\alpha\beta}^2 + g_{\alpha1\alpha2} \cdot (g_{\beta1\beta1} + g_{\beta1\beta2})}{(g_{\alpha1\alpha1} - g_{\alpha1\alpha2}) \cdot \left(-4 \cdot g_{\alpha\beta}^2 + (g_{\alpha1\alpha1} + g_{\alpha1\alpha2}) \cdot (g_{\beta1\beta1} + g_{\beta1\beta2})\right)} \\ \cdot \left(-3 \cdot g_{\alpha\beta} \cdot (L_{md} - L_{mq}) \cdot cos(2 \cdot \theta_r) - g_{\alpha1\alpha2} \cdot \left(r_s - \frac{3}{2} \cdot (L_{md} - L_{mq}) \cdot sin(2 \cdot \theta_r)\right) + \frac{3}{2} \cdot g_{\alpha1\alpha1} \\ \cdot (L_{md} - L_{mq}) \cdot sin(2 \cdot \theta_r)\right)$$

$$k_{st2} = \frac{-3 \cdot g_{\alpha\beta}^2 \cdot (L_{md} - L_{mq}) \cdot cos(2 \cdot \theta_r)}{-4 \cdot g_{\alpha\beta}^2 + (g_{\alpha1\alpha1} + g_{\alpha1\alpha2}) \cdot (g_{\beta1\beta1} + g_{\beta1\beta2})} \\ - \frac{g_{\alpha\beta} \cdot g_{\beta1\beta2} \cdot \left(r_s + \frac{3}{2} \cdot (L_{md} - L_{mq}) \cdot sin(2 \cdot \theta_r)\right) - \frac{3}{2} \cdot g_{\alpha\beta} \cdot g_{\beta1\beta1} \cdot (L_{md} - L_{mq}) \cdot sin(2 \cdot \theta_r)}{-4 \cdot g_{\alpha\beta}^2 + (g_{\alpha1\alpha1} + g_{\alpha1\alpha2}) \cdot (g_{\beta1\beta1} + g_{\beta1\beta2})}$$

(4.26)

$$k_{st3} = \frac{-2 \cdot g_{\alpha\beta}^2 + g_{\alpha1\alpha1} \cdot (g_{\beta1\beta1} + g_{\beta1\beta2})}{(g_{\alpha1\alpha1} - g_{\alpha1\alpha2}) \cdot \left(-4 \cdot g_{\alpha\beta}^2 + (g_{\alpha1\alpha1} + g_{\alpha1\alpha2}) \cdot (g_{\beta1\beta1} + g_{\beta1\beta2})\right)} \\ \cdot \left(3 \cdot g_{\alpha\beta} \cdot (L_{md} - L_{mq}) \cdot cos(2 \cdot \theta_r) + g_{\alpha1\alpha2} \cdot \left(r_s - \frac{3}{2} \cdot (L_{md} - L_{mq}) \cdot sin(2 \cdot \theta_r)\right) - \frac{3}{2} \cdot g_{\alpha1\alpha1} \\ \cdot (L_{md} - L_{mq}) \cdot sin(2 \cdot \theta_r)\right)$$

$$k_{st4} = \frac{-3 \cdot g_{\alpha\beta}^2 \cdot (L_{md} - L_{mq}) \cdot cos(2 \cdot \theta_r)}{-4 \cdot g_{\alpha\beta}^2 + (g_{\alpha1\alpha1} + g_{\alpha1\alpha2}) \cdot (g_{\beta1\beta1} + g_{\beta1\beta2})}$$
$$- \frac{g_{\alpha\beta} \cdot g_{\alpha1\alpha2} \cdot \left(r_s - \frac{3}{2} \cdot (L_{md} - L_{mq}) \cdot sin(2 \cdot \theta_r)\right) - \frac{3}{2} \cdot g_{\alpha\beta} \cdot g_{\alpha1\alpha1} \cdot (L_{md} - L_{mq}) \cdot sin(2 \cdot \theta_r)}{-4 \cdot g_{\alpha\beta}^2 + (g_{\alpha1\alpha1} + g_{\alpha1\alpha2}) \cdot (g_{\beta1\beta1} + g_{\beta1\beta2})}$$

$$k_{st5} = \frac{-2 \cdot g_{\alpha\beta}^2 + g_{\beta1\beta2} \cdot (g_{\alpha1\alpha1} + g_{\alpha1\alpha2})}{(g_{\beta1\beta1} - g_{\beta1\beta2}) \cdot \left(-4 \cdot g_{\alpha\beta}^2 + (g_{\alpha1\alpha1} + g_{\alpha1\alpha2}) \cdot (g_{\beta1\beta1} + g_{\beta1\beta2})\right)}$$
$$\cdot \left(-3 \cdot g_{\alpha\beta} \cdot (L_{md} - L_{mq}) \cdot cos(2 \cdot \theta_r) - g_{\beta1\beta2} \cdot \left(r_s + \frac{3}{2} \cdot (L_{md} - L_{mq}) \cdot sin(2 \cdot \theta_r)\right) + \frac{3}{2} \cdot g_{\beta1\beta1}\right.$$
$$\left. \cdot (L_{md} - L_{mq}) \cdot sin(2 \cdot \theta_r)\right)$$

$$k_{st6} = \frac{-2 \cdot g_{\alpha\beta}^2 + g_{\beta1\beta1} \cdot (g_{\alpha1\alpha1} + g_{\alpha1\alpha2})}{(g_{\beta1\beta1} - g_{\beta1\beta2}) \cdot \left(-4 \cdot g_{\alpha\beta}^2 + (g_{\alpha1\alpha1} + g_{\alpha1\alpha2}) \cdot (g_{\beta1\beta1} + g_{\beta1\beta2})\right)}$$
$$\cdot \left(3 \cdot g_{\alpha\beta} \cdot (L_{md} - L_{mq}) \cdot cos(2 \cdot \theta_r) + g_{\beta1\beta2} \cdot \left(r_s + \frac{3}{2} \cdot (L_{md} - L_{mq}) \cdot sin(2 \cdot \theta_r)\right) + \frac{3}{2} \cdot g_{\beta1\beta1}\right.$$
$$\left. \cdot (L_{md} - L_{mq}) \cdot sin(2 \cdot \theta_r)\right)$$

Now the only cross-coupling left is the one regarding the inputs, which implies that the stator's voltage in one three-phase system affects the currents in the other system(s) making the control of each of them difficult. To overcome this limitation, a gain K_{in} can be introduced in the input path so that

$$[B] \cdot [K_{in}] = [I] \tag{4.27}$$

where [I] is the identity matrix. Then, the input gain matrix can be calculated as

$$[K_{in}] = [B]^{-1} = \begin{bmatrix} k_{in1} & k_{in2} & k_{in3} & k_{in2} \\ k_{in2} & k_{in4} & k_{in2} & k_{in5} \\ k_{in3} & k_{in2} & k_{in1} & k_{in2} \\ k_{in2} & k_{in5} & k_{in2} & k_{in4} \end{bmatrix}$$

$$k_{in1} = \frac{-\left(2 \cdot g_{\alpha\beta}^2 - g_{\alpha1\alpha1} \cdot (g_{\beta1\beta1} + g_{\beta1\beta2})\right)}{(g_{\alpha1\alpha1} - g_{\alpha1\alpha2}) \cdot \left(-4 \cdot g_{\alpha\beta}^2 + (g_{\alpha1\alpha1} + g_{\alpha1\alpha2}) \cdot (g_{\beta1\beta1} + g_{\beta1\beta2})\right)} \tag{4.28}$$

$$k_{in2} = \frac{-g_{\alpha\beta}}{-4 \cdot g_{\alpha\beta}^2 + (g_{\alpha1\alpha1} + g_{\alpha1\alpha2}) \cdot (g_{\beta1\beta1} + g_{\beta1\beta2})}$$

$$k_{in3} = \frac{\left(2 \cdot g_{\alpha\beta}^2 - g_{\alpha1\alpha2} \cdot (g_{\beta1\beta1} + g_{\beta1\beta2})\right)}{(g_{\alpha1\alpha1} - g_{\alpha1\alpha2}) \cdot \left(-4 \cdot g_{\alpha\beta}^2 + (g_{\alpha1\alpha1} + g_{\alpha1\alpha2}) \cdot (g_{\beta1\beta1} + g_{\beta1\beta2})\right)}$$

$$k_{in4} = \frac{\left(-2 \cdot g_{\alpha\beta}^2 + g_{\beta1\beta1} \cdot (g_{\alpha1\alpha1} + g_{\alpha1\alpha2})\right)}{(g_{\beta1\beta1} - g_{\beta1\beta2}) \cdot \left(-4 \cdot g_{\alpha\beta}^2 + (g_{\alpha1\alpha1} + g_{\alpha1\alpha2}) \cdot (g_{\beta1\beta1} + g_{\beta1\beta2})\right)}$$

$$k_{in5} = \frac{\left(2 \cdot g_{\alpha\beta}^2 - g_{\beta1\beta2} \cdot (g_{\alpha1\alpha1} + g_{\alpha1\alpha2})\right)}{(g_{\beta1\beta1} - g_{\beta1\beta2}) \cdot \left(-4 \cdot g_{\alpha\beta}^2 + (g_{\alpha1\alpha1} + g_{\alpha1\alpha2}) \cdot (g_{\beta1\beta1} + g_{\beta1\beta2})\right)}$$

Applying this complete decoupling strategy, the machine equations in the stationary reference frame get fully decoupled as both the states and the input matrices are diagonal in form. An important remark here is that the decoupling terms $g_{\alpha i \alpha j}$, $g_{\beta i \beta j}$ and $g_{\alpha\beta}$ depend on the rotor position (θ_r); hence its values need to be updated at each sampling period of the control, thus increasing the computational burden.

The combination of all these manipulations leads to a totally decoupled model of a machine with multiple three-phase systems in the stationary reference frame with the following state space representation:

$$[\dot{X}] = [A_{\alpha\beta st}] \cdot [X] + [I] \cdot [u_c] \qquad [Y] = [X] \qquad [X] = [i_{\alpha 1}, i_{\beta 1}, i_{\alpha 2}, i_{\beta 2}]^T \qquad [u_c] = [v_{\alpha 1c}, v_{\beta 1c}, v_{\alpha 2c}, v_{\beta 2c}]^T \qquad \textbf{(4.29)}$$

Writing the equations on per axis basis, the following equations apply for the current control loops:

$$\frac{di_{\alpha 1}}{dt} = -r_s \cdot g_{\alpha 1 \alpha 1} \cdot i_{\alpha 1} + v_{\alpha 1c} \qquad \frac{di_{\beta 1}}{dt} = -r_s \cdot g_{\beta 1 \beta 1} \cdot i_{\beta 1} + v_{\beta 1c}$$

$$\textbf{(4.30)}$$

$$\frac{di_{\alpha 2}}{dt} = -r_s \cdot g_{\alpha 1 \alpha 1} \cdot i_{\alpha 2} + v_{\alpha 2c} \qquad \frac{di_{\beta 2}}{dt} = -r_s \cdot g_{\beta 1 \beta 1} \cdot i_{\beta 2} + v_{\beta 2c}$$

resulting in a fully decoupled model with a first-order inductive plant in each of the axis. Again, it has to be noted that the plant of the current regulators has time-varying coefficients that make difficult the proper tuning. The effects of each decoupling term can be seen in Fig. 4.1, where Bode plots are shown for a set of transfer functions that relate outputs and inputs. The 2-pt black line represents the behaviour when both $K_{\alpha\beta}$ and K_{st} decouplings are activated. It can be seen how only the plots on the diagonal (those representing the effect of one input on its corresponding output) are near the 0 dB line meaning a unitary gain. The non-diagonal terms are almost zero meaning that the other inputs have no effect on the output (decoupled behaviour). The individual contribution of each of the decoupling terms can be seen in the 2-pt grey line (only K_{st} is activated) and in the 1-pt grey one (only $K_{\alpha\beta}$ is active). The 1-pt black line represents the machine's original behaviour (both decoupling terms deactivated).
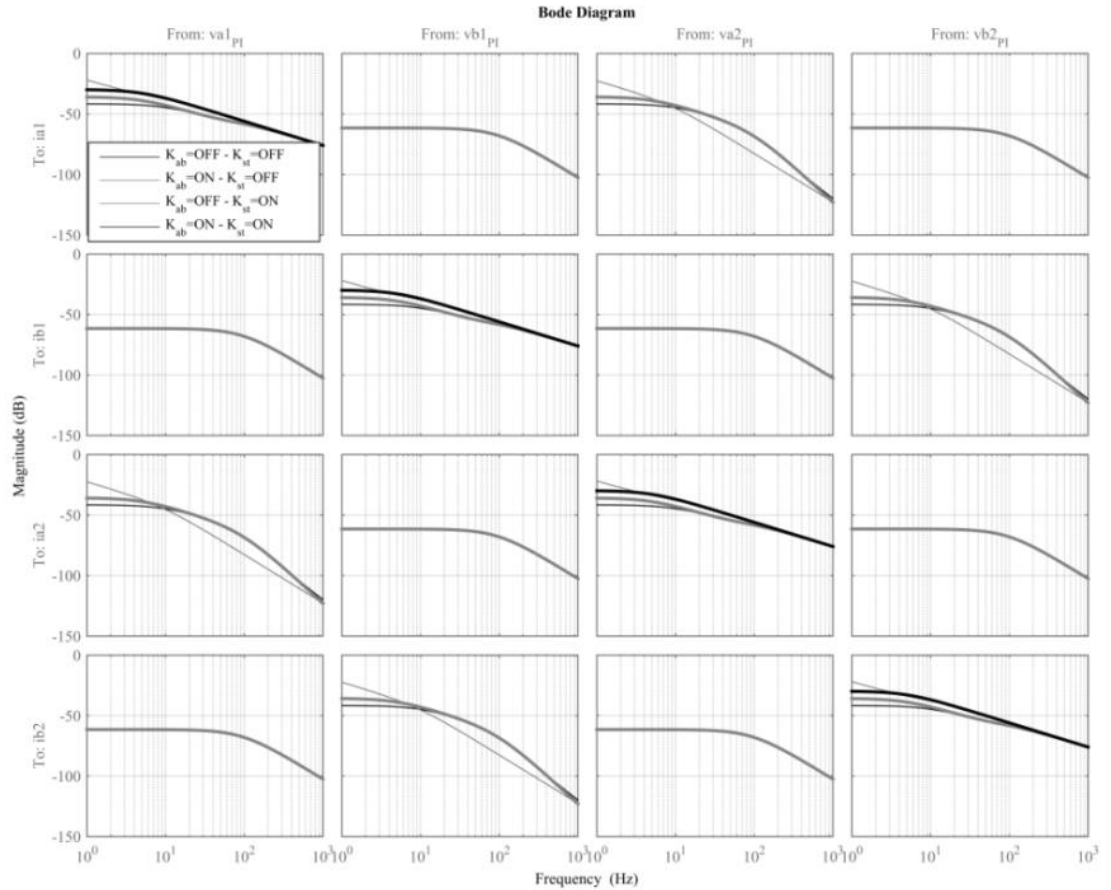
Fig. 4.1 Magnitude Bode plots for transfer functions from inputs $v_{\alpha 1c}$, $v_{\beta 1c}$, $v_{\alpha 2c}$, $v_{\beta 2c}$ (columns 1 to 4, respectively) to outputs $i_{\alpha 1}$, $i_{\beta 1}$, $i_{\alpha 2}$, $i_{\beta 2}$ (rows 1 to 4, respectively) with different decoupling setups. The frequency is expressed with respect to the stationary reference frame.

From equations (4.10) and (4.11), it can be seen that the terms in the inductance matrix and the transformed rotor flux are dependent on the rotor angle (θ_r). This means that the application of the rotational transformation into the synchronous reference may be beneficial, resulting in

$$[L_s]_{t+r} = \begin{bmatrix} L_{ls} + \frac{3}{2} \cdot L_{md} & 0 & 0 & \frac{3}{2} \cdot L_{md} & 0 & 0 \\ 0 & L_{ls} + \frac{3}{2} \cdot L_{mq} & 0 & 0 & \frac{3}{2} \cdot L_{mq} & 0 \\ 0 & 0 & L_{ls} & 0 & 0 & 0 \\ \frac{3}{2} \cdot L_{md} & 0 & 0 & L_{ls} + \frac{3}{2} \cdot L_{md} & 0 & 0 \\ 0 & \frac{3}{2} \cdot L_{mq} & 0 & 0 & L_{ls} + \frac{3}{2} \cdot L_{mq} & 0 \\ 0 & 0 & 0 & 0 & 0 & L_{ls} \end{bmatrix}$$ **(4.31)**

$$[\Psi_{PM}]_{t+r} = \psi_{PM} \cdot [1 \quad 0 \quad 0 \quad 1 \quad 0 \quad 0]^T \qquad [T] \cdot \frac{d([T]^{-1})}{dt} = \omega_r \cdot \begin{pmatrix} [a] & [b] \\ [b] & [a] \end{pmatrix}$$

where the dependence on the rotor position is eliminated, thus obtaining the inductance matrix with constant coefficients. From (4.31), it can be concluded that applying the double d-q transformation to a six-phase machine yields a constant coefficient inductance matrix, but it is not diagonal in form. This highlights the cross-coupling present between the different three-phase systems in the machine.

Substituting all the terms in equation (4.6) and re-arranging the terms to follow the state-space representation,

$$\frac{d([i_s]_{t+r})}{dt} = [L_s]_{t+r}^{-1} \cdot \left([V_s]_{t+r} - [R_s] \cdot [i_s]_{t+r} - \omega_r \cdot \begin{pmatrix} [a] & [b] \\ [b] & [a] \end{pmatrix} \cdot ([L_s]_{t+r} \cdot [i_s]_{t+r} + [\Psi_{PM}]_{t+r}) \right)$$ **(4.32)**

results. To simplify the representation, the following matrices

$$[a] = \begin{bmatrix} 0 & -1 & 0 \\ 1 & 0 & 0 \\ 0 & 0 & 0 \end{bmatrix} \qquad [b] = \begin{bmatrix} 0 & 0 & 0 \\ 0 & 0 & 0 \\ 0 & 0 & 0 \end{bmatrix}$$ **(4.33)**

have been defined. The expressions of the equations for each of the axes can be obtained for a six-phase machine in the following form:

$$\frac{di_{d1}}{dt} = g_{d11} \cdot \left(v_{d1} - r_s \cdot i_{d1} + \omega_r \cdot \left(\left(L_{ls} + \frac{3}{2} \cdot L_{mq} \right) \cdot i_{q1} + \frac{3}{2} \cdot L_{mq} \cdot i_{q2} \right) \right) + g_{d12}$$
$$\cdot \left(v_{d2} - r_s \cdot i_{d2} + \omega_r \cdot \left(\frac{3}{2} \cdot L_{mq} \cdot i_{q1} + \left(L_{ls} + \frac{3}{2} \cdot L_{mq} \right) \cdot i_{q2} \right) \right)$$

$$\frac{di_{q1}}{dt} = g_{q11} \cdot \left(v_{q1} - r_s \cdot i_{q1} - \omega_r \cdot \left(\psi_{PM} + \left(L_{ls} + \frac{3}{2} \cdot L_{md} \right) \cdot i_{d1} + \frac{3}{2} \cdot L_{md} \cdot i_{d2} \right) \right) + g_{q12}$$
$$\cdot \left(v_{q2} - r_s \cdot i_{q2} - \omega_r \cdot \left(\psi_{PM} + \frac{3}{2} \cdot L_{md} \cdot i_{d1} + \left(L_{ls} + \frac{3}{2} \cdot L_{md} \right) \cdot i_{d2} \right) \right)$$

$$\frac{di_{d2}}{dt} = g_{d21} \cdot \left(v_{d1} - r_s \cdot i_{d1} + \omega_r \cdot \left(\left(L_{ls} + \frac{3}{2} \cdot L_{mq} \right) \cdot i_{q1} + \frac{3}{2} \cdot L_{mq} \cdot i_{q2} \right) \right) + g_{d22}$$ **(4.34)**
$$\cdot \left(v_{d2} - r_s \cdot i_{d2} + \omega_r \cdot \left(\frac{3}{2} \cdot L_{mq} \cdot i_{q1} + \left(L_{ls} + \frac{3}{2} \cdot L_{mq} \right) \cdot i_{q2} \right) \right)$$

$$\frac{di_{q2}}{dt} = g_{q21} \cdot \left(v_{q1} - r_s \cdot i_{q1} - \omega_r \cdot \left(\psi_{PM} + \left(L_{ls} + \frac{3}{2} \cdot L_{md} \right) \cdot i_{d1} + \frac{3}{2} \cdot L_{mq} \cdot i_{d2} \right) \right) + g_{q22}$$
$$\cdot \left(v_{q2} - r_s \cdot i_{q2} - \omega_r \cdot \left(\psi_{PM} + \frac{3}{2} \cdot L_{md} \cdot i_{d1} + \left(L_{ls} + \frac{3}{2} \cdot L_{md} \right) \cdot i_{d2} \right) \right)$$

where v_{dk}, v_{qk} and i_{dk}, i_{qk} are the d- and q-axis voltages and currents in the three-phase system number k and the coefficients g_d and g_q can be calculated as

$$g_{d11} = g_{d22} = \frac{2 \cdot L_{ls} + 3 \cdot L_{md}}{2 \cdot L_{ls} \cdot (L_{ls} + 3 \cdot L_{md})} \qquad g_{d12} = g_{d21} = \frac{-3 \cdot L_{md}}{2 \cdot L_{ls} \cdot (L_{ls} + 3 \cdot L_{md})}$$

$$g_{q12} = g_{q21} = \frac{-3 \cdot L_{mq}}{2 \cdot L_{ls} \cdot (L_{ls} + 3 \cdot L_{mq})} \qquad g_{q11} = g_{q22} = \frac{2 \cdot L_{ls} + 3 \cdot L_{mq}}{2 \cdot L_{ls} \cdot (L_{ls} + 3 \cdot L_{mq})}$$

(4.35)

The g_{dij} and g_{qij} coefficients with $i{\neq}j$ account for the cross-coupling that exists between the different three-phase systems in the machine. It can be seen how, as the leakage inductance (L_{ls}) increases, the weight of these terms is reduced in comparison with those with $i{=}j$. These cross-coupling terms make it very difficult to tune the current regulators in both d and q axes as the d-axis current in the three-phase system number one is influenced, through g_{d12}, by the d-axis voltage (v_{d2}) in the three-phase system number two. All this implies that the d-axis (q-axis) current in any of the three-phase systems in the machine will be governed by two, in principle independent, inputs v_{d1} and v_{d2} (v_{q1} and v_{q2}).

By compensating the inputs in the q-axis with the terms related to the flux of the permanent magnets, equation (4.34) is simplified as

$$\frac{di_{q1}}{dt} = g_{q11} \cdot \left(v_{q1c} - r_s \cdot i_{q1} - \omega_r \cdot \left(\left(L_{ls} + \frac{3}{2} \cdot L_{md} \right) \cdot i_{d1} + \frac{3}{2} \cdot L_{md} \cdot i_{d2} \right) \right) + g_{q12}$$
$$\cdot \left(v_{q2c} - r_s \cdot i_{q2} - \omega_r \cdot \left(\frac{3}{2} \cdot L_{md} \cdot i_{d1} + \left(L_{ls} + \frac{3}{2} \cdot L_{md} \right) \cdot i_{d2} \right) \right)$$

$$\frac{di_{q2}}{dt} = g_{q21} \cdot \left(v_{q1c} - r_s \cdot i_{q1} - \omega_r \cdot \left(\left(L_{ls} + \frac{3}{2} \cdot L_{md} \right) \cdot i_{d1} + \frac{3}{2} \cdot L_{mq} \cdot i_{d2} \right) \right) + g_{q22}$$
$$\cdot \left(v_{q2c} - r_s \cdot i_{q2} - \omega_r \cdot \left(\frac{3}{2} \cdot L_{md} \cdot i_{d1} + \left(L_{ls} + \frac{3}{2} \cdot L_{md} \right) \cdot i_{d2} \right) \right)$$

(4.36)

where v_{qkc} are the compensated inputs of the q-axis in the k-th three-phase system,

$$v_{dkc} = v_{dk}$$
$$v_{qkc} = v_{qk} + \omega_r \cdot \psi_{PM}$$

(4.37)

Constructing the matrices of the state-space representation, while considering the output matrix $[C]$ as equal to an identity matrix, yields:

$$[\dot{X}] = [A] \cdot [X] + [B] \cdot [u_c] \qquad [Y] = [X]$$

$$[X] = [i_{d1}, i_{q1}, i_{d2}, i_{q2}]^T \qquad [u_c] = [v_{d1c}, v_{q1c}, v_{d2c}, v_{q2c}]^T$$

$$[A] = \begin{bmatrix} a_{11} & a_{12} & a_{13} & a_{14} \\ a_{21} & a_{22} & a_{23} & a_{24} \\ a_{13} & a_{14} & a_{11} & a_{12} \\ a_{23} & a_{24} & a_{21} & a_{22} \end{bmatrix}$$

(4.38)

$$a_{11} = -g_{d11} \cdot r_s \qquad a_{12} = g_{d11} \cdot \omega_r \cdot \left(L_{ls} + \frac{3}{2} \cdot L_{mq} \right) + g_{d12} \cdot \omega_r \cdot \frac{3}{2} \cdot L_{mq}$$

$$a_{13} = -g_{d12} \cdot r_s \qquad a_{14} = g_{d11} \cdot \omega_r \cdot \frac{3}{2} \cdot L_{mq} + g_{d12} \cdot \omega_r \cdot \left(L_{ls} + \frac{3}{2} \cdot L_{mq} \right)$$

$$a_{21} = -g_{q11} \cdot \omega_r \cdot \left(L_{ls} + \frac{3}{2} \cdot L_{md} \right) - g_{q12} \cdot \omega_r \cdot \frac{3}{2} \cdot L_{md} \qquad a_{22} = -g_{q11} \cdot r_s$$

$$a_{23} = -g_{q11} \cdot \omega_r \cdot \frac{3}{2} \cdot L_{md} - g_{q12} \cdot \omega_r \cdot \left(L_{ls} + \frac{3}{2} \cdot L_{md} \right) \qquad a_{24} = -g_{q12} \cdot r_s$$

$$[B] = \begin{bmatrix} g_{d11} & 0 & g_{d12} & 0 \\ 0 & g_{q11} & 0 & g_{q12} \\ g_{d12} & 0 & g_{d11} & 0 \\ 0 & g_{q12} & 0 & g_{q11} \end{bmatrix}$$

The system's cross-couplings become evident in the matrix [A]. This matrix has non-zero elements in all the positions, meaning a heavy cross-coupling. The reduction of these cross-couplings can be made in a similar manner as done above for the stationary reference frame, yielding the following decoupling matrices:

$$[K_{dq}] = [B]^{-1} \cdot ([A_{dq}] - [A]) = \begin{bmatrix} 0 & k_{d1} & 0 & k_{d2} \\ k_{q1} & 0 & k_{q2} & 0 \\ 0 & k_{d2} & 0 & k_{d1} \\ k_{q2} & 0 & k_{q1} & 0 \end{bmatrix} \qquad \textbf{(4.39)}$$

$$k_{d1} = -\omega_r \cdot \left(L_{ls} + \frac{3}{2} \cdot L_{mq}\right) \quad k_{d2} = -\omega_r \cdot \frac{3}{2} \cdot L_{mq} \quad k_{q1} = \omega_r \cdot \left(L_{ls} + \frac{3}{2} \cdot L_{md}\right) \quad k_{q2} = \omega_r \cdot \frac{3}{2} \cdot L_{md}$$

$$[K_{st}] = [B]^{-1} \cdot ([A_{dqst}] - [A_{dq}]) = \begin{bmatrix} k_{st1} & 0 & k_{st2} & 0 \\ 0 & k_{st3} & 0 & k_{st4} \\ k_{st2} & 0 & k_{st1} & 0 \\ 0 & k_{st4} & 0 & k_{st3} \end{bmatrix} \qquad \textbf{(4.40)}$$

$$k_{st1} = -\frac{g_{d12}^2}{g_{d11}^2 - g_{d12}^2} \cdot r_s \qquad k_{st2} = \frac{g_{d11} \cdot g_{d12}}{g_{d11}^2 - g_{d12}^2} \cdot r_s \qquad k_{st3} = -\frac{g_{q12}^2}{g_{q11}^2 - g_{q12}^2} \cdot r_s \qquad k_{st4} = \frac{g_{q11} \cdot g_{q12}}{g_{q11}^2 - g_{q12}^2} \cdot r_s$$

$$[K_{in}] = [B]^{-1} = \begin{bmatrix} k_{in1} & 0 & k_{in2} & 0 \\ 0 & k_{in3} & 0 & k_{in4} \\ k_{in2} & 0 & k_{in1} & 0 \\ 0 & k_{in4} & 0 & k_{in3} \end{bmatrix} \qquad \textbf{(4.41)}$$

$$k_{in1} = \frac{g_{d11}}{g_{d11}^2 - g_{d12}^2} \qquad k_{in2} = -\frac{g_{d12}}{g_{d11}^2 - g_{d12}^2} \qquad k_{in3} = \frac{g_{q11}}{g_{q11}^2 - g_{q12}^2} \qquad k_{in4} = -\frac{g_{q12}}{g_{q11}^2 - g_{q12}^2}$$

The combination of all these manipulations leads to a totally decoupled model of a multiple three-phase systems machine following the multiple *dq* approach with the following state space representation

$$[\dot{X}] = [A_{dqst}] \cdot [X] + [I] \cdot [u_c] \qquad [Y] = [X] \qquad \textbf{(4.42)}$$

$$[X] = [i_{d1}, i_{q1}, i_{d2}, i_{q2}]^T \qquad [u_c] = [v_{d1c}, v_{q1c}, v_{d2c}, v_{q2c}]^T$$

Writing the equations on per axis basis, the following equations apply for the current control loops:

$$\frac{di_{d1}}{dt} = -r_s \cdot g_{d11} \cdot i_{d1} + v_{d1c} \qquad \frac{di_{q1}}{dt} = -r_s \cdot g_{q11} \cdot i_{q1} + v_{q1c} \qquad \textbf{(4.43)}$$

$$\frac{di_{d2}}{dt} = -r_s \cdot g_{d11} \cdot i_{d2} + v_{d2c} \qquad \frac{di_{q2}}{dt} = -r_s \cdot g_{q11} \cdot i_{q2} + v_{q2c}$$

resulting in a fully decoupled model with a first-order inductive plant on each of the axes. The effects of each decoupling terms can be seen in Fig. 4.2, where Bode plots are shown for a set of transfer functions that relate outputs and inputs. The 2-pt black line represents the behaviour when both K_{dq} and K_{st} decouplings are activated. It can be seen how only the plots in the diagonal (those representing the effect of one input on its corresponding output) are near the 0 dB line meaning a unitary gain. The non-diagonal terms are almost zero meaning that the other inputs have no effect on the output (decoupled behaviour). The individual contribution of each of the decoupling terms can be seen in the 1-pt grey line (only K_{dq} is activated) and in the 2-pt grey one (only K_{st} is active). The 1-pt black line represents the machine's original behaviour (both decoupling terms deactivated).
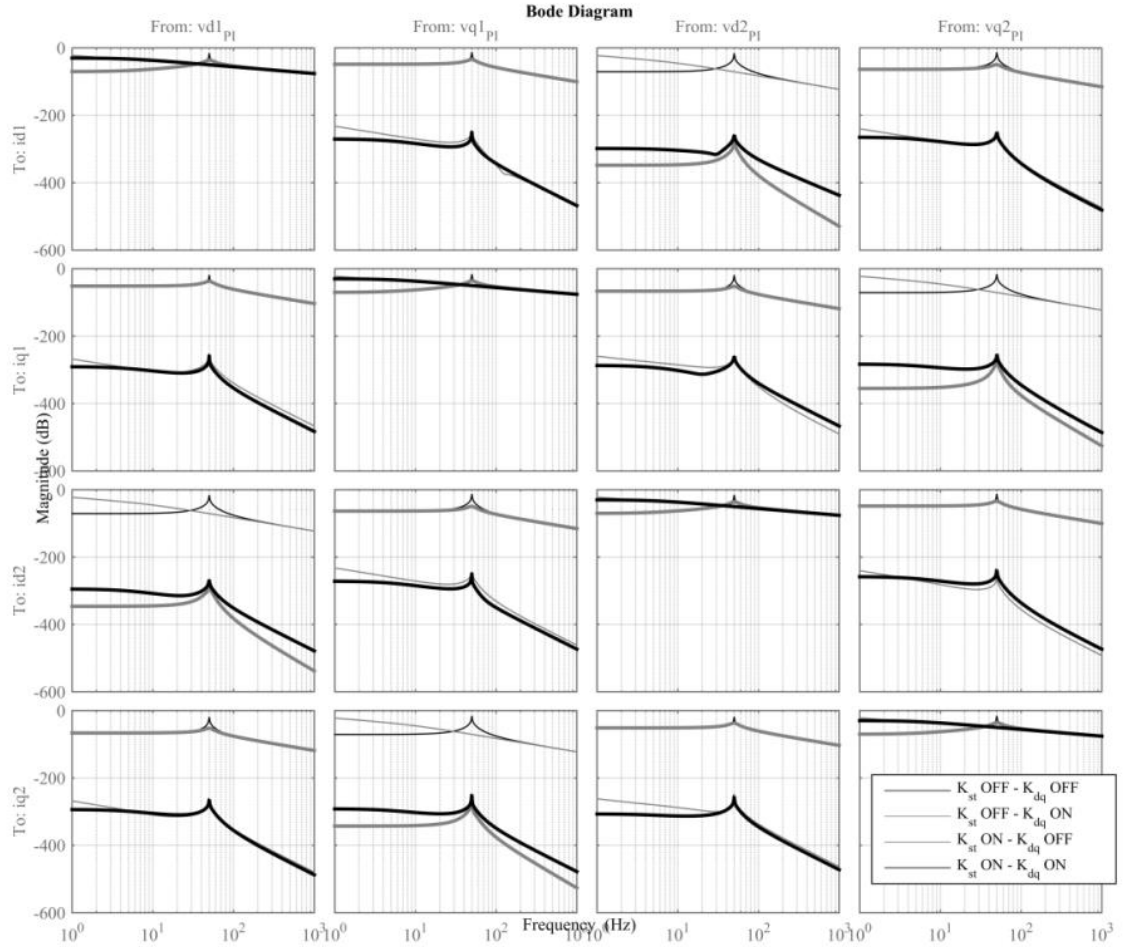
Fig. 4.2 Magnitude Bode plots for transfer functions from inputs v_{d1}, v_{q1}, v_{d2}, v_{q2} (columns 1 to 4, respectively) to outputs i_{d1}, i_{q1}, i_{d2}, i_{q2} (rows 1 to 4, respectively) with different decoupling setups. The frequency is expressed relative to the rotating reference frame (50 Hz).

The electromagnetic torque equation can be derived from the equation of the stator's electrical power,

$$P_s = \frac{3}{2} \cdot \sum_{j=1}^{k} \left(v_{dj} \cdot i_{dj} + v_{qj} \cdot i_{qj} \right) \tag{4.44}$$

by substituting the voltage terms with their steady state expressions obtained from equation (4.6). In (4.44), taking away the stator's winding losses, substituting the fluxes by their expressions as functions of the stator's currents and dividing by the mechanical speed, the torque expression is obtained as

$$T_{elec} = \frac{3}{2} \cdot p \cdot \sum_{j=1}^{k} \left(\psi_{PM} \cdot i_{qj} + \left(L_d - L_q \right) \cdot i_{dj} \cdot i_{qj} \right) \tag{4.45}$$

where p stands for the number of pole pairs and k is the number of three-phase systems in the machine. Two distinct terms can be observed:

- $\psi_{PM} \cdot i_{qj}$, which accounts for the torque produced due to the interaction between the stator's and rotor's fluxes
- $\left(L_d - L_q \right) \cdot i_{dj} \cdot i_{qj}$, which represents the torque produced by the variation in the reluctance of the magnetic circuit (reluctance torque). In machines without saliency, this is negligible but it becomes more important as the saliency increases.

Defining α_c as the angle between the stator's current vector and the rotor's flux, the equation (4.45) can be rewritten as,

$$i_{dj} = I_{sj} \cdot cos(\alpha_c) \qquad i_{qj} = I_{sj} \cdot sin(\alpha_c)$$

$$T_{elec} = \frac{3}{2} \cdot p \cdot \sum_{j=1}^{k} \left(\psi_{PM} \cdot I_{sj} \cdot sin(\alpha_c) + \frac{1}{2} \cdot \left(L_d - L_q \right) \cdot I_{sj}^2 \cdot sin(2 \cdot \alpha_c) \right) \tag{4.46}$$

giving an expression of the torque as a function of the stator current amplitude (I_{sj}) and its relative angle with respect to the rotor flux (α_c).

Manipulating the equation (4.45) to isolate the sum of the q-axis currents,

$$\sum_{j=1}^{k} (i_{qj})^* = \frac{T_{elec}^*}{\frac{3}{2} \cdot p \cdot \left(k \cdot \psi_{PM} + \left(L_d - L_q \right) \cdot \sum_{j=1}^{k} (i_{dj}) \right)} \tag{4.47}$$

an expression of the required sum of the q-axis currents, required to produce a certain torque, is obtained. The superscript * stands for references. By means of equation (4.47), a torque command can be translated into a current command.

4.2.1.2 Models resulting from vector space decomposition approach

To follow the VSD approach, the same procedure followed in 4.2.1.1 is to be applied, with the only difference in the transformation matrix to be used. In this case, the transformation matrix required is the one shown in (3.20) for a six-phase machine.

Calculating the unknown terms (4.9) for a six-phase machine,

$$[L_s]_t = \begin{bmatrix} L_{ls} + 2 \cdot L_{\alpha\alpha} & 2 \cdot L_{\alpha\beta} & 0 & 0 & 0 & 0 \\ 2 \cdot L_{\alpha\beta} & L_{ls} + 2 \cdot L_{\beta\beta} & 0 & 0 & 0 & 0 \\ 0 & 0 & L_{ls} & 0 & 0 & 0 \\ 0 & 0 & 0 & L_{ls} & 0 & 0 \\ 0 & 0 & 0 & 0 & L_{ls} & 0 \\ 0 & 0 & 0 & 0 & 0 & L_{ls} \end{bmatrix} \tag{4.48}$$

$$[\Psi_{PM}]_t = \psi_{PM} \cdot [cos(\theta_r) \quad sin(\theta_r) \quad 0 \quad 0 \quad 0 \quad 0]^T$$

the transformed inductance matrix and permanent magnet's flux vector are obtained where the values of $L_{\alpha\alpha}$, $L_{\beta\beta}$ and $L_{\alpha\beta}$ are those shown in (4.11). It can be seen that the terms in the inductance matrix and the transformed rotor flux are dependent on the rotor angle (θ_r), but comparing the inductance matrices in (4.10) and (4.48), it easy to see that the VSD approach yields a sparser inductance matrix (closer to the diagonal one in form). Another important aspect to highlight is that the inductance matrix would be diagonal in form if the terms $L_{\alpha\beta}$ were zero. With the definition in (4.11), it can be seen how this

happens if L_{md} equals L_{mq}, meaning a lack of saliency in the machine. Rearranging the equations to follow the state space notation,

$$\frac{di_\alpha}{dt} = g_{\alpha\alpha} \cdot (v_\alpha - r_s \cdot i_\alpha + \omega_r \cdot \psi_{PM} \cdot sin(\theta_r) + 3 \cdot (L_{md} - L_{mq}) \cdot (i_\alpha \cdot sin(2 \cdot \theta_r) - i_\beta \cdot cos(2 \cdot \theta_r)) + g_{\alpha\beta}$$
$$\cdot (v_\beta - r_s \cdot i_\beta - \omega_r \cdot \psi_{PM} \cdot cos(\theta_r) - 3 \cdot (L_{md} - L_{mq}) \cdot (i_\alpha \cdot cos(2 \cdot \theta_r) + i_\beta \cdot sin(2 \cdot \theta_r)))$$

$$\frac{di_\beta}{dt} = g_{\alpha\beta} \cdot (v_\alpha - r_s \cdot i_\alpha + \omega_r \cdot \psi_{PM} \cdot sin(\theta_r) + 3 \cdot (L_{md} - L_{mq}) \cdot (i_\alpha \cdot sin(2 \cdot \theta_r) - i_\beta \cdot cos(2 \cdot \theta_r)) + g_{\beta\beta}$$
$$\cdot (v_\beta - r_s \cdot i_\beta - \omega_r \cdot \psi_{PM} \cdot cos(\theta_r) - 3 \cdot (L_{md} - L_{mq}) \cdot (i_\alpha \cdot cos(2 \cdot \theta_r) + i_\beta \cdot sin(2 \cdot \theta_r)))$$

(4.49)

$$\frac{di_x}{dt} = g_{xy} \cdot (v_x - r_s \cdot i_x) \qquad \frac{di_y}{dt} = g_{xy} \cdot (v_y - r_s \cdot i_y)$$

where v_α, v_β, v_x, v_y and i_α, i_β, i_x, i_y are the α-, β-, x- and y-axis voltages and currents in the machine and the coefficients $g_{\alpha\alpha}$, $g_{\alpha\beta}$, $g_{\beta\beta}$ and g_{xy} can be calculated as

$$g_{\alpha\alpha} = \frac{2 \cdot L_{ls} + 3 \cdot (L_{md} + L_{mq}) - 3 \cdot (L_{md} - L_{mq}) \cdot cos(2 \cdot \theta_r)}{2 \cdot (L_{ls} + 3 \cdot L_{md}) \cdot (L_{ls} + 3 \cdot L_{mq})}$$

$$g_{\beta\beta} = \frac{2 \cdot L_{ls} + 3 \cdot (L_{md} + L_{mq}) + 3 \cdot (L_{md} - L_{mq}) \cdot cos(2 \cdot \theta_r)}{2 \cdot (L_{ls} + 3 \cdot L_{md}) \cdot (L_{ls} + 3 \cdot L_{mq})}$$

(4.50)

$$g_{\alpha\beta} = \frac{-3 \cdot (L_{md} - L_{mq}) \cdot sin(2 \cdot \theta_r)}{2 \cdot (L_{ls} + 3 \cdot L_{md}) \cdot (L_{ls} + 3 \cdot L_{mq})} \qquad g_{xy} = \frac{1}{L_{ls}}$$

By compensating the inputs with the terms related to the flux of the permanent magnets, the first two equations in (4.49) are simplified into

$$\frac{di_\alpha}{dt} = g_{\alpha\alpha} \cdot (v_{\alpha c} - r_s \cdot i_\alpha + 3 \cdot (L_{md} - L_{mq}) \cdot (i_\alpha \cdot sin(2 \cdot \theta_r) - i_\beta \cdot cos(2 \cdot \theta_r)) + g_{\alpha\beta}$$
$$\cdot (v_{\beta c} - r_s \cdot i_\beta - 3 \cdot (L_{md} - L_{mq}) \cdot (i_\alpha \cdot cos(2 \cdot \theta_r) + i_\beta \cdot sin(2 \cdot \theta_r)))$$

(4.51)

$$\frac{di_\beta}{dt} = g_{\alpha\beta} \cdot (v_{\alpha c} - r_s \cdot i_\alpha + 3 \cdot (L_{md} - L_{mq}) \cdot (i_\alpha \cdot sin(2 \cdot \theta_r) - i_\beta \cdot cos(2 \cdot \theta_r)) + g_{\beta\beta}$$
$$\cdot (v_{\beta c} - r_s \cdot i_\beta - 3 \cdot (L_{md} - L_{mq}) \cdot (i_\alpha \cdot cos(2 \cdot \theta_r) + i_\beta \cdot sin(2 \cdot \theta_r)))$$

where $v_{\alpha c}$ and $v_{\beta c}$ are the compensated voltages in the α and β axes in the machine, and their expressions are,

$$v_{\alpha c} = v_\alpha - \omega_r \cdot \psi_{PM} \cdot sin(\theta_r) \qquad v_{\beta c} = v_\beta + \omega_r \cdot \psi_{PM} \cdot cos(\theta_r)$$

(4.52)

Constructing the matrices of the state-space representation from equation (4.49), while considering the output matrix $[C]$ as equal to an identity matrix, yields:

$$[\dot{X}] = [A] \cdot [X] + [B] \cdot [u] \qquad [Y] = [X] \qquad [X] = [i_\alpha, i_\beta, i_x, i_y]^T \qquad [u_c] = [v_{\alpha c}, v_{\beta c}, v_x, v_y]^T$$

$$[A] = \begin{bmatrix} a_{11} & a_{12} & 0 & 0 \\ a_{21} & a_{22} & 0 & 0 \\ 0 & 0 & a_{33} & 0 \\ 0 & 0 & 0 & a_{44} \end{bmatrix}$$

(4.53)

$$a_{11} = -g_{\alpha\alpha} \cdot (r_s - 3 \cdot (L_{md} - L_{mq}) \cdot sin(2 \cdot \theta_r)) - g_{\alpha\beta} \cdot 3 \cdot (L_{md} - L_{mq}) \cdot cos(2 \cdot \theta_r)$$

$$a_{12} = -g_{\alpha\alpha} \cdot 3 \cdot (L_{md} - L_{mq}) \cdot cos(2 \cdot \theta_r) - g_{\alpha\beta} \cdot (r_s + 3 \cdot (L_{md} - L_{mq}) \cdot sin(2 \cdot \theta_r))$$

$$a_{21} = -g_{\beta\beta} \cdot 3 \cdot (L_{md} - L_{mq}) \cdot cos(2 \cdot \theta_r) - g_{\alpha\beta} \cdot (r_s - 3 \cdot (L_{md} - L_{mq}) \cdot sin(2 \cdot \theta_r))$$

$$a_{22} = -g_{\beta\beta} \cdot (r_s + 3 \cdot (L_{md} - L_{mq}) \cdot sin(2 \cdot \theta_r)) - g_{\alpha\beta} \cdot 3 \cdot (L_{md} - L_{mq}) \cdot cos(2 \cdot \theta_r)$$

$$a_{33} = a_{44} = -g_{xy} \cdot r_s$$

$$[B] = \begin{bmatrix} g_{\alpha\alpha} & g_{\alpha\beta} & 0 & 0 \\ g_{\alpha\beta} & g_{\beta\beta} & 0 & 0 \\ 0 & 0 & g_{xy} & 0 \\ 0 & 0 & 0 & g_{xy} \end{bmatrix}$$

where the cross-couplings present between the first two axes can be clearly seen in both $[A]$ and $[B]$ matrices. The reduction of these cross-couplings can be made progressively following a similar procedure as the one shown in section 4.2.1.1, yielding the following decoupling matrices:

$$[K_{\alpha\beta}] = [B]^{-1} \cdot ([A_{\alpha\beta}] - [A]) = \begin{bmatrix} k_{\alpha\alpha} & k_{\alpha\beta} & 0 & 0 \\ k_{\beta\alpha} & k_{\alpha\alpha} & 0 & 0 \\ 0 & 0 & 0 & 0 \\ 0 & 0 & 0 & 0 \end{bmatrix} \qquad (4.54)$$

$$k_{\alpha\alpha} = -3 \cdot sin(2 \cdot \theta_r) \cdot (L_{md} - L_{mq}) - \frac{g_{\alpha\beta}{}^2 \cdot r_s}{(g_{\alpha\alpha} \cdot g_{\beta\beta} - g_{\alpha\beta}{}^2)} \quad k_{\alpha\beta}$$
$$= 3 \cdot cos(2 \cdot \theta_r) \cdot (L_{md} - L_{mq}) + \frac{g_{\alpha\beta} \cdot g_{\beta\beta} \cdot r_s}{(g_{\alpha\alpha} \cdot g_{\beta\beta} - g_{\alpha\beta}{}^2)}$$

$$k_{\beta\alpha} = 3 \cdot cos(2 \cdot \theta_r) \cdot (L_{md} - L_{mq}) + \frac{g_{\alpha\beta} \cdot g_{\alpha\alpha} \cdot r_s}{(g_{\alpha\alpha} \cdot g_{\beta\beta} - g_{\alpha\beta}{}^2)}$$

$$[K_{in}] = [B]^{-1} = \begin{bmatrix} k_{in1} & k_{in2} & 0 & 0 \\ k_{in2} & k_{in3} & 0 & 0 \\ 0 & 0 & 1 & 0 \\ 0 & 0 & 0 & 1 \end{bmatrix} \qquad (4.55)\ [3]$$

$$k_{in1} = \frac{g_{\beta\beta}}{g_{\alpha\alpha} \cdot g_{\beta\beta} - g_{\alpha\beta}{}^2} \qquad k_{in2} = \frac{-g_{\alpha\beta}}{g_{\alpha\alpha} \cdot g_{\beta\beta} - g_{\alpha\beta}{}^2} \qquad k_{in3} = \frac{g_{\alpha\alpha}}{g_{\alpha\alpha} \cdot g_{\beta\beta} - g_{\alpha\beta}{}^2}$$

The combination of all these manipulations leads to a totally decoupled model of a machine with two three-phase systems in the stationary reference frame, with the following state space representation

$$[\dot{X}] = [A_{\alpha\beta}] \cdot [X] + [I] \cdot [u_c] \qquad [Y] = [X] \qquad [X] = [i_\alpha, i_\beta, i_x, i_y]^T \qquad [u_c] = [v_{\alpha c}, v_{\beta c}, v_x, v_y]^T \qquad (4.56)$$

Writing the equations on per axis basis, the following equations apply for the current control loops:

$$\frac{di_\alpha}{dt} = -r_s \cdot g_{\alpha\alpha} \cdot i_\alpha + v_{\alpha c} \qquad \frac{di_\beta}{dt} = -r_s \cdot g_{\beta\beta} \cdot i_\beta + v_{\beta c}$$
$$\frac{di_x}{dt} = -r_s \cdot g_{xy} \cdot i_x + v_x \qquad \frac{di_y}{dt} = -r_s \cdot g_{xy} \cdot i_y + v_y \qquad (4.57)$$

---

[3] The terms on the diagonal in the third and fourth rows in the matrix $[K_{in}]$ have been made intentionally equal to one to avoid scaling unnecessarily the x-y subspace.

resulting in a fully decoupled model with a first-order inductive plant in each of the axis. The effects of each decoupling term can be seen in Fig. 4.3, where Bode plots are shown for a set of transfer functions that relate outputs and inputs. The 2-pt black line represents the behaviour when $K_{\alpha\beta}$ decoupling is activated. It can be seen how only the plots in the diagonal (those representing the effect of one input on its corresponding output) are near the 0 dB line meaning a unitary gain. The non-diagonal terms are almost zero meaning that the other inputs have no effect on the output (decoupled behaviour). The 1-pt black line represents the machine's original behaviour (both decoupling terms deactivated).
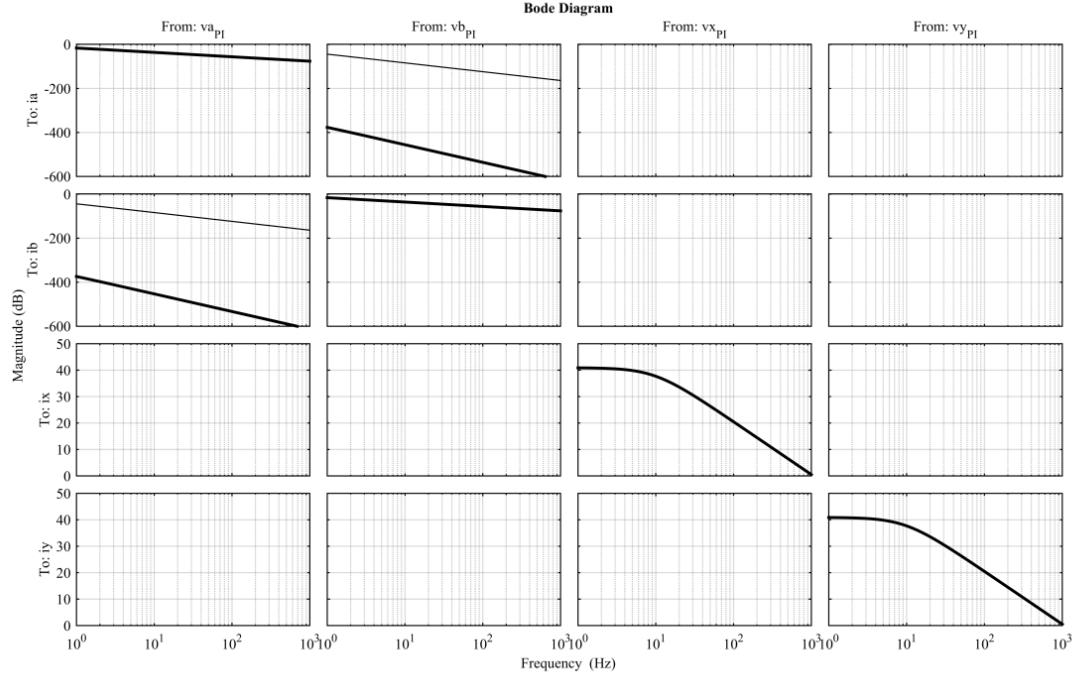
Fig. 4.3 Magnitude Bode plots for transfer functions from inputs v_α, v_β, v_x and v_y (columns 1 to 4, respectively) to outputs i_α, i_β, i_x and i_y (rows 1 to 4, respectively) with different decoupling setups. The frequency is expressed with respect to the stationary reference frame.

To obtain a fully diagonal inductance matrix regardless of the saliency in the machine, it is again required to apply a rotational transformation but, in this case, only to the first two rows yielding the following matrices:

$$[L_s]_{t+r} = \begin{bmatrix} L_{ls} + 3 \cdot L_{md} & 0 & 0 & 0 & 0 & 0 \\ 0 & L_{ls} + 3 \cdot L_{mq} & 0 & 0 & 0 & 0 \\ 0 & 0 & L_{ls} & 0 & 0 & 0 \\ 0 & 0 & 0 & L_{ls} & 0 & 0 \\ 0 & 0 & 0 & 0 & L_{ls} & 0 \\ 0 & 0 & 0 & 0 & 0 & L_{ls} \end{bmatrix} \qquad \textbf{(4.58)}$$

$$[\Psi_{PM}]_{t+r} = \psi_{PM} \cdot [1 \quad 0 \quad 0 \quad 0 \quad 0 \quad 0]^T \qquad [T] \cdot \frac{d([T]^{-1})}{dt} = \omega_r \cdot \begin{pmatrix} [a] & [b] \\ [b] & [a] \end{pmatrix}$$

where the following conclusions can be extracted:

- the inductance in the flux/torque producing subspace (*d-q* subspace herein after) is the result of the addition of the stator leakage inductance (L_{ls}) and a magnetising inductance (see 3.2.1).
- the inductance in all the non-flux/torque producing subspaces is the same and equals the stator leakage inductance.

Substituting all the terms in equation (4.6) and re-arranging the terms to follow the state-space representation, the equations for each of the axes can be obtained in the following form:

$$\frac{di_d}{dt} = \frac{1}{L_{ls} + 3 \cdot L_{md}} \cdot \left(v_d - r_s \cdot i_d + \omega_r \cdot (L_{ls} + 3 \cdot L_{mq}) \cdot i_q\right)$$

$$\frac{di_q}{dt} = \frac{1}{L_{ls} + 3 \cdot L_{mq}} \cdot \left(v_q - r_s \cdot i_q - \omega_r \cdot (\psi_{PM} + (L_{ls} + 3 \cdot L_{md}) \cdot i_d)\right)$$

$$\frac{di_x}{dt} = \frac{1}{L_{ls}} \cdot (v_x - r_s \cdot i_x)$$

$$\frac{di_y}{dt} = \frac{1}{L_{ls}} \cdot (v_y - r_s \cdot i_y)$$

(4.59)

A significant simplification over the equations for the multiple *dq* approach (4.34), in terms of cross-coupling, is achieved. It can be immediately seen how the equations for the *d-q* axes are exactly the same as those for a three-phase machine, thus allowing to tune the current regulators following the same rules. Additionally, it can be seen that the equations in the non-flux/torque producing subspace are fully decoupled, allowing to independently control each of the corresponding current terms. The only cross-coupling present in this model is that of the *d-* and *q*-axes which can be compensated for as in 4.2.1.1 with a state feedback of the form

$$[K_{dqVSD}] = \begin{bmatrix} 0 & k_d & 0 & 0 \\ k_q & 0 & 0 & 0 \\ 0 & 0 & 0 & 0 \\ 0 & 0 & 0 & 0 \end{bmatrix}$$

(4.60)

$$k_d = -\omega_r \cdot (L_{ls} + 3 \cdot L_{mq}) \qquad k_q = \omega_r \cdot (L_{ls} + 3 \cdot L_{md})$$

With this feedback, the model becomes fully decoupled,

$$[\dot{X}] = [A_{VSD}] \cdot [X] + [I] \cdot [u] \qquad [Y] = [X]$$

$$[X] = [i_d, i_q, i_x, i_y]^T \qquad [u] = [v_d, v_q, v_x, v_y]^T$$

(4.61)

Writing the equations on per axis basis, the following equations apply for the current control loops:

$$\frac{di_d}{dt} = \frac{v_d - r_s \cdot i_d}{L_{ls} + 3 \cdot L_{md}} \qquad \frac{di_q}{dt} = \frac{v_q - r_s \cdot i_q}{L_{ls} + 3 \cdot L_{mq}}$$

$$\frac{di_x}{dt} = \frac{v_x - r_s \cdot i_x}{L_{ls}} \qquad \frac{di_y}{dt} = \frac{v_y - r_s \cdot i_y}{L_{ls}}$$

(4.62)

which are very similar to those of the three-phase counterpart. Again the effect of the decoupling terms can be seen by plotting the frequency responses of the plant seen by the controller when the decoupling term is activated and deactivated (2- and 1-pt black line, respectively, in Fig. 4.4).
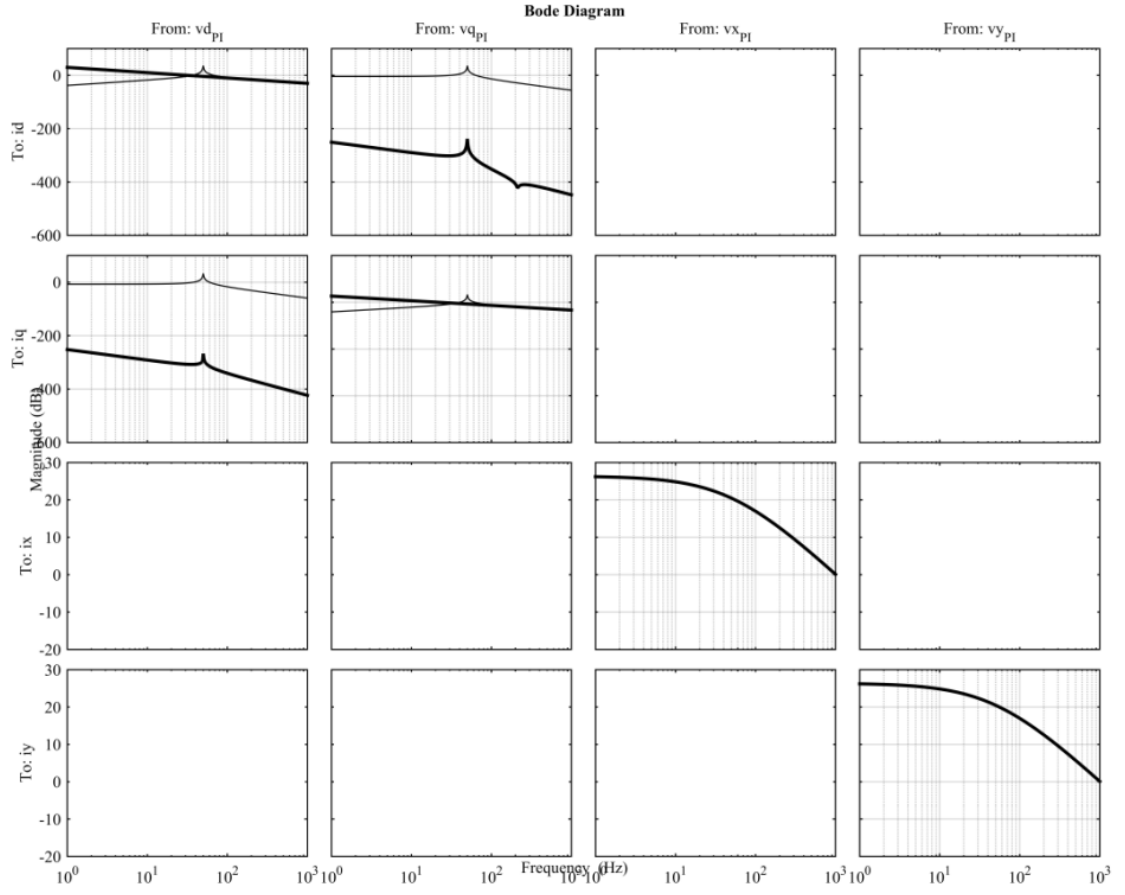
Fig. 4.4 Magnitude Bode plots for transfer functions from inputs v_d, v_q, v_x and v_y (columns 1 to 4 respectively) to outputs i_d, i_q, i_x and i_y (rows 1 to 4 respectively) with different decoupling setups. The frequency is expressed relative to the rotating reference frame (50 Hz).

Following a similar procedure as in 4.2.1.1, the torque expression can be calculated for the VSD approach,

$$T_{elec} = \frac{n}{2} \cdot p \cdot \left(\psi_{PM} \cdot i_q + \left(L_d - L_q \right) \cdot i_d \cdot i_q \right) \tag{4.63}$$

where n stands for the number of stator phases in the machine.

Using the relative angle between the stator current vector and the rotor flux α_c, the equation (4.63) can be transformed as follows:

$$i_d = I_s \cdot cos(\alpha_c) \qquad i_q = I_s \cdot sin(\alpha_c)$$

$$T_{elec} = \frac{n}{2} \cdot p \cdot \left(\psi_{PM} \cdot I_s \cdot sin(\alpha_c) + \frac{1}{2} \cdot \left(L_d - L_q \right) \cdot I_s^2 \cdot sin(2 \cdot \alpha_c) \right) \tag{4.64}$$

Thus an expression of the torque as a function of the stator current vector amplitude (I_s) and its relative angle with respect to the rotor flux (α_c) results.

Manipulating equation (4.63) to isolate the q-axis current,

$$i_q{}^* = \frac{T_{elec}{}^*}{\frac{n}{2} \cdot p \cdot \left(\psi_{PM} + \left(L_d - L_q \right) \cdot i_d \right)} \tag{4.65}$$

the expression of the required q-axis reference current to produce certain torque is obtained.

4.2.1.3   Models resulting from the novel transformation approach

Applying the transformation with the novel transformation matrix shown in (3.32) for a six-phase machine, the same results as in (4.58) are obtained.

4.2.2   Triple three-phase windings

4.2.2.1   Models resulting from multiple *dq* approach

The transformation matrices for a nine-phase machine are given by (3.27). Substituting in equations (4.4) and in (4.8) the generic transformation matrix $[T]$ by C_{Tdq} (3.27), the transformed equations for a nine-phase machine are obtained.

Calculating the unknown terms (4.9) for a nine-phase machine,

$$[L_s]_t = \begin{bmatrix} L_{ls}+L_{\alpha\alpha} & L_{\alpha\beta} & 0 & L_{\alpha\alpha} & L_{\alpha\beta} & 0 & L_{\alpha\alpha} & L_{\alpha\beta} & 0 \\ L_{\alpha\beta} & L_{ls}+L_{\beta\beta} & 0 & L_{\alpha\beta} & L_{\beta\beta} & 0 & L_{\alpha\beta} & L_{\beta\beta} & 0 \\ 0 & 0 & L_{ls} & 0 & 0 & 0 & 0 & 0 & 0 \\ L_{\alpha\alpha} & L_{\alpha\beta} & 0 & L_{ls}+L_{\alpha\alpha} & L_{\alpha\beta} & 0 & L_{\alpha\alpha} & L_{\alpha\beta} & 0 \\ L_{\alpha\beta} & L_{\beta\beta} & 0 & L_{\alpha\beta} & L_{ls}+L_{\beta\beta} & 0 & L_{\alpha\beta} & L_{\beta\beta} & 0 \\ 0 & 0 & 0 & 0 & 0 & L_{ls} & 0 & 0 & 0 \\ L_{\alpha\alpha} & L_{\alpha\beta} & 0 & L_{\alpha\alpha} & L_{\alpha\beta} & 0 & L_{ls}+L_{\alpha\alpha} & L_{\alpha\beta} & 0 \\ L_{\alpha\beta} & L_{\beta\beta} & 0 & L_{\alpha\beta} & L_{\beta\beta} & 0 & L_{\alpha\beta} & L_{ls}+L_{\beta\beta} & 0 \\ 0 & 0 & 0 & 0 & 0 & 0 & 0 & 0 & L_{ls} \end{bmatrix} \tag{4.66}$$

$$[\Psi_{PM}]_t = \psi_{PM} \cdot [cos(\theta_r) \quad sin(\theta_r) \quad 0 \quad cos(\theta_r) \quad sin(\theta_r) \quad 0 \quad cos(\theta_r) \quad sin(\theta_r) \quad 0]^T$$

Re-arranging the terms to follow the state-space representation with currents as state variables,

$$\frac{d([i_s]_t)}{dt} = [L_s]_t^{-1} \cdot \left([V_s]_t - [R_s] \cdot [i_s]_t - \frac{d[\Psi_{PM}]_t}{dt} - \frac{d[L_s]_t}{dt} \cdot [i_s]_t \right) \tag{4.67}$$

the expressions of the equations for each of the axes can be obtained for a nine-phase machine in the following form:

$$\frac{di_{\alpha1}}{dt} = g_{\alpha1\alpha1} \cdot (v_{\alpha1} - r_s \cdot i_{\alpha1} + \omega_r \cdot \psi_{PM} \cdot sin(\theta_r) + sal_\alpha) + g_{\alpha\beta} \cdot (v_{\beta1} - r_s \cdot i_{\beta1} - \omega_r \cdot \psi_{PM} \cdot cos(\theta_r) + sal_\beta)$$
$$+ g_{\alpha1\alpha2} \cdot (v_{\alpha2} - r_s \cdot i_{\alpha2} + \omega_r \cdot \psi_{PM} \cdot sin(\theta_r) + sal_\alpha) + g_{\alpha\beta}$$
$$\cdot (v_{\beta2} - r_s \cdot i_{\beta2} - \omega_r \cdot \psi_{PM} \cdot cos(\theta_r) + sal_\beta) + g_{\alpha1\alpha3}$$
$$\cdot (v_{\alpha3} - r_s \cdot i_{\alpha3} + \omega_r \cdot \psi_{PM} \cdot sin(\theta_r) + sal_\alpha) + g_{\alpha\beta} \cdot (v_{\beta3} - r_s \cdot i_{\beta3} - \omega_r \cdot \psi_{PM} \cdot cos(\theta_r) + sal_\beta)$$

$$\frac{di_{\beta1}}{dt} = g_{\alpha\beta} \cdot (v_{\alpha1} - r_s \cdot i_{\alpha1} + \omega_r \cdot \psi_{PM} \cdot sin(\theta_r) + sal_\alpha) + g_{\beta1\beta1} \cdot (v_{\beta1} - r_s \cdot i_{\beta1} - \omega_r \cdot \psi_{PM} \cdot cos(\theta_r) + sal_\beta) + g_{\alpha\beta}$$
$$\cdot (v_{\alpha2} - r_s \cdot i_{\alpha2} + \omega_r \cdot \psi_{PM} \cdot sin(\theta_r) + sal_\alpha) + g_{\beta1\beta2}$$
$$\cdot (v_{\beta2} - r_s \cdot i_{\beta2} - \omega_r \cdot \psi_{PM} \cdot cos(\theta_r) + sal_\beta) + g_{\alpha\beta} \cdot (v_{\alpha3} - r_s \cdot i_{\alpha3} + \omega_r \cdot \psi_{PM} \cdot sin(\theta_r) + sal_\alpha)$$
$$+ g_{\beta1\beta3} \cdot (v_{\beta3} - r_s \cdot i_{\beta3} - \omega_r \cdot \psi_{PM} \cdot cos(\theta_r) + sal_\beta)$$

$$\tag{4.68}$$

$$\frac{di_{\alpha 2}}{dt} = g_{\alpha 2\alpha 1} \cdot (v_{\alpha 1} - r_s \cdot i_{\alpha 1} + \omega_r \cdot \psi_{PM} \cdot sin(\theta_r) + sal_\alpha) + g_{\alpha\beta} \cdot (v_{\beta 1} - r_s \cdot i_{\beta 1} - \omega_r \cdot \psi_{PM} \cdot cos(\theta_r) + sal_\beta)$$
$$+ g_{\alpha 2\alpha 2} \cdot (v_{\alpha 2} - r_s \cdot i_{\alpha 2} + \omega_r \cdot \psi_{PM} \cdot sin(\theta_r) + sal_\alpha) + g_{\alpha\beta}$$
$$\cdot (v_{\beta 2} - r_s \cdot i_{\beta 2} - \omega_r \cdot \psi_{PM} \cdot cos(\theta_r) + sal_\beta) + g_{\alpha 2\alpha 3}$$
$$\cdot (v_{\alpha 3} - r_s \cdot i_{\alpha 3} + \omega_r \cdot \psi_{PM} \cdot sin(\theta_r) + sal_\alpha) + g_{\alpha\beta} \cdot (v_{\beta 3} - r_s \cdot i_{\beta 3} - \omega_r \cdot \psi_{PM} \cdot cos(\theta_r) + sal_\beta)$$

$$\frac{di_{\beta 2}}{dt} = g_{\alpha\beta} \cdot (v_{\alpha 1} - r_s \cdot i_{\alpha 1} + \omega_r \cdot \psi_{PM} \cdot sin(\theta_r) + sal_\alpha) + g_{\beta 2\beta 1} \cdot (v_{\beta 1} - r_s \cdot i_{\beta 1} - \omega_r \cdot \psi_{PM} \cdot cos(\theta_r) + sal_\beta) + g_{\alpha\beta}$$
$$\cdot (v_{\alpha 2} - r_s \cdot i_{\alpha 2} + \omega_r \cdot \psi_{PM} \cdot sin(\theta_r) + sal_\alpha) + g_{\beta 2\beta 2}$$
$$\cdot (v_{\beta 2} - r_s \cdot i_{\beta 2} - \omega_r \cdot \psi_{PM} \cdot cos(\theta_r) + sal_\beta) + g_{\alpha\beta} \cdot (v_{\alpha 3} - r_s \cdot i_{\alpha 3} + \omega_r \cdot \psi_{PM} \cdot sin(\theta_r) + sal_\alpha)$$
$$+ g_{\beta 2\beta 3} \cdot (v_{\beta 3} - r_s \cdot i_{\beta 3} - \omega_r \cdot \psi_{PM} \cdot cos(\theta_r) + sal_\beta)$$

$$\frac{di_{\alpha 3}}{dt} = g_{\alpha 3\alpha 1} \cdot (v_{\alpha 1} - r_s \cdot i_{\alpha 1} + \omega_r \cdot \psi_{PM} \cdot sin(\theta_r) + sal_\alpha) + g_{\alpha\beta} \cdot (v_{\beta 1} - r_s \cdot i_{\beta 1} - \omega_r \cdot \psi_{PM} \cdot cos(\theta_r) + sal_\beta)$$
$$+ g_{\alpha 3\alpha 2} \cdot (v_{\alpha 2} - r_s \cdot i_{\alpha 2} + \omega_r \cdot \psi_{PM} \cdot sin(\theta_r) + sal_\alpha) + g_{\alpha\beta}$$
$$\cdot (v_{\beta 2} - r_s \cdot i_{\beta 2} - \omega_r \cdot \psi_{PM} \cdot cos(\theta_r) + sal_\beta) + g_{\alpha 3\alpha 3}$$
$$\cdot (v_{\alpha 3} - r_s \cdot i_{\alpha 3} + \omega_r \cdot \psi_{PM} \cdot sin(\theta_r) + sal_\alpha) + g_{\alpha\beta} \cdot (v_{\beta 3} - r_s \cdot i_{\beta 3} - \omega_r \cdot \psi_{PM} \cdot cos(\theta_r) + sal_\beta)$$

$$\frac{di_{\beta 3}}{dt} = g_{\alpha\beta} \cdot (v_{\alpha 1} - r_s \cdot i_{\alpha 1} + \omega_r \cdot \psi_{PM} \cdot sin(\theta_r) + sal_\alpha) + g_{\beta 3\beta 1} \cdot (v_{\beta 1} - r_s \cdot i_{\beta 1} - \omega_r \cdot \psi_{PM} \cdot cos(\theta_r) + sal_\beta) + g_{\alpha\beta}$$
$$\cdot (v_{\alpha 2} - r_s \cdot i_{\alpha 2} + \omega_r \cdot \psi_{PM} \cdot sin(\theta_r) + sal_\alpha) + g_{\beta 3\beta 2}$$
$$\cdot (v_{\beta 2} - r_s \cdot i_{\beta 2} - \omega_r \cdot \psi_{PM} \cdot cos(\theta_r) + sal_\beta) + g_{\alpha\beta} \cdot (v_{\alpha 3} - r_s \cdot i_{\alpha 3} + \omega_r \cdot \psi_{PM} \cdot sin(\theta_r) + sal_\alpha)$$
$$+ g_{\beta 3\beta 3} \cdot (v_{\beta 3} - r_s \cdot i_{\beta 3} - \omega_r \cdot \psi_{PM} \cdot cos(\theta_r) + sal_\beta)$$

$$sal_\alpha = \frac{3}{2} \cdot (L_{md} - L_{mq}) \cdot ((i_{\alpha 1} + i_{\alpha 2} + i_{\alpha 3}) \cdot sin(2 \cdot \theta_r) - (i_{\beta 1} + i_{\beta 2} + i_{\beta 3}) \cdot cos(2 \cdot \theta_r))$$

$$sal_\beta = \frac{-3}{2} \cdot (L_{md} - L_{mq}) \cdot ((i_{\alpha 1} + i_{\alpha 2} + i_{\alpha 3}) \cdot cos(2 \cdot \theta_r) + (i_{\beta 1} + i_{\beta 2} + i_{\beta 3}) \cdot sin(2 \cdot \theta_r))$$

where $v_{\alpha k}$, $v_{\beta k}$ and $i_{\alpha k}$, $i_{\beta k}$ are the α- and β-axis voltages and currents in the three-phase system number k and the coefficients $g_{\alpha\alpha}$ and $g_{\beta\beta}$ can be calculated as

$$g_{\alpha 1\alpha 1} = g_{\alpha 2\alpha 2} = g_{\alpha 3\alpha 3} = \frac{4 \cdot L_{ls}^2 + 15 \cdot L_{ls} \cdot (L_{md} + L_{mq}) + 54 \cdot L_{md} \cdot L_{mq} - 3 \cdot L_{ls} \cdot (L_{md} - L_{mq}) \cdot cos(2 \cdot \theta_r)}{L_{ls} \cdot (2 \cdot L_{ls} + 9 \cdot L_{md}) \cdot (2 \cdot L_{ls} + 9 \cdot L_{mq})}$$

$$g_{\alpha 1\alpha 2} = g_{\alpha 2\alpha 1} = g_{\alpha 1\alpha 3} = g_{\alpha 3\alpha 1} = g_{\alpha 2\alpha 3} = g_{\alpha 3\alpha 2}$$
$$= \frac{-3 \cdot L_{ls} \cdot (L_{md} + L_{mq}) - 27 \cdot L_{md} \cdot L_{mq} - 3 \cdot L_{ls} \cdot (L_{md} - L_{mq}) \cdot cos(2 \cdot \theta_r)}{L_{ls} \cdot (2 \cdot L_{ls} + 9 \cdot L_{md}) \cdot (2 \cdot L_{ls} + 9 \cdot L_{mq})}$$

$$g_{\alpha\beta} = \frac{-3 \cdot (L_{md} - L_{mq}) \cdot sin(2 \cdot \theta_r)}{(2 \cdot L_{ls} + 9 \cdot L_{md}) \cdot (2 \cdot L_{ls} + 9 \cdot L_{mq})} \quad \textbf{(4.69)}$$

$$g_{\beta 1\beta 1} = g_{\beta 2\beta 2} = g_{\beta 3\beta 3} = \frac{4 \cdot L_{ls}^2 + 15 \cdot L_{ls} \cdot (L_{md} + L_{mq}) + 54 \cdot L_{md} \cdot L_{mq} + 3 \cdot L_{ls} \cdot (L_{md} - L_{mq}) \cdot cos(2 \cdot \theta_r)}{L_{ls} \cdot (2 \cdot L_{ls} + 9 \cdot L_{md}) \cdot (2 \cdot L_{ls} + 9 \cdot L_{mq})}$$

$$g_{\beta 1\beta 2} = g_{\beta 2\beta 1} = g_{\beta 1\beta 3} = g_{\beta 3\beta 1} = g_{\beta 2\beta 3} = g_{\beta 3\beta 2}$$
$$= \frac{-3 \cdot L_{ls} \cdot (L_{md} + L_{mq}) - 27 \cdot L_{md} \cdot L_{mq} + 3 \cdot L_{ls} \cdot (L_{md} - L_{mq}) \cdot cos(2 \cdot \theta_r)}{L_{ls} \cdot (2 \cdot L_{ls} + 9 \cdot L_{md}) \cdot (2 \cdot L_{ls} + 9 \cdot L_{mq})}$$

The terms sal_α and sal_β in (4.68) represent the effect of the saliency of the magnetic circuit in the time derivative of the stator's flux. The $g_{\alpha i\alpha j}$ and $g_{\beta i\beta j}$ coefficients with $i \neq j$ account for the cross-coupling that exists between the different three-phase systems in the machine. Additionally, the $g_{\alpha\beta}$ coefficient represents the cross-coupling of the α-β axes. It can be clearly seen how this coupling is directly proportional to the saliency of the machine (i.e. the difference between the inductances in the d and q axes). These cross-coupling terms make it very difficult to tune the current regulators in both α and β axes as the α-axis current in the three-phase system number one is influenced, through $g_{\alpha 1\alpha 2}$, by the α-axis voltage ($v_{\alpha 2}$) in the three-phase system number two and through $g_{\alpha\beta}$ by the voltages in β-axis. All this implies that the α-axis and/or the β-axis current in any of the three-phase systems in the machine will be governed by six inputs $v_{\alpha 1}$, $v_{\alpha 2}$, $v_{\alpha 3}$, $v_{\beta 1}$, $v_{\beta 2}$ and $v_{\beta 3}$.

By compensating the inputs with the terms related to the flux of the permanent magnets, equation (4.68) is simplified into

$$\frac{di_{\alpha1}}{dt} = g_{\alpha1\alpha1} \cdot (v_{\alpha1c} - r_s \cdot i_{\alpha1} + sal_\alpha) + g_{\alpha\beta} \cdot (v_{\beta1c} - r_s \cdot i_{\beta1} + sal_\beta) + g_{\alpha1\alpha2} \cdot (v_{\alpha2c} - r_s \cdot i_{\alpha2} + sal_\alpha) + g_{\alpha\beta}$$
$$\cdot (v_{\beta2c} - r_s \cdot i_{\beta2} + sal_\beta) + g_{\alpha1\alpha3} \cdot (v_{\alpha3c} - r_s \cdot i_{\alpha3} + sal_\alpha) + g_{\alpha\beta} \cdot (v_{\beta3c} - r_s \cdot i_{\beta3} + sal_\beta)$$

$$\frac{di_{\beta1}}{dt} = g_{\alpha\beta} \cdot (v_{\alpha1c} - r_s \cdot i_{\alpha1} + +sal_\alpha) + g_{\beta1\beta1} \cdot (v_{\beta1c} - r_s \cdot i_{\beta1} + sal_\beta) + g_{\alpha\beta} \cdot (v_{\alpha2} - r_s \cdot i_{\alpha2} + sal_\alpha) + g_{\beta1\beta2}$$
$$\cdot (v_{\beta2c} - r_s \cdot i_{\beta2} + sal_\beta) + g_{\alpha\beta} \cdot (v_{\alpha3c} - r_s \cdot i_{\alpha3} + sal_\alpha) + g_{\beta1\beta3} \cdot (v_{\beta3c} - r_s \cdot i_{\beta3} + sal_\beta)$$

$$\frac{di_{\alpha2}}{dt} = g_{\alpha2\alpha1} \cdot (v_{\alpha1c} - r_s \cdot i_{\alpha1} + sal_\alpha) + g_{\alpha\beta} \cdot (v_{\beta1c} - r_s \cdot i_{\beta1} + sal_\beta) + g_{\alpha2\alpha2} \cdot (v_{\alpha2c} - r_s \cdot i_{\alpha2} + sal_\alpha) + g_{\alpha\beta}$$
$$\cdot (v_{\beta2c} - r_s \cdot i_{\beta2} + sal_\beta) + g_{\alpha2\alpha3} \cdot (v_{\alpha3c} - r_s \cdot i_{\alpha3} + sal_\alpha) + g_{\alpha\beta} \cdot (v_{\beta3c} - r_s \cdot i_{\beta3} + sal_\beta)$$

$$\frac{di_{\beta2}}{dt} = g_{\alpha\beta} \cdot (v_{\alpha1c} - r_s \cdot i_{\alpha1} + sal_\alpha) + g_{\beta2\beta1} \cdot (v_{\beta1c} - r_s \cdot i_{\beta1} + sal_\beta) + g_{\alpha\beta} \cdot (v_{\alpha2c} - r_s \cdot i_{\alpha2} + sal_\alpha) + g_{\beta2\beta2}$$
$$\cdot (v_{\beta2c} - r_s \cdot i_{\beta2} + sal_\beta) + g_{\alpha\beta} \cdot (v_{\alpha3c} - r_s \cdot i_{\alpha3} + sal_\alpha) + g_{\beta2\beta3} \cdot (v_{\beta3c} - r_s \cdot i_{\beta3} + sal_\beta)$$

$$\frac{di_{\alpha3}}{dt} = g_{\alpha3\alpha1} \cdot (v_{\alpha1c} - r_s \cdot i_{\alpha1} + sal_\alpha) + g_{\alpha\beta} \cdot (v_{\beta1c} - r_s \cdot i_{\beta1} + sal_\beta) + g_{\alpha3\alpha2} \cdot (v_{\alpha2c} - r_s \cdot i_{\alpha2} + sal_\alpha) + g_{\alpha\beta}$$
$$\cdot (v_{\beta2c} - r_s \cdot i_{\beta2} + sal_\beta) + g_{\alpha3\alpha3} \cdot (v_{\alpha3c} - r_s \cdot i_{\alpha3} + sal_\alpha) + g_{\alpha\beta} \cdot (v_{\beta3c} - r_s \cdot i_{\beta3} + sal_\beta)$$

$$\frac{di_{\beta3}}{dt} = g_{\alpha\beta} \cdot (v_{\alpha1c} - r_s \cdot i_{\alpha1} + sal_\alpha) + g_{\beta3\beta1} \cdot (v_{\beta1c} - r_s \cdot i_{\beta1} + sal_\beta) + g_{\alpha\beta} \cdot (v_{\alpha2c} - r_s \cdot i_{\alpha2} + sal_\alpha) + g_{\beta3\beta2}$$
$$\cdot (v_{\beta2c} - r_s \cdot i_{\beta2} + sal_\beta) + g_{\alpha\beta} \cdot (v_{\alpha3c} - r_s \cdot i_{\alpha3} + sal_\alpha) + g_{\beta3\beta3} \cdot (v_{\beta3c} - r_s \cdot i_{\beta3} + sal_\beta)$$

(4.70)

where $v_{\alpha kc}$ and $v_{\beta kc}$ are the compensated voltages in the α and β axes in the three-phase system number k and their expressions are,

$$v_{\alpha kc} = v_{\alpha k} - \omega_r \cdot \psi_{PM} \cdot sin(\theta_r)$$
$$v_{\beta kc} = v_{\beta k} + \omega_r \cdot \psi_{PM} \cdot cos(\theta_r)$$

(4.71)

Constructing the matrices of the state-space representation from equation (4.70), while considering the output matrix [C] as equal to an identity matrix, yields:

$$[\dot{X}] = [A] \cdot [X] + [B] \cdot [u] \qquad [Y] = [X]$$

$$[X] = [i_{\alpha1}, i_{\beta1}, i_{\alpha2}, i_{\beta2}, i_{\alpha3}, i_{\beta3}]^T \qquad [u] = [v_{\alpha1}, v_{\beta1}, v_{\alpha2}, v_{\beta2}, v_{\alpha3}, v_{\beta3}]^T$$

$$[A] = \begin{bmatrix} a_{11} & a_{12} & a_{13} & a_{14} & a_{15} & a_{16} \\ a_{21} & a_{22} & a_{23} & a_{24} & a_{25} & a_{26} \\ a_{31} & a_{32} & a_{33} & a_{34} & a_{35} & a_{36} \\ a_{41} & a_{42} & a_{43} & a_{44} & a_{45} & a_{46} \\ a_{51} & a_{52} & a_{53} & a_{54} & a_{55} & a_{56} \\ a_{61} & a_{62} & a_{63} & a_{64} & a_{65} & a_{66} \end{bmatrix}$$

(4.72)

$$a_{11} = -g_{\alpha\beta} \cdot \frac{9}{2} \cdot (L_{md} - L_{mq}) \cdot cos(2 \cdot \theta_r) - g_{\alpha1\alpha1} \cdot \left(r_s - \frac{3}{2} \cdot (L_{md} - L_{mq}) \cdot sin(2 \cdot \theta_r)\right) + (g_{\alpha1\alpha2} + g_{\alpha1\alpha3}) \cdot \frac{3}{2}$$
$$\cdot (L_{md} - L_{mq}) \cdot sin(2 \cdot \theta_r)$$

$$a_{12} = -(g_{\alpha1\alpha1} + g_{\alpha1\alpha2} + g_{\alpha1\alpha3}) \cdot \frac{3}{2} \cdot (L_{md} - L_{mq}) \cdot cos(2 \cdot \theta_r) - g_{\alpha\beta} \cdot \left(r_s + \frac{9}{2} \cdot (L_{md} - L_{mq}) \cdot sin(2 \cdot \theta_r)\right)$$

$$a_{13} = -g_{\alpha\beta} \cdot \frac{9}{2} \cdot (L_{md} - L_{mq}) \cdot cos(2 \cdot \theta_r) + (g_{\alpha1\alpha1} + g_{\alpha1\alpha3}) \cdot \frac{3}{2} \cdot (L_{md} - L_{mq}) \cdot sin(2 \cdot \theta_r) - g_{\alpha1\alpha2}$$
$$\cdot \left(r_s - \frac{3}{2} \cdot (L_{md} - L_{mq}) \cdot sin(2 \cdot \theta_r)\right)$$

$$a_{14} = -(g_{\alpha1\alpha1} + g_{\alpha1\alpha2} + g_{\alpha1\alpha3}) \cdot \frac{3}{2} \cdot (L_{md} - L_{mq}) \cdot cos(2 \cdot \theta_r) - g_{\alpha\beta} \cdot \left(r_s + \frac{9}{2} \cdot (L_{md} - L_{mq}) \cdot sin(2 \cdot \theta_r)\right)$$

$$a_{15} = -g_{\alpha\beta} \cdot \frac{9}{2} \cdot (L_{md} - L_{mq}) \cdot cos(2 \cdot \theta_r) + (g_{\alpha1\alpha1} + g_{\alpha1\alpha2}) \cdot \frac{3}{2} \cdot (L_{md} - L_{mq}) \cdot sin(2 \cdot \theta_r) - g_{\alpha1\alpha3}$$
$$\cdot \left(r_s - \frac{3}{2} \cdot (L_{md} - L_{mq}) \cdot sin(2 \cdot \theta_r)\right)$$

$$a_{16} = -(g_{\alpha1\alpha1} + g_{\alpha1\alpha2} + g_{\alpha1\alpha3}) \cdot \frac{3}{2} \cdot (L_{md} - L_{mq}) \cdot cos(2 \cdot \theta_r) - g_{\alpha\beta} \cdot \left(r_s + \frac{9}{2} \cdot (L_{md} - L_{mq}) \cdot sin(2 \cdot \theta_r)\right)$$

$$a_{21} = -(g_{\beta1\beta1} + g_{\beta1\beta2} + g_{\beta1\beta3}) \cdot \frac{3}{2} \cdot (L_{md} - L_{mq}) \cdot cos(2 \cdot \theta_r) - g_{\alpha\beta} \cdot \left(r_s - \frac{9}{2} \cdot (L_{md} - L_{mq}) \cdot sin(2 \cdot \theta_r)\right)$$

$$a_{22} = -g_{\alpha\beta} \cdot \frac{9}{2} \cdot (L_{md} - L_{mq}) \cdot cos(2 \cdot \theta_r) - g_{\beta1\beta1} \cdot \left(r_s + \frac{3}{2} \cdot (L_{md} - L_{mq}) \cdot sin(2 \cdot \theta_r)\right) - (g_{\beta1\beta2} + g_{\beta1\beta3}) \cdot \frac{3}{2}$$
$$\cdot (L_{md} - L_{mq}) \cdot sin(2 \cdot \theta_r)$$

$$a_{23} = -(g_{\beta1\beta1} + g_{\beta1\beta2} + g_{\beta1\beta3}) \cdot \frac{3}{2} \cdot (L_{md} - L_{mq}) \cdot cos(2 \cdot \theta_r) - g_{\alpha\beta} \cdot \left(r_s - \frac{9}{2} \cdot (L_{md} - L_{mq}) \cdot sin(2 \cdot \theta_r)\right)$$

$$a_{24} = -g_{\alpha\beta} \cdot \frac{9}{2} \cdot (L_{md} - L_{mq}) \cdot cos(2 \cdot \theta_r) - (g_{\beta1\beta1} + g_{\beta1\beta3}) \cdot \frac{3}{2} \cdot (L_{md} - L_{mq}) \cdot sin(2 \cdot \theta_r) - g_{\beta1\beta2}$$
$$\cdot \left(r_s + \frac{3}{2} \cdot (L_{md} - L_{mq}) \cdot sin(2 \cdot \theta_r)\right)$$

$$a_{25} = -(g_{\beta1\beta1} + g_{\beta1\beta2} + g_{\beta1\beta3}) \cdot \frac{3}{2} \cdot (L_{md} - L_{mq}) \cdot cos(2 \cdot \theta_r) - g_{\alpha\beta} \cdot \left(r_s - \frac{9}{2} \cdot (L_{md} - L_{mq}) \cdot sin(2 \cdot \theta_r)\right)$$

$$a_{26} = -g_{\alpha\beta} \cdot \frac{9}{2} \cdot (L_{md} - L_{mq}) \cdot cos(2 \cdot \theta_r) - (g_{\beta1\beta1} + g_{\beta1\beta2}) \cdot \frac{3}{2} \cdot (L_{md} - L_{mq}) \cdot sin(2 \cdot \theta_r) - g_{\beta1\beta3}$$
$$\cdot \left(r_s + \frac{3}{2} \cdot (L_{md} - L_{mq}) \cdot sin(2 \cdot \theta_r)\right)$$

$$a_{31} = -g_{\alpha\beta} \cdot \frac{9}{2} \cdot (L_{md} - L_{mq}) \cdot cos(2 \cdot \theta_r) + (g_{\alpha2\alpha2} + g_{\alpha2\alpha3}) \cdot \frac{3}{2} \cdot (L_{md} - L_{mq}) \cdot sin(2 \cdot \theta_r) - g_{\alpha2\alpha1}$$
$$\cdot \left(r_s - \frac{3}{2} \cdot (L_{md} - L_{mq}) \cdot sin(2 \cdot \theta_r)\right)$$

$$a_{32} = -(g_{\alpha2\alpha1} + g_{\alpha2\alpha2} + g_{\alpha2\alpha3}) \cdot \frac{3}{2} \cdot (L_{md} - L_{mq}) \cdot cos(2 \cdot \theta_r) - g_{\alpha\beta} \cdot \left(r_s + \frac{9}{2} \cdot (L_{md} - L_{mq}) \cdot sin(2 \cdot \theta_r)\right)$$

$$a_{33} = -g_{\alpha\beta} \cdot \frac{9}{2} \cdot (L_{md} - L_{mq}) \cdot cos(2 \cdot \theta_r) - g_{\alpha2\alpha2} \cdot \left(r_s - \frac{3}{2} \cdot (L_{md} - L_{mq}) \cdot sin(2 \cdot \theta_r)\right) + (g_{\alpha2\alpha1} + g_{\alpha2\alpha3}) \cdot \frac{3}{2}$$
$$\cdot (L_{md} - L_{mq}) \cdot si\,n(2 \cdot \theta_r)$$

$$a_{34} = -(g_{\alpha2\alpha1} + g_{\alpha2\alpha2} + g_{\alpha2\alpha3}) \cdot \frac{3}{2} \cdot (L_{md} - L_{mq}) \cdot cos(2 \cdot \theta_r) - g_{\alpha\beta} \cdot \left(r_s + \frac{9}{2} \cdot (L_{md} - L_{mq}) \cdot sin(2 \cdot \theta_r)\right)$$

$$a_{35} = -g_{\alpha\beta} \cdot \frac{9}{2} \cdot (L_{md} - L_{mq}) \cdot cos(2 \cdot \theta_r) - g_{\alpha2\alpha3} \cdot \left(r_s - \frac{3}{2} \cdot (L_{md} - L_{mq}) \cdot sin(2 \cdot \theta_r)\right) + (g_{\alpha2\alpha1} + g_{\alpha2\alpha2}) \cdot \frac{3}{2}$$
$$\cdot (L_{md} - L_{mq}) \cdot si\,n(2 \cdot \theta_r)$$

$$a_{36} = -(g_{\alpha2\alpha1} + g_{\alpha2\alpha2} + g_{\alpha2\alpha3}) \cdot \frac{3}{2} \cdot (L_{md} - L_{mq}) \cdot cos(2 \cdot \theta_r) - g_{\alpha\beta} \cdot \left(r_s + \frac{9}{2} \cdot (L_{md} - L_{mq}) \cdot sin(2 \cdot \theta_r)\right)$$

$$a_{41} = -(g_{\beta2\beta1} + g_{\beta2\beta2} + g_{\beta2\beta3}) \cdot \frac{3}{2} \cdot (L_{md} - L_{mq}) \cdot cos(2 \cdot \theta_r) - g_{\alpha\beta} \cdot \left(r_s - \frac{9}{2} \cdot (L_{md} - L_{mq}) \cdot sin(2 \cdot \theta_r)\right)$$

$$a_{42} = -g_{\alpha\beta} \cdot \frac{9}{2} \cdot (L_{md} - L_{mq}) \cdot cos(2 \cdot \theta_r) - g_{\beta2\beta1} \cdot \left(r_s + \frac{3}{2} \cdot (L_{md} - L_{mq}) \cdot sin(2 \cdot \theta_r)\right) - (g_{\beta2\beta2} + g_{\beta2\beta3}) \cdot \frac{3}{2}$$
$$\cdot (L_{md} - L_{mq}) \cdot sin(2 \cdot \theta_r)$$

$$a_{43} = -(g_{\beta2\beta1} + g_{\beta2\beta2} + g_{\beta2\beta3}) \cdot \frac{3}{2} \cdot (L_{md} - L_{mq}) \cdot cos(2 \cdot \theta_r) - g_{\alpha\beta} \cdot \left(r_s - \frac{9}{2} \cdot (L_{md} - L_{mq}) \cdot sin(2 \cdot \theta_r)\right)$$

$$a_{44} = -g_{\alpha\beta} \cdot \frac{9}{2} \cdot (L_{md} - L_{mq}) \cdot cos(2 \cdot \theta_r) - (g_{\beta2\beta1} + g_{\beta2\beta3}) \cdot \frac{3}{2} \cdot (L_{md} - L_{mq}) \cdot sin(2 \cdot \theta_r) - g_{\beta2\beta2}$$
$$\cdot \left(r_s + \frac{3}{2} \cdot (L_{md} - L_{mq}) \cdot sin(2 \cdot \theta_r)\right)$$

$$a_{45} = -(g_{\beta2\beta1} + g_{\beta2\beta2} + g_{\beta2\beta3}) \cdot \frac{3}{2} \cdot (L_{md} - L_{mq}) \cdot cos(2 \cdot \theta_r) - g_{\alpha\beta} \cdot \left(r_s - \frac{9}{2} \cdot (L_{md} - L_{mq}) \cdot sin(2 \cdot \theta_r)\right)$$

$$a_{46} = -g_{\alpha\beta} \cdot \frac{9}{2} \cdot (L_{md} - L_{mq}) \cdot cos(2 \cdot \theta_r) - (g_{\beta2\beta1} + g_{\beta2\beta2}) \cdot \frac{3}{2} \cdot (L_{md} - L_{mq}) \cdot sin(2 \cdot \theta_r) - g_{\beta2\beta3}$$
$$\cdot \left(r_s + \frac{3}{2} \cdot (L_{md} - L_{mq}) \cdot sin(2 \cdot \theta_r)\right)$$

$$a_{51} = -g_{\alpha\beta} \cdot \frac{9}{2} \cdot (L_{md} - L_{mq}) \cdot cos(2 \cdot \theta_r) + (g_{\alpha3\alpha2} + g_{\alpha3\alpha3}) \cdot \frac{3}{2} \cdot (L_{md} - L_{mq}) \cdot sin(2 \cdot \theta_r) - g_{\alpha3\alpha1}$$
$$\cdot \left(r_s - \frac{3}{2} \cdot (L_{md} - L_{mq}) \cdot sin(2 \cdot \theta_r) \right)$$

$$a_{52} = -(g_{\alpha3\alpha1} + g_{\alpha3\alpha2} + g_{\alpha3\alpha3}) \cdot \frac{3}{2} \cdot (L_{md} - L_{mq}) \cdot cos(2 \cdot \theta_r) - g_{\alpha\beta} \cdot \left(r_s + \frac{9}{2} \cdot (L_{md} - L_{mq}) \cdot sin(2 \cdot \theta_r) \right)$$

$$a_{53} = -g_{\alpha\beta} \cdot \frac{9}{2} \cdot (L_{md} - L_{mq}) \cdot cos(2 \cdot \theta_r) - g_{\alpha3\alpha2} \cdot \left(r_s - \frac{3}{2} \cdot (L_{md} - L_{mq}) \cdot sin(2 \cdot \theta_r) \right) + (g_{\alpha3\alpha1} + g_{\alpha3\alpha3}) \cdot \frac{3}{2}$$
$$\cdot (L_{md} - L_{mq}) \cdot sin(2 \cdot \theta_r)$$

$$a_{54} = -(g_{\alpha3\alpha1} + g_{\alpha3\alpha2} + g_{\alpha3\alpha3}) \cdot \frac{3}{2} \cdot (L_{md} - L_{mq}) \cdot cos(2 \cdot \theta_r) - g_{\alpha\beta} \cdot \left(r_s + \frac{9}{2} \cdot (L_{md} - L_{mq}) \cdot sin(2 \cdot \theta_r) \right)$$

$$a_{55} = -g_{\alpha\beta} \cdot \frac{9}{2} \cdot (L_{md} - L_{mq}) \cdot cos(2 \cdot \theta_r) - g_{\alpha3\alpha3} \cdot \left(r_s - \frac{3}{2} \cdot (L_{md} - L_{mq}) \cdot sin(2 \cdot \theta_r) \right) + (g_{\alpha3\alpha1} + g_{\alpha3\alpha2}) \cdot \frac{3}{2}$$
$$\cdot (L_{md} - L_{mq}) \cdot sin(2 \cdot \theta_r)$$

$$a_{56} = -(g_{\alpha3\alpha1} + g_{\alpha3\alpha2} + g_{\alpha3\alpha3}) \cdot \frac{3}{2} \cdot (L_{md} - L_{mq}) \cdot cos(2 \cdot \theta_r) - g_{\alpha\beta} \cdot \left(r_s + \frac{9}{2} \cdot (L_{md} - L_{mq}) \cdot sin(2 \cdot \theta_r) \right)$$

$$a_{61} = -(g_{\beta3\beta1} + g_{\beta3\beta2} + g_{\beta3\beta3}) \cdot \frac{3}{2} \cdot (L_{md} - L_{mq}) \cdot cos(2 \cdot \theta_r) - g_{\alpha\beta} \cdot \left(r_s - \frac{9}{2} \cdot (L_{md} - L_{mq}) \cdot sin(2 \cdot \theta_r) \right)$$

$$a_{62} = -g_{\alpha\beta} \cdot \frac{9}{2} \cdot (L_{md} - L_{mq}) \cdot cos(2 \cdot \theta_r) - g_{\beta3\beta1} \cdot \left(r_s + \frac{3}{2} \cdot (L_{md} - L_{mq}) \cdot sin(2 \cdot \theta_r) \right) - (g_{\beta3\beta2} + g_{\beta3\beta3}) \cdot \frac{3}{2}$$
$$\cdot (L_{md} - L_{mq}) \cdot sin(2 \cdot \theta_r)$$

$$a_{63} = -(g_{\beta3\beta1} + g_{\beta3\beta2} + g_{\beta3\beta3}) \cdot \frac{3}{2} \cdot (L_{md} - L_{mq}) \cdot cos(2 \cdot \theta_r) - g_{\alpha\beta} \cdot \left(r_s - \frac{9}{2} \cdot (L_{md} - L_{mq}) \cdot sin(2 \cdot \theta_r) \right)$$

$$a_{64} = -g_{\alpha\beta} \cdot \frac{9}{2} \cdot (L_{md} - L_{mq}) \cdot cos(2 \cdot \theta_r) - (g_{\beta3\beta1} + g_{\beta3\beta3}) \cdot \frac{3}{2} \cdot (L_{md} - L_{mq}) \cdot sin(2 \cdot \theta_r) - g_{\beta3\beta2}$$
$$\cdot \left(r_s + \frac{3}{2} \cdot (L_{md} - L_{mq}) \cdot sin(2 \cdot \theta_r) \right)$$

$$a_{65} = -(g_{\beta3\beta1} + g_{\beta3\beta2} + g_{\beta3\beta3}) \cdot \frac{3}{2} \cdot (L_{md} - L_{mq}) \cdot cos(2 \cdot \theta_r) - g_{\alpha\beta} \cdot \left(r_s - \frac{9}{2} \cdot (L_{md} - L_{mq}) \cdot sin(2 \cdot \theta_r) \right)$$

$$a_{66} = -g_{\alpha\beta} \cdot \frac{9}{2} \cdot (L_{md} - L_{mq}) \cdot cos(2 \cdot \theta_r) - (g_{\beta3\beta1} + g_{\beta3\beta2}) \cdot \frac{3}{2} \cdot (L_{md} - L_{mq}) \cdot sin(2 \cdot \theta_r) - g_{\beta3\beta3}$$
$$\cdot \left(r_s + \frac{3}{2} \cdot (L_{md} - L_{mq}) \cdot sin(2 \cdot \theta_r) \right)$$

$$[B] = \begin{bmatrix} g_{\alpha1\alpha1} & g_{\alpha\beta} & g_{\alpha1\alpha2} & g_{\alpha\beta} & g_{\alpha1\alpha3} & g_{\alpha\beta} \\ g_{\alpha\beta} & g_{\beta1\beta1} & g_{\alpha\beta} & g_{\beta1\beta2} & g_{\alpha\beta} & g_{\beta1\beta3} \\ g_{\alpha2\alpha1} & g_{\alpha\beta} & g_{\alpha1\alpha1} & g_{\alpha\beta} & g_{\alpha2\alpha3} & g_{\alpha\beta} \\ g_{\alpha\beta} & g_{\beta2\beta1} & g_{\alpha\beta} & g_{\beta1\beta1} & g_{\alpha\beta} & g_{\beta2\beta3} \\ g_{\alpha3\alpha1} & g_{\alpha\beta} & g_{\alpha3\alpha2} & g_{\alpha\beta} & g_{\alpha1\alpha1} & g_{\alpha\beta} \\ g_{\alpha\beta} & g_{\beta3\beta1} & g_{\alpha\beta} & g_{\beta3\beta2} & g_{\alpha\beta} & g_{\beta1\beta1} \end{bmatrix}$$

where the cross-couplings can be clearly seen in both [A] and [B] matrices. The reduction of these cross-couplings can be made progressively following a similar procedure as in the earlier section.

The decoupling matrix for the axes decoupling is,

$$[K_{\alpha\beta}] = \begin{bmatrix} k_{\alpha\alpha} & k_{\alpha\beta} & k_{\alpha\alpha} & k_{\alpha\beta} & k_{\alpha\alpha} & k_{\alpha\beta} \\ k_{\beta\alpha} & k_{\beta\beta} & k_{\beta\alpha} & k_{\beta\beta} & k_{\beta\alpha} & k_{\beta\beta} \\ k_{\alpha\alpha} & k_{\alpha\beta} & k_{\alpha\alpha} & k_{\alpha\beta} & k_{\alpha\alpha} & k_{\alpha\beta} \\ k_{\beta\alpha} & k_{\beta\beta} & k_{\beta\alpha} & k_{\beta\beta} & k_{\beta\alpha} & k_{\beta\beta} \\ k_{\alpha\alpha} & k_{\alpha\beta} & k_{\alpha\alpha} & k_{\alpha\beta} & k_{\alpha\alpha} & k_{\alpha\beta} \\ k_{\beta\alpha} & k_{\beta\beta} & k_{\beta\alpha} & k_{\beta\beta} & k_{\beta\alpha} & k_{\beta\beta} \end{bmatrix}$$

$$k_{\alpha\alpha} = \frac{-3 \cdot g_{\alpha\beta}{}^2 \cdot \left(r_s - \frac{9}{2} \cdot (L_{md} - L_{mq}) \cdot sin(2 \cdot \theta_r)\right) - g_{\alpha\beta} \cdot \frac{9}{2} \cdot (L_{md} - L_{mq}) \cdot (g_{\beta 1\beta 1} + 2 \cdot g_{\beta 1\beta 2}) \cdot cos(2 \cdot \theta_r)}{-9 \cdot g_{\alpha\beta}{}^2 + (g_{\alpha 1\alpha 1} + 2 \cdot g_{\alpha 1\alpha 2}) \cdot (g_{\beta 1\beta 1} + 2 \cdot g_{\beta 1\beta 2})} \qquad \textbf{(4.73)}$$

$$k_{\beta\beta} = \frac{-3 \cdot g_{\alpha\beta}{}^2 \cdot \left(r_s + \frac{9}{2} \cdot (L_{md} - L_{mq}) \cdot sin(2 \cdot \theta_r)\right) - g_{\alpha\beta} \cdot \frac{9}{2} \cdot (L_{md} - L_{mq}) \cdot (g_{\alpha 1\alpha 1} + 2 \cdot g_{\alpha 1\alpha 2}) \cdot cos(2 \cdot \theta_r)}{-9 \cdot g_{\alpha\beta}{}^2 + (g_{\alpha 1\alpha 1} + 2 \cdot g_{\alpha 1\alpha 2}) \cdot (g_{\beta 1\beta 1} + 2 \cdot g_{\beta 1\beta 2})}$$

$$k_{\alpha\beta} = \frac{\frac{3}{2} \cdot (g_{\alpha 1\alpha 1} + 2 \cdot g_{\alpha 1\alpha 2}) \cdot (g_{\beta 1\beta 1} + 2 \cdot g_{\beta 1\beta 2}) \cdot (L_{md} - L_{mq}) \cdot cos(2 \cdot \theta_r)}{-9 \cdot g_{\alpha\beta}{}^2 + (g_{\alpha 1\alpha 1} + 2 \cdot g_{\alpha 1\alpha 2}) \cdot (g_{\beta 1\beta 1} + 2 \cdot g_{\beta 1\beta 2})}$$
$$+ \frac{g_{\alpha\beta} \cdot (g_{\beta 1\beta 1} + 2 \cdot g_{\beta 1\beta 2}) \cdot (r_s + \frac{9}{2} \cdot (L_{md} - L_{mq}) \cdot sin(2 \cdot \theta_r))}{-9 \cdot g_{\alpha\beta}{}^2 + (g_{\alpha 1\alpha 1} + 2 \cdot g_{\alpha 1\alpha 2}) \cdot (g_{\beta 1\beta 1} + 2 \cdot g_{\beta 1\beta 2})}$$

$$k_{\beta\alpha} = \frac{\frac{3}{2} \cdot (g_{\alpha 1\alpha 1} + 2 \cdot g_{\alpha 1\alpha 2}) \cdot (g_{\beta 1\beta 1} + 2 \cdot g_{\beta 1\beta 2}) \cdot (L_{md} - L_{mq}) \cdot cos(2 \cdot \theta_r)}{-9 \cdot g_{\alpha\beta}{}^2 + (g_{\alpha 1\alpha 1} + 2 \cdot g_{\alpha 1\alpha 2}) \cdot (g_{\beta 1\beta 1} + 2 \cdot g_{\beta 1\beta 2})}$$
$$+ \frac{g_{\alpha\beta} \cdot (g_{\alpha 1\alpha 1} + 2 \cdot g_{\alpha 1\alpha 2}) \cdot (r_s - \frac{9}{2} \cdot (L_{md} - L_{mq}) \cdot sin(2 \cdot \theta_r))}{-9 \cdot g_{\alpha\beta}{}^2 + (g_{\alpha 1\alpha 1} + 2 \cdot g_{\alpha 1\alpha 2}) \cdot (g_{\beta 1\beta 1} + 2 \cdot g_{\beta 1\beta 2})}$$

whereas the matrix for the stator decouplings can be expressed as

$$[K_{st}] = \begin{bmatrix} k_{st1} & k_{st2} & k_{st3} & k_{st2} & k_{st3} & k_{st2} \\ k_{st4} & k_{st5} & k_{st4} & k_{st6} & k_{st4} & k_{st6} \\ k_{st3} & k_{st2} & k_{st1} & k_{st2} & k_{st3} & k_{st2} \\ k_{st4} & k_{st6} & k_{st4} & k_{st5} & k_{st4} & k_{st6} \\ k_{st3} & k_{st2} & k_{st3} & k_{st2} & k_{st1} & k_{st2} \\ k_{st4} & k_{st6} & k_{st4} & k_{st6} & k_{st4} & k_{st5} \end{bmatrix} \qquad \textbf{(4.74)}$$

The inputs decoupling matrix is,

$$[K_{in}] = \begin{bmatrix} k_{in1} & k_{in2} & k_{in3} & k_{in2} & k_{in3} & k_{in2} \\ k_{in2} & k_{in4} & k_{in2} & k_{in5} & k_{in2} & k_{in5} \\ k_{in3} & k_{in2} & k_{in1} & k_{in2} & k_{in3} & k_{in2} \\ k_{in2} & k_{in5} & k_{in2} & k_{in4} & k_{in2} & k_{in5} \\ k_{in3} & k_{in2} & k_{in3} & k_{in2} & k_{in1} & k_{in2} \\ k_{in2} & k_{in5} & k_{in2} & k_{in5} & k_{in2} & k_{in4} \end{bmatrix} \qquad \textbf{(4.75)}$$

where the expressions of the terms have been omitted here due to their complex nature; but, they are detailed in the Appendix 3 with a nomenclature that allows a direct integration into DSP code.

From equation (4.68), it can be seen that the terms in the inductance matrix and the transformed rotor flux are dependent on the rotor angle (θ_r). This means that the rotational transformation into the synchronous reference frame needs to be applied to the equations, resulting in

$$[L_s]_{t+r} = \begin{bmatrix} L_{ls}+\frac{3}{2}\cdot L_{md} & 0 & 0 & \frac{3}{2}\cdot L_{md} & 0 & 0 & \frac{3}{2}\cdot L_{md} & 0 & 0 \\ 0 & L_{ls}+\frac{3}{2}\cdot L_{mq} & 0 & 0 & \frac{3}{2}\cdot L_{mq} & 0 & 0 & \frac{3}{2}\cdot L_{mq} & 0 \\ 0 & 0 & L_{ls} & 0 & 0 & 0 & 0 & 0 & 0 \\ \frac{3}{2}\cdot L_{md} & 0 & 0 & L_{ls}+\frac{3}{2}\cdot L_{md} & 0 & 0 & \frac{3}{2}\cdot L_{md} & 0 & 0 \\ 0 & \frac{3}{2}\cdot L_{mq} & 0 & 0 & L_{ls}+\frac{3}{2}\cdot L_{mq} & 0 & 0 & \frac{3}{2}\cdot L_{mq} & 0 \\ 0 & 0 & 0 & 0 & 0 & L_{ls} & 0 & 0 & 0 \\ \frac{3}{2}\cdot L_{md} & 0 & 0 & \frac{3}{2}\cdot L_{md} & 0 & 0 & L_{ls}+\frac{3}{2}\cdot L_{md} & 0 & 0 \\ 0 & \frac{3}{2}\cdot L_{mq} & 0 & 0 & \frac{3}{2}\cdot L_{mq} & 0 & 0 & L_{ls}+\frac{3}{2}\cdot L_{mq} & 0 \\ 0 & 0 & 0 & 0 & 0 & 0 & 0 & 0 & L_{ls} \end{bmatrix}$$

(4.76)

$$[\Psi_{PM}]_{t+r} = \psi_{PM}\cdot[1\quad 0\quad 0\quad 1\quad 0\quad 0\quad 1\quad 0\quad 0]^T \qquad [T]\cdot\frac{d([T]^{-1})}{dt} = \omega_r\cdot\begin{pmatrix}[a] & [b] & [b] \\ [b] & [a] & [b] \\ [b] & [b] & [a]\end{pmatrix}$$

Substituting all the terms in equation (4.6) and re-arranging the terms to follow the state-space representation,

$$\frac{d([i_s]_{t+r})}{dt} = [L_s]_{t+r}^{-1}\cdot\left([V_s]_{t+r} - [R_s]\cdot[i_s]_{t+r} - \omega_r\cdot\begin{pmatrix}[a] & [b] & [b] \\ [b] & [a] & [b] \\ [b] & [b] & [a]\end{pmatrix}\cdot([L_s]_{t+r}\cdot[i_s]_{t+r} + [\Psi_{PM}]_{t+r})\right)$$

(4.77)

the expressions of the equations for each of the axes can be obtained for a nine-phase machine in the following form:

$$\frac{di_{d1}}{dt} = g_{d11}\cdot\left(v_{d1} - r_s\cdot i_{d1} + \omega_r\cdot\left(\left(L_{ls}+\frac{3}{2}\cdot L_{mq}\right)\cdot i_{q1} + \frac{3}{2}\cdot L_{mq}\cdot(i_{q2}+i_{q3})\right)\right) + g_{d12}$$
$$\cdot\left(v_{d2} - r_s\cdot i_{d2} + \omega_r\cdot\left(\frac{3}{2}\cdot L_{mq}\cdot(i_{q1}+i_{q3}) + \left(L_{ls}+\frac{3}{2}\cdot L_{mq}\right)\cdot i_{q2}\right)\right) + g_{d13}$$
$$\cdot\left(v_{d3} - r_s\cdot i_{d3} + \omega_r\cdot\left(\frac{3}{2}\cdot L_{mq}\cdot(i_{q1}+i_{q2}) + \left(L_{ls}+\frac{3}{2}\cdot L_{mq}\right)\cdot i_{q3}\right)\right)$$

(4.78)

$$\frac{di_{q1}}{dt} = g_{q11}\cdot\left(v_{q1} - r_s\cdot i_{q1} - \omega_r\cdot\left(\psi_{PM} + \left(L_{ls}+\frac{3}{2}\cdot L_{md}\right)\cdot i_{d1} + \frac{3}{2}\cdot L_{md}\cdot(i_{d2}+i_{d3})\right)\right) + g_{q12}$$
$$\cdot\left(v_{q2} - r_s\cdot i_{q2} - \omega_r\cdot\left(\psi_{PM} + \frac{3}{2}\cdot L_{md}\cdot(i_{d1}+i_{d3}) + \left(L_{ls}+\frac{3}{2}\cdot L_{md}\right)\cdot i_{d2}\right)\right) + g_{q13}$$
$$\cdot\left(v_{q3} - r_s\cdot i_{q3} - \omega_r\cdot\left(\psi_{PM} + \frac{3}{2}\cdot L_{md}\cdot(i_{d1}+i_{d2}) + \left(L_{ls}+\frac{3}{2}\cdot L_{md}\right)\cdot i_{d3}\right)\right)$$

$$\frac{di_{d2}}{dt} = g_{d21} \cdot \left(v_{d1} - r_s \cdot i_{d1} + \omega_r \cdot \left(\left(L_{ls} + \frac{3}{2} \cdot L_{mq} \right) \cdot i_{q1} + \frac{3}{2} \cdot L_{mq} \cdot (i_{q2} + i_{q3}) \right) \right) + g_{d22}$$
$$\cdot \left(v_{d2} - r_s \cdot i_{d2} + \omega_r \cdot \left(\frac{3}{2} \cdot L_{mq} \cdot (i_{q1} + i_{q3}) + \left(L_{ls} + \frac{3}{2} \cdot L_{mq} \right) \cdot i_{q2} \right) \right) + g_{d23}$$
$$\cdot \left(v_{d3} - r_s \cdot i_{d3} + \omega_r \cdot \left(\frac{3}{2} \cdot L_{mq} \cdot (i_{q1} + i_{q2}) + \left(L_{ls} + \frac{3}{2} \cdot L_{mq} \right) \cdot i_{q3} \right) \right)$$

$$\frac{di_{q2}}{dt} = g_{q21} \cdot \left(v_{q1} - r_s \cdot i_{q1} - \omega_r \cdot \left(\psi_{PM} + \left(L_{ls} + \frac{3}{2} \cdot L_{md} \right) \cdot i_{d1} + \frac{3}{2} \cdot L_{md} \cdot (i_{d2} + i_{d3}) \right) \right) + g_{q22}$$
$$\cdot \left(v_{q2} - r_s \cdot i_{q2} - \omega_r \cdot \left(\psi_{PM} + \frac{3}{2} \cdot L_{md} \cdot (i_{d1} + i_{d3}) + \left(L_{ls} + \frac{3}{2} \cdot L_{md} \right) \cdot i_{d2} \right) \right) + g_{q23}$$
$$\cdot \left(v_{q3} - r_s \cdot i_{q3} - \omega_r \cdot \left(\psi_{PM} + \frac{3}{2} \cdot L_{md} \cdot (i_{d1} + i_{d2}) + \left(L_{ls} + \frac{3}{2} \cdot L_{md} \right) \cdot i_{d3} \right) \right)$$

$$\frac{di_{d3}}{dt} = g_{d31} \cdot \left(v_{d1} - r_s \cdot i_{d1} + \omega_r \cdot \left(\left(L_{ls} + \frac{3}{2} \cdot L_{mq} \right) \cdot i_{q1} + \frac{3}{2} \cdot L_{mq} \cdot (i_{q2} + i_{q3}) \right) \right) + g_{d32}$$
$$\cdot \left(v_{d2} - r_s \cdot i_{d2} + \omega_r \cdot \left(\frac{3}{2} \cdot L_{mq} \cdot (i_{q1} + i_{q3}) + \left(L_{ls} + \frac{3}{2} \cdot L_{mq} \right) \cdot i_{q2} \right) \right) + g_{d33}$$
$$\cdot \left(v_{d3} - r_s \cdot i_{d3} + \omega_r \cdot \left(\frac{3}{2} \cdot L_{mq} \cdot (i_{q1} + i_{q2}) + \left(L_{ls} + \frac{3}{2} \cdot L_{mq} \right) \cdot i_{q3} \right) \right)$$

$$\frac{di_{q3}}{dt} = g_{q31} \cdot \left(v_{q1} - r_s \cdot i_{q1} - \omega_r \cdot \left(\psi_{PM} + \left(L_{ls} + \frac{3}{2} \cdot L_{md} \right) \cdot i_{d1} + \frac{3}{2} \cdot L_{md} \cdot (i_{d2} + i_{d3}) \right) \right) + g_{q32}$$
$$\cdot \left(v_{q2} - r_s \cdot i_{q2} - \omega_r \cdot \left(\psi_{PM} + \frac{3}{2} \cdot L_{md} \cdot (i_{d1} + i_{d3}) + \left(L_{ls} + \frac{3}{2} \cdot L_{md} \right) \cdot i_{d2} \right) \right) + g_{q33}$$
$$\cdot \left(v_{q3} - r_s \cdot i_{q3} - \omega_r \cdot \left(\psi_{PM} + \frac{3}{2} \cdot L_{md} \cdot (i_{d1} + i_{d2}) + \left(L_{ls} + \frac{3}{2} \cdot L_{md} \right) \cdot i_{d3} \right) \right)$$

where v_{dk}, v_{qk} and i_{dk}, i_{qk} are the *d*- and *q*-axis voltages and currents in the three-phase system number *k* and the coefficients g_d and g_q can be calculated as

$$g_{d11} = g_{d22} = g_{d33} = \frac{2 \cdot L_{ls} + 6 \cdot L_{md}}{L_{ls} \cdot (2 \cdot L_{ls} + 9 \cdot L_{md})}$$

$$g_{q11} = g_{q22} = g_{q33} = \frac{2 \cdot L_{ls} + 6 \cdot L_{mq}}{L_{ls} \cdot (2 \cdot L_{ls} + 9 \cdot L_{mq})}$$

$$g_{d12} = g_{d21} = g_{d13} = g_{d31} = g_{d23} = g_{d32} = \frac{-3 \cdot L_{md}}{L_{ls} \cdot (2 \cdot L_{ls} + 9 \cdot L_{md})}$$

$$g_{q12} = g_{q21} = g_{q13} = g_{q31} = g_{q23} = g_{q32} = \frac{-3 \cdot L_{mq}}{L_{ls} \cdot (2 \cdot L_{ls} + 9 \cdot L_{mq})}$$

(4.79)

By compensating the inputs in the *q*-axis with the terms related to the flux of the permanent magnets, equation (4.34) is simplified as

$$\frac{di_{qk}}{dt} = g_{qk1} \cdot \left(v_{q1c} - r_s \cdot i_{q1} - \omega_r \cdot \left(\left(L_{ls} + \frac{3}{2} \cdot L_{md} \right) \cdot i_{d1} + \frac{3}{2} \cdot L_{md} \cdot (i_{d2} + i_{d3}) \right) \right) + g_{qk2}$$
$$\cdot \left(v_{q2c} - r_s \cdot i_{q2} - \omega_r \cdot \left(\frac{3}{2} \cdot L_{md} \cdot (i_{d1} + i_{d3}) + \left(L_{ls} + \frac{3}{2} \cdot L_{md} \right) \cdot i_{d2} \right) \right) + g_{qk3}$$
$$\cdot \left(v_{q3c} - r_s \cdot i_{q3} - \omega_r \cdot \left(\frac{3}{2} \cdot L_{md} \cdot (i_{d1} + i_{d2}) + \left(L_{ls} + \frac{3}{2} \cdot L_{md} \right) \cdot i_{d3} \right) \right)$$

(4.80)

where v_{qkc} is the compensated input of the *q*-axis in the *k*-th three-phase system,

$$v_{dkc} = v_{dk}$$
$$v_{qkc} = v_{qk} + \omega_r \cdot \psi_{PM}$$

(4.81)

Constructing the matrices of the state-space representation having in mind the equalities shown in (4.79), while considering the output matrix [*C*] as equal to an identity matrix, yields:

$$[\dot{X}] = [A] \cdot [X] + [B] \cdot [u_c]$$

$$[Y] = [X]$$

$$[X] = \left[i_{d1}, i_{q1}, i_{d2}, i_{q2}, i_{d3}, i_{q3}\right]^T$$

$$[u_c] = \left[v_{d1c}, v_{q1c}, v_{d2c}, v_{q2c}, v_{d3c}, v_{q3c}\right]^T$$

$$[A] = \begin{bmatrix} a_{11} & a_{12} & a_{13} & a_{14} & a_{15} & a_{16} \\ a_{21} & a_{22} & a_{23} & a_{24} & a_{25} & a_{26} \\ a_{31} & a_{32} & a_{33} & a_{34} & a_{35} & a_{36} \\ a_{41} & a_{42} & a_{43} & a_{44} & a_{45} & a_{46} \\ a_{51} & a_{52} & a_{53} & a_{54} & a_{55} & a_{56} \\ a_{61} & a_{62} & a_{63} & a_{64} & a_{65} & a_{66} \end{bmatrix}$$

$$a_{11} = a_{33} = a_{55} = -g_{d11} \cdot r_s$$

$$a_{12} = a_{34} = a_{56} = g_{d11} \cdot \omega_r \cdot \left(L_{ls} + \frac{3}{2} \cdot L_{mq}\right) + 3 \cdot g_{d12} \cdot \omega_r \cdot L_{mq}$$

$$a_{13} = a_{15} = a_{31} = a_{35} = a_{51} = a_{53} = -g_{d12} \cdot r_s$$

$$a_{14} = a_{16} = g_{d11} \cdot \omega_r \cdot \frac{3}{2} \cdot L_{mq} + g_{d12} \cdot \omega_r \cdot \left(L_{ls} + 3 \cdot L_{mq}\right)$$ **(4.82)**

$$a_{21} = a_{43} = a_{65} = -g_{q11} \cdot \omega_r \cdot \left(L_{ls} + \frac{3}{2} \cdot L_{md}\right) - g_{q12} \cdot \omega_r \cdot 3 \cdot L_{md}$$

$$a_{22} = a_{44} = a_{66} = -g_{q11} \cdot r_s$$

$$a_{24} = a_{26} = a_{42} = a_{46} = a_{62} = a_{64} = -g_{q12} \cdot r_s$$

$$a_{23} = a_{25} = a_{41} = -g_{q11} \cdot \omega_r \cdot \frac{3}{2} \cdot L_{md} - g_{q12} \cdot \omega_r \cdot (L_{ls} + 3 \cdot L_{md})$$

$$a_{32} = a_{36} = a_{52} = a_{54} = g_{d11} \cdot \omega_r \cdot \frac{3}{2} \cdot L_{mq} + g_{d12} \cdot \omega_r \cdot \left(L_{ls} + 3 \cdot L_{mq}\right)$$

$$a_{45} = a_{61} = a_{63} = -g_{q11} \cdot \omega_r \cdot \frac{3}{2} \cdot L_{md} - g_{q12} \cdot \omega_r \cdot (L_{ls} + 3 \cdot L_{md})$$

$$[B] = \begin{bmatrix} g_{d11} & 0 & g_{d12} & 0 & g_{d12} & 0 \\ 0 & g_{q11} & 0 & g_{q12} & 0 & g_{q12} \\ g_{d12} & 0 & g_{d11} & 0 & g_{d12} & 0 \\ 0 & g_{q12} & 0 & g_{q11} & 0 & g_{q12} \\ g_{d12} & 0 & g_{d12} & 0 & g_{d11} & 0 \\ 0 & g_{q12} & 0 & g_{q12} & 0 & g_{q11} \end{bmatrix}$$

The system's cross-couplings become evident in the matrix [A]. This matrix has non-zero elements in all the positions, meaning a heavy cross-coupling. The reduction of these cross-couplings can be made in a similar manner as done above for the stationary reference frame, yielding the following decoupling matrices:

$$[K_{dq}] = [B]^{-1} \cdot ([A_{dq}] - [A]) = \begin{bmatrix} 0 & k_{d1} & 0 & k_{d2} & 0 & k_{d2} \\ k_{q1} & 0 & k_{q2} & 0 & k_{q2} & 0 \\ 0 & k_{d2} & 0 & k_{d1} & 0 & k_{d2} \\ k_{q2} & 0 & k_{q1} & 0 & k_{q2} & 0 \\ 0 & k_{d2} & 0 & k_{d2} & 0 & k_{d1} \\ k_{q2} & 0 & k_{q2} & 0 & k_{q1} & 0 \end{bmatrix}$$

(4.83)

$$k_{d1} = -\omega_r \cdot \left(L_{ls} + \frac{3}{2} \cdot L_{mq} \right) \qquad k_{d2} = -\omega_r \cdot \frac{3}{2} \cdot L_{mq} \qquad k_{q1} = \omega_r \cdot \left(L_{ls} + \frac{3}{2} \cdot L_{md} \right) \qquad k_{q2} = \omega_r \cdot \frac{3}{2} \cdot L_{md}$$

$$[K_{st}] = [B]^{-1} \cdot ([A_{dqst}] - [A_{dq}]) = \begin{bmatrix} k_{st1} & 0 & k_{st2} & 0 & k_{st2} & 0 \\ 0 & k_{st3} & 0 & k_{st4} & 0 & k_{st4} \\ k_{st2} & 0 & k_{st1} & 0 & k_{st2} & 0 \\ 0 & k_{st4} & 0 & k_{st3} & 0 & k_{st4} \\ k_{st2} & 0 & k_{st2} & 0 & k_{st1} & 0 \\ 0 & k_{st4} & 0 & k_{st4} & 0 & k_{st3} \end{bmatrix}$$

(4.84)

$$k_{st1} = -\frac{2 \cdot g_{d12}{}^2}{g_{d11}{}^2 + g_{d11} \cdot g_{d12} - 2 \cdot g_{d12}{}^2} \cdot r_s \qquad k_{st2} = \frac{g_{d11} \cdot g_{d12}}{g_{d11}{}^2 + g_{d11} \cdot g_{d12} - 2 \cdot g_{d12}{}^2} \cdot r_s$$

$$k_{st3} = -\frac{2 \cdot g_{q12}{}^2}{g_{q11}{}^2 + g_{q11} \cdot g_{q12} - 2 \cdot g_{q12}{}^2} \cdot r_s \qquad k_{st4} = \frac{g_{q11} \cdot g_{q12}}{g_{q11}{}^2 + g_{q11} \cdot g_{q12} - 2 \cdot g_{q12}{}^2} \cdot r_s$$

$$[K_{in}] = [B]^{-1} = \begin{bmatrix} k_{in1} & 0 & k_{in2} & 0 & k_{in2} & 0 \\ 0 & k_{in3} & 0 & k_{in4} & 0 & k_{in4} \\ k_{in2} & 0 & k_{in1} & 0 & k_{in1} & 0 \\ 0 & k_{in4} & 0 & k_{in3} & 0 & k_{in4} \\ k_{in2} & 0 & k_{in2} & 0 & k_{in1} & 0 \\ 0 & k_{in4} & 0 & k_{in4} & 0 & k_{in3} \end{bmatrix}$$

(4.85)

$$k_{in1} = \frac{g_{d11} + g_{d12}}{g_{d11}{}^2 + g_{d11} \cdot g_{d12} - 2 \cdot g_{d12}{}^2} \qquad k_{in2} = -\frac{g_{d12}}{g_{d11}{}^2 + g_{d11} \cdot g_{d12} - 2 \cdot g_{d12}{}^2}$$

$$k_{in3} = \frac{g_{q11} + g_{q12}}{g_{q11}{}^2 + g_{q11} \cdot g_{q12} - 2 \cdot g_{q12}{}^2} \qquad k_{in4} = -\frac{g_{q12}}{g_{q11}{}^2 + g_{q11} \cdot g_{q12} - 2 \cdot g_{q12}{}^2}$$

The combination of all these manipulations leads to a totally decoupled model of a triple three-phase systems machine following the multiple dq approach with the following state space representation

$$[\dot{X}] = [A_{dqst}] \cdot [X] + [I] \cdot [u_c] \qquad [Y] = [X]$$

$$[X] = [i_{d1}, i_{q1}, i_{d2}, i_{q2}, i_{d3}, i_{q3}]^T \qquad [u_c] = [v_{d1c}, v_{q1c}, v_{d2c}, v_{q2c}, v_{d3c}, v_{q3c}]^T$$

(4.86)

Writing the equations on per axis basis, the following equations apply for the current control loops:

$$\frac{di_{d1}}{dt} = -r_s \cdot g_{d11} \cdot i_{d1} + v_{d1c} \qquad \frac{di_{q1}}{dt} = -r_s \cdot g_{q11} \cdot i_{q1} + v_{q1c}$$

$$\frac{di_{d2}}{dt} = -r_s \cdot g_{d11} \cdot i_{d2} + v_{d2c} \qquad \frac{di_{q2}}{dt} = -r_s \cdot g_{q11} \cdot i_{q2} + v_{q2c}$$

$$\frac{di_{d3}}{dt} = -r_s \cdot g_{d11} \cdot i_{d3} + v_{d3c} \qquad \frac{di_{q3}}{dt} = -r_s \cdot g_{q11} \cdot i_{q3} + v_{q3c}$$

(4.87)

resulting again in a fully decoupled model with a first-order inductive plant in each of the axes.

4.2.2.2 Models resulting from vector space decomposition approach

In this case, the transformation matrix required is the one shown in (3.20) for a nine-phase machine.

Calculating the unknown terms (4.9) for a nine-phase machine,

$$[L_s]_t = \begin{bmatrix} L_{ls} + 2 \cdot L_{\alpha\alpha} & 2 \cdot L_{\alpha\beta} & 0 & 0 & 0 & 0 \\ 2 \cdot L_{\alpha\beta} & L_{ls} + 2 \cdot L_{\beta\beta} & 0 & 0 & 0 & 0 \\ 0 & 0 & L_{ls} & 0 & 0 & 0 \\ 0 & 0 & 0 & L_{ls} & 0 & 0 \\ 0 & 0 & 0 & 0 & L_{ls} & 0 \\ 0 & 0 & 0 & 0 & 0 & L_{ls} \end{bmatrix}$$

(4.88)

$$[\Psi_{PM}]_t = \psi_{PM} \cdot [cos(\theta_r) \quad sin(\theta_r) \quad 0 \quad 0 \quad 0 \quad 0]^T$$

the transformed inductance matrix and permanent magnet's flux vector are obtained where the values of $L_{\alpha\alpha}$, $L_{\beta\beta}$ and $L_{\alpha\beta}$ are those shown in (4.11). In the inductance matrix shown in (4.88), the rows and columns corresponding to the zero-sequence components have been omitted for the sake of simplicity. Rearranging the equations to follow the state space notation,

$$\frac{di_\alpha}{dt} = g_{\alpha\alpha} \cdot \left(v_\alpha - r_s \cdot i_\alpha + \omega_r \cdot \psi_{PM} \cdot sin(\theta_r) + 3 \cdot (L_{md} - L_{mq}) \cdot (i_\alpha \cdot sin(2 \cdot \theta_r) - i_\beta \cdot cos(2 \cdot \theta_r)) + g_{\alpha\beta} \right.$$
$$\left. \cdot \left(v_\beta - r_s \cdot i_\beta - \omega_r \cdot \psi_{PM} \cdot cos(\theta_r) - 3 \cdot (L_{md} - L_{mq}) \cdot (i_\alpha \cdot cos(2 \cdot \theta_r) + i_\beta \cdot sin(2 \cdot \theta_r))\right)\right)$$

$$\frac{di_\beta}{dt} = g_{\alpha\beta} \cdot \left(v_\alpha - r_s \cdot i_\alpha + \omega_r \cdot \psi_{PM} \cdot sin(\theta_r) + 3 \cdot (L_{md} - L_{mq}) \cdot (i_\alpha \cdot sin(2 \cdot \theta_r) - i_\beta \cdot cos(2 \cdot \theta_r)) + g_{\beta\beta} \right.$$
$$\left. \cdot \left(v_\beta - r_s \cdot i_\beta - \omega_r \cdot \psi_{PM} \cdot cos(\theta_r) - 3 \cdot (L_{md} - L_{mq}) \cdot (i_\alpha \cdot cos(2 \cdot \theta_r) + i_\beta \cdot sin(2 \cdot \theta_r))\right)\right)$$

(4.89)

$$\frac{di_{x1}}{dt} = g_{xy} \cdot (v_{x1} - r_s \cdot i_{x1}) \qquad \frac{di_{y1}}{dt} = g_{xy} \cdot (v_{y1} - r_s \cdot i_{y1})$$

$$\frac{di_{x2}}{dt} = g_{xy} \cdot (v_{x2} - r_s \cdot i_{x2}) \qquad \frac{di_{y2}}{dt} = g_{xy} \cdot (v_{y2} - r_s \cdot i_{y2})$$

where v_α, v_β, v_{x1}, v_{y1}, v_{x2}, v_{y2} and i_α, i_β, i_{x1}, i_{y1}, i_{x2}, i_{y2} are the α-, β-, $x1$-, $y1$-, $x2$- and $y2$-axis voltages and currents in the machine and the coefficients $g_{\alpha\alpha}$, $g_{\alpha\beta}$, $g_{\beta\beta}$ and g_{xy} can be calculated as

$$g_{\alpha\alpha} = \frac{4 \cdot L_{ls} + 9 \cdot (L_{md} + L_{mq}) - 9 \cdot (L_{md} - L_{mq}) \cdot \cos(2 \cdot \theta_r)}{(2 \cdot L_{ls} + 9 \cdot L_{md}) \cdot (2 \cdot L_{ls} + 9 \cdot L_{mq})}$$

$$g_{\beta\beta} = \frac{4 \cdot L_{ls} + 9 \cdot (L_{md} + L_{mq}) + 9 \cdot (L_{md} - L_{mq}) \cdot \cos(2 \cdot \theta_r)}{(2 \cdot L_{ls} + 9 \cdot L_{md}) \cdot (2 \cdot L_{ls} + 9 \cdot L_{mq})}$$

$$g_{\alpha\beta} = \frac{-9 \cdot (L_{md} - L_{mq}) \cdot \sin(2 \cdot \theta_r)}{(2 \cdot L_{ls} + 9 \cdot L_{md}) \cdot (2 \cdot L_{ls} + 9 \cdot L_{mq})}$$

$$g_{xy} = \frac{1}{L_{ls}}$$

(4.90)

Constructing the matrices of the state-space representation from equation (4.89), while considering the output matrix $[C]$ as equal to an identity matrix, yields:

$$[\dot{X}] = [A] \cdot [X] + [B] \cdot [u] \qquad [Y] = [X]$$

$$[X] = [i_\alpha, i_\beta, i_{x1}, i_{y1}, i_{x2}, i_{y2}]^T \qquad [u_c] = [v_{\alpha c}, v_{\beta c}, v_{x1}, v_{y1}, v_{x2}, v_{y2}]^T$$

$$[A] = \begin{bmatrix} a_{11} & a_{12} & 0 & 0 & 0 & 0 \\ a_{21} & a_{22} & 0 & 0 & 0 & 0 \\ 0 & 0 & a_{33} & 0 & 0 & 0 \\ 0 & 0 & 0 & a_{33} & 0 & 0 \\ 0 & 0 & 0 & 0 & a_{33} & 0 \\ 0 & 0 & 0 & 0 & 0 & a_{33} \end{bmatrix}$$

$$a_{11} = -g_{\alpha\alpha} \cdot \left(r_s - \frac{9}{2} \cdot (L_{md} - L_{mq}) \cdot \sin(2 \cdot \theta_r)\right) - g_{\alpha\beta} \cdot \frac{9}{2} \cdot (L_{md} - L_{mq}) \cdot \cos(2 \cdot \theta_r)$$

$$a_{12} = -g_{\alpha\alpha} \cdot \frac{9}{2} \cdot (L_{md} - L_{mq}) \cdot \cos(2 \cdot \theta_r) - g_{\alpha\beta} \cdot \left(r_s + \frac{9}{2} \cdot (L_{md} - L_{mq}) \cdot \sin(2 \cdot \theta_r)\right)$$

(4.91)

$$a_{21} = -g_{\beta\beta} \cdot \frac{9}{2} \cdot (L_{md} - L_{mq}) \cdot \cos(2 \cdot \theta_r) - g_{\alpha\beta} \cdot \left(r_s - \frac{9}{2} \cdot (L_{md} - L_{mq}) \cdot \sin(2 \cdot \theta_r)\right)$$

$$a_{22} = -g_{\beta\beta} \cdot \left(r_s + \frac{9}{2} \cdot (L_{md} - L_{mq}) \cdot \sin(2 \cdot \theta_r)\right) - g_{\alpha\beta} \cdot \frac{9}{2} \cdot (L_{md} - L_{mq}) \cdot \cos(2 \cdot \theta_r)$$

$$a_{33} = -g_{xy} \cdot r_s$$

$$[B] = \begin{bmatrix} g_{\alpha\alpha} & g_{\alpha\beta} & 0 & 0 & 0 & 0 \\ g_{\alpha\beta} & g_{\beta\beta} & 0 & 0 & 0 & 0 \\ 0 & 0 & g_{xy} & 0 & 0 & 0 \\ 0 & 0 & 0 & g_{xy} & 0 & 0 \\ 0 & 0 & 0 & 0 & g_{xy} & 0 \\ 0 & 0 & 0 & 0 & 0 & g_{xy} \end{bmatrix}$$

where the cross-couplings present between the first two axes can be clearly seen in both $[A]$ and $[B]$ matrices. The reduction of these cross-couplings yields the following decoupling matrices:

$$[K_{\alpha\beta}] = [B]^{-1} \cdot ([A_{\alpha\beta}] - [A]) = \begin{bmatrix} k_{\alpha\alpha} & k_{\alpha\beta} & 0 & 0 & 0 & 0 \\ k_{\beta\alpha} & k_{\alpha\alpha} & 0 & 0 & 0 & 0 \\ 0 & 0 & 0 & 0 & 0 & 0 \\ 0 & 0 & 0 & 0 & 0 & 0 \\ 0 & 0 & 0 & 0 & 0 & 0 \\ 0 & 0 & 0 & 0 & 0 & 0 \end{bmatrix}$$

(4.92)

$$k_{\alpha\alpha} = -\frac{9}{2} \cdot sin(2 \cdot \theta_r) \cdot (L_{md} - L_{mq}) - \frac{g_{\alpha\beta}^2 \cdot r_s}{(g_{\alpha\alpha} \cdot g_{\beta\beta} - g_{\alpha\beta}^2)}$$

$$k_{\alpha\beta} = \frac{9}{2} \cdot cos(2 \cdot \theta_r) \cdot (L_{md} - L_{mq}) + \frac{g_{\alpha\beta} \cdot g_{\beta\beta} \cdot r_s}{(g_{\alpha\alpha} \cdot g_{\beta\beta} - g_{\alpha\beta}^2)}$$

$$k_{\beta\alpha} = \frac{9}{2} \cdot cos(2 \cdot \theta_r) \cdot (L_{md} - L_{mq}) + \frac{g_{\alpha\beta} \cdot g_{\alpha\alpha} \cdot r_s}{(g_{\alpha\alpha} \cdot g_{\beta\beta} - g_{\alpha\beta}^2)}$$

$$[K_{in}] = [B]^{-1} = \begin{bmatrix} k_{in1} & k_{in2} & 0 & 0 & 0 & 0 \\ k_{in2} & k_{in3} & 0 & 0 & 0 & 0 \\ 0 & 0 & 1 & 0 & 0 & 0 \\ 0 & 0 & 0 & 1 & 0 & 0 \\ 0 & 0 & 0 & 0 & 1 & 0 \\ 0 & 0 & 0 & 0 & 0 & 1 \end{bmatrix}$$

(4.93) [4]

$$k_{in1} = \frac{g_{\beta\beta}}{g_{\alpha\alpha} \cdot g_{\beta\beta} - g_{\alpha\beta}^2} \qquad k_{in2} = \frac{-g_{\alpha\beta}}{g_{\alpha\alpha} \cdot g_{\beta\beta} - g_{\alpha\beta}^2} \qquad k_{in3} = \frac{g_{\alpha\alpha}}{g_{\alpha\alpha} \cdot g_{\beta\beta} - g_{\alpha\beta}^2}$$

The combination of all these manipulations leads to a totally decoupled model of a machine with multiple three-phase systems following the VSD approach in the stationary reference frame, with the following state space representation:

$$[\dot{X}] = [A_{\alpha\beta}] \cdot [X] + [I] \cdot [u_c] \qquad [Y] = [X]$$

$$[X] = [i_\alpha, i_\beta, i_{x1}, i_{y1}, i_{x2}, i_{y2}]^T \qquad [u_c] = [v_{\alpha c}, v_{\beta c}, v_{x1}, v_{y1}, v_{x2}, v_{y2}]^T$$

(4.94)

Writing the equations on per axis basis, the following equations apply for the current control loops:

$$\frac{di_\alpha}{dt} = -r_s \cdot g_{\alpha\alpha} \cdot i_\alpha + v_{\alpha c} \qquad \frac{di_\beta}{dt} = -r_s \cdot g_{\beta\beta} \cdot i_\beta + v_{\beta c}$$

$$\frac{di_{x1}}{dt} = -r_s \cdot g_{xy} \cdot i_{x1} + v_{x1} \qquad \frac{di_{y1}}{dt} = -r_s \cdot g_{xy} \cdot i_{y1} + v_{y1}$$

$$\frac{di_{x2}}{dt} = -r_s \cdot g_{xy} \cdot i_{x2} + v_{x2} \qquad \frac{di_{y2}}{dt} = -r_s \cdot g_{xy} \cdot i_{y2} + v_{y2}$$

(4.95)

---

[4] The terms on the diagonal in the third to the sixth rows in the matrix $[K_{in}]$ have been made intentionally equal to one to avoid scaling unnecessarily the x-y subspaces.

resulting in a fully decoupled model with a first-order inductive plant in each of the axis.

To obtain a fully diagonal inductance matrix regardless of the saliency in the machine, it is again required to apply a rotational transformation but, in this case, only to the first two rows yielding the following matrices:

$$
[L_s]_{t+r} =
\begin{bmatrix}
L_{ls} + \frac{9}{2} \cdot L_{md} & 0 & 0 & 0 & 0 & 0 & 0 & 0 & 0 \\
0 & L_{ls} + \frac{9}{2} \cdot L_{mq} & 0 & 0 & 0 & 0 & 0 & 0 & 0 \\
0 & 0 & L_{ls} & 0 & 0 & 0 & 0 & 0 & 0 \\
0 & 0 & 0 & L_{ls} & 0 & 0 & 0 & 0 & 0 \\
0 & 0 & 0 & 0 & L_{ls} & 0 & 0 & 0 & 0 \\
0 & 0 & 0 & 0 & 0 & L_{ls} & 0 & 0 & 0 \\
0 & 0 & 0 & 0 & 0 & 0 & L_{ls} & 0 & 0 \\
0 & 0 & 0 & 0 & 0 & 0 & 0 & L_{ls} & 0 \\
0 & 0 & 0 & 0 & 0 & 0 & 0 & 0 & L_{ls}
\end{bmatrix}
\tag{4.96}
$$

$$
[\Psi_{PM}]_{t+r} = \psi_{PM} \cdot [1 \quad 0 \quad 0 \quad 0 \quad 0 \quad 0 \quad 0 \quad 0 \quad 0]^T \qquad [T] \cdot \frac{d([T]^{-1})}{dt} = \omega_r \cdot \begin{pmatrix} [a] & [b] & [b] \\ [b] & [a] & [b] \\ [b] & [b] & [a] \end{pmatrix}
$$

where the following conclusions can be extracted:

- the inductance in the flux/torque producing subspace (*d-q* subspace herein after) is the result of the addition of the stator leakage inductance (L_{ls}) and a magnetising inductance (see 3.2.1).
- the inductance in all the non-flux/torque producing subspaces is the same and equals the stator leakage inductance.

Substituting all the terms in equation (4.6) and re-arranging the terms to follow the state-space representation, the equations for each of the axes can be obtained in the following form:

$$
\frac{di_d}{dt} = \frac{1}{L_{ls} + \frac{9}{2} \cdot L_{md}} \cdot \left(v_d - r_s \cdot i_d + \omega_r \cdot \left(L_{ls} + \frac{9}{2} \cdot L_{mq} \right) \cdot i_q \right)
$$

$$
\frac{di_q}{dt} = \frac{1}{L_{ls} + \frac{9}{2} \cdot L_{mq}} \cdot \left(v_q - r_s \cdot i_q - \omega_r \cdot \left(\psi_{PM} + \left(L_{ls} + \frac{9}{2} \cdot L_{md} \right) \cdot i_d \right) \right)
$$

$$
\frac{di_{x1}}{dt} = \frac{1}{L_{ls}} \cdot (v_{x1} - r_s \cdot i_{x1}) \tag{4.97}
$$

$$
\frac{di_{y1}}{dt} = \frac{1}{L_{ls}} \cdot (v_{y1} - r_s \cdot i_{y1})
$$

$$
\frac{di_{x2}}{dt} = \frac{1}{L_{ls}} \cdot (v_{x2} - r_s \cdot i_{x2})
$$

$$
\frac{di_{y2}}{dt} = \frac{1}{L_{ls}} \cdot (v_{y2} - r_s \cdot i_{y2})
$$

The only cross-coupling present in this model is that of the *d*- and *q*-axes, which can be compensated for as in 4.2.1.1 with a state feedback of the form

$$[K_{dqVSD}] = \begin{bmatrix} 0 & k_d & 0 & 0 & 0 & 0 \\ k_q & 0 & 0 & 0 & 0 & 0 \\ 0 & 0 & 0 & 0 & 0 & 0 \\ 0 & 0 & 0 & 0 & 0 & 0 \\ 0 & 0 & 0 & 0 & 0 & 0 \\ 0 & 0 & 0 & 0 & 0 & 0 \end{bmatrix}$$

(4.98)

$$k_d = -\omega_r \cdot \left(L_{ls} + \frac{9}{2} \cdot L_{mq}\right) \qquad k_q = \omega_r \cdot \left(L_{ls} + \frac{9}{2} \cdot L_{md}\right)$$

With this feedback, the model becomes fully decoupled,

$$[\dot{X}] = [A_{VSD}] \cdot [X] + [I] \cdot [u] \quad [Y] = [X]$$

$$[X] = [i_d, i_q, i_{x1}, i_{y1}, i_{x2}, i_{y2}]^T \qquad [u] = [v_d, v_q, v_{x1}, v_{y1}, v_{x2}, v_{y2}]^T$$

(4.99)

Writing the equations on per axis basis, the following equations apply for the current control loops:

$$\frac{di_d}{dt} = \frac{v_d - r_s \cdot i_d}{L_{ls} + \frac{9}{2} \cdot L_{md}} \qquad \frac{di_q}{dt} = \frac{v_q - r_s \cdot i_q}{L_{ls} + \frac{9}{2} \cdot L_{mq}}$$

$$\frac{di_{xi}}{dt} = \frac{v_{xi} - r_s \cdot i_{xi}}{L_{ls}} \qquad \frac{di_{yi}}{dt} = \frac{v_{yi} - r_s \cdot i_{yi}}{L_{ls}}$$

(4.100)

which are very similar to those of the three-phase counterpart (subscript $i = 1,2$).

4.2.2.3 Models resulting from the novel transformation approach

Applying the transformation with the novel transformation matrix shown in (3.38) for a nine-phase machine, the same results as in (4.96) are obtained, thus leading to the same model equations.

4.3 Summary

As it has been demonstrated in this chapter, the equations of a multiphase machine depend on the modelling approach followed. To be more precise, two different sets of equations, one for the multiple dq approach and the other for the VSD (and the novel approach) can be used to control the machine.

In the case of the multiple dq approach, the resultant equations show a high cross-coupling between the three-phase systems in the machine making it necessary to use different decoupling terms to virtually eliminate the cross-couplings (as seen in 4.2.1.1 and in 4.2.2.1). These terms depend on machine parameters (mainly inductances and resistances) which can be poorly estimated or may vary during the machine operation, thus reducing the accuracy of the decoupling. In the case of the VSD and the novel approach, the equations are much better decoupled from the outset, thus minimising the dependence on machine's parameters.

CHAPTER 5

Control of multiphase machines with two three-phase windings

5.1 Introduction

From the control perspective, a multiple three-phase winding machine is very similar to its three-phase counterpart. Regardless of this, applying a control directly derived from the latter machine usually results in a poor dynamic response and even instability. This is so since the multiple three-phase machines present mutual cross-couplings between its three-phase windings. These couplings strongly affect the operation, thus requiring the introduction of some compensation to mitigate them.

In this chapter, a detailed model of the current loops for the machines with two three-phase windings is developed. It includes all the couplings and the decoupling terms that apply to permanent magnet machines with two three-phase windings. Following this, a tuning algorithm for the current loops is also provided yielding PI parameters satisfying different optimization criteria. This tuning algorithm includes all the non-idealities and limitations that industrial control hardware has, such as sample and computation times, delays, filters, etc. Finally, a correlation of the results with experimental data obtained from a test-bench has been established. This correlation has been obtained on the step-by-step basis, firstly using the machine model developed for Matlab's SimPowerSystems, next the control block including all the non-idealities, and finally the entire system.

The most important results of this chapter have been published in (Zabaleta et al., 2017a) and (Zabaleta et al., 2017b).

5.2 Field oriented control of permanent magnet machines with multiple three-phase windings

5.2.1 Basic notions

The basic idea behind the FOC is to align the reference frame with one of the magnetic fields present in a rotating machine. The fields usually considered in permanent magnets machines are as follows:
- The permanent magnet flux (rotor flux orientation)
- The airgap flux (airgap flux orientation)
- The stator flux (stator flux orientation)

The selection of the field to align with is not a trivial issue, as it has serious implications on the cross-couplings between the torque and flux equations. But, as it will be seen next, none of them provides the perfect solution, so that the selection of one or the other is merely a designer's preference.

When the reference frame is aligned with a magnetic flux (ψ in Fig 5.1), the current in the axis aligned with the selected magnetic flux (usually d-axis) creates a magnetic flux that adds (if the current is positive) arithmetically with the selected flux, thus increasing its magnitude without altering its position (see Fig 5.1(a)). The current in the orthogonal axis (usually q-axis) creates a flux which is orthogonal to the initial one, thus altering the angular position of the resultant flux with a slight influence on its magnitude (see Fig 5.1(b)). Hence it can be concluded that, when aligning the reference frame with a magnetic flux, the current in one axis can modify directly the amplitude of the flux, while the current in the other axis mainly affects its angular position.

(a)   (b)
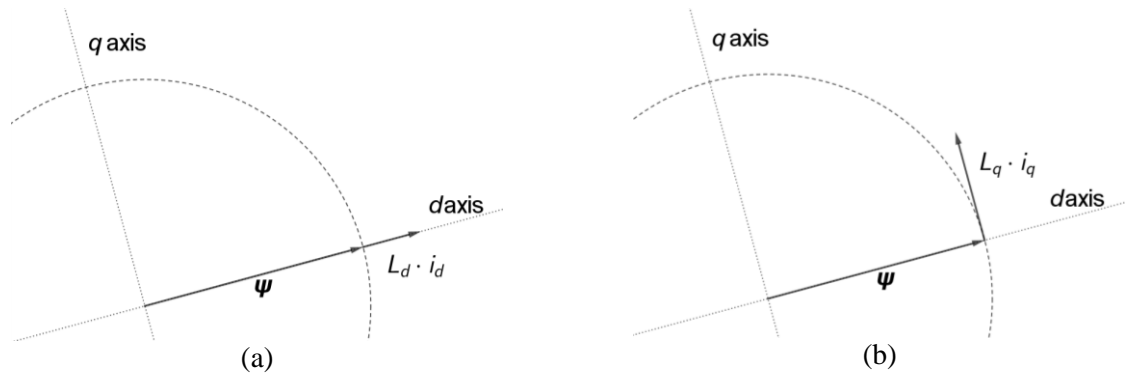
Fig. 5.1 Schematic representation of a magnetic flux modified by currents (a) in the d-axis, (b) in the q-axis.

The behaviour described above resembles that of an independently excited dc machine in which the excitation current governs the amplitude of the magnetic flux, while the armature current determines the torque produced by the machine. This is the main idea of the FOC theory, as it seeks to provide decoupled control of the torque and the flux of a rotating ac machine.

Different alignments are possible, mainly affecting the torque-flux cross-coupling and the plants that are seen by the current regulators. As a brief comparison, Table 5.1 shows the characteristics of each of the alignments mentioned above. To avoid ambiguity with the name of the axes in the different alignments, the following nomenclature will be applied:

- The axes, when alignment with the rotor flux is used, are denoted *d* and *q*
- The axes, when alignment with the airgap flux is used, are denoted *d'* and *q'*
- The axes, when alignment with the stator flux is used, are denoted *M* and *T*

Table 5.1 Summary of the different reference frame orientations commonly used in the literature.

ROTOR FLUX ORIENTATION	
Torque expression	$T_{elec} = \dfrac{n}{2} \cdot p \cdot \left(\psi_{PM} \cdot i_q + \left(L_d - L_q \right) \cdot i_d \cdot i_q \right)$
Stator flux amplitude	$\psi_s = \sqrt{\left(L_q \cdot i_q \right)^2 + (\psi_{PM} + L_d \cdot i_d)^2}$
Transformation angle (θ_{mec})	Easy to obtain as it can be measured by means of rotary encoder. There are several techniques to estimate it eliminating the need for the encoder.
Plant for the current controllers	Constant inductances, good performance.
AIRGAP FLUX ORIENTATION	
Torque expression	$T_{elec} = \dfrac{n}{2} \cdot p \cdot \psi_{airgap} \cdot i_{q'}$
Airgap flux amplitude	$\psi_{airgap} = 2 \cdot L_{mq} \cdot \dfrac{L_{md} \cdot i_{d'} + \psi_{PM} \cdot cos(\theta_f)}{L_{md} + L_{mq} + \left(L_q - L_d \right) \cdot cos(2 \cdot \theta_f)}$
Transformation angle (θ_f)	It could be measured by means of hall-effect sensors located in the airgap; but this yields a less robust machine. Not widely used in industrial applications.
Plant for the current controllers	Variable inductances as the transformation angle differs from θ_{mec} (machine is being loaded), so difficult tuning is to be expected. This applies to machines with saliency.
STATOR FLUX ORIENTATION	
Torque expression	$T_{elec} = \dfrac{n}{2} \cdot p \cdot \psi_s \cdot i_T$
Stator flux amplitude	$\psi_s = \left(\dfrac{2 \cdot L_d \cdot L_q \cdot i_F + 2 \cdot L_q \cdot \psi_{PM} \cdot cos(\delta)}{L_d \cdot (1 - cos(2 \cdot \delta)) + L_q \cdot (1 + cos(2 \cdot \delta))} \right)$
Transformation angle (δ)	It is not possible to measure it, so estimation techniques are compulsory.
Plant for the current controllers	Variable inductances as the transformation angle differs from θ_{mec} (machine is being loaded), so difficult tuning is to be expected. This applies to machines with saliency.

To summarise, the FOC basically consists of controlling the torque and flux of the machine (as much independently as possible) by means of two orthogonal currents. Beyond this point, the rotor flux orientation will be considered unless explicitly stated.

In order to optimise the conversion stage design, the power converter ratings are always matched with those of the machine. This means that the maximum voltage and current output of the power converter coincide with the rated stator values of the machine. The main implication of this is that the stator's voltage and current values should be kept inside a circle of unitary radius at all times to avoid exceeding the power converter maximum values. In Fig. 5.2 (a), the vector diagram of a machine with L_d and L_q equal to 0.8 p.u. is shown when i_d is zero, i_q is 1 p.u. and ω_r equals 0.78 p.u.. It can be seen how at a speed lower than the rated one (1 p.u.), even though the emf phasor (E_{pm}) is smaller than 1 p.u., the stator voltage phasor (V_s) reaches the maximum allowable value when d-axis current is kept at zero and q-axis current is at the rated value. This means that the speed could not be increased any more without lowering the q-axis current (and so the torque). This limitation makes it necessary to adopt a different strategy than keeping the d-axis current zero even below rated speed. As it has been widely studied in the literature, by introducing a negative d-axis current, the magnitude of the stator voltage can be reduced, thus allowing to increase the speed without surpassing the maximum voltage threshold. In Fig. 5.2 (b), the same machine is controlled with d-axis current equal to -0.5 p.u. while q-axis current is kept at 1 p.u. and speed is increased to 1 p.u. while keeping the stator voltage amplitude at rated value. In this last example, it is obvious that the stator current is higher than 1 p.u. so it is not a long-term feasible operating point, but it has been used here to highlight the effect of the negative d-axis current.

In generating applications such as windpower, where the rotating speed of the machine is controlled by very slow dynamic actuators (the blade pitch actuators), the speed can experience big excursions (above current speed) when a sudden wind gust reaches the rotor. If the speed increase yields a stator voltage higher than the power converter's maximum, the converter controller needs to introduce a more negative d-axis current so as to reduce the stator terminal voltage below the maximum value and thus avoid losing the control of the currents.

(a)   (b)
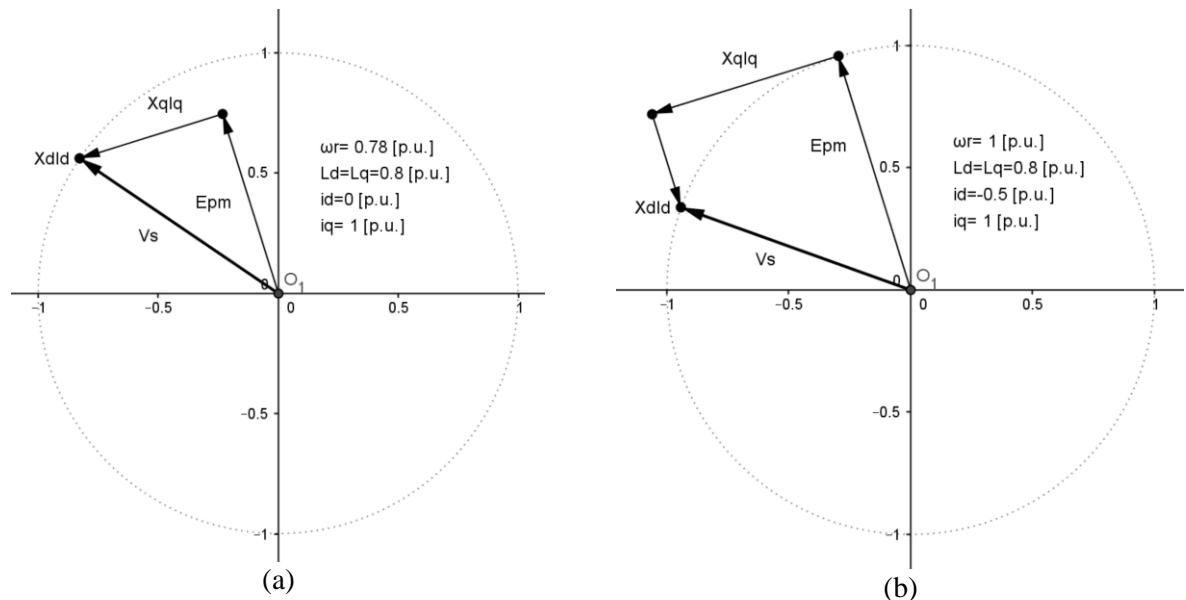
Fig. 5.2 Vector diagrams of a PMSM and the effects of d-axis current: (a) with zero d-axis current and (b) with negative d-axis current.

Regarding the d-axis current reference calculation, several control strategies may arise such as:
- d-axis current reference kept at zero: keeps d-axis current at zero at all times yielding optimal torque per ampere strategy for non-salient machines. It may reach the power converter's maximum voltage below rated speed – hence this strategy reduces the operating speed range.

- Maximum torque per ampere (MTPA) strategy: especially applied in conjunction with salient machines, this strategy generates the *d*-axis current reference that maximises the torque per ampere by means of taking advantage of the reluctance torque. The optimal angle α_c^{opt} can be obtained by differentiating the equation (4.46) with respect to the angle α_c.
- Unity power factor (UPF) operation: consists in setting the *d*-axis current reference in such a way as to obtain unity power factor at the machine's terminals. Depending on the magnetic design of the machine, this strategy can lead to high flux weakening at high loads that can lead to unstable operation (this is of special concern in motoring applications).
- Stator voltage control: consists of setting the *d*-axis current reference in such a way as to obtain the desired stator voltage amplitude. This strategy is the adequate one at high speeds to avoid surpassing the maximum voltage of the power converter.

5.2.2 Controller structure

Because the FOC controls the machine's output by means of currents, current controllers are inevitably required and form the inner-most loop of the control system. A typical structure of the controller (for a three-phase machine) consists of two current controllers (one for the torque- and other for the flux-related currents) whose outputs are the voltage references for the stator. These are fed into a modulation stage which calculates the switching instants of the semiconductor devices. The commands for the current regulators are derived by means of the FOC algorithm which translates the external commands (torque and stator voltage) into current commands (Fig. 5.3).
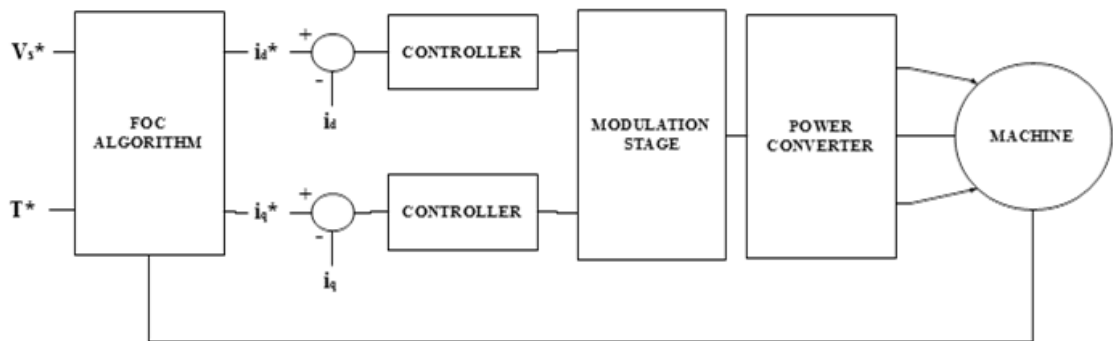
Fig. 5.3 Schematic structure of a FOC controller for a three-phase machine.

The controller structure for a multiphase machine remains the same as the one shown in Fig. 5.3, with the addition of two more current controllers for each of the auxiliary subspaces (or additional three-phase systems in the multiple *dq* approach) present in the machine. These current regulators in the auxiliary subspaces are usually commanded with zero current setpoint when VSD based model is used, but, as it has been demonstrated in CHAPTER 3, commanding non-zero currents in the auxiliary subspaces can lead to unequal current sharing within the three-phase systems in the machine.

5.2.3 Effects of the controller delays

The effects of the delays in the control loops have been widely studied in the literature as they greatly affect the performance of the digital control loops [(Harnefors et al., 2015), (Kim et al., 2010), (Shen et al., 2012)]. Basically, delays introduce a phase drop which is proportional to the frequency. This effect directly affects the phase margin of the system, as it reduces the overall system's phase, thus altering the dynamic behaviour and even affecting the stability as can be seen in Fig. 5.4. In this figure, the frequency response of a controlled system has been plotted with solid line when no delay is included and with dashed line, for the same system in which a delay of 625 μs has been introduced. It can be seen how the phase margin of the system is reduced when the delay is present and, additionally, the delay produces a crossover point with -180º on the phase plot, thus defining a finite gain margin. The consequence of this latter effect is that the gain of the controller should be limited to a certain

value when delays are present (Holmes et al., 2009). To reduce the effect of the delays, a compensation term is usually introduced in the loop which corrects the phase drop at a frequency of interest (usually the fundamental frequency). As stated in (Shen et al., 2012), this compensation shifts upwards the phase plot to get 0 degrees phase shift at desired frequency, but it does not alter the slope of the phase drop. This can be seen in Fig. 5.4 where the dotted line represents the frequency response of the delayed system in which a delay compensation at 100 Hz has been introduced. It can be seen how the phase of the compensated system coincides with that of the one without delay only at said frequency (100 Hz).
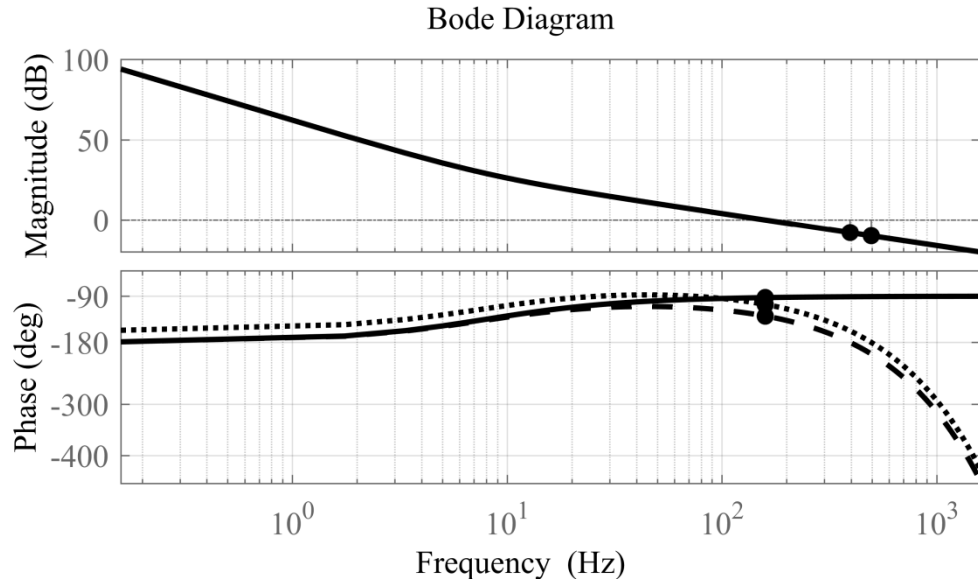
Fig. 5.4 Bode plot of first order system with no delay (solid), delayed system (dashed) and delayed and compensated at 100 Hz (dotted).

When the synchronous frame is chosen, it is important to guarantee that the dynamic behaviour of the current regulators is adequate at all the rotating speeds within the operational range. In the case of motor / generator drives, the entire operational speed range of the machine should be checked. In such applications an additional negative effect of the delays becomes noticeable as the fundamental frequency increases. When the fundamental frequency gets closer to the sampling frequency, the slope of the phase drop introduced by the delay increases (see Fig. 5.4), thus increasing the effect of the delay at the non-compensated frequencies. This effect is translated into the cross-coupling decoupling terms (see K_{dq} and K_{dqVSD} in 4.2.1.1 and 4.2.1.2 for the synchronous reference frame) not being able to fully decouple the d- and q-axes, resulting in the appearance of anomalous gain peaks in the closed loop frequency response that lead to an increased overshoot and stabilization time. This can be seen in Fig. 5.5(a), where the closed loop frequency responses of three controllers in a rotating reference frame, all tuned with 15 Hz bandwidth (BW) and 70º phase margin (PM), are plotted for different rotating speeds. The solid line represents the response when the reference frame rotates at 25 Hz and the smoothness of the magnitude and phase plots recalls a controlled response without oscillations and low overshoot (peak response 12%), as expected from a PM of 70º. The dashed line and the dash-dotted line represent the response when the reference frame rotates at 50 Hz and 75 Hz, respectively, and make obvious the above-mentioned effect showing steep slopes in both gain and phase plots. These abrupt frequency responses lead to oscillatory responses (even instability) and increased overshoot when step changes in the reference occur, as shown in Fig. 5.5(b).

(a)

(b)
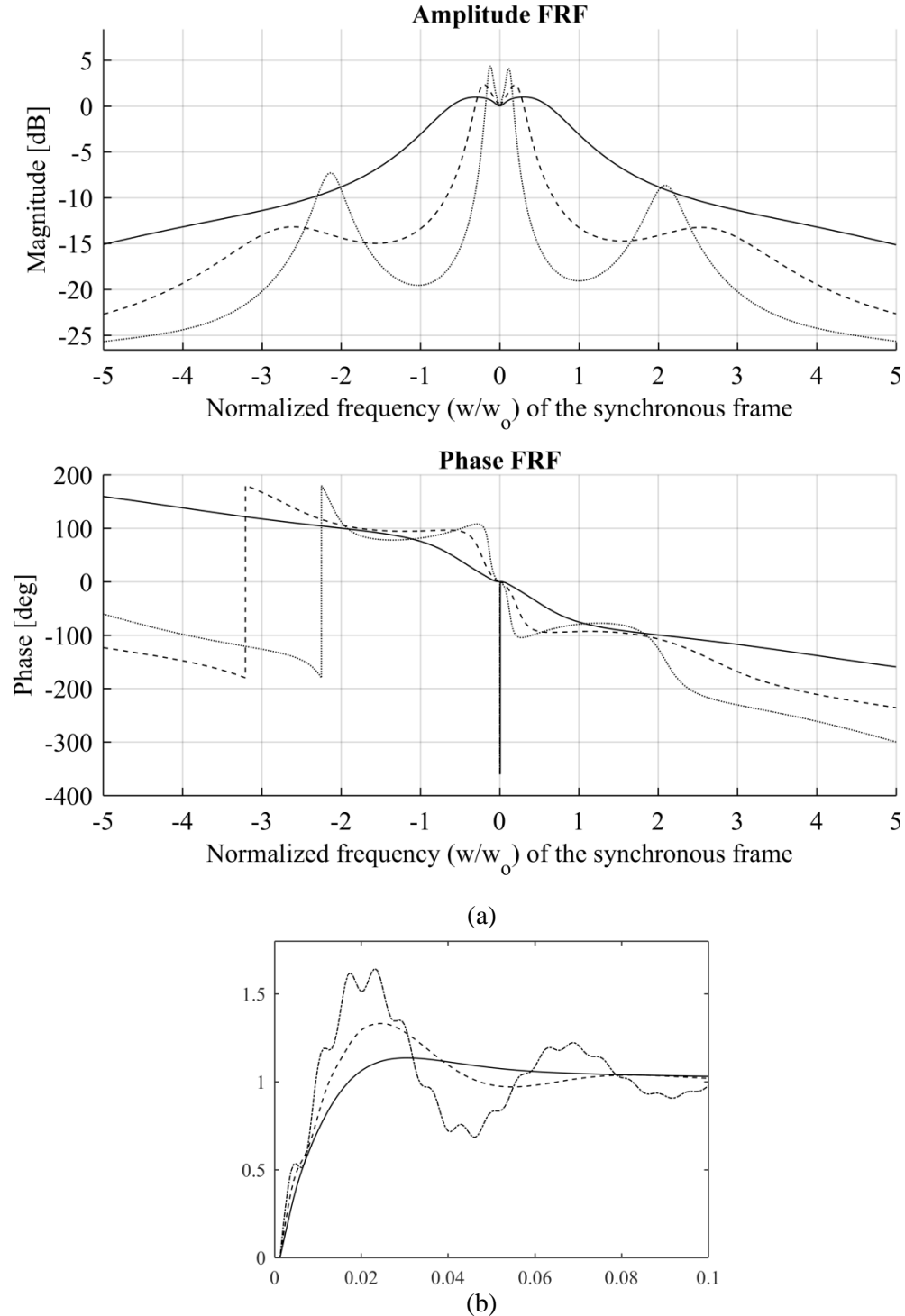
Fig. 5.5 Frequency response function (a) and step responses (b) of closed loop digital controllers (sampling at $T_s = 625$ μs and delayed with $1.5T_s$) in the synchronous frame with the same BW and PM and different rotating speeds: 25 Hz solid line, 50 Hz dashed line and 75 Hz the dash-dotted line.

An important conclusion can be extracted from the previous considerations, relevant for the tuning of current regulators in a rotating reference frame. The BW and PM of the system do not faithfully represent the behaviour of the closed loop, as anomalous peak gains can appear in the frequency response, introducing unexpected oscillations and overshoot. To highlight this limitation, Fig. 5.6 shows the open loop frequency responses of the controllers used in the previous figure. As it

can be seen, all of them present the same BW and PM in the rotating reference frame. The solid line represents the response of the controller tuned for rotating at 25 Hz and the dashed line and the dash-dotted line represent the response when the reference frame rotates at 50 Hz and 75 Hz, respectively. It should be born in mind that the horizontal axis in the figure is referred to the rotating reference frame speed; this explains why the same 15 Hz BW corresponds to different 0 dB crossing points.
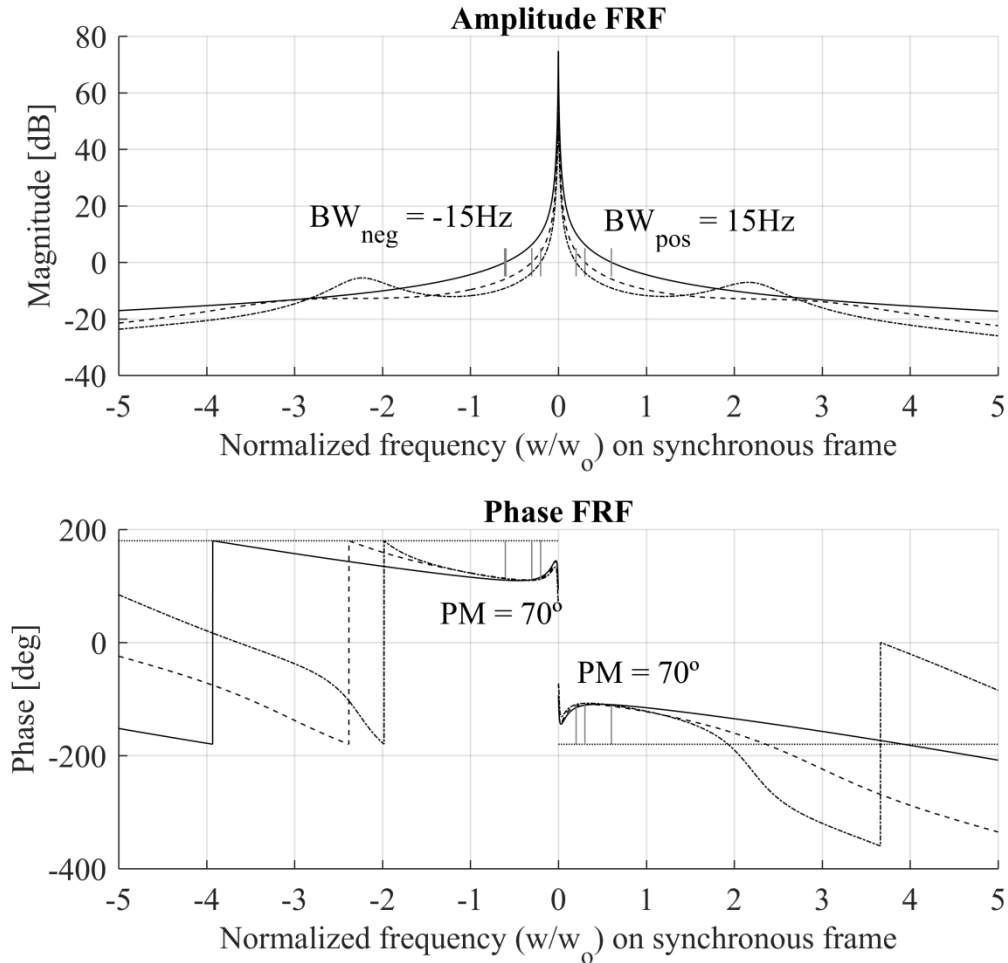
Fig. 5.6 Frequency response function of open loop digital controllers (sampling at 625 μs) in the synchronous frame with the same BW and PM and different rotating speeds: 25 Hz solid line, 50 Hz dashed line and 75 Hz the dash-dotted line.

Another important conclusion extracted from this is that, as the sampling frequency is reduced, it is of vital importance to modify the regulator parameters as the fundamental frequency varies in order to obtain smooth dynamic responses. This is not necessary when the sampling frequency is several times (>40) bigger than the fundamental frequency as it usually happens in low-voltage applications, but it becomes a must when dealing with sampling to fundamental ratios around 20 or below.

5.2.4 Tuning of the current regulators in the synchronous frame

As mentioned in previous sections, the plant for the current regulators depends on the alignment of the reference frame. The rotor of the PMSM is usually the main source for the saliency of the magnetic circuit; so if the rotor flux orientation is chosen, the inductances in the transformed d- and q-axes are constant at all times, as these are fixed to the rotor. It can be seen in Fig. 5.7 how the airgap and the stator fluxes deviate from the rotor's as the machine is loaded with q-axis current. This deviation modifies the effective inductance seen in the axes (aligned with airgap and stator fluxes),

yielding an inductance dependant on the operating point (in machines with saliency). This issue introduces a difficulty when tuning the current regulators as their parameters may need to be varied as the machine operating point is changed.
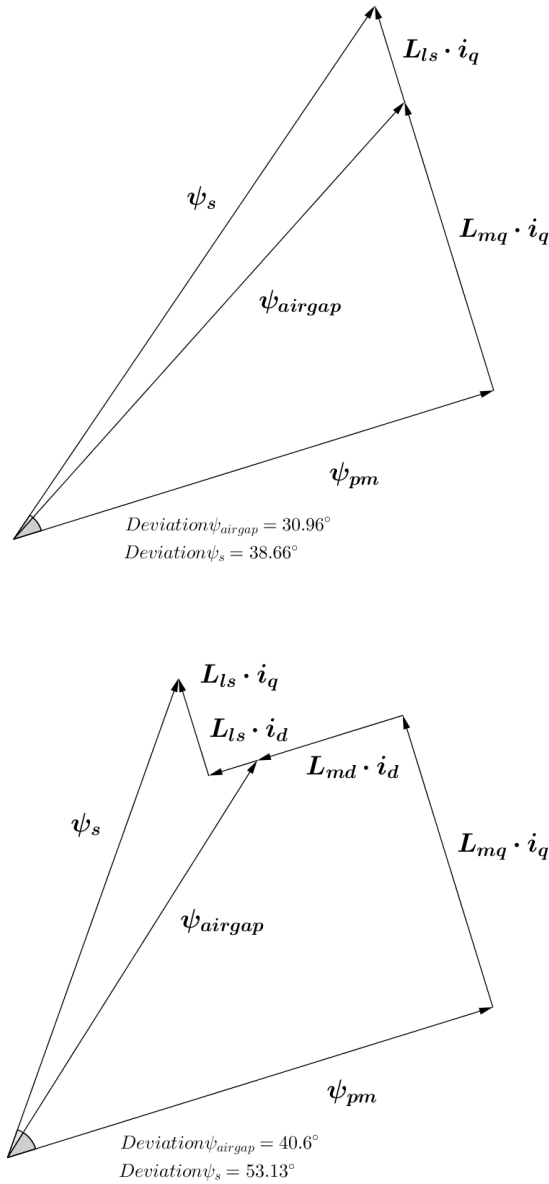
Fig. 5.7 Vector diagram for q-axis current equal to 1 [p.u.] with zero d-axis current (upper) and q-axis current equal to 0.85 [p.u.] with d-axis current equal to -0.5 [p.u.] (lower).

It can be concluded, on the basis of the considerations given above, that, when using a synchronous reference frame, the best option is to align the current regulators' reference frame with the rotor flux. This provides constant inductances and so the current regulators may have the same dynamic response regardless of the operating point of the machine.

Applying the Laplace transformation to the equations resulting from the multiple *dq* approach (4.43), these can be converted from the time domain into the frequency (*s*) domain,

$$\frac{i_{dj}}{v_{dj}} = \frac{1}{s + r_s \cdot g_{d11}}$$

$$\frac{i_{qj}}{v_{qj}} = \frac{1}{s + r_s \cdot g_{q11}}$$

(5.1)

where $j = 1$ to k (the number of the three phase system). The original differential equations are thus converted into simple algebraic ones allowing the construction of the transfer function of the plant for the current regulator design. From equation (5.1), it can be concluded that the plants for the current regulators are a simple first-order system; hence almost any tuning method can be applied to obtain a PI regulator for d- and q-axis. This process will need to be repeated for each of the three-phase systems in the machine as current regulators are needed in all of them. The block diagram shown in Fig. 5.8 represents schematically the structure of the current loop, following the multiple dq approach, to achieve decoupled operation.
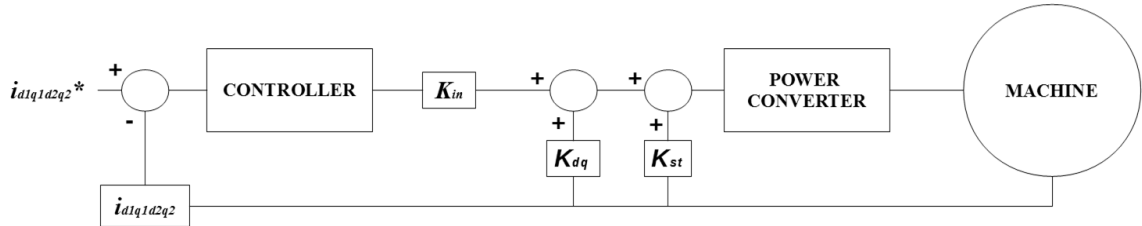
Fig. 5.8 Schematic representation of the current loops with the multiple dq approach.

By constructing the control loop (including the decoupling terms) in Matlab, the transfer function seen by the controller can be obtained and compared with that of the theoretical analysis performed above (equations (5.1)). In Fig. 5.9, the frequency response functions (FRF) of both the theoretical and the analytically obtained transfer functions are shown for the d-axis and a randomly chosen machine parameters, which are at this stage irrelevant. It can be seen how both are perfectly overlapped meaning that they are identical. In this figure, w_o stands for the rotational speed of the synchronous reference frame.
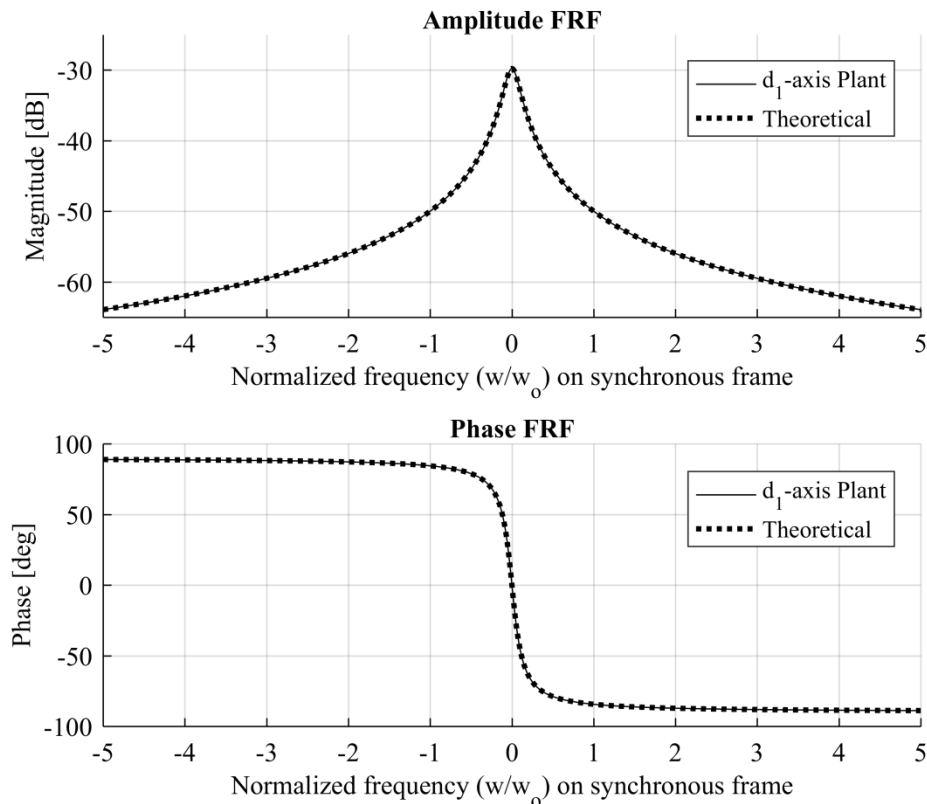
Fig. 5.9 Frequency response functions of the plants seen by the controller in the d-axis after decoupling strategy.

Manipulating now equation (4.62) in a similar manner, the equations to tune the current regulators in the VSD approach can be obtained:

$$\frac{i_d}{v_d} = \frac{1}{\left(L_{ls} + \frac{n}{2} \cdot L_{md}\right) \cdot s + r_s}$$

$$\frac{i_q}{v_q} = \frac{1}{\left(L_{ls} + \frac{n}{2} \cdot L_{mq}\right) \cdot s + r_s}$$

(5.2)

$$\frac{i_x}{v_x} = \frac{1}{L_{ls} \cdot s + r_s}$$

$$\frac{i_y}{v_y} = \frac{1}{L_{ls} \cdot s + r_s}$$

which are very similar to those obtained with the multiple dq approach (5.1). The main difference is that, in this case, no additional transformations in the model are required (see decoupling procedure in 4.2.2.1), thus yielding a simpler and more robust model as it does not rely on machine's parameter values to obtain decoupled operation. In the Fig. 5.10, the schematic representation of the current loop following the VSD or novel approach is shown. It can be seen how the required decoupling terms are reduced to a single d-q decoupling term.
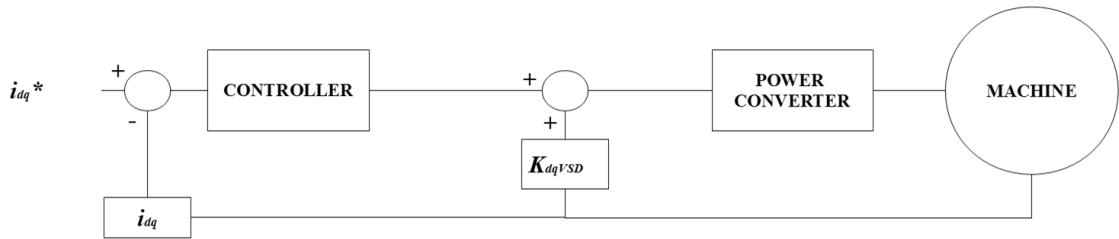
Fig. 5.10 Schematic representation of the current loops with the VSD and novel approaches.

Once the transfer functions of the current regulator plants are obtained, the tuning of the regulators can be accomplished. The most widely used current regulator in the synchronous reference frame is the proportional-integral (PI) one thanks to its good trade-off between dynamic performance and robustness. PI controllers can be tuned following a wide variety of techniques already available in the existing literature (Ho et al., 1996) that lead to slight differences in the load disturbance response and the reference response. In what follows, any PI controller used in this work will be tuned following the procedure described in the Appendix 4 unless explicitly stated. This method is preferred as it implicitly defines the actuation limits (bandwidth) for the controllers facilitating the integration of outer regulators (for stator's power and voltage) and it allows to reliably predict the performance of the control under distorted conditions such as switching harmonics.

As it has been shown in 5.2.3, the delays in the control loop introduce side-effects that strongly impact on the dynamic performance of the loops. A tuning procedure for the current controllers has been designed taking into account almost every single relevant feature present in the real application.
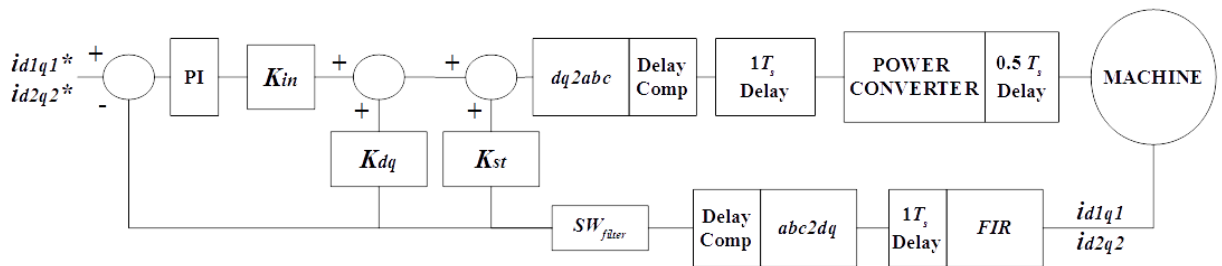
Fig. 5.11 Detailed representation of the current loop used for the tuning procedure following double dq (DDQ) approach. The model used for VSD and novel approaches is exactly the same but removing the K_{in} and K_{st} decoupling terms.

In Fig. 5.11, the detailed current control loop used for the tuning is shown. The entire loop is defined in the digital frame with the sampling time as a parameter (typically 625 µs). The delays present in the direct chain (1 T_s and 0.5 T_s) are those representing the computation time of the DSP and the modulation update time respectively. These can be clearly represented, as in Fig. 5.12, where T_s and T_{sw} stand for the sampling and the switching periods, respectively.
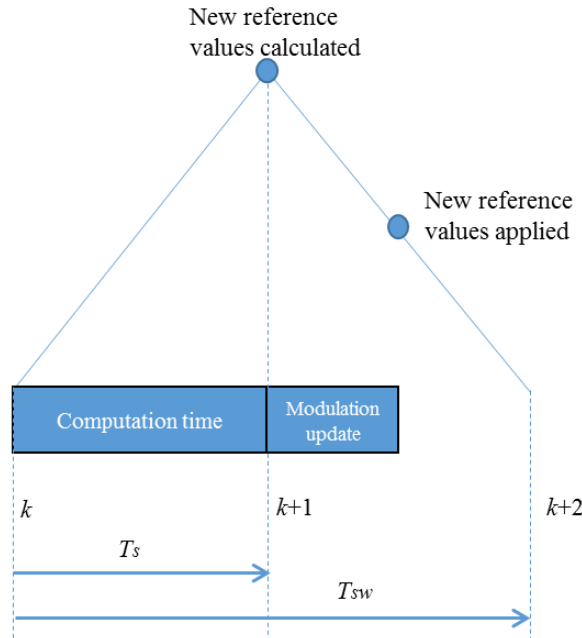
Fig. 5.12 Direct chain delays explanation.

When sampling at low frequencies, there is not enough separation between the control bandwidth (typically 10-20 Hz) and the frequency of the ripple (typically 700-800 Hz), so that a conventional first or second order low-pass filter cannot provide a good ripple-free signal. In these cases, it might be more interesting to use moving average filters to completely remove the switching frequency. The side effect of this filter is that it introduces a delay equal to one sampling time at all frequencies. The one sampling time delay associated with the finite impulse response (FIR) filter can be explained with the help of the Fig. 5.13. The FIR filter is programmed as a moving average filter that completely removes the switching frequency (and its integer multiples) from the measured stator currents. For this purpose, it samples the currents at a high frequency (around 100 kHz) and it provides to the DSP the sum of the values of all the samples across the previous (*k*-1) sampling period (T_s). The DSP keeps in memory the value of the sum across the *k*-2 period and it performs the arithmetical mean between both sums (corresponding to two sampling periods). In the Fig. 5.13, it can be seen how a signal at the switching frequency will provide accumulated sums with opposite signs in *k*-2 and *k*-1 periods thus cancelling it when the mean value is calculated.
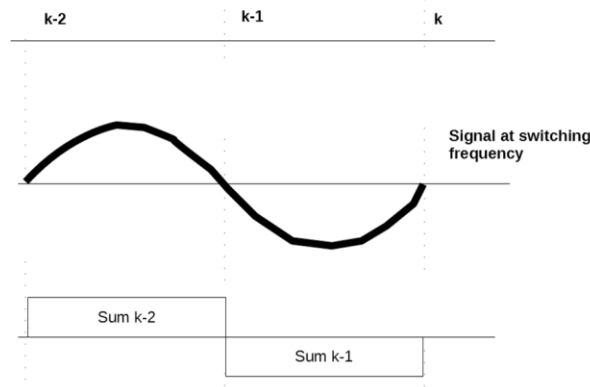
Fig. 5.13 FIR filter delay.

These types of filters can be modelled by a transfer function

$$\frac{i_{filtered}}{i_{sampled}} = \frac{1 - e^{(-s \cdot numTs \cdot Ts)}}{s \cdot numTs \cdot Ts} \tag{5.3}$$

where *numTs* is the number of sampling times that are averaged (2 in this case). The frequency response of said filter can be seen on Fig. 5.14 where it is clear how it completely removes the switching frequency components and all its integer multiples.
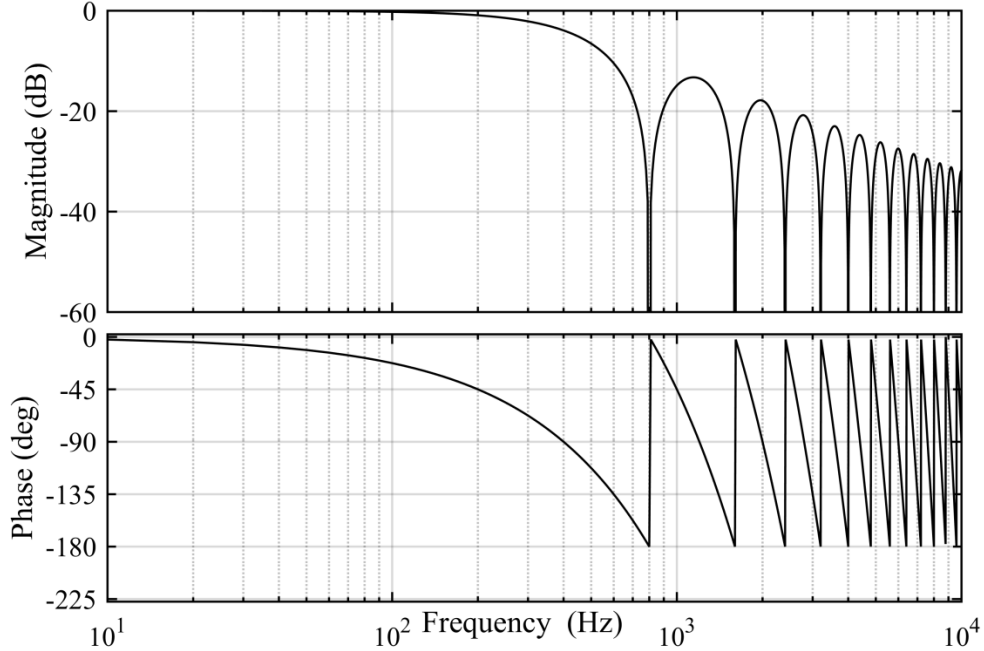
Fig. 5.14 FIR filter frequency response for 800 Hz switching frequency.

To compensate these delays inherent to the system itself, some compensation terms are introduced in the transformation (and in the inverse transformation) to (from) the *d-q* frame. These terms are the usual ones already described in the literature,

$$Delay\ Compensation = e^{\pm j \cdot p \cdot \omega_s \cdot T_s} \tag{5.4}$$

where *p* is a scalar value representing the number of sampling periods that are to be compensated for. As it was described in section 5.2.3, this compensation is exact only at one frequency, ω_s in (5.4) leaving all the other frequencies uncompensated.

To obtain a good behaviour along the operational speed range of the machine, a tuning procedure has been developed; it iterates along a vector of values of rotor speed, and it obtains the PI parameters that satisfy the BW and PM requirements, those that keep the overshoot at a desired level or those that fulfil any other condition such as minimizing the quadratic error (MQE) or the settling time (MSS) of a step response. The tuning procedure follows the flowchart shown in Fig. 5.15. Firstly, a vector containing all the rotational speeds (ω_s) desired is to be set, followed by vectors containing the bandwidths (BW) and phase margins (PM) to be analysed. The tuning algorithm iterates for each rotational speed across the desired bandwidths and phase margins evaluating for each point (ω_s, BW, PM) the desired optimization criteria. Once all the BW and PM have been analysed for a given rotational speed, the next speed is assigned and the procedure starts again.
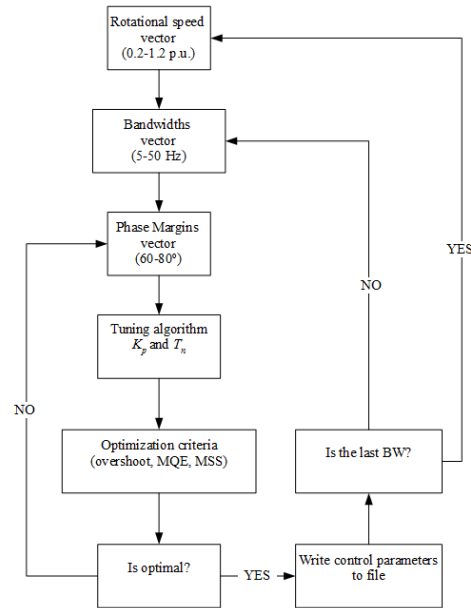
Fig. 5.15 Tuning algorithm flowchart.

The output of the tuning algorithm shown in Fig. 5.15 is a text file as shown in Appendix 5 for the case of the machine used in the test rig. To obtain a reliable tuning procedure, all the elements (both hardware and software) that affect the behaviour of the system should be taken into account inside the tuning algorithm. This is of special concern as the rotational speed gets closer to the sampling frequency as the effects of delays, compensating terms and filters may become crucial.

Several different optimization criteria can be selected for the tuning of the current regulators, each of them having benefits and drawbacks. In the following, these optimization criteria are described. All the tunings have been made considering the machine's parameters shown in Table 5.6.

5.2.4.1   Setting a fixed bandwidth and phase margin

The straightforward criteria might be to set a fixed BW and PM for all the operating speeds of the machine. This, as it was described in 5.2.3, may yield some undesired effects in terms of dynamic performance, such as oscillations and increased overshoot, as the rotational speed gets closer to the sampling frequency. In the Fig. 5.16(a), the evolution of the overshoot for a controller tuned at BW=25 Hz and PM=70º is shown and the abovementioned undesired effect can be observed at rotating speeds above 70 Hz, where the controller becomes critically stable yielding oscillatory response.

(a)   (b)
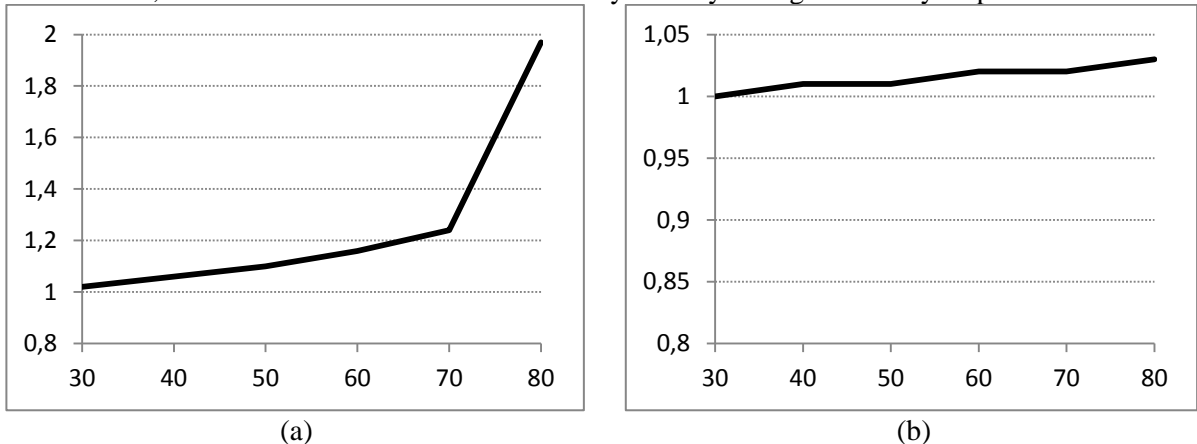
Fig. 5.16 Overshoot across the different rotating speeds for a controller tuned at BW=25 Hz and PM=70º (a) and tuned at BW=15 Hz and PM=70º. In both plots vertical axes represent the current overshoot in p.u. and the horizontals represent the rotational speed in Hz.

In order to obtain a stable operation across the entire rotational speed range, a more conservative tuning may be required Fig. 5.16(b). This criterion has the main drawback in the fact that the slow dynamic response required for the high rotational speed range is forced across the entire rotational speed range thus leading to slower dynamics in the low- and mid-range.

5.2.4.2 Setting a fixed overshoot

A way to improve the control dynamics in the low- and mid-speed range might be to set up a constant overshoot across the entire speed range. With this criterion, at low rotational speeds the dynamic is high (high BW) and it is steadily reduced as the rotational speed increases. These effects can be easily seen in Fig. 5.17. In the figure (a), the overshoot for the different controller settings is plotted for a low rotational speed of 30 Hz. It can be seen how even at the fastest settings (higher BW), the overshoot is kept low. On the other hand, in the figure (b) the same plot is shown for a high rotational speed (80 Hz) and it can be seen how the overshoot rapidly increases as the dynamic of the controller is increased.

(a)

(b)
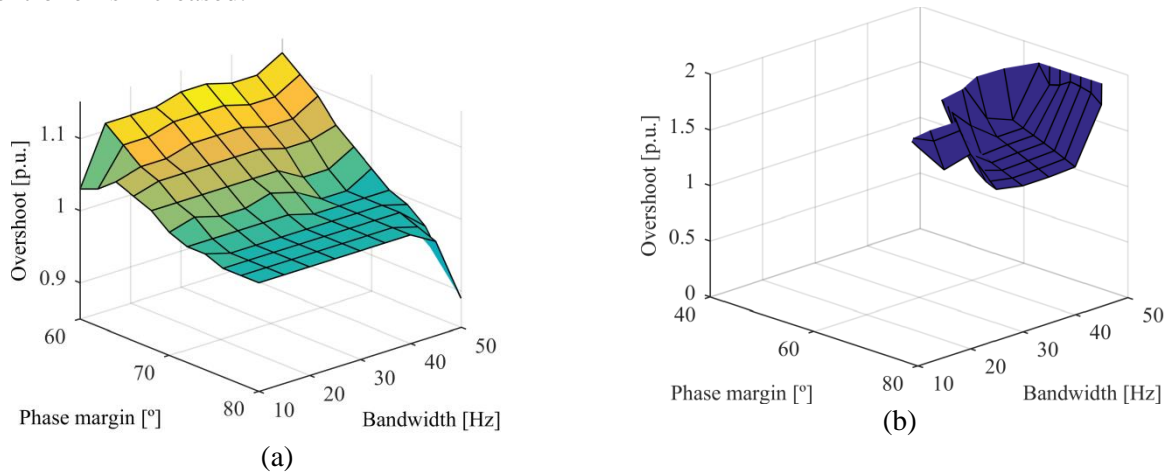
Fig. 5.17 Maximum overshoot for different controller settings at rotational speeds equal to 30 Hz (a) and 80 Hz (b).

5.2.4.3 Minimising the step response quadratic error

The quadratic error of step responses can be calculated as the squared sum of all the areas where there is a difference between the step reference and the system's response (Fig. 5.18). This criterion penalises heavily the initial instants of the step (where the error is very high) thus leading to controller with high initial dynamics and favours longer settling times (where the reference and the response are closer so the error is low). Minimising the quadratic error of a step response usually yields fast reacting controllers with moderate overshoot and high damping with responses similar to second order systems.
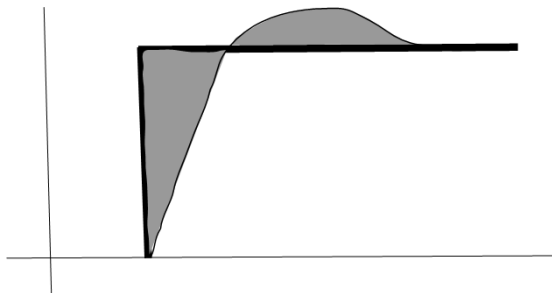
Fig. 5.18 Quadratic error of a step response. Grey shadowed areas are what the criterion tends to minimise.

The Fig. 5.19 shows the evolution of the quadratic error with different settings for the current controllers. It can be seen how with low rotational speeds (Fig. 5.19 (a)) there is a wide range of

controller settings that lead to a low quadratic error; but, as the rotational speed increases (Fig. 5.19 (b)), the range of settings for the current controllers is greatly reduced as in this situation the effect of the delays of the system makes it impossible to obtain a stable regulator.
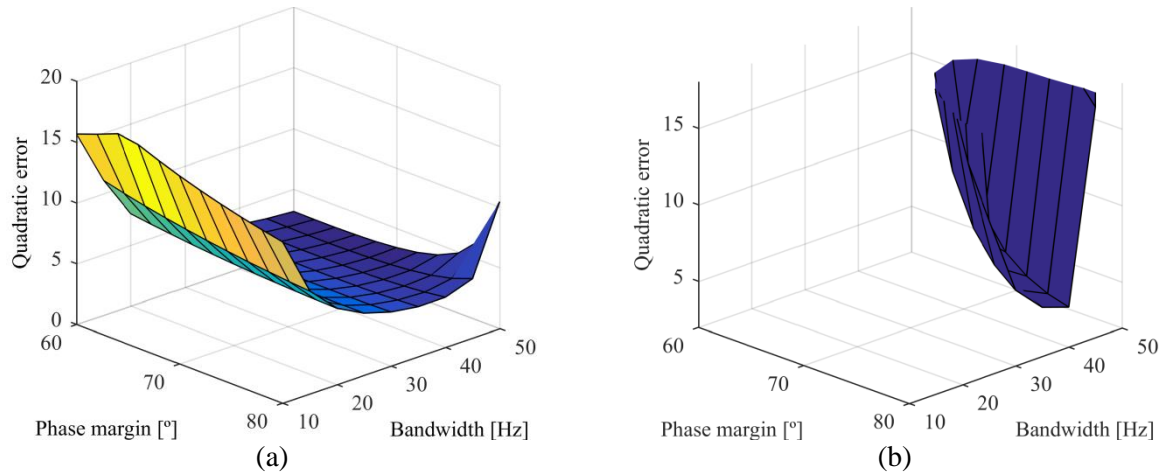

Fig. 5.19 Quadratic error for different controller settings for rotational speeds equal to 30 Hz (a) and 80 Hz (b).

5.2.4.4   Minimising the settling time

The settling time can be defined in different manners depending on the limits considered. In this work, the settling time is considered as the time when the response to a step input reaches and stays further within the ±5% band around the reference.

Minimising the settling time normally leads to slow reacting controllers with very low or zero overshoot with responses similar to first order systems.

The Fig. 5.20 shows the evolution of the settling time with different settings for the current controllers. It can be seen how with low rotational speeds (Fig. 5.20 (a)) there is a wide range of controller settings that lead to reduced settling times but as the rotational speed increases (Fig. 5.20 (b)), the range of settings for the current controllers is greatly reduced as in this situation the effect of the delays of the system makes it impossible to obtain a stable regulator.
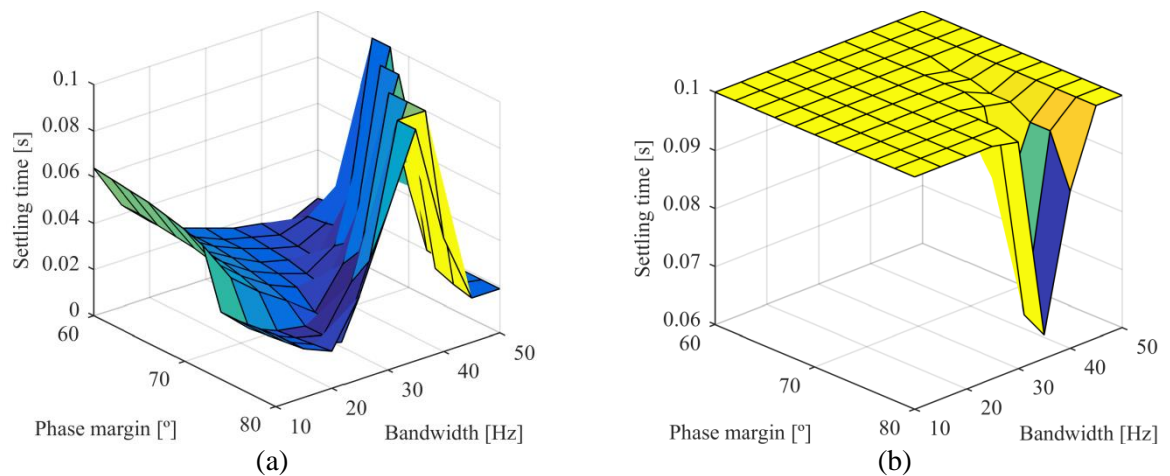
Fig. 5.20 Settling time for different controller settings, for rotational speeds equal to 30 Hz (a) and 80 Hz (b).

5.2.5   Tuning of the flux/torque regulators

When using the reference frame aligned with the stator's flux, it is common to assign the *d*-axis current to the control of the flux, and the *q*-axis current to the control of the torque. As it has been

seen in section 5.2.1, the expressions of torque and flux in the rotor reference frame do not depend on only one current, so that it is not possible to obtain decoupled control of torque and flux in this frame (with salient machines). From the expression of the stator's flux in Table 5.1, the reference for the d-axis current can be obtained for a desired stator's voltage reference V_s^* as

$$i_d = \frac{-\psi_{PM}}{L_d} + \sqrt{\left(\frac{V_s^*}{\omega_s \cdot L_d}\right)^2 - \frac{(L_q \cdot i_q)^2}{L_d^2}} \qquad (5.5)$$

where ω_s is the electrical speed of the machine. Similarly, the expression of the q-axis current for a certain torque command T_{elec}^* can be obtained as

$$i_q = \frac{T_{elec}^*}{\frac{n}{2} \cdot p \cdot (\psi_{PM} + (L_d - L_q) \cdot i_d)} \qquad (5.6)$$

The expressions in (5.5) and (5.6) can be used as references for the current regulators once the references for torque and stator voltage have been received from the master controller. The drawback of these expressions is that they rely on machine's parameters, such as inductances and the permanent magnet's flux, that vary noticeably with the operational point of the machine. The consequence of this variation is that the calculated current references will not coincide with the actual needed values, thus not producing the desired torque and stator voltage. Fig. 5.21 shows, as an example, the d-axis current calculation provided by (5.5) when the inductances have been overestimated by 20% (dash-dotted), by 15% (dashed) and by 10% (solid). It can be seen how the calculated current in these cases is sometimes lower and at other times higher (in terms of the absolute value) than the really needed one (100%). The overestimation of the inductances is a typical issue as the machine manufacturers usually provide the unsaturated values and, when the machine is loaded, the magnetic circuit saturates and the inductance values are reduced by 10 to 20% in the common electromagnetic designs.
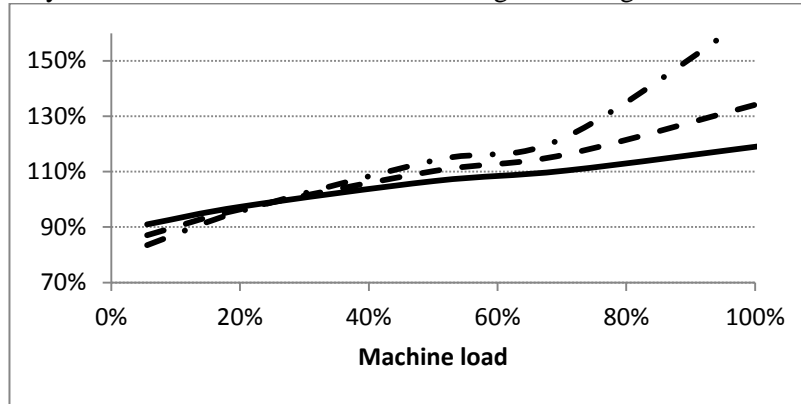
Fig. 5.21 d-axis current reference calculation using (5.5) when the inductances are 20% overestimated (dash-dotted), 15% (dashed) and 10% (solid) for the case of a generic machine rotating at its rated speed and aiming at rated stator voltage.

To overcome this effect, a torque and voltage regulator, as shown in Fig. 5.22, may be introduced that would take care of compensating the parameter mismatch. The expressions (5.5) and (5.6) will act as feedforward terms to reduce the burden on the controller and increase transient response; whereas the controller will take care exclusively of cancelling the steady state error under any load condition due to parameter variations.
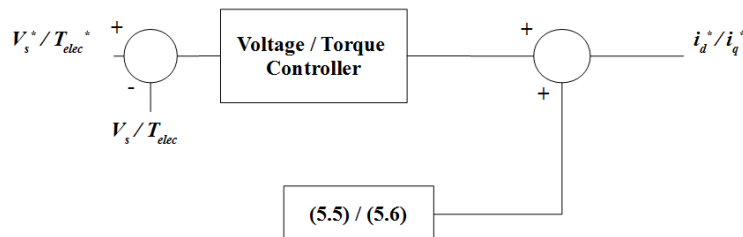

Fig. 5.22 d- and q-axis current reference generation.

Special care needs to be taken when tuning the parameters of the voltage/torque controller in Fig. 5.22 as it is actually an outer loop to the current regulators; hence, its bandwidth should be kept below one tenth of that of the current regulators. If the rotor reference frame is used, the expressions of torque and stator's voltage are non-linear and depend on both *d-* and *q-* axes currents so theoretical tuning procedures for PI regulators cannot be followed. This drawback is partially overcome by the experience of the designer who needs to experimentally obtain some parameters that yield an acceptable behaviour.

5.3   Simulation procedure and results

In what follows, results of simulations in Matlab's SimPower Systems ® will be presented. This simulation environment runs in Simulink ® but instead of using transfer functions and differential equations to model the system, it allows to use physical devices such as inductors, resistances, semiconductor devices etc. directly in the model. It basically transforms Simulink into an electromagnetic transient simulator. The good point of it is that the model can be divided into the control side that runs in Simulink and the power side that runs in SimPower, thus providing an easy-to-use, yet powerful tool.

SimPower provides a library with standard power blocks such as inductors, resistors, capacitors, semiconductor devices and electrical machines. Unfortunately, it does not include multiphase machine models, but it is possible to construct user-defined models, similarly as in Simulink. For this work, a new model for six- and nine-phase machines has been developed for SimPower and it has been encapsulated under a mask (Fig. 5.23(a)) to facilitate its use. Double-clicking the mask, the model can be parameterised by means of a dialog (Fig. 5.23(b)), where several machine aspects can be configured to accommodate it to any kind of simulation.

(a)   (b)
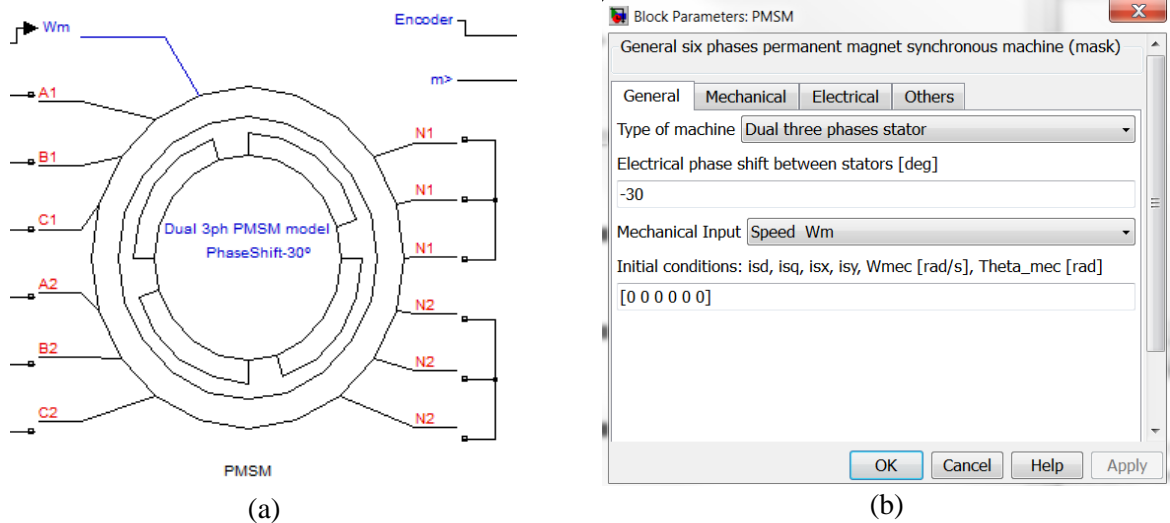
Fig. 5.23 SimPower model block mask for six-phase machines (a) and its configuration dialog (b).

The multiphase machine in this work has been modelled using the VSD approach in the synchronously rotating frame. This reduces the online calculation requirements as the inductance matrix has constant coefficients and so it optimizes the simulation. The model can be configured to accept load torque or speed as the mechanical input.

5.3.1   Simulation procedure

Wind turbine applications require a wide speed range of operation to optimize the energy yield and reduce the mechanical demands on the drivetrain. This requires the power converter to control the electrical machine at low and high speed values. In the high end, the operation includes a safety feature as the converter is required to keep a smooth braking torque to avoid over-speeding of the wind turbine that may lead to important damages in the drivetrain. This especially applies when sudden wind gusts

reach the blades while the generator is already rotating at rated speed. In such a case, the rotor accelerates due to the gust and so the frequency of the converter increases transiently over the rated one (while the blade actuators remove the extra energy), reaching around 10% higher speeds. In extreme cases (worst case scenario), the possibility of a huge sudden gust reaching the blades should be taken into account and this may require the converter to keep applying the required braking torque even at speeds 30% higher than rated (Germanischer Lloyd, 2012).

This work is focused on high-voltage and high-power conversion stages with switching frequencies limited below 800 Hz (sampling at 1600 Hz) due to thermal constraints. The conversion stage should be able to properly control the torque and flux of the machine up to fundamental frequencies slightly above one tenth of the switching (i.e. 80 Hz) to fulfil the requirements across the entire operational range. This is so as the machines usually foreseen for multi-MW wind power applications are in the medium-speed range (around 350 rpm); this type of machines eliminates the need for the high-speed stage of the gearbox (which is the weakest part of the gearbox). The electromagnetic construction usually includes a pole pair number around 10 to 12 yielding a rated frequency between 60 and 70 Hz.

Unless explicitly stated, the machine to be used in the simulations is a six-phase permanent magnet synchronous machine with two three-phase systems in the stator and with two independent neutral points. Machine's and simulation's parameters are detailed in Table 5.2.

Table 5.2 Test bench machine's and simulation's parameters.

Machine	
Parameter	**Value**
Pole pairs	8
d-axis magnetic inductance (L_{md})	0.825 mH
q-axis magnetic inductance (L_{mq})	0.825 mH
Leakage inductance (L_{ls})	0.7868 mH
Phase winding resistance (R_s)	76.9 mOhms
Nominal frequency (f_{nom})	66.6 Hz
No-load voltage (V_0) at f_{nom}	751 V$_{ph-ph}$
Nominal voltage (V_{nom})	690 V$_{ph-ph}$
Number of phases (n)	6
Shift angle (σ)	0 or 30 (configurable)
Rated torque	3 kNm
Control	
Parameter	**Value**
Converter type	3L-NPC
Switching frequency (f_{sw})	800 Hz
Controller nature	Digital, sample time 625 us
Control type	FOC
d-q current controller	Dual PI controller
x-y current controller	Proportional resonant controller (PR)
Machine mechanical input	Speed, infinite inertia

5.3.2 Current regulator dynamic response

To simulate the behaviour of the current regulators across the entire rotational speed range, a ramp on the speed of the machine is implemented taking it from 30 to 80 Hz. Along the simulation time, several steps with 35A amplitude (and negative in sign so that the torque of the machine is braking torque) are performed in the q-axis current to highlight how the dynamic response varies.

5.3.2.1 Tuning algorithm correlation

In order to determine whether the results from the tuning algorithm match those obtained in simulations and in the experimental test bench, a comparison between the three of them is performed

firstly. The tuning algorithm is run and the details regarding the dynamic response to a step input are saved to a file for further comparison with simulation and experimental data.

The Table 5.3 and Fig. 5.24 show the comparison between the predicted overshoot by the tuning algorithm (following DDQ approach) and the overshoot seen in simulation for the case of minimising the settling time, respectively. It can be seen how the values from the tuning algorithm match very well with those from simulation.

Table 5.3 Comparison between the DDQ tuning algorithm and the simulation results.

ω_s [Hz]	Overshoot tuning	Overshoot simulation
30	1.04	1.04
40	1.03	1.03
50	1.29	1.29
60	1.34	1.34
70	1.31	1.31
80	1.31	1.42
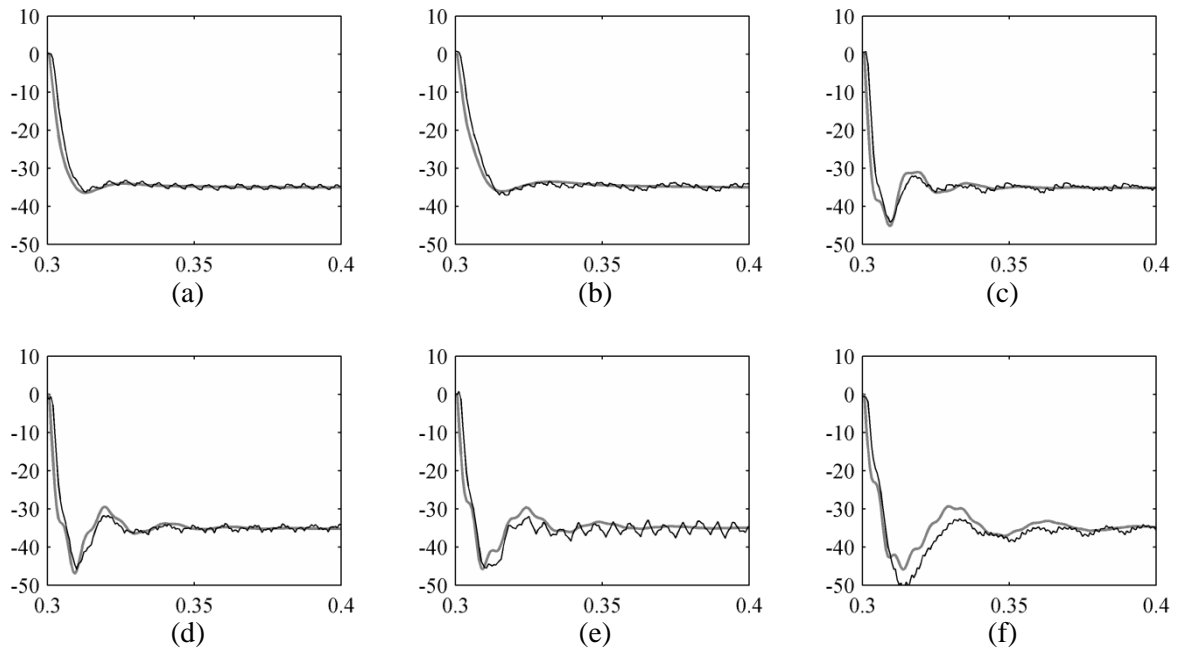
Fig. 5.24 Comparison of the step response predicted by the DDQ tuning algorithm (thick grey trace) and the simulated result for different rotating speeds (a) 30 Hz, (b) 40 Hz, (c) 50 Hz, (d) 60 Hz, (e) 70 Hz and (f) 80 Hz. The control parameters have been chosen to minimise the settling time. The horizontal axis represents the time [s] while the vertical one represents the q-axis current in [A].

The tuning algorithm has also been programmed to accept the VSD approach, so that it can yield tuning parameters for controlling the machine following any of the two approaches. The same study has also been done using the VSD approach, leading to a similar match as the one obtained for DDQ (Fig. 5.25).
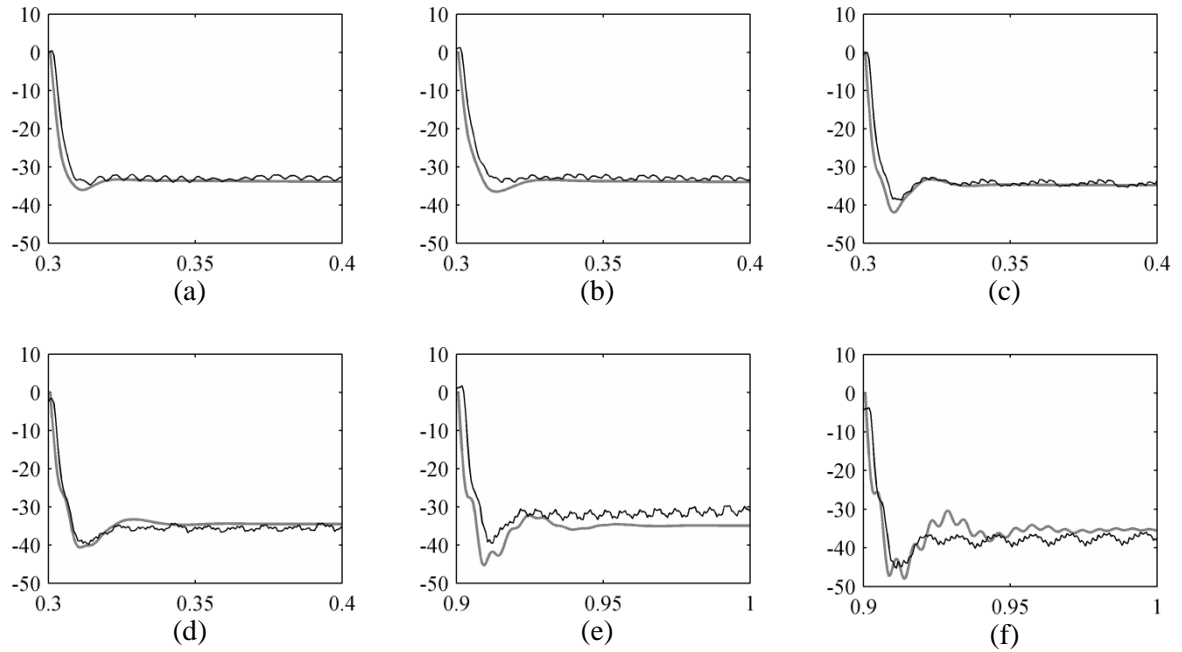
Fig. 5.25 Comparison of the step response predicted by the VSD tuning algorithm (thick grey trace) and the simulated result for different rotating speeds (a) 30 Hz, (b) 40 Hz, (c) 50 Hz, (d) 60 Hz, (e) 70 Hz and (f) 80 Hz. The control parameters have been chosen to minimise the settling time. The horizontal axis represents the time [s] while the vertical one represents the q-axis current in [A].

5.3.2.2 Setting a fixed bandwidth and phase margin

As it can be easily deduced from 5.2.2, tuning the current regulators in the synchronous frame by keeping constant the BW and PM may yield an increase in the overshoot and a reduction in the dynamic stability (oscillations) as the rotational speed increases. This can be seen in Fig. 5.26 where the dynamic response of the *d-q* current regulators for different rotational speeds is shown (*d*-axis current kept constant at -250A). In the upper and middle plot of the figure, the *d*- and *q*-currents are shown, respectively. It can be clearly seen how the overshoot increases with the rotational speed; in the upper range of the speeds, a slightly oscillatory response is obtained.
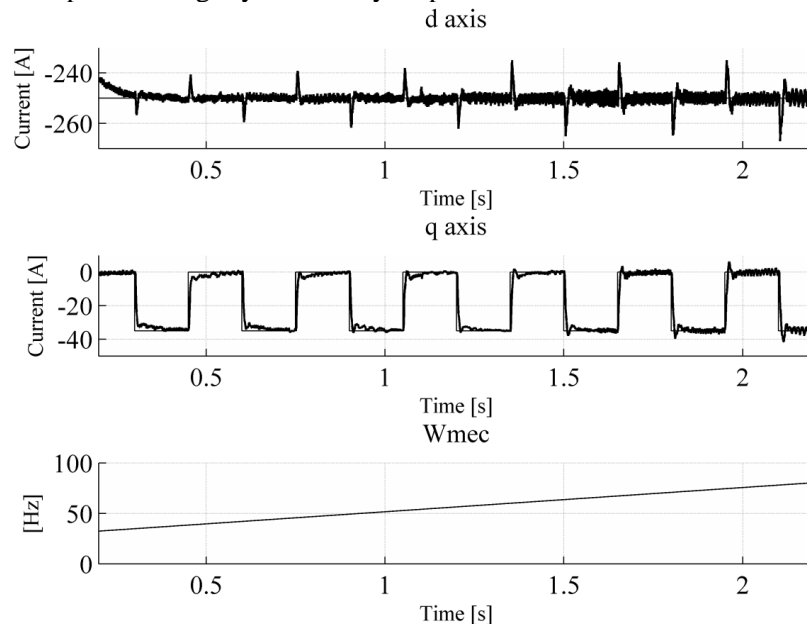
Fig. 5.26 Dynamic response of the current regulators in the synchronous frame (upper and mid plot) for fixed BW=35 Hz and PM=78° for varying rotational speed (lower plot).

5.3.2.3   Setting a fixed overshoot

Setting a fixed overshoot across the entire speed range allows the regulators to enhance the dynamic response in the low- and mid-speed range while keeping a moderate overshoot in the high-end. This is accomplished by setting the highest BW possible to keep constant overshoot across the speed range. The *d*-axis current was once more kept constant at -250A.

In the Fig. 5.27, it can be seen how the overshoot is kept constant at all rotating speeds and equal to the desired value (1.1 p.u. ±0.05). An important aspect to be observed in the figure is that, as the tuning algorithm maximises the BW while keeping the desired overshoot, some of the resultant tunings can make the response too fast yielding high ripple in the currents and a certain tendency to oscillate.
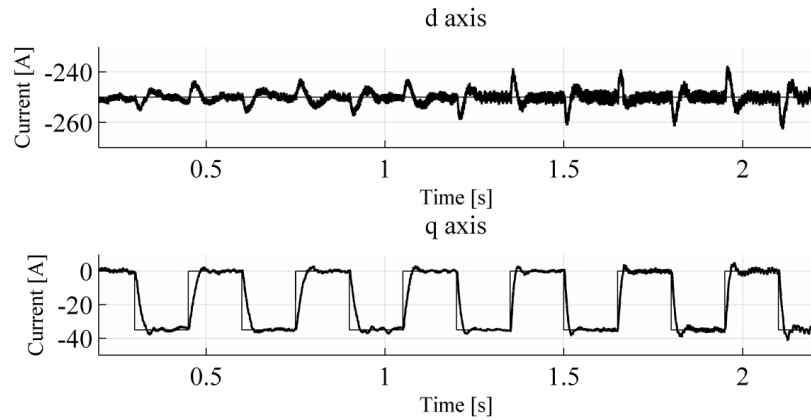
Fig. 5.27 Dynamic response of the current regulators in the synchronous frame (upper and mid plot) for fixed overshoot at 1.1±0.05 p.u. for varying rotational speed (same as in Fig. 5.26). The tunings are those that maximise the BW while achieving desired overshoot.

5.3.2.4   Minimising the step response quadratic error

Minimising the quadratic error yields settings with fast reaction (low rise time), as can be seen in Fig. 5.28. The *d*-axis current was kept constant at -200A.
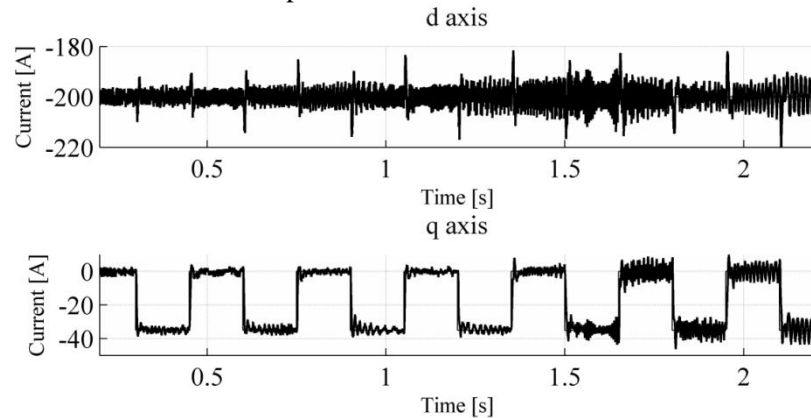
Fig. 5.28 Dynamic response of the current regulators in the synchronous frame (upper and mid plot) minimising the quadratic error on a step input, for varying rotational speeds (same as in Fig. 5.26).

5.3.2.5   Minimising the 5% settling time

By minimising the settling time, the dynamic response oscillations are reduced yielding smoother and more dampened behaviour especially in the high-speed region (Fig. 5.29). On the other hand, it can be seen in 5.3.2.1 that this criterion yields quite high overshoots, especially in the high-speed region. In this region, these high overshoots might be undesired as they may be translated into high torque (and hence power) surges in the drivetrain. The *d*-axis current was kept constant at -250A.

d axis

q axis
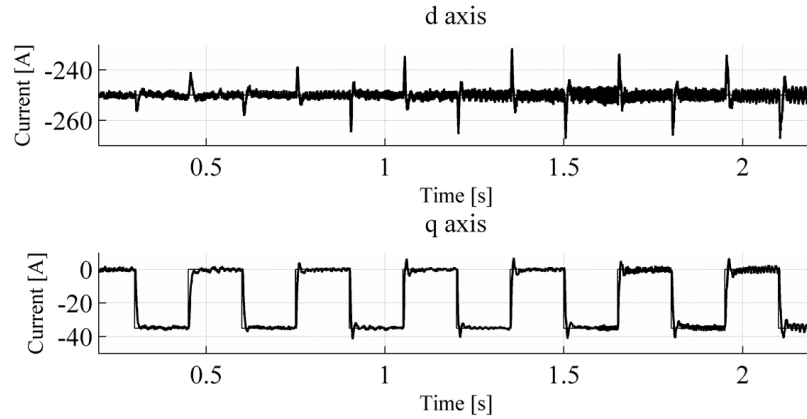
*Fig. 5.29 Dynamic response of the current regulators in the synchronous frame (upper and mid plot) minimising the settling time on a step input, for varying rotational speeds (same as in Fig. 5.26).*

5.3.3 Flux/torque regulator dynamic response

The dynamic response of the torque and flux in a machine, when using FOC, is highly influenced by the current regulator's response as these are responsible for setting up the needed currents for certain torque and flux values. This is the reason why so much effort has been placed on modelling the current regulators and properly tuning them in this research.

In this section, simulations for flux/torque reference changes have been performed, having programmed said loops with only the feedforward terms in Fig. 5.22. The simulation results shown in Fig. 5.30 cover the same situation as in the section 5.3.2 where the performance of the current regulators was tested across the entire rotational speed range of the machine. In this case, torque steps of 1 p.u. (3 kNm) are being performed at different speeds, while keeping the stator's voltage reference value at rated. This has been done this way to test the regulators under the most severe transient conditions.

The Fig. 5.30 (a) covers the entire speed range of the machine. Around $t = 2$ s, it can be seen how the torque command (thick black line in the lower figure) and the actual torque delivered by the machine (1-pt black line) start to drift away meaning the converter is losing the control of the torque. In this part of the simulation, the stator voltage is very close to the converter's voltage limit (fixed by the dc-link voltage) and due to converter non-idealities and parameter mismatch, the d-axis current calculated by (5.5) is not capable of keeping the stator's voltage at the desired value and it starts to drift until it surpasses the converter's limit.

It can also be seen how the performance of the torque regulator is asymmetrical as it behaves slightly differently depending on the torque step sign. To be more precise, if the step goes towards the negative side (applying more braking torque), the behaviour is very fast, reaching the target value in less than 10 ms; whereas if the step goes towards the positive side (reducing the braking torque), the behaviour is slower as it takes around 30 ms to reach the target value (especially at higher speeds). Looking at the behaviour of the stator voltage amplitude, the explanation for said asymmetrical behaviour can be found. When the step increases the braking torque (step at 1.5 s in Fig. 5.30 (b)), the converter needs to reduce the terminal voltage of the machine to pull out more q-axis current from the stator in order to increase the torque. In this situation, no regulator saturation occurs as the stator voltage is temporarily reduced. On the other hand, when the step reduces the braking torque (step at 1.65 s in Fig. 5.30 (b)), the converter needs to increase the machine's terminal voltage to reduce the q-axis current as fast as possible. As the operating point is close to the converter's voltage limit, this sudden increase in the machine terminal's voltage yields a saturation of the converter that can be seen in the flat part of the stator's voltage plot (Morimoto et al., 1994). This phenomenon is completely irrelevant in windpower applications as there is no situation in which the braking torque should be removed as fast as possible; but it is extremely important for motoring applications, as in these applications the saturation occurs when increasing the motoring torque (when the converter needs to

deliver more *q*-axis current), directly affecting the performance of the speed controller (Sudhoff et al., 1995).
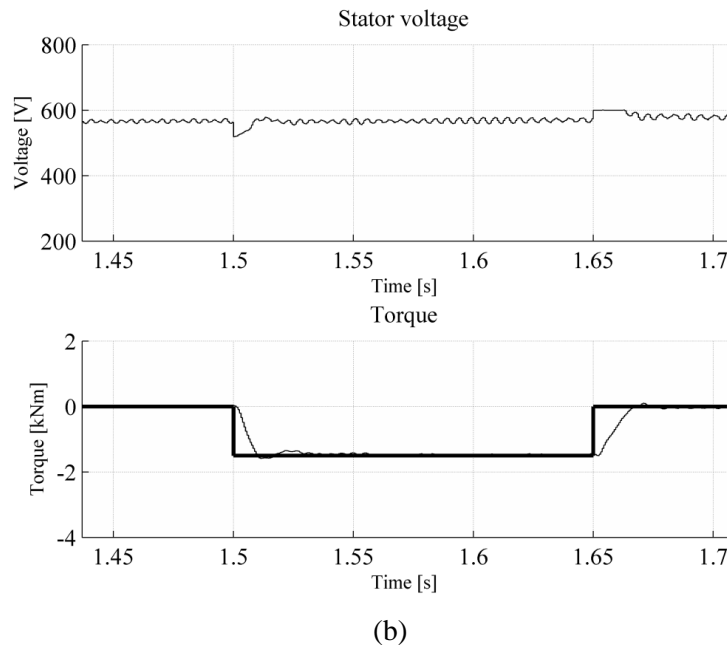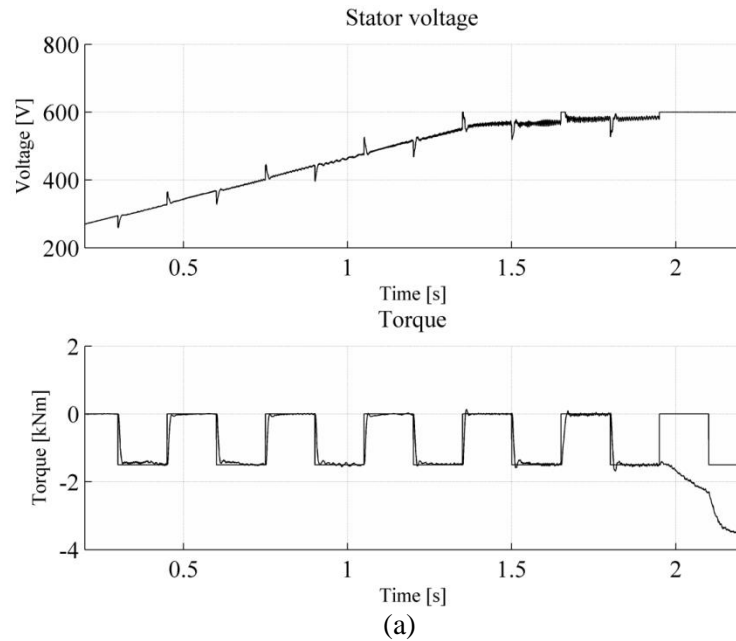

Fig. 5.30 Dynamic response of the torque regulator (lower plots of (a) and (b)) while varying rotational speed as in Fig. 5.29. In the upper plots of (a) and (b), the stator's voltage amplitude is shown which reflects the performance of the flux regulator. A zoomed plot can be seen in (b).

An improvement of this behaviour can be obtained by implementing an anti-saturation regulator that basically consists of a controller that introduces a negative term in the *d*-axis current reference whenever the stator voltage goes above the reference value. This scheme is the same as the one shown in Fig. 5.22, but with saturating the controller output to provide only negative outputs.
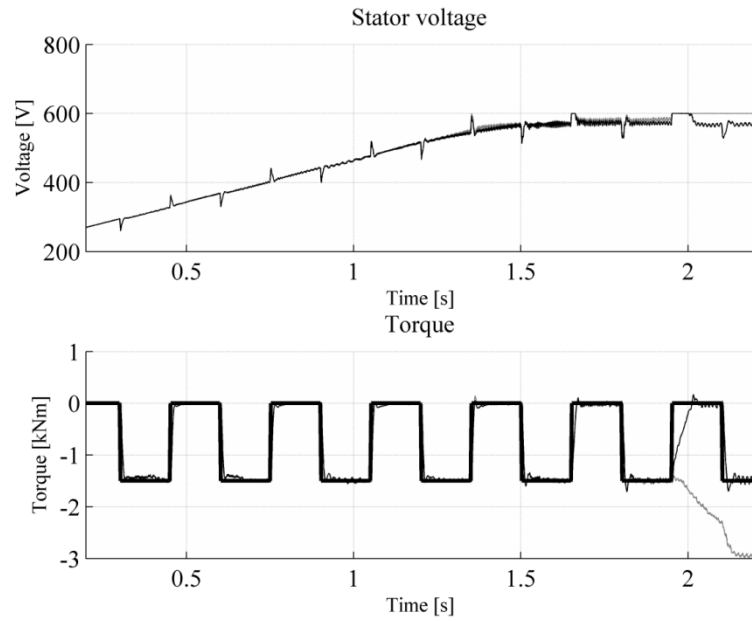
Fig. 5.31 Comparison of the behaviour with (black) and without (grey) anti-saturation controller.

Fig. 5.31 shows the comparison of the performance with and without the anti-saturation controller, as described in 5.2.5. It can be seen how the duration of the flat part in the stator voltage is reduced so the amount of time that the current regulators are saturated is also reduced, thus increasing the responsiveness of the regulation and avoiding the instability. Furthermore, it can be seen how the anti-saturation controller is active only when the torque steps are in the direction of reducing the braking torque. As it was mentioned in section 5.2.5, the tuning of this anti-saturation controller is purely empirical as the relationship between stator voltage and *d-q* currents is highly non-linear.

5.4   Experimental test bench

The test bench used for this research is the test rig where Ingeteam emulates the behaviour of offshore windconverters. In order to obtain realistic results, the rig includes not only the machines and the converters to be tested, but also a control cabinet emulating the windturbine PLC. This way, the windturbine behaviour can be reproduced taking into account every single intervening device. The general overview of the test rig can be seen on Fig. 5.32.

Additionally, the grid side of the test rig can be connected directly to a real stiff grid (by means of a configurable inductance to simulate different grid impedances) or can be connected to a virtual grid emulator. This virtual grid emulator is a power converter that can simulate any grid condition such as frequency drifts, low and high voltage conditions, symmetric and asymmetric voltage sags and surges, etc.
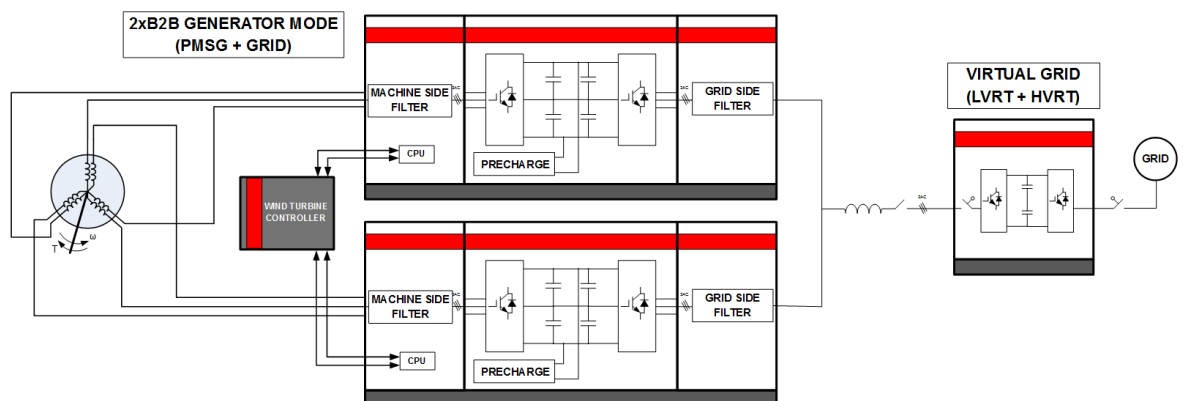

Fig. 5.32 Testbench overview.

In conclusion, this test rig can faithfully reproduce almost any situation that can appear in a real offshore application both from the grid and the machine side point of view.

5.4.1 Electrical machines

The test rig has three machine arrangements to cover the three electrical machines already used in windturbines (i.e. electrically excited synchronous machine, asynchronous machine and permanent magnets machine). Each of the machine arrangements consist of a 150 kW dc machine that acts as a motor regulating the rotational speed and the ac machine arranged in a back-to-back configuration as seen in Fig. 5.33 (a).

(a)   (b)
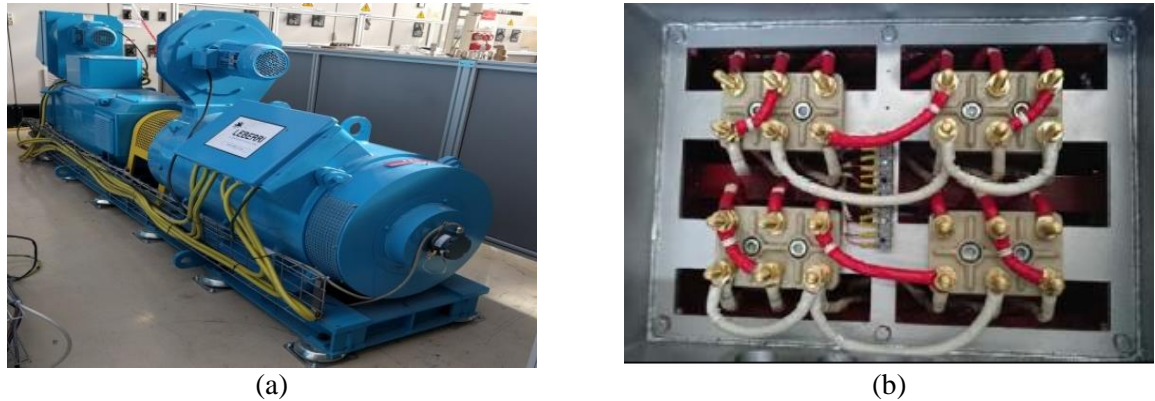
Fig. 5.33 Electrical machine arrangement (a) and end windings connections in the terminal box (b).

For the purpose of this research, and to cover the situations where double three-phase machines are used, the original three-phase permanent magnet machine of the test rig was replaced by a new one that can accommodate different end-winding connections (Fig. 5.33 (b)) yielding different stator configurations such as:

- Single 690 V 150 kW three-phase winding (parallel connection)
- Dual 690 V 2x 75 kW three-phase windings with 0 degrees shift
- Dual 690 V 2x 75 kW three-phase windings with 30 degrees shift
- Single 1380 V 150 kW three-phase winding (serial connection)

For this research, the stator winding configuration yielding two 0 degrees shifted three-phase systems was chosen due to Ingeteam's high interest in such configuration.

5.4.2 Conversion lines

The test rig includes two 150 kW, 690V conversion lines, each of which is constituted by two three-level NPC converters arranged in back-to-back configuration as shown in Fig. 5.32. Additionally to the converters, each conversion line includes a grid side inductor (configurable from 200 to 800 µH in 200 µH steps) and a machine side dv/dt filter to reduce the voltage derivatives applied to the motor windings (Fig. 5.34).

Fig. 5.34 Picture of one of the conversion lines.

The typical ratings of the conversion lines are summarized in Table 5.4.

Table 5.4 Conversion line typical values.

Conversion line	
Parameter	**Value**
ac voltage	690 – 1380 V
dc bus voltage	1050 – 2300 V
Maximum current	125 A
IGBT dead time [5]	10 μs
IGBT minimum ON time [5]	15 μs
Switching frequency [5]	600-6000 Hz
Cooling	Forced air-cooled

Each of the three-phase windings of the permanent magnet machine is connected to a conversion line.

5.4.3 Control architecture

The conversion lines are equipped with the same controllers as in the converters for real applications, so that the results obtained here can be directly extrapolated to real scenarios. The control architecture is distributed so that the measurements are taken as close as possible to the source of the measurement (the sensor) by means of a so called remote power management module (PMM), Fig. 5.35 (a). The measurements are sent via a fibre optic link to the central processing unit (CPU), seen in Fig. 5.35 (b), where the algorithms are running and the next sampling interval references are calculated. The references are sent back to the PMM where the modulation is programmed in a FPGA yielding the switching signals to the semiconductor switches. This architecture (as illustrated in Fig. 5.35 (c)) minimizes the cabling within the converter, thus reducing its complexity and enhancing its noise immunity.

(a)   (b)

(c)
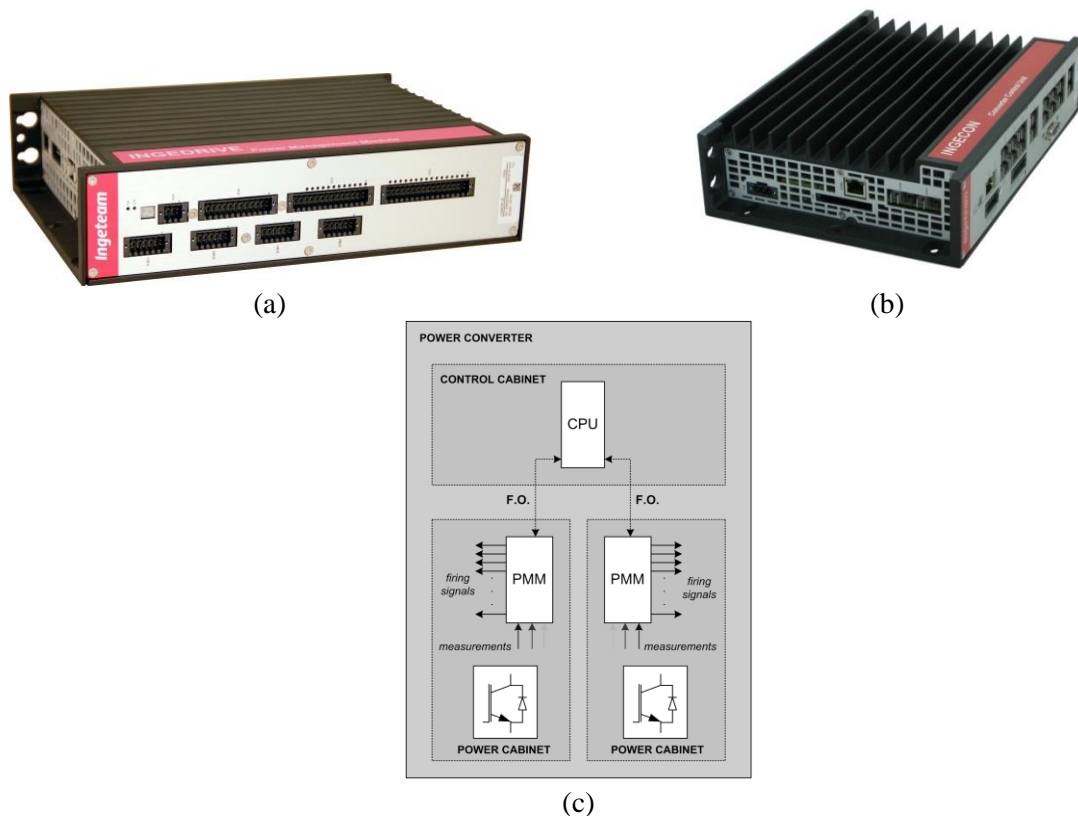
Fig. 5.35 Control hardware: power management module (a), central processing unit (b) and schematic (c).

---

[5] These values are configurable through software

The CPU has a built in oscilloscope and recorder (Fig. 5.36) that can log several analog variables (those available in the DSP) at a maximum sampling rate equal to the sampling time of the DSP. The recorded data can be easily integrated in Matlab, Excel or any other graphics software. These features make it unnecessary to use external oscilloscopes and probes, as the measurements of e.g. voltages, currents and temperatures are already available through the DSP.
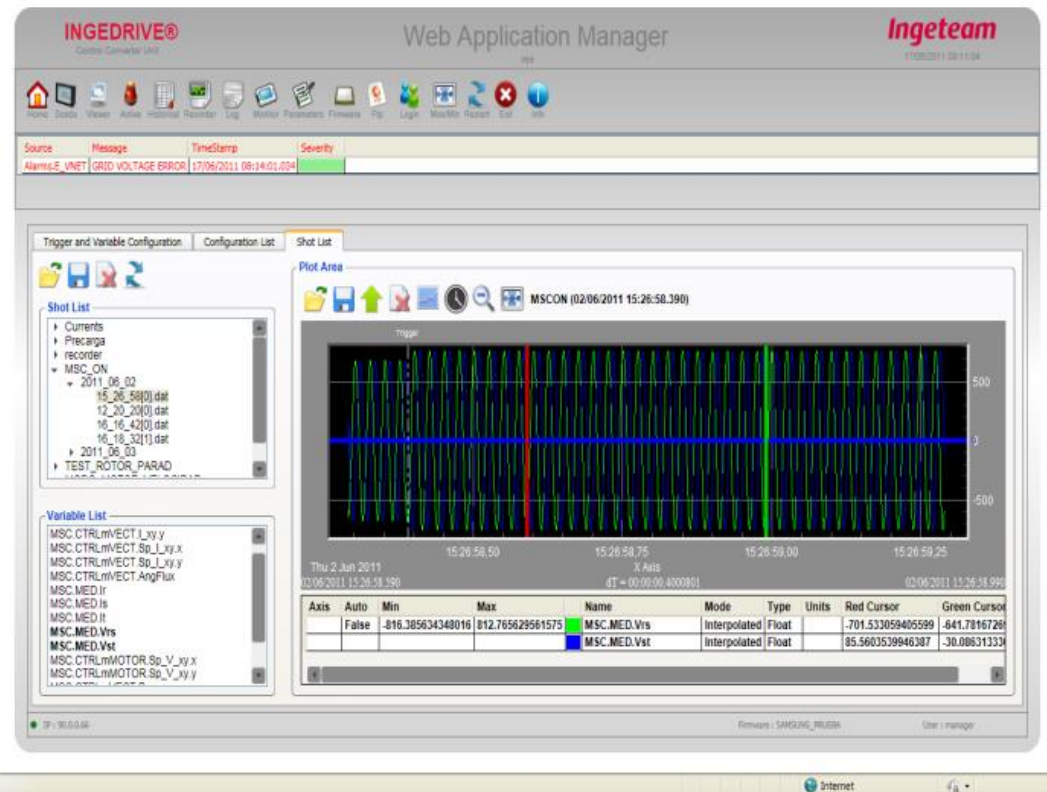

Fig. 5.36 CPU built-in oscilloscope.

5.5   Correlation between simulation and experimental test rig

As mentioned in 5.3, SimPower Systems does not provide a model for multiple three-phase winding machines within the model library. This led to the development of a model for such machines within the SimPower Systems environment.

5.5.1   Correlation of the experimental and simulation results

In order to examine the validity of the model derived, a correlation with the experimental test-bench results was established in the following manner:
- The voltages and currents of the machine in the test bench have been recorded during a step change of the *q*-axis current
- A simulation model that accepts the recorded voltages was prepared allowing to compare the output currents between the model and the experimental results
- An optimization procedure was launched in order to find the machine's parameters that optimally match the response of the actual machine

With the initial parameters given by the machine manufacturer, the response shown in Fig. 5.37 was obtained. As it can be seen, the differences in the responses are quite significant, both in terms of dynamic and steady state performance. This response mismatch was at first associated to the variation in the speed caused by the low dynamic performance of the dc motor drive, but after including the actual speed variation in the simulation, the response was still very far from the one obtained experimentally.
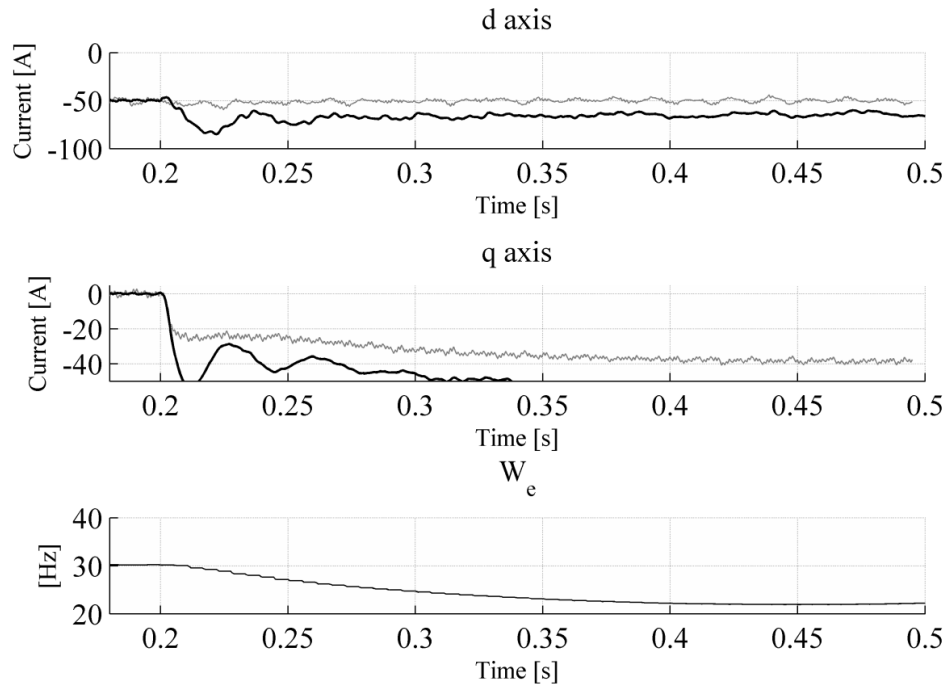
Fig. 5.37 Simulated (black) and experimental (grey) response to -35A current step in the q-axis. The top picture shows the d-axis current, the middle the q-axis current and the bottom one shows the speed variation as recorded from the test bench. The simulated results were obtained using the machine's parameters as per the manufacturer's data.

After the optimization procedure, the response in Fig. 5.38 was obtained. This response is much closer to the response recorded form the experimental test bench (both in terms of the dynamic response and ripple amplitude) and therefore, it appears that the developed machine's model can virtually behave as a real plant, once the adequate parameters are found.
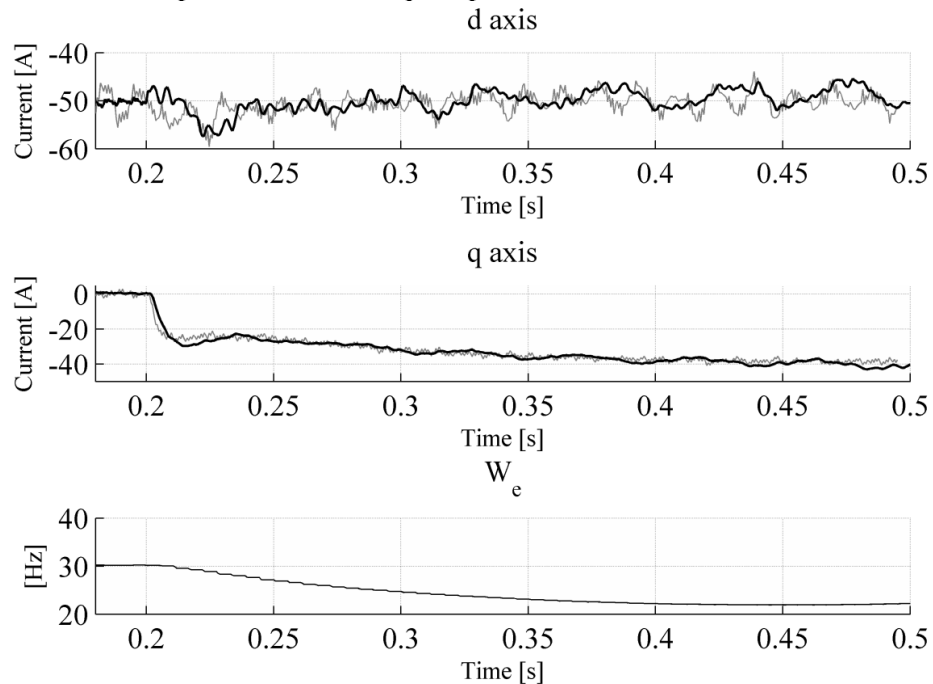
Fig. 5.38 Simulated (black) and experimental (grey) response to -35A current step in the q-axis. The top picture shows the d-axis current (note the difference in scale, compared to Fig. 5.37), the middle the q-axis current and the bottom one shows the speed variation as recorded from the test bench. The simulated results were obtained with the machine's parameters obtained from the optimization process.

119
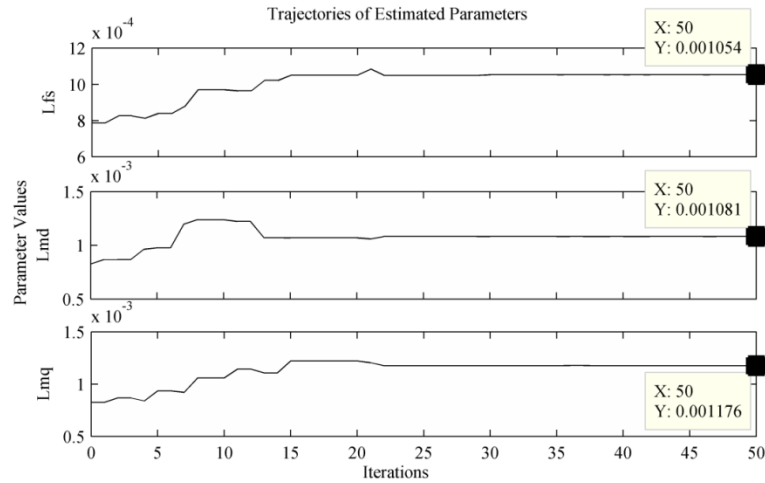
Fig. 5.39 Parameter trajectories during the optimization procedure.

The parameter optimization process, illustrated in Fig. 5.39, yielded the parameter values listed in Table 5.5 (manufacturer's parameters, already listed in Table 5.2 are included for an easier comparison):

Table 5.5 Test bench machine's parameters after the identification performed by means of the optimization procedure.

Identified machine parameters		Manufacturer given
Parameter	Value	Value
d-axis magnetic inductance (L_{md})	1.081 mH	0.825 mH
q-axis magnetic inductance (L_{mq})	1.176 mH	0.825 mH
Leakage inductance (L_{ls})	1.054 mH	0.7868 mH

5.5.2 Machine's parameter identification

In order to double-check the validity of the parameters found by the optimization process, a set of experiments were carried out in order to obtain the parameters following an alternative way. To obtain an estimation of the inductance values theoretically the following procedure was carried out:

- First test
    o A torque reference of -500 Nm is set
    o A voltage reference that yields d-axis current equal to zero is set
    o The following variables are to be recorded from the DSP
        ▪ the output of the torque regulator
        ▪ d- and q-axis currents
        ▪ stator's voltage
        ▪ electrical frequency of the stator
    o With the theoretical expression of the q-axis current vs. torque (5.6) and the output of the torque regulator, the permanent magnet's flux under certain load is obtained. This demonstrates that the magnet's flux hardly varied when increasing the q-axis current.
- Second test
    o The torque reference is set to zero
    o The voltage reference is set so that the d-axis current is big enough to measure it properly (50 A)
    o The following variables are to be recorded from the DSP
        ▪ the output of the voltage regulator
        ▪ d- and q-axis currents
        ▪ stator's voltage

- electrical frequency of the stator
  - With the theoretical expression of the *d*-axis current vs. stator's voltage (5.5) and the output of the voltage regulator, the *d*-axis inductance can be obtained.
- Now repeating the first test with a stator's voltage reference that yields a *d*-axis current different from zero, the (L_d-L_q) term can be calculated and provided that the *d*-axis inductance has been calculated from the second test, the *q*-axis current is the only unknown.

This procedure was performed at different speeds and the results obtained were very similar at all speeds. In fact, the value for the *d*- and *q*-axis inductances obtained from the above procedure was 2.1 and 2.4 mH respectively. At this point, it would be very complicated to analytically derive the contribution of the stator's leakage inductance to the above calculated inductances; so the same value as the one yielded from the optimization process above was assumed. The values obtained from the experimental characterization are shown in Table 5.6. These values are very similar to those obtained from the optimization process (Table 5.5), indicating that the performed optimization can be regarded as sufficiently reliable.

Table 5.6 Test bench machine's parameters after the identification performed experimentally.

Machine	
Parameter	**Value**
d-axis magnetic inductance (L_{md})	1.046 mH
q-axis magnetic inductance (L_{mq})	1.346 mH
Leakage inductance (L_{ls})	1.054 mH

In what follows, the inductance values of the machine will be taken as those listed in Table 5.5, as these values are those that minimise the actual difference between the simulation and experimental results.

5.5.3   Response correlation of the control algorithm

To certify that the responses of the control algorithm implemented in the simulation and those of the one actually downloaded to the converter control unit (CCU) match, a modified model was built. This model accepted at certain time (time instant 0.2 seconds), the current references and measurements from an external source (such as those recorded in the test-bench). Under these conditions, the outputs of the control algorithms (stator voltage references) should match. Eventually, the responses shown on Fig. 5.40 were obtained showing a significant mismatch in the *q*-axis response.
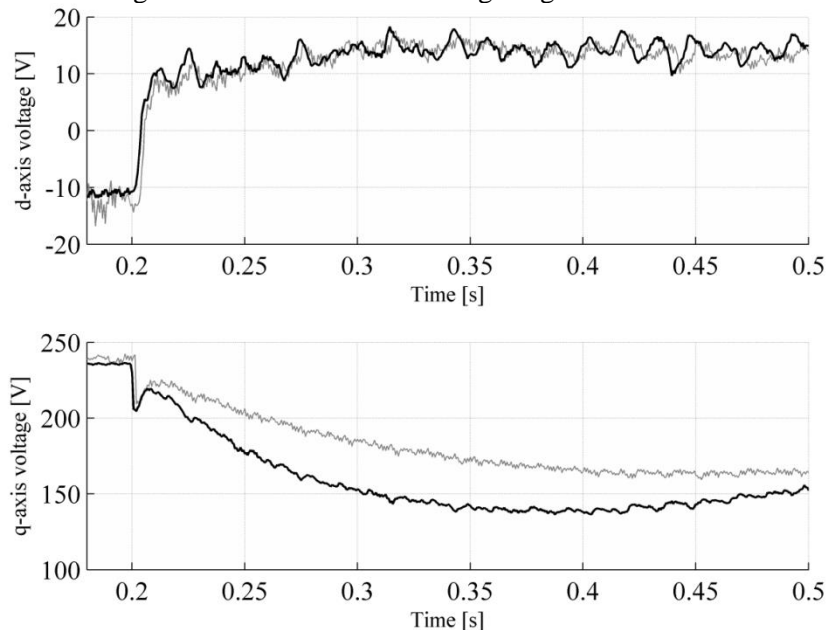

Fig. 5.40 Simulated (black) and experimental (grey) voltage references while forcing the current references and measurements in simulation to the experimental values. The experiment consisted of

a q-axis current step of -35A while keeping d-axis current at -50A and the speed at 225 rpm. In this figure, the filter for the speed measurement was not implemented in the simulation.

While carefully analysing where this difference may come from, a filter for the speed measurement was found to be set at a very low frequency (10 Hz) in the CCU code. The setting of this filter is adequate for big machines with high inertia where the speed variation is very slow. This was not the case in the test-bench used here as the machines have low inertia and the speed regulation is not very fast, leading to quite big speed variations when torque steps are applied (see lower plot in Fig. 5.38).After including in the simulation the filter for the speed measurement, the responses matched considerably better, as can be seen in Fig. 5.41.
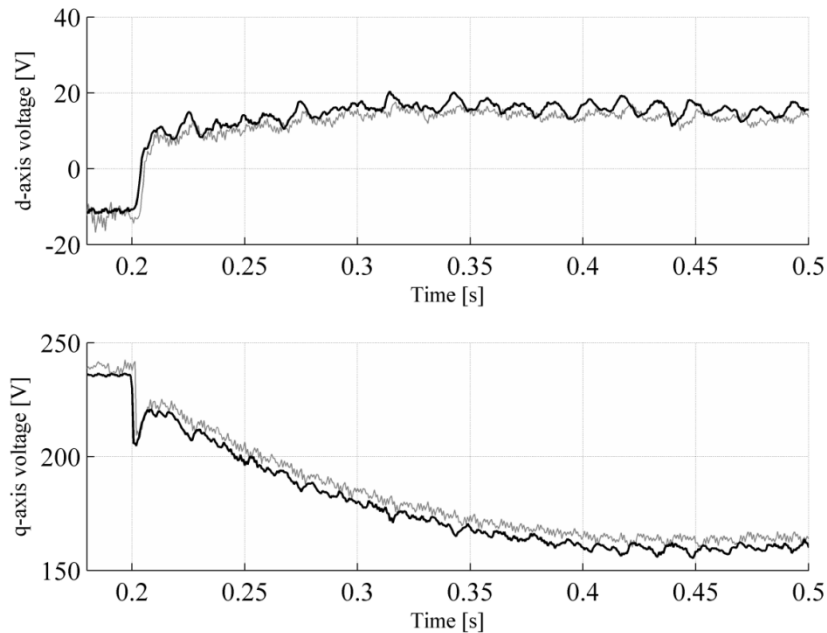
Fig. 5.41 Simulated (black) and experimental (grey) voltage references while forcing the current references and measurements in the simulation to the experimental values. The experiment consisted of a q-axis current step of -35A while keeping d-axis current at -50A and the speed at 225 rpm. In this figure, the filter for the speed measurement was set at 10Hz as in the test-bench code.

As can be concluded from the figures above, the tuning of the speed filter has a big impact on the dynamic performance of the current regulators. This is so as the speed variation observed in the test-bench is quite important due to the low inertia of the machines and the poor dynamic performance of the speed regulator of the motor drive. In order to remove the effect of this filter, a filter frequency of 200 Hz will be used herein after.

5.5.4   Simulation vs. experimental dynamic response of the current regulators

To correlate the dynamic response of the current regulators in simulation with the results from the experimental test-bench, a series of steps in the *q*-axis current are performed at different rotating speeds, Fig. 5.42. It can be seen how the dynamic response obtained from the test-bench (grey trace) follows closely the response obtained from the simulation model (black trace). In the figure, the plot at 80 Hz has been omitted because the motor drive could not handle such a big power step and it tripped.

In order to determine the validity of the identified parameters across the entire operational range of the machine, an experiment with different *d*-axis current was performed. Fig. 5.43 shows the comparison of the responses to a step on the *d*-axis current from 0 to -75A while the machine is rotating at 53Hz. It can be seen how the identified parameters still provide a very good match between experimental and simulated results.
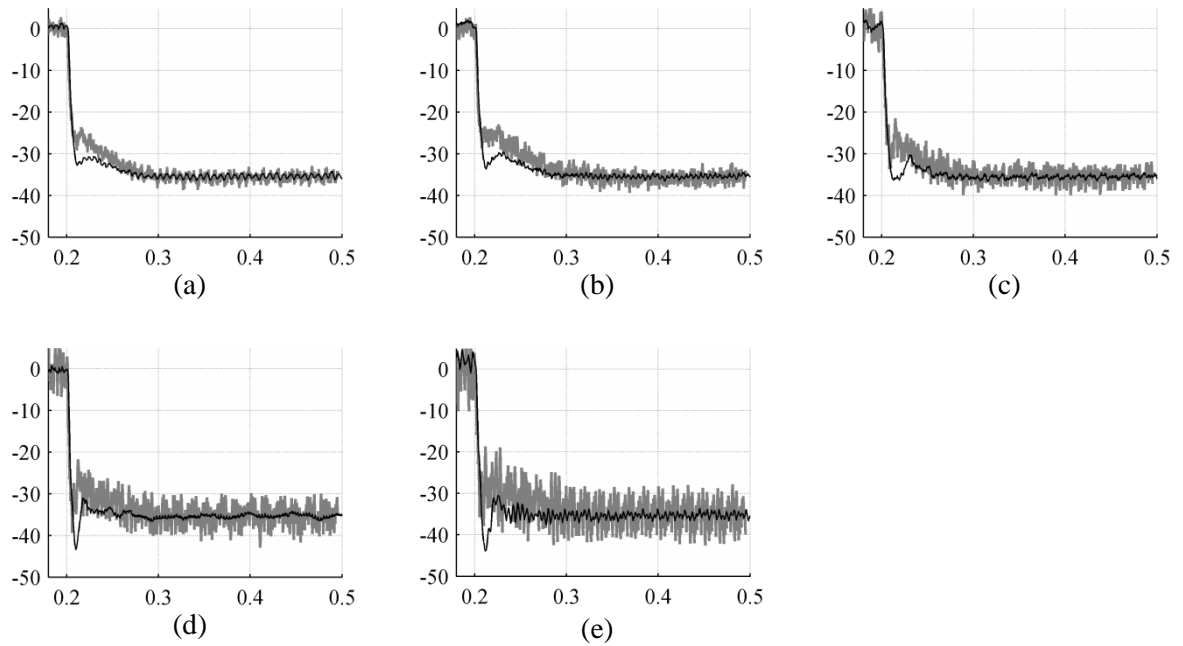
Fig. 5.42 Comparison of the q-axis current step response obtained from simulation (black trace) and the experimental results (thick grey trace) for different rotating speeds (a) 30 Hz, (b) 40 Hz, (c) 50 Hz, (d) 60 Hz, (e) 70 Hz. The control parameters have been chosen to minimise the settling time.
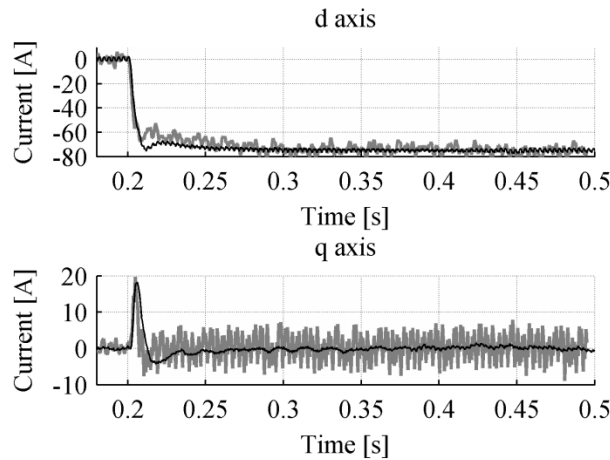

Fig. 5.43 Comparison of the dynamic responses obtained from simulation (black trace) and the experimental results (thick grey trace) for a -75A d-axis current step at 53Hz.

Another experiment to examine the validity of the identified parameters is to compare the stator voltages (directly dependant on machine's parameters) under different stator current levels (Fig. 5.44 and Fig. 5.45). Fig. 5.44 represents the comparison of the stator voltages for different q-axis current levels. It can be seen how the simulation (black trace) and the experimental results (grey trace) match very well for all current levels. This implies that the identified parameters are valid for any q-axis current, indicating a very low q-axis saturation.
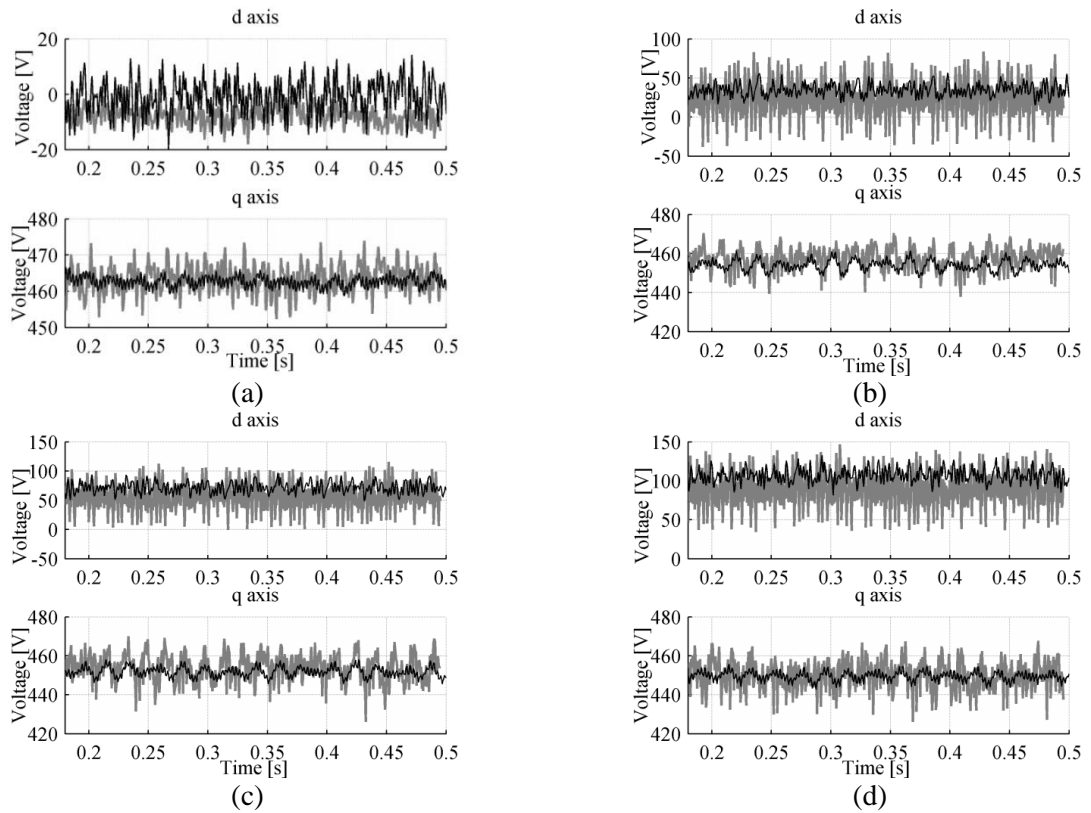
Fig. 5.44 Comparison of the d- and q-axis voltages (top and bottom plots, respectively) for different q-axis current (a) 0A, (b) -25A, (c) -50A, (d) -75A and constant d-axis current set at 0A. The black trace is simulation data and the thick grey trace represents the experimental data.
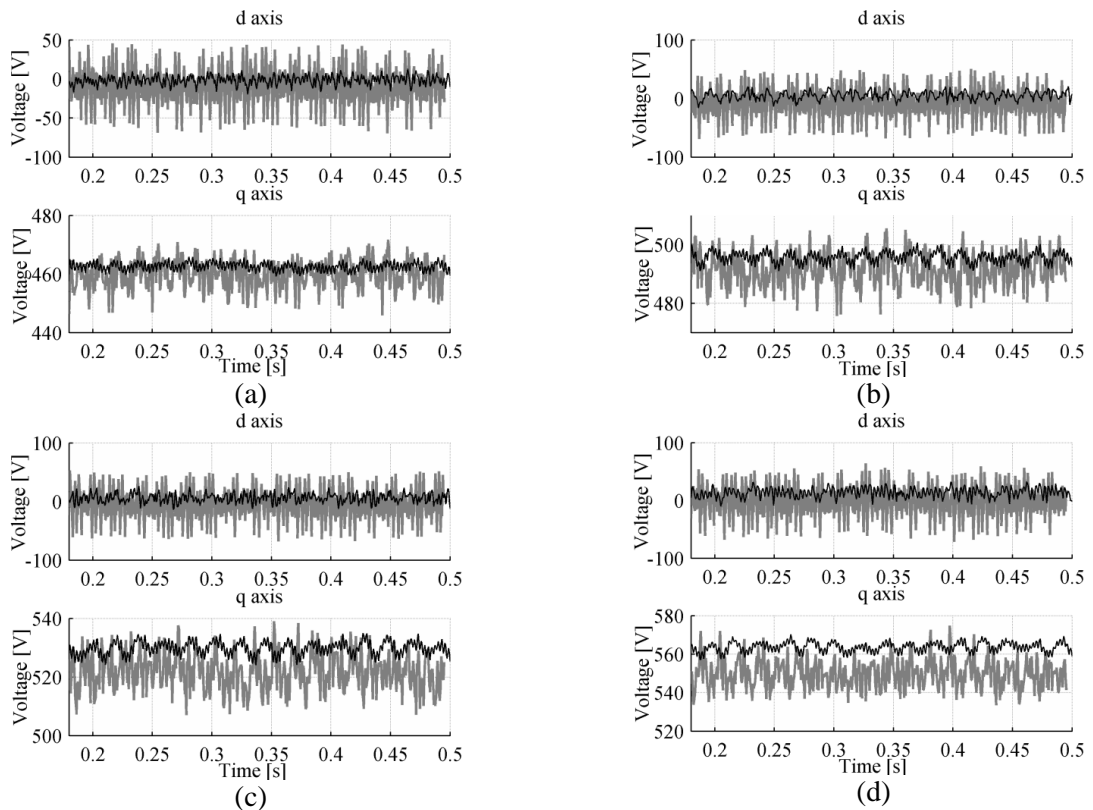

Fig. 5.45 Comparison of the d- and q-axis voltages (top and bottom plots, respectively) for different d-axis current (a) 0A, (b) 25A, (c) 50A, (d) 75A and constant q-axis current set at 0A. The black trace is simulation data and the thick grey trace represents the experimental data.

Fig. 5.45 shows the comparison of the stator's voltages when varying the *d*-axis current from 0 to 75A (in 25A steps). It can be seen how as the *d*-axis current is increased, the plots of the *q*-axis voltages (lower plots) start to differ showing the effect of the *d*-axis magnetic saturation (reduction of the actual *d*-axis inductance). The parameter estimation algorithm could be run in these cases to obtain the variation of the *d*-axis inductance as the *d*-axis current is increased. For regulation purposes, the inductance variation shown in this case is almost negligible and so the machine's parameters can be considered almost constant and equal to those shown in Table 5.5 across the entire operational range.

5.6   Effect of the decoupling terms

5.6.1   Omission of the *d-q* axis decoupling terms

By removing the *d-q* decoupling terms, the effect of changing the current in either *d*- or *q*-axis on the current of the other axis becomes more noticeable, as can be seen in Fig. 5.46. In this figure, it can be seen that the effect of the *q*-axis current step on the *d*-axis current is more pronounced (and lasts longer) when the decoupling terms are deactivated (black trace).
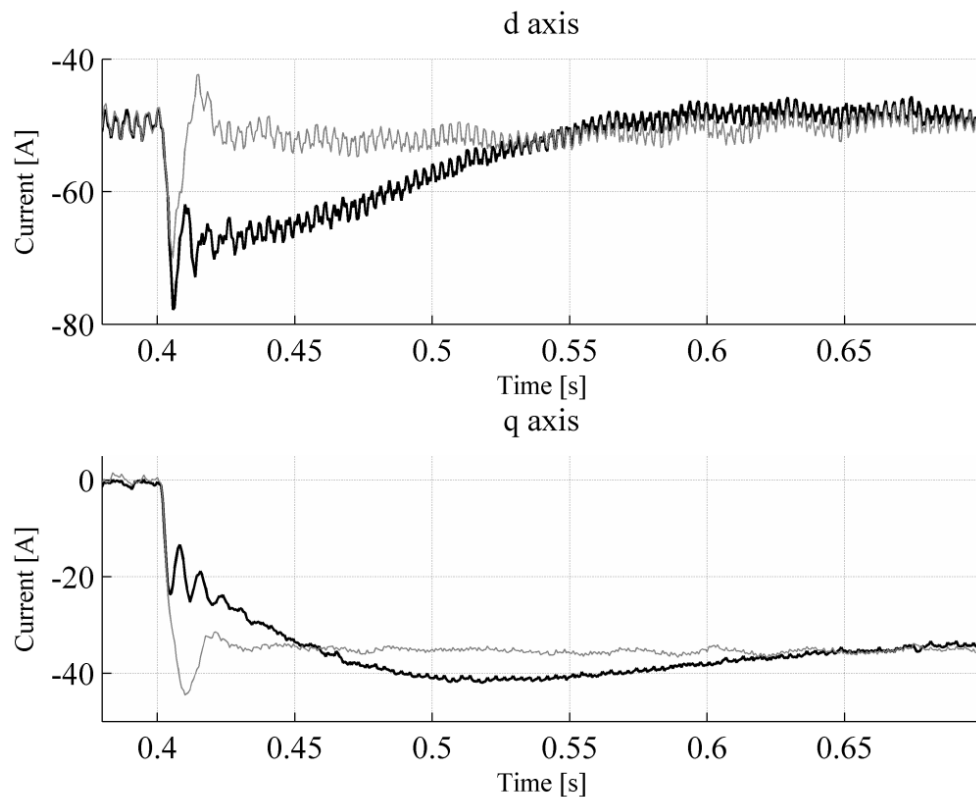

Fig. 5.46 Comparison of the step response obtained from simulation when the d-q decoupling term is deactivated (black trace) and activated (grey trace) for a speed of 60 Hz. The control parameters have been chosen to minimise the settling time.

A set of *q*-axis current steps at different rotational speeds are performed both in simulation and in the test-bench in order to check how the decoupling terms affect the behaviour of the current loops. It can be seen that the effect of disabling the decoupling terms becomes more detrimental as the rotational speed increases. This is expected since the *d-q* decoupling terms include multiplication with the electrical speed (4.39) – hence the effect becomes more pronounced as the speed increases. In fact, the coefficients that are multiplied with the speed are rather small, as can be seen in

Table 5.7.

Table 5.7 Test bench machine's d-q decoupling term coefficients.

| Parameter	Value
K_{d1}	0.00071
K_{d2}	-0.00176
K_{q1}	0.002676
K_{q2}	0.001622
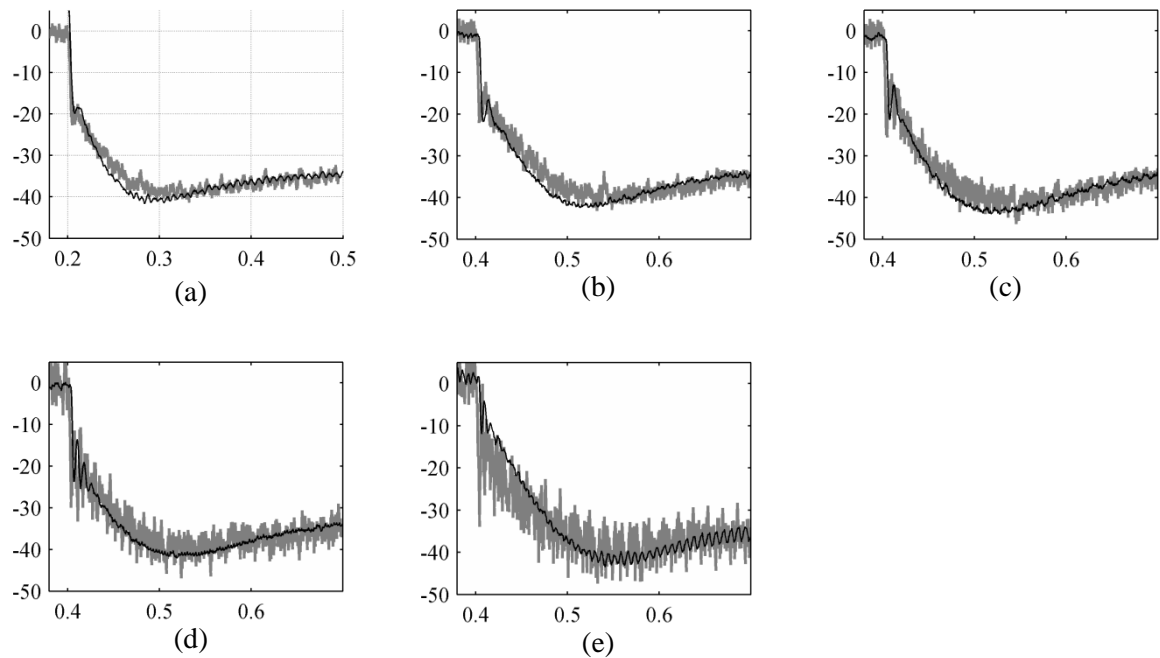
Fig. 5.47 Comparison of the step response obtained from simulation (black trace) and the experimental results (thick grey trace) for different rotating speeds (a) 30 Hz, (b) 40 Hz, (c) 50 Hz when the d-q decoupling terms are deactivated. The control parameters have been chosen to minimise the settling time.

The dynamic response of the current loops becomes affected experiencing a clear reduction in the dynamic performance and an increase in the overshoot and the settling time. The effect of this decoupling can be easily explained looking at the frequency response function (FRF) of the current regulator's transfer functions Fig. 5.48. It clearly shows how the inclusion of the decoupling terms provides a smooth plot without anomalous gain peaks. Furthermore, in Fig. 5.48 (c), it can be seen how the deactivation of the decoupling terms yields the apparition of an additional 0 db cross-over point at a very low frequency (±2 Hz in this case) that greatly reduces the dynamic performance of the loop.

In the closed-loop plots (b) and (d), the reduction in the bandwidth when disabling the decoupling terms can be clearly seen. With the decoupling activated (b), the gain plot shows a wide region near the unitary gain threshold (0 dB), whereas with the decoupling deactivated (d), this region is greatly reduced. This is translated into a limitation of the frequency range at which the loop is able to respond.

(a)   (b)

(c)   (d)
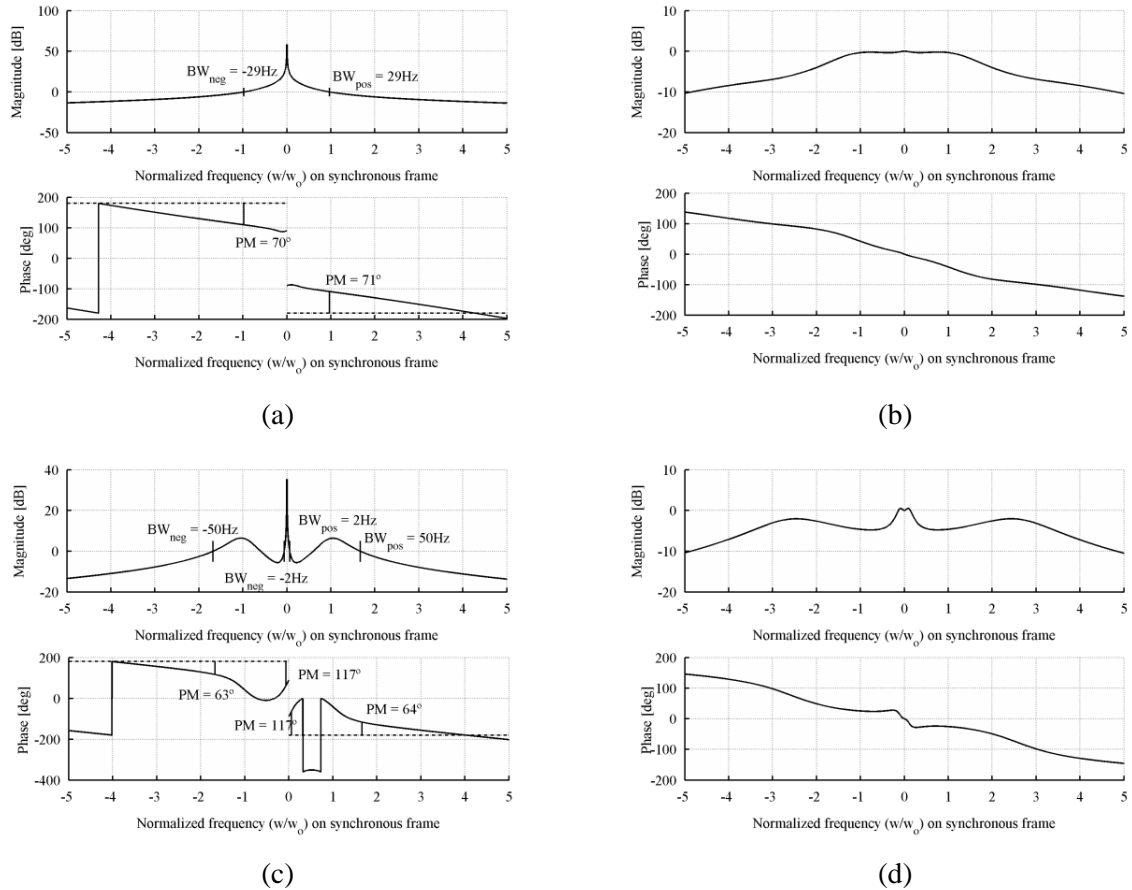
Fig. 5.48 FRF of the current regulator's open ((a) and (c)) and closed ((b) and (d)) loop transfer function when the d-q decoupling terms are activated (a) and (b) and deactivated (c) and (d). The electrical speed is set to 30 Hz.

5.6.2   Decoupling between stators

The effect of the stator-stator decoupling can be seen in Fig. 5.49. In this figure, the responses to a *q*-axis step current in the stator number 1 are shown, while keeping *q*-axis current in stator 2 at zero. In this situation, the change in the *q*-axis current in the stator 1 can be seen as a perturbation to the current regulators of the stator 2. Comparing the two results, it can be concluded that the effect of this perturbation is almost negligible, as it hardly affects the current in the stator 2. Table 5.8 shows the decoupling parameters for the machine parameters shown in Table 5.5; it can be seen how the values are rather small thus yielding a small amplitude perturbation. This is so because these coefficients are only multiplied with the current (and not with the electrical speed, as in 5.6.1); as a consequence, the effect is much smaller.

Table 5.8 Test bench machine's stator-stator decoupling coefficients.

Parameter	Value
K_{st1}	0.030652
K_{st2}	-0.05058
K_{st3}	0.03402
K_{st4}	-0.05435

(a)   (b)
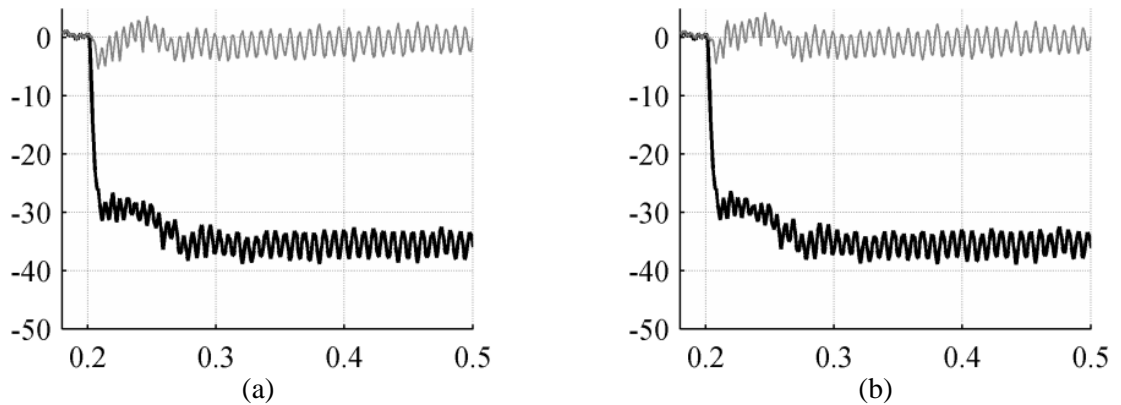
Fig. 5.49 Step responses of q-axis current obtained from simulation when the stator-stator decoupling is disabled (a) and enabled (b) for a rotating speed of 30 Hz. The black trace is the stator's 1 q-axis current while the grey trace is the stator's 2 q-axis current. The control parameters have been chosen to minimise the settling time.

Looking at the expressions for the decoupling terms (4.40) it can be seen how the values of the decoupling terms increase as the leakage inductance decreases (see Fig. 5.50). This may imply that in high-power machines, where the leakage inductances are small, the effect of these decoupling terms might become more dominant.
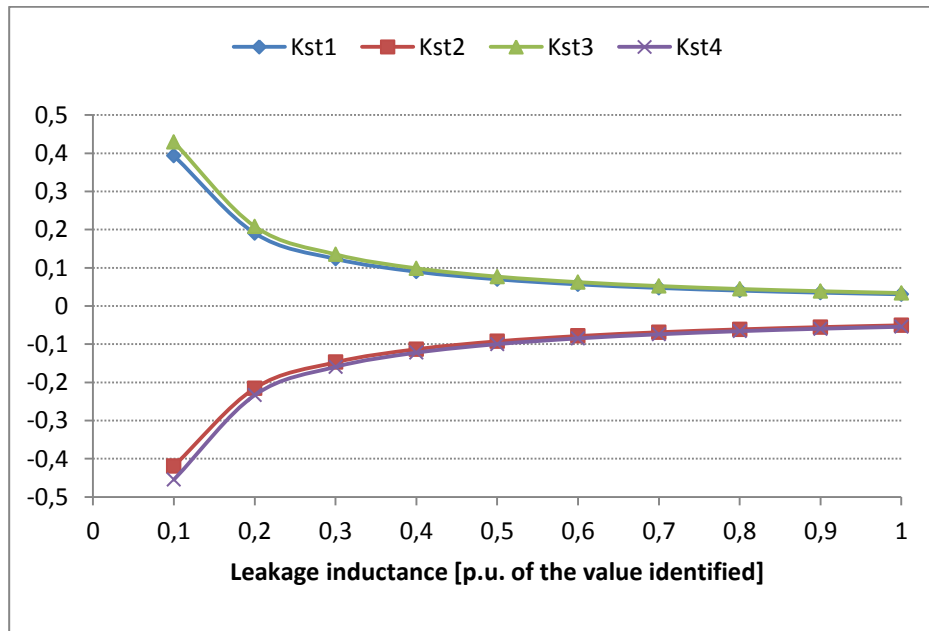

Fig. 5.50 Evolution of the stator-stator decoupling terms when varying the leakage inductance from 0.1 to 1 p.u. of the value shown in Table 5.5.

5.6.3   Inputs decoupling

The input decoupling tries to compensate the effect that a change in the voltage in the stator 1 has on the stator 2. For this purpose, a step in the q-axis current (and so in the q-axis voltage) of the stator 1 is performed keeping constant the currents of the stator 2. Fig. 5.51 shows the difference in the responses when the decoupling is disabled (a) an enabled (b). When the decoupling is disabled, the step in the stator 1 transiently affects the current in the stator 2 (a), while enabling the decoupling clearly compensates said effect making the two stators practically independent.

Table 5.9 Test bench machine's inputs decoupling coefficients.

Parameter	Value
K_{in1}	0.002675
K_{in2}	0.001621
K_{in3}	0.002818
K_{in4}	0.001764

(a)   (b)
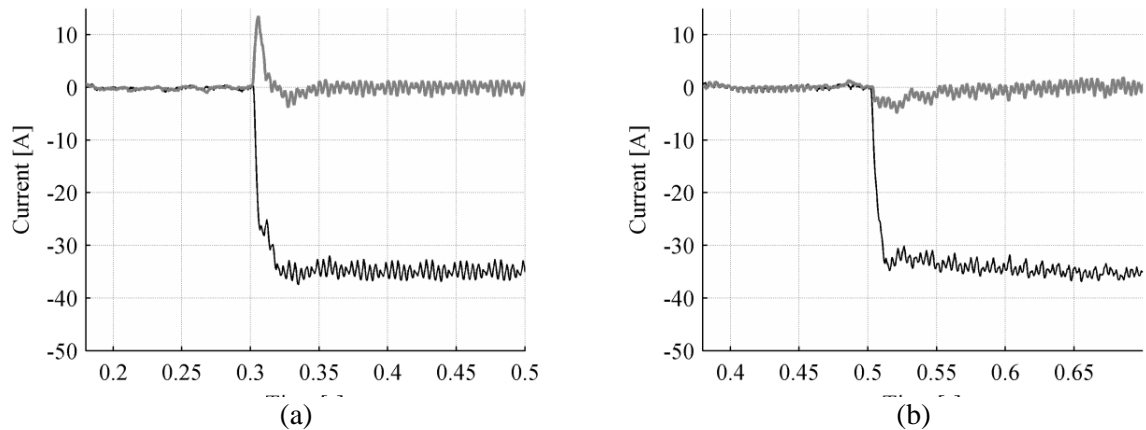
Fig. 5.51 Step responses obtained from simulation when the input decoupling is disabled (a) and enabled (b) for a rotating speed of 40 Hz. The black trace is the stator's 1 q-axis current while the grey trace is the stator's 2. A step in the q-axis current of the stator 1 is requested while keeping stator's 2 at zero. The control parameters have been chosen to minimise the settling time.

The effect of this decoupling is only appreciable when both stators are operating independently in terms of current sharing. If the two stators are operated with equal currents, there is hardly any difference between disabling and enabling this decoupling, as can be seen in Fig. 5.52.


(a)   (b)
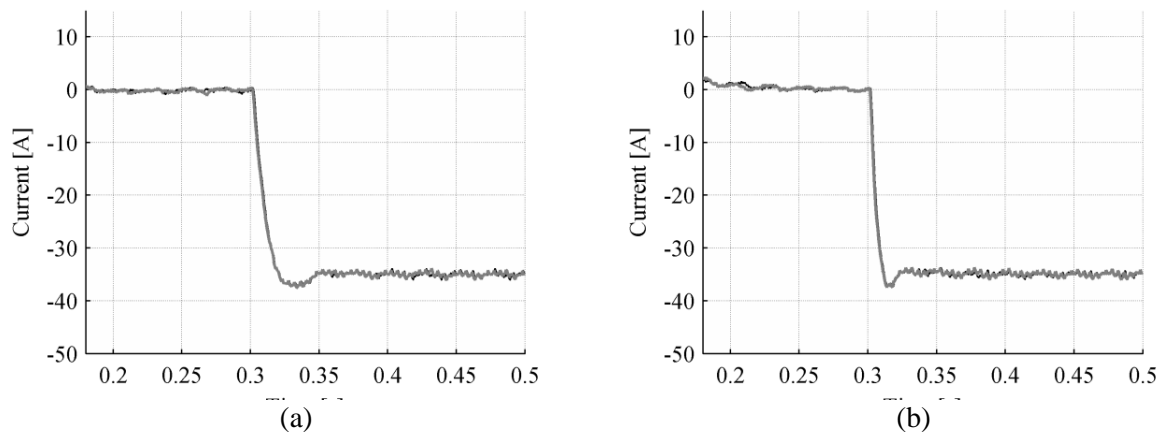
Fig. 5.52 Step responses obtained from simulation when the input decoupling is disabled (a) and enabled (b) for a rotating speed of 40 Hz. The black trace is the stator's 1 q-axis current while the grey trace is the stator's 2 q-axis current. A step in the q-axis current of both stators is commanded. The control parameters have been chosen to minimise the settling time.

5.7   Summary

In this chapter, the development of the current control loops for a machine with two three-phase windings has been presented. The procedure includes the non-idealities of an industrial control hardware in order to make the algorithm directly transferrable to a real test-bench. These non-idealities make the modelling of the current loops much more complex since internal delays and phase-shifts cannot be easily represented accurately. Furthermore, the modelling of the current loops has been developed following a multidimensional approach with multiple input and multiple output (MIMO) models. This allows to take into account all the mutual couplings actually present in the real system and design the decoupling terms accordingly. With the MIMO representation of the current loops, a tuning algorithm has also been derived allowing to obtain regulator's parameters that satisfy certain optimization criteria while taking into account the residual mutual couplings after the decoupling terms are applied.

Theoretical considerations and simulation results have been satisfactorily verified using experimental data obtained from an Ingeteam's low-power test-bench.

CHAPTER 6

Power sharing in multiphase machines with multiple three-phase windings

6.1 Introduction

The ability to operate a multiple three-phase machine with different loads on its three-phase systems can be highly interesting in applications where the energy managed by the conversion stage (machine and power converter) is to be maximized at all times. One of such applications is wind power where, without this ability, in case for example of an overheating in a component of one of the converters, it should be completely shut down thus losing its production. If different load sharing is available, in this latter case, the overheated converter could reduce its power (instead of fully shutting down) while the healthy ones are kept at maximum. This way, the overheating does not lead to a thermal runaway and trip of the converter; instead, the converter keeps operating minimizing the loss of energy.

In general, the way the power sharing is performed depends on the modelling approach used for the machine control scheme. In the multiple *dq* approach, the power sharing is as simple as just changing the current reference values on the different three-phase windings. On the other hand, if the VSD approach is followed, the power sharing strategy depends on the number of phases of the machine and it always involves the injection of fundamental frequency currents in the non-flux/torque producing subspaces.

6.2 Power sharing in a double three-phase machine

6.2.1 Double *dq* approach

Throughout this section, the control scheme used both in simulations and in the experimental rig is the same as the one derived in the section 5.2.4. The control structure is identical to the one shown in Fig. 5.11. With this control structure in the synchronously rotating frame, as was demonstrated in section 4.2.1.1, the initial four-input/four-output (MIMO) plant with heavy cross-couplings is simplified to four independent single channel plants thus allowing to increase the performance of the current loops without compromising the stability. The current regulators have been tuned following the optimization criterion of minimising the settling time (see section 5.2.4.4) and considering the machine's inductances identified in section 5.5.2. With these inputs, the tuning algorithm yielded the control parameters shown in Table 6.1.

Table 6.1 Current regulator parameters (proportional gain k_p and integral time constant T_i) for the double dq control approach.

Machine's speed [Hz]	*d*-axis		*q*-axis	
	k_p	T_i	k_p	T_i
30	212.3	0.026	212.3	0.026
40	227.1	0.035	227.0	0.036
50	238.1	0.026	238.1	0.026
60	402.8	0.034	402.8	0.034
70	378.3	0.046	378.2	0.047
80	378.3	0.052	378.6	0.065

Following the double *dq* approach, the power sharing amongst the different three-phase windings in the machine is very straightforward. This is so since this approach yields two independent sets of current controllers (one for each three-phase winding); then, different current commands can be set to each of them.

In Fig. 6.1, it can be seen how both windings can easily handle different power by simply modifying the current commands for each of them. The top two plots represent the *q*-axis current commands and responses, respectively, applied to the winding 1 (black trace) and to the winding 2 (grey trace). The third plot shows the currents for the phase one phase winding 1 (black trace) and for another phase of winding 2 (grey trace). The last plot shows the resultant active power handled by each of the windings. By setting different *q*-axis current references to each of the three-phase windings (as in Fig. 6.1), different power will be handled by each of them.
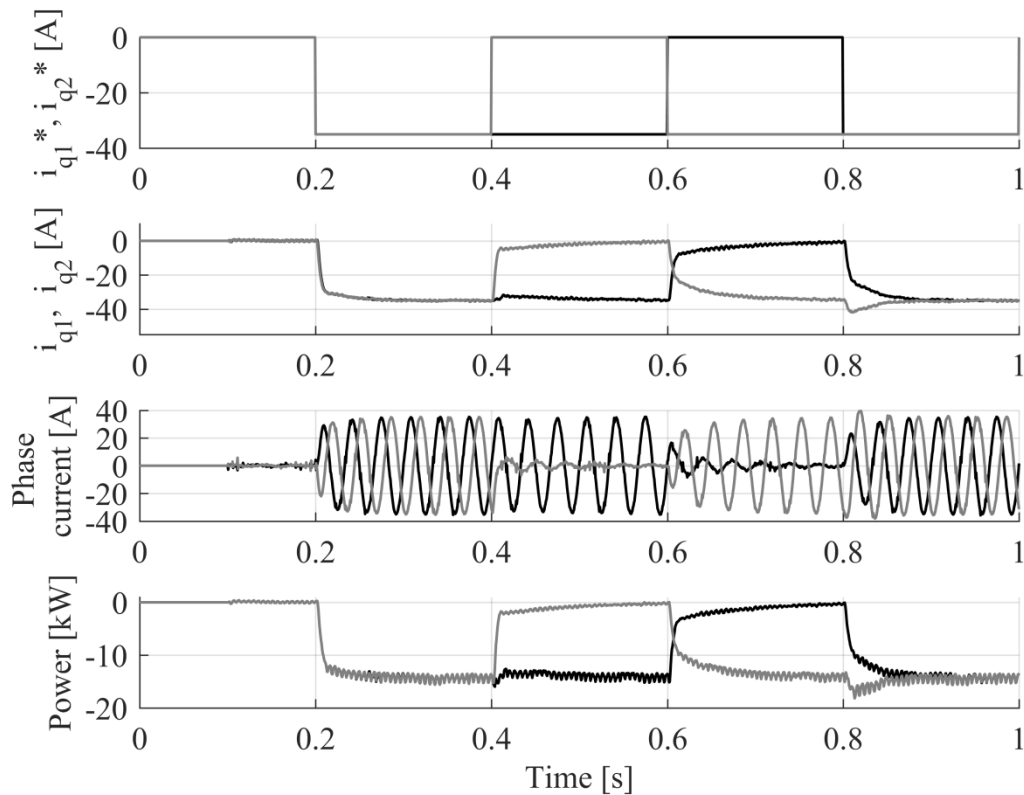

Fig. 6.1 Simulation of different current sharing situations in a double three-phase machine following double dq approach. The black trace corresponds to the values in winding 1 and the grey to the winding 2. The d-axis current has been kept at 0 in both windings at all times and the machine rotates at 20 Hz.

Fig. 6.2 shows the comparison between the simulation model and the experimental test rig results in a situation in which both three-phase windings were initially with the same current level (-35A); at time instant $t = 0.2$ s the currents of the first three-phase winding are driven to zero with a step command (Fig. 6.2(a)) and the currents are then again driven to -35A (Fig. 6.2(b)). It can be seen how the decoupling between the different axes in the machine is perfectly accomplished since hardly any perturbation can be noticed when the step commands are applied to the *q*-axis current. In Fig. 6.2(b), it can be noticed how the dynamic response of the current step is poorer than the one obtained in (a). This is so since the current step in (b) increases the braking torque of the generator and it results in a steep and wide speed variation due to poor dynamics of the motor drive that reduces the dynamic response of the current loop (see section 5.5).

With this approach, the power sharing between the three-phase systems simply requires the command of different currents for each of the windings, exactly the same as if they were two independent three-phase machines. This makes it very intuitive and easy to understand.


(a)

(b)
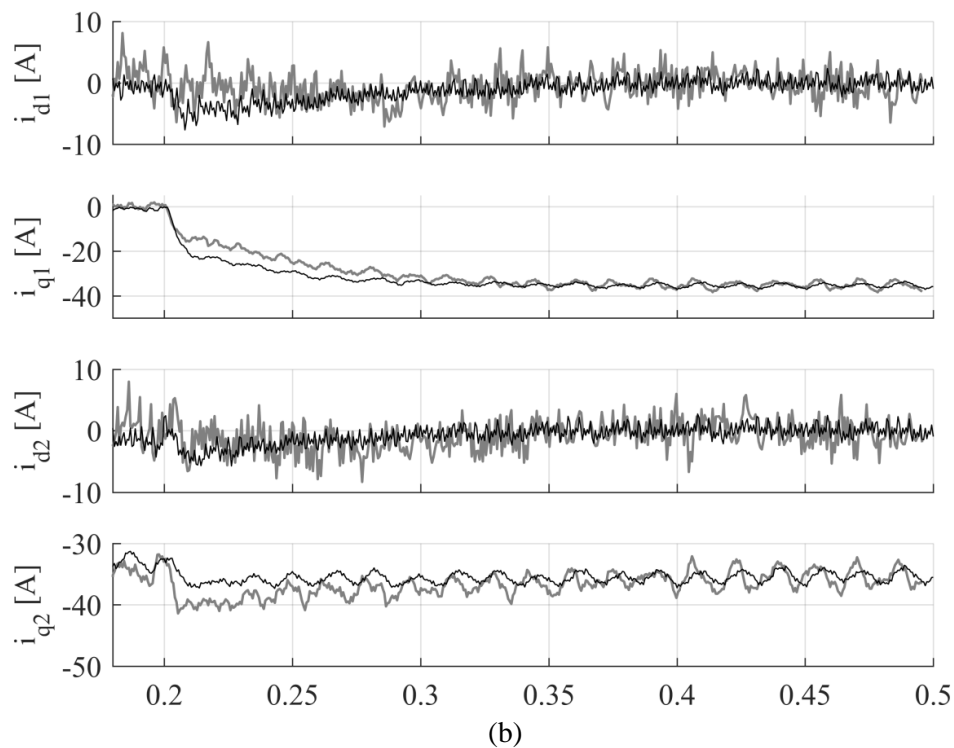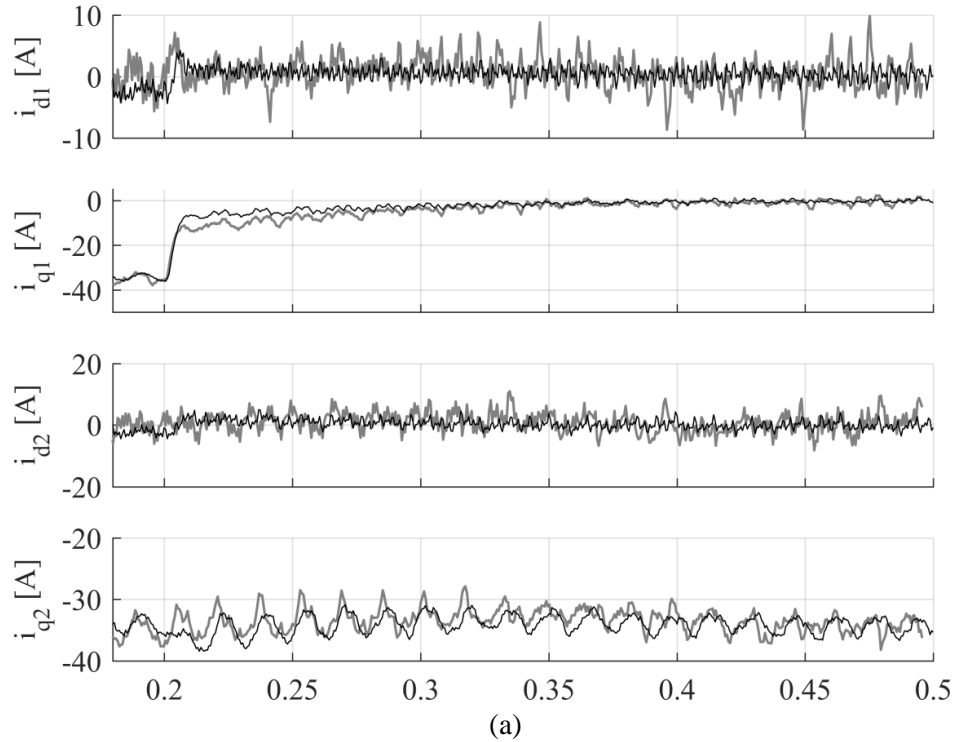
Fig. 6.2 Simulation and experimental results of different current sharing situations in a double three-phase machine following double dq approach. Current step command from -35 to 0 (a) and from 0 to -35 (b) on winding 1. The black trace corresponds to the results from simulation, whereas the grey shows the experimentally obtained ones. The machine rotates at 40 Hz.

A somewhat special case of power sharing situation can be found when one of the three-phase windings is operated as generator (with negative q-axis current), while the other is operated as motor (with positive q-axis current). This situation is shown in Fig. 6.3 where it can be seen how the winding 1 is motoring with q-axis current equal to 35A while the winding 2 is generating with -35A. This special power sharing situation can be very interesting from the industrial point of view since it allows testing the machine and the converter up to full rated power without the need of an additional driving machine and converter. The comparison between the traditional test-bench for machines and/or converters and the proposed one using this ability can be seen in Fig. 6.4. It is obvious that important savings in terms of cost and required footprint are obtained by taking advantage of this ability.
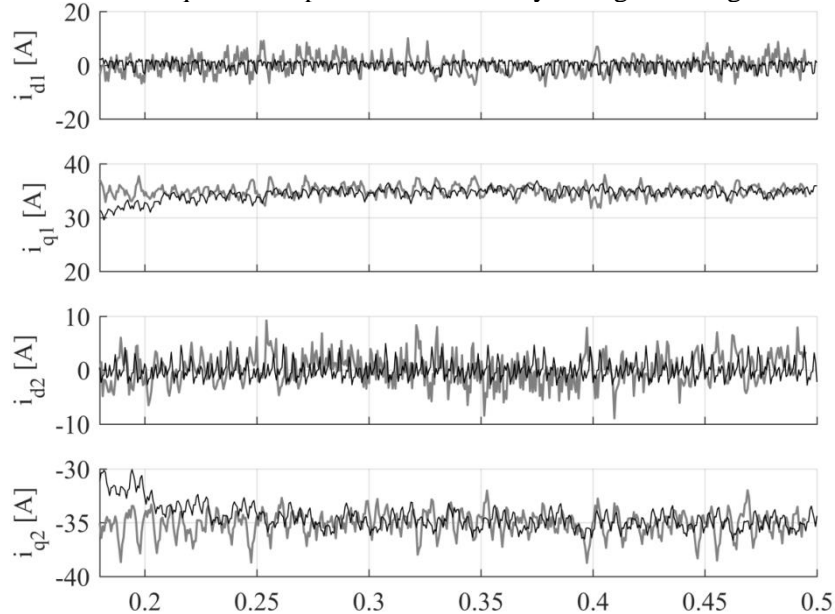

Fig. 6.3 Simulation and experimental results of a current sharing situation in which one three-phase winding is motoring and the other generating. The black trace corresponds to the results from simulation whereas the grey shows the experimentally obtained one. The d-axis current has been kept at 0 in both windings at all times and the machine rotates at 40 Hz.


(a)

(b)
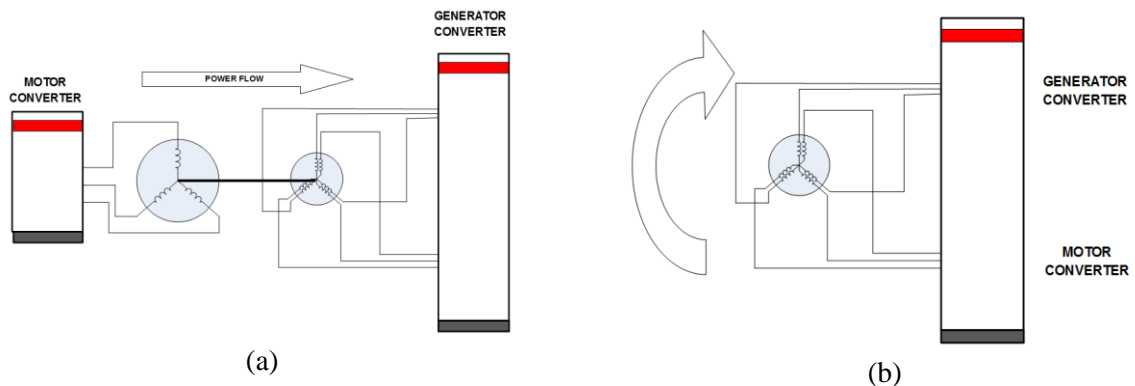
Fig. 6.4 Test-bench layouts for testing the machine and/or converter: (a) the standard one with a driving machine and converter in back-to-back configuration and (b) the proposed one with one winding motoring and the other generating.

Further details and experimental results from the proposed test bench layout can be found in (Zabaleta et al., 2018a) and (Zabaleta et al., 2018b).

6.2.2 VSD approach

In this section, the control structure used is the one shown in Fig. 5.11, in which the decoupling terms relative to the inputs (K_{in}) and between the three-phase windings (K_{st}) are not required. This is so

since, as described in section 4.2.1.2, the plant model resultant from the VSD approach only presents a *dq* cross-coupling in the flux/torque producing subspace. The current regulators have been tuned following the optimization criterion of minimising the step response quadratic error (see section 5.2.4.3) and considering the machine's inductances identified in section 5.5.2. With these inputs, the tuning algorithm yielded the control parameters shown in Table 6.2.

Table 6.2 Current regulator parameters for the VSD control approach.

Machine's speed [Hz]	*d*-axis		*q*-axis	
	k_p	T_i	k_p	T_i
30	1.337	0.221	1.426	0.289
40	1.361	0.199	1.45	0.164
50	1.387	0.272	1.479	0.381
60	1.387	0.401	1.478	0.401
70	1.325	0.1	1.413	0.112
80	1.175	0.072	1.252	0.078

For the current regulation in the non-flux/torque producing subspace, resonant controllers in the stationary reference frame have been used. This type of the controller has been chosen since it provides excellent tracking for the currents at the resonant frequency (continuously varied to ensure it corresponds to the fundamental frequency of the machine) in both positive and negative sequences.
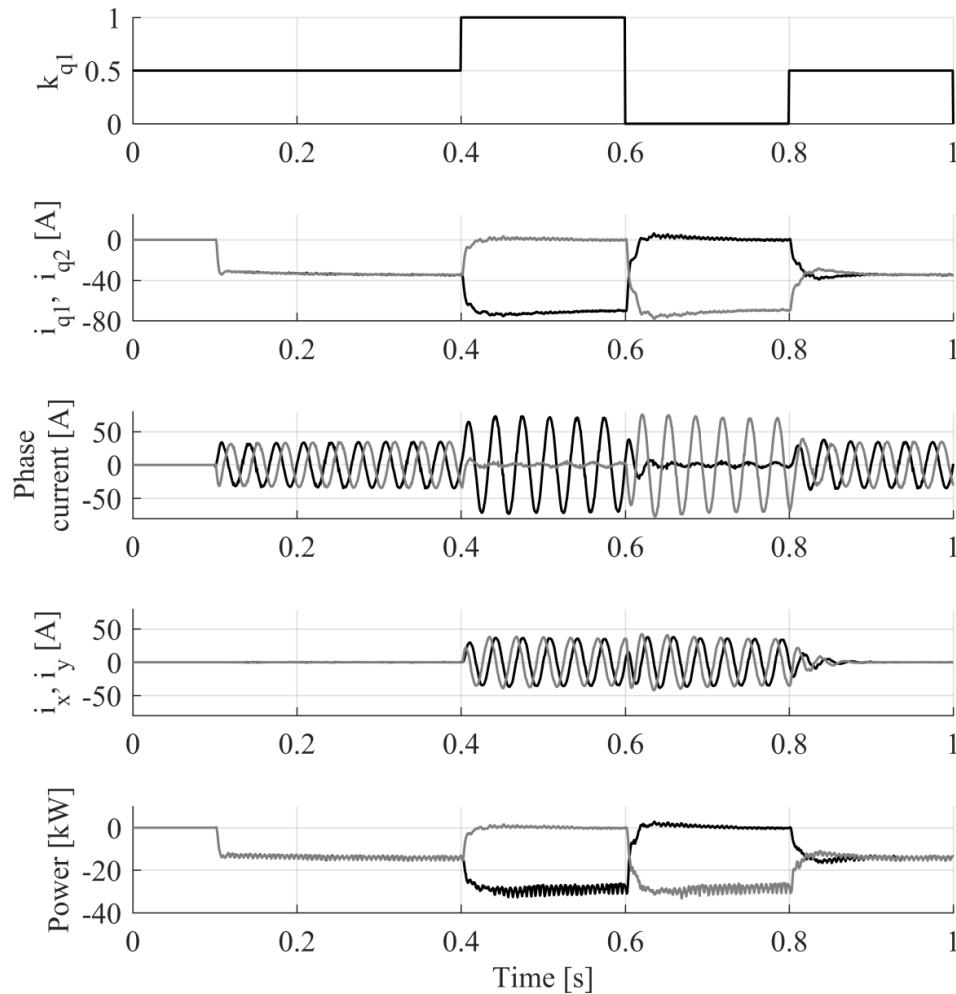

Fig. 6.5 Simulation of different current sharing situations in a double three-phase machine following VSD approach. The black trace corresponds to the values of winding 1 and the grey to the winding 2. The d-axis current has been kept at 0 in both windings at all times and the machine rotates at 20 Hz. Coefficient k_{q1} defines the power sharing between two windings.

When the VSD approach is followed, to obtain different power sharing amongst the three-phase windings in the machine, a fundamental frequency current needs to be injected in the non-flux/torque subspace.

Fig. 6.5 shows the same experiment as the one shown in Fig. 6.1 where, at different instants, the current in the different three-phase windings is varied between -35A and 0A. An important remark here is that the power sharing using the VSD approach is a little bit more complicated than with the multiple *dq* approach. This is so since in the latter case, to modify the power of one winding, only the current reference relative to that winding needs to be modified keeping the rest unchanged. On the other hand, in the VSD approach, it is not just enough to introduce fundamental frequency currents in the non-flux/torque producing subspace, but also the current reference for the flux/torque producing subspace needs to be modified to avoid overloading the other winding. This effect can be seen in Fig. 6.5 where only the currents in the non-flux/torque producing subspace are introduced. When (at instant 0.4 s) the currents in the winding 2 are driven to 0, the currents in the winding 1 are doubled to compensate for the lack of torque from winding 2. This may clearly overload the winding 1 and could trip its converter due to overcurrent.

To avoid overloading the windings, the flux/torque subspace current reference needs to be modified accordingly. This effect can be seen in Fig. 6.6 where the flux/torque subspace current reference has been modified in order to keep the current of each three-phase winding below or equal to its rated value.
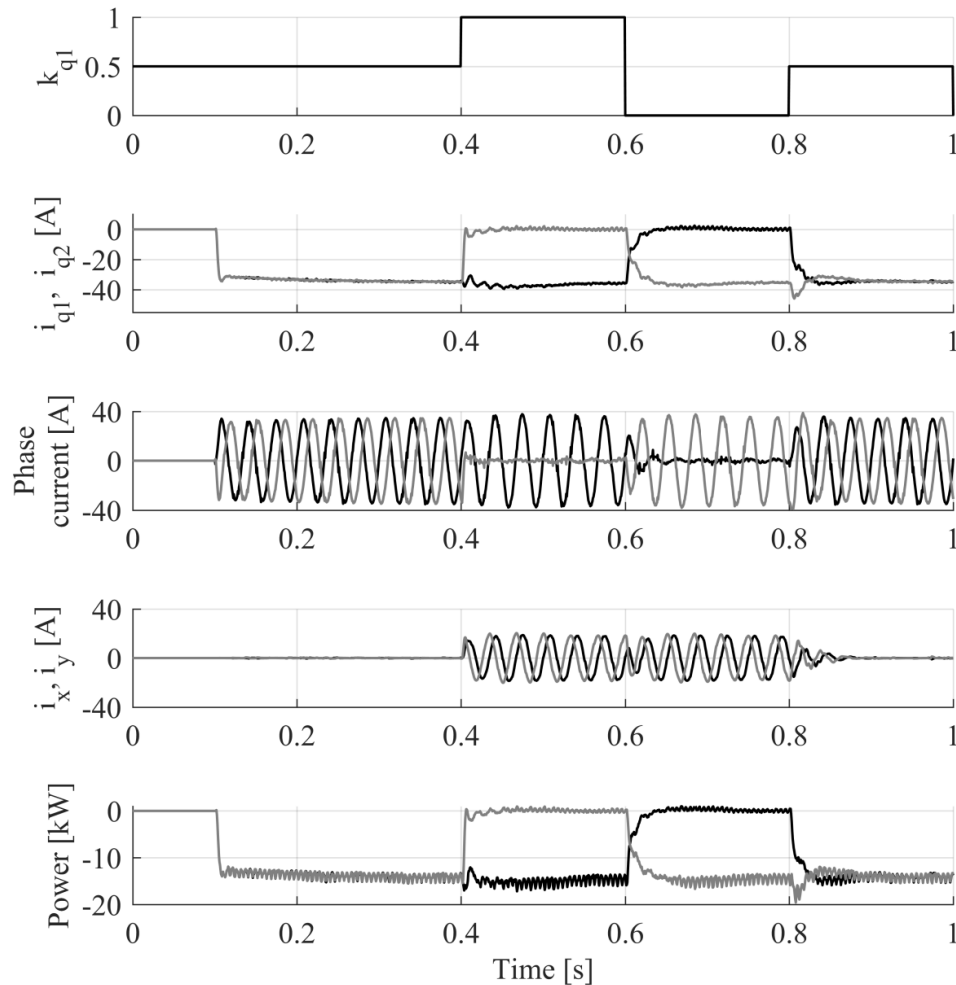

Fig. 6.6 Different current sharing situations in a double three-phase machine following VSD approach with limiting of the flux/torque subspace current reference. The black trace corresponds to the values in winding 1 and the grey to the winding 2. The d-axis current has been kept at 0 in both windings at all times and the machine rotates at 20 Hz. Coefficient k_{q1} again defines the power sharing between two windings.

For the case of a double three-phase machine, the VSD and the novel transformation approach yield the same transformation matrix, as explained in section 3.7.2. For this reason, both approaches are identical for this type of the machine and, in this section, only the VSD approach was analysed.

6.3   Power sharing in a triple three-phase machine

For the triple three-phase machine, all the results are obtained from simulations as no experimental rig was available with a nine-phase machine. The simulation approach is the same as the one used for the six-phase machine, which has been thoroughly described and investigated in CHAPTER 5. As has been demonstrated in the said chapter, the simulation model represents very precisely the behavior of the experimental rig. Similarly as in CHAPTER 5, a nine-phase machine's model has been developed for Matlab's SimPower Systems as there were no available models for nine-phase machines in this simulation platform. As the case was for the six-phase machine, the spatial 0º shift between the different three-phase windings has been considered.

For the machine model, the same machine's parameters as the ones shown in the identified parameter column in Table 5.5 are considered. The rated value of the phase current has been taken as 35A.

6.3.1   Triple *dq* approach

Throughout this section, the control scheme used in simulations is the same as the one derived in the section 5.2.4. The control structure corresponds to the one shown in Fig. 5.11. With this control structure in the synchronously rotating frame, as was demonstrated in section 4.2.2.1, the initial six-input/six-output (MIMO) plant with heavy cross-couplings is simplified to six independent single channel plants. As the machine's inductances are considered equal to those of the six-phase machine, the control parameters shown in Table 5.5 have been used.

Following the multiple *dq* approach in a nine-phase machine, the power sharing between the three-phase windings is again extremely straightforward. This is so since the controls of the different windings are completely independent. As can be seen in Fig. 6.7, the current sharing is obtained by simply varying the current references for each of the three-phase windings. As each three-phase winding has its own controller, setting up the limits for its variables (e.g. currents, powers, etc.) becomes very simple and is in essence independent of the number of three-phase windings that are actually being used at a certain time instant.
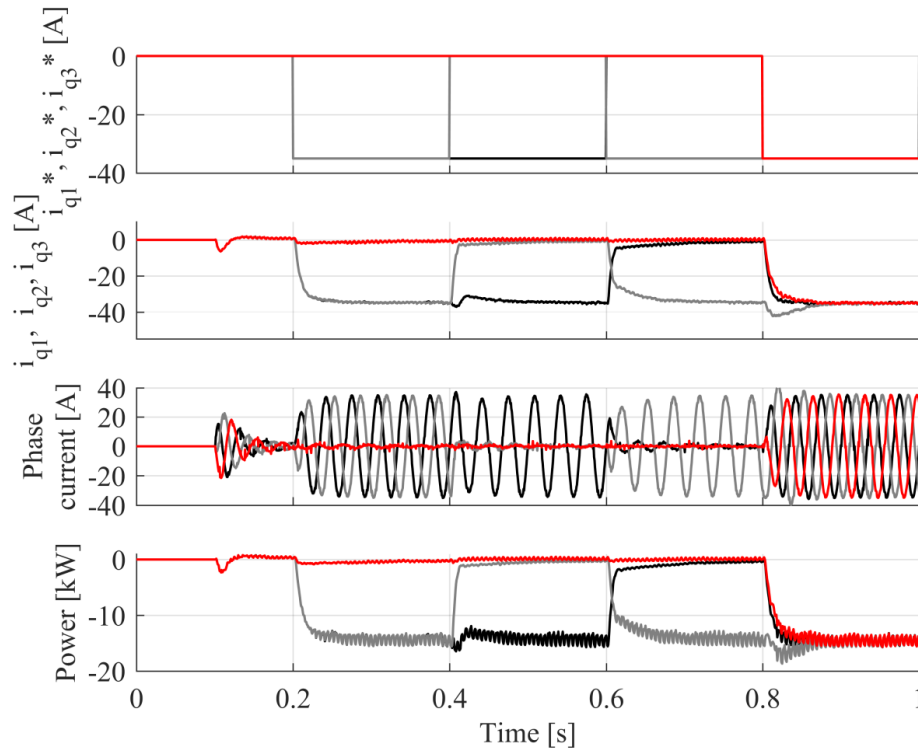
Fig. 6.7 Different current sharing situations in a triple three-phase machine following triple dq approach. The black trace corresponds to the values of winding 1, the grey to the winding 2 and the red to the winding 3. The d-axis current has been kept at 0 at all times and the machine is rotates at 20 Hz.

6.3.2 VSD approach

As the machine parameters have been taken equal to those of the six-phase machine, the current regulator parameters are the same as for the six-phase machine (Table 6.2).

The current sharing following the VSD approach for a nine-phase machine has been derived in (Zoric et al., 2017). In this paper, it was demonstrated how a set of current references for the x_iy_i subspaces can be found so that any current sharing can be obtained. Slightly modifying the scaling of the current references for the x_iy_i subspaces, the same results as in the previous subsection can be obtained. This scaling comes from the fact that the sharing coefficients used here are defined so that their sum should be equal to one (instead of three as in (Zoric et al., 2017)).

As the case was with the six-phase machine, the current reference in the flux/torque producing subspace needs to be adapted in order to avoid overloading the windings of the machine. This technique has been implemented in Fig. 6.8, where it can be seen how, when some windings are disconnected, the currents in the others are kept within the rated value.
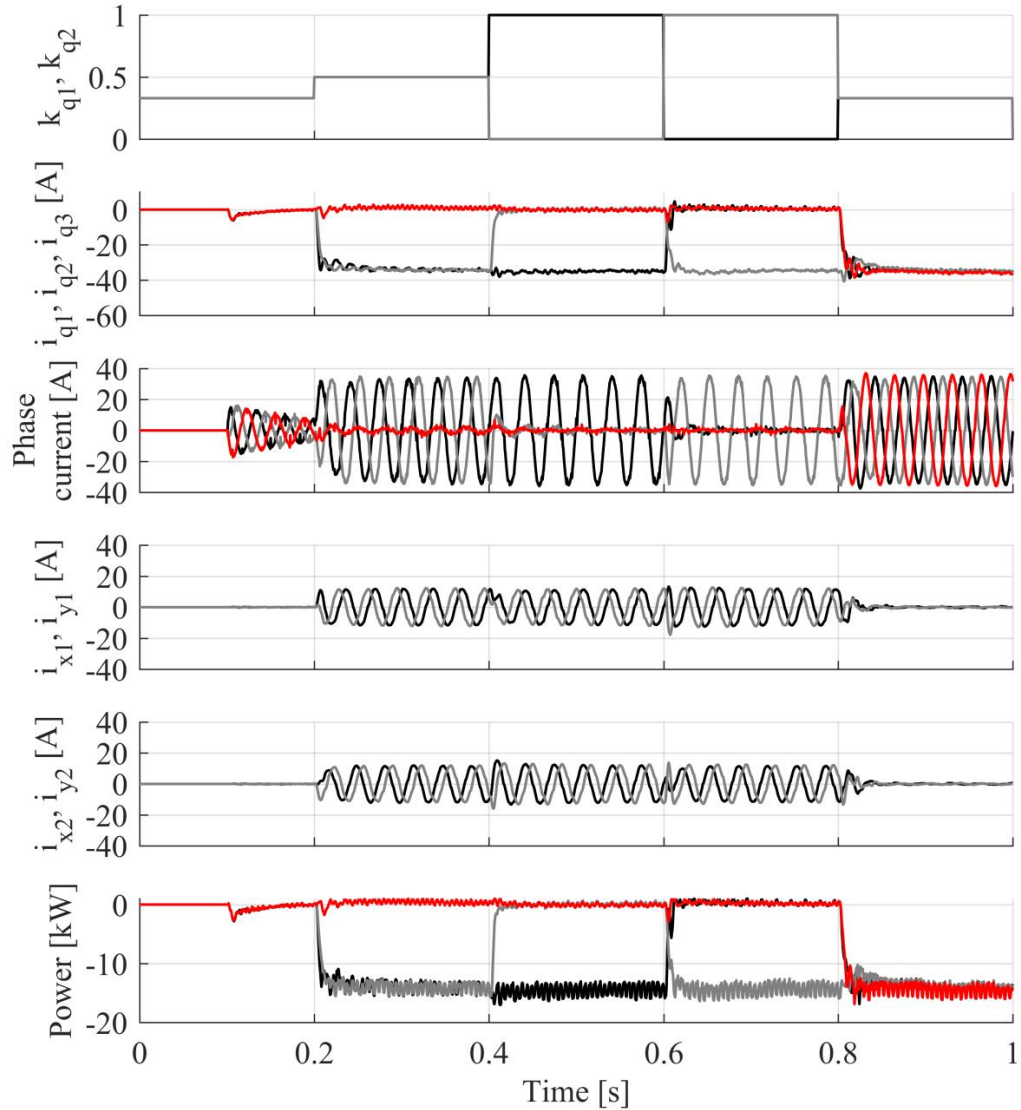
Fig. 6.8 Different current sharing situations in a triple three-phase machine following the VSD approach. The black trace corresponds to the values in winding 1, the grey to the winding 2 and the red to the winding 3. The d-axis current has been kept at 0 at all times and the machine rotates at 20 Hz. Coefficients k_{q1} and k_{q2} define the fractions of the power provided by windings 1 and 2 with respect to the total power.

      The implementation of the current limiter is not straightforward since the limits for the current regulators depend on the actual operating point. More specifically, they depend on the instantaneous power sharing amongst the different three-phase windings. For example, in the case of connecting/disconnecting three-phase windings in an on/off manner (i.e., all the active windings are with the same current and the inactive ones are with zero current), the flux/torque producing current limit might be

$$I_{dqmax} = \frac{k_{act} \cdot I_{rated}}{k}$$

(6.1)

where k is the total number of three-phase windings in the machine, k_{act} is the number of active windings and I_{rated} is the rated phase current. This is the limiting technique used in the Fig. 6.8.

      The current limiting technique described in (6.1) is not adequate when power sharing coefficients are varied in a continuous manner. In this case, the power handled by one of the windings can be for example 80% of the power handled by the others. Another example can be very insightful: in case that two of the converters are overheated and need to reduce their handled power, if the limiting technique described in (6.1) is used, there would still be three active windings and so the maximum

flux/torque producing current should be set as equal to the rated phase current. Situations like the one shown in Fig. 6.9a can happen where the healthy three-phase winding would be handling a higher than rated current because other windings are handling a reduced power due to some circumstance.


(a)   (b)
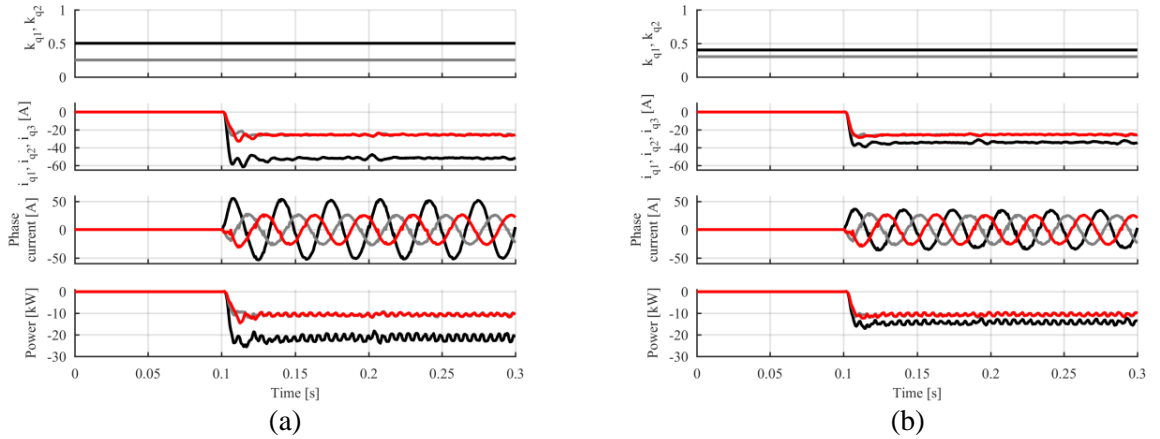
Fig. 6.9 Application of the current limiting technique described in (6.1) (a) and implementation of the limiting technique described in (6.2) (b).

In order to avoid the undesired overload of a winding, an availability factor (AF) per three-phase winding is introduced. This factor indicates the amount of current (power) that each of the three-phase windings can handle in the following manner: the availability factor of a winding is between 0 and 1 indicating the amount of the current that said winding can handle relative to the rated current. With these AFs, the flux/torque producing subspace maximum current can be set as

$$I_{dqmax} = \frac{\sum_{i=1}^{k} AF_i}{k} \cdot I_{rated}$$

(6.2)

where k is the number of three-phase windings. Additionally, in order to satisfy that the current in any of the windings does not go beyond the one defined by its AF, the current sharing coefficients (k_{dqi}) are then calculated by solving

$$\sum_{i=1}^{k} k_{dqi} = 1$$

(6.3)

$$k_{dq1} = \frac{AF_1}{AF_2} \cdot k_{dq2} \quad k_{dq2} = \frac{AF_2}{AF_3} \cdot k_{dq3} \quad \dots \quad k_{dqk-1} = \frac{AF_{k-1}}{AF_k} \cdot k_{dqk}$$

Applying this new limiting technique with $AF_1 = 1$, $AF_2 = AF_3 = 0.75$, the current sharing shown in Fig. 6.9b is obtained. It can be seen how the current in every winding is kept within its desired operational margins.

6.3.3   Novel approach

As was indicated in section 4.2.2.3, the model of the machine resulting from the application of the novel transformation approach is exactly the same as the one obtained by applying VSD. This makes it possible to use the same current regulator's tunings as in the latter case.

With the novel approach, the current sharing between the three-phase windings in the machine is also straightforward. This is so since the transformation has been derived having this in mind. As the auxiliary subspaces gather the information about the differences in currents between the different windings, injecting currents in said subspaces will lead to current differences between the windings in the machine. This can be seen in Fig. 6.10 where different current sharing situations are shown for a nine-phase machine. By varying the current sharing coefficients defined in (3.41), the same situations as in section 6.3.1 can be obtained. It has to be said here that, as it happens with the VSD approach, the current reference in the flux/torque producing subspace needs to be continuously updated in order to avoid overloading the windings of the machine. A scaling factor of 1/3 has been introduced in the

auxiliary subspaces in order to obtain a one-to-one relationship between the current sharing coefficients.
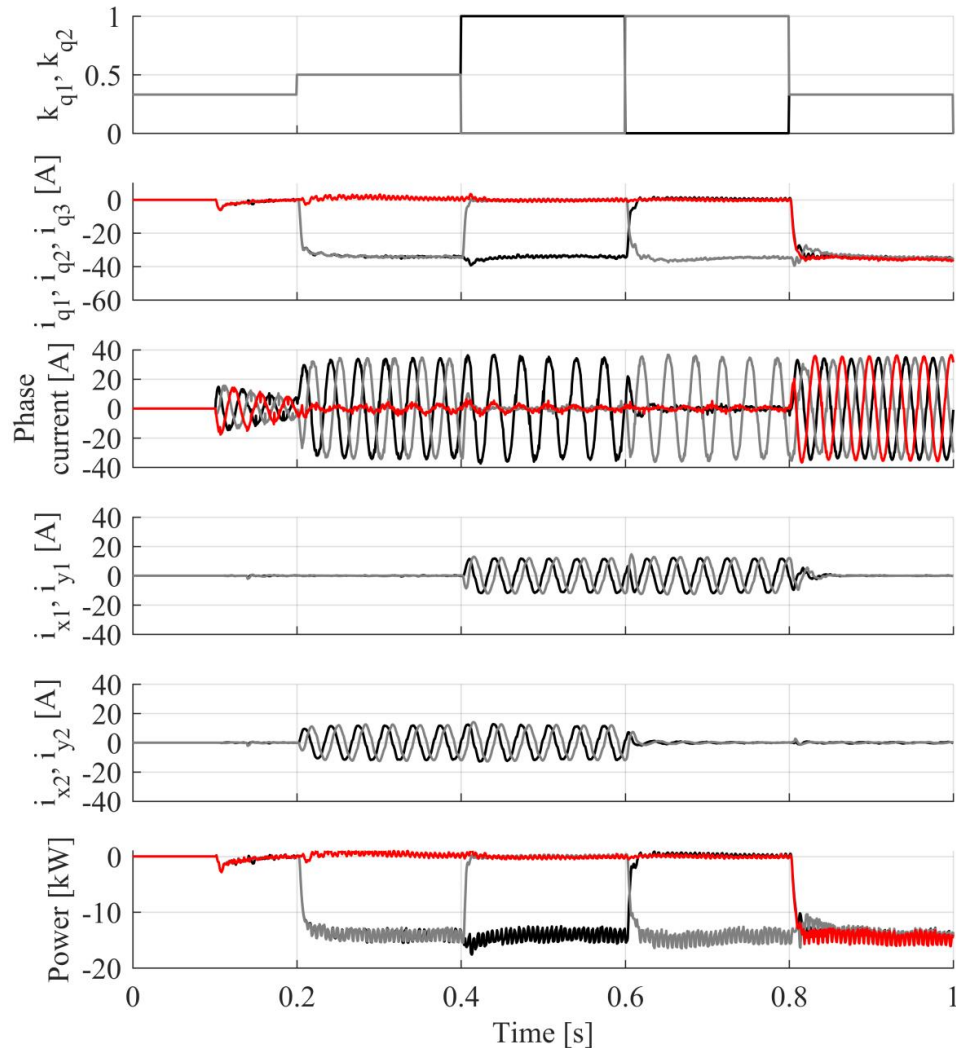

Fig. 6.10 Different current sharing situations in a triple three-phase machine following the novel modelling approach. The black trace corresponds to the values in winding 1, the grey to the winding 2 and the red to the winding 3. The d-axis current has been kept at 0 at all times and the machine rotates at 20 Hz.

Regarding the x_1y_1 and x_2y_2 current plots in Fig. 6.8 and Fig. 6.10, the main difference between the VSD and the novel transformation can be seen. In the former, as soon as there is a three-phase winding with a different power sharing, fundamental frequency currents need to be introduced in both xy subspaces. To the contrary, when using the novel transformation, fundamental frequency currents need to be introduced only in the subspace relative to the winding that has a different power value (compared to the reference one).

6.4 Summary

At the first sight, the multiple *dq* approach may seem to yield more complex control structures than VSD since it requires more cross-coupling decoupling structures. This initial drawback is overcome by the easier and more straightforward ability to apply different power sharing conditions between the three-phase windings of the machine.

Comparing the VSD and the novel transformation, both transformations can be used even in the case of different power sharing. The main benefits from the novel transformation in comparison to the VSD are:

- the transformation matrix can be easily obtained for any number of phases and spatial phase shifts.
- the physical interpretation of the auxiliary subspaces makes it easy to derive the required auxiliary subspace currents needed for certain power sharing.

When using VSD and novel approaches, it is important to implement a current limiting technique similar to the one proposed in 6.3.2 to avoid overloading any of the three-phase windings. With said technique, the desired current (power) sharing between the windings is also guaranteed.

CHAPTER 7

Conclusion and future work

7.1 Summary

This thesis covers the modelling and control of multiphase machines when a low switching to fundamental frequency ratio is required. This is the case of medium voltage converters where the switching frequency needs to be taken as low as possible in order to keep losses at a manageable level. Different multiphase machine construction types have been analysed and the emphasis is further placed on multiple three-phase winding machines, as the most frequent type in real-world applications. Along this work, the implications of a real industrial hardware have been taken into account when modelling the control loops, thus including non-idealities such as delays, sampling, filters, etc. The aim of the presented current control loops is to fully reproduce the behaviour observed in real industrial applications, thus allowing to predict dynamic behaviour under any condition. The current control loops have been modelled in Matlab but the implementation has been carried out in C code (to allow direct translation to a real DSP code). The simulations have been performed using the latter C code in the Simulink's SimPower environment. For the case of double three-phase machines, the modelling and simulation results have been experimentally validated within Ingeteam's offshore wind testbench.

Literature survey provided in Chapter 2 proves that a lot of research effort has been invested into the multiphase power conversion stage. Despite of this, the applications of these topologies in the industry are still limited and can be mainly found in electrical ship propulsion and aerospace, where the extra initial cost of the conversion stage has little effect on the overall cost. As it has been emphasised in previous chapters, multiphase conversion stage provides an inherent fault tolerance, which can provide a fail-safe mode that allows to keep operating it in the event of a failure. This behaviour opens a wide range of prospective industrial applications to which the multiphase conversion stages may fit perfectly. One of these applications is the offshore windpower, where unscheduled maintenance actions are extremely costly. In offshore, this fail-safe mode is very interesting as it allows the windfarm operator to keep operating the wind turbine, with a non-fatal failure within the power converter, instead of fully stopping it. This increases the energy harvest and it also helps to reduce the maintenance costs as the repair becomes less urgent. From this survey, it can also be concluded that the multiphase conversion stages introduce additional difficulties in terms of control and modulation strategies (such as low-order harmonic current flow and magnetic cross-couplings) that need to be taken into account to obtain stable operation. Additionally, it is clear that post-fault control strategy highly influences the amount of available power that can be handled by the conversion stage during the fail-safe mode, thus requiring further detailed analysis to reach an optimal solution.

The analysis performed in Chapter 3 unveils that there basically exist two well differentiated modelling approaches for multiphase machines, the VSD and the multiple *dq* modelling. The former treats the multiphase machine as a whole; hence, it is general and can be applied to any multiphase machine with minor changes. On the contrary, the latter treats the machine as several three-phase machines; therefore, it is only applicable to multiple three-phase winding machines. Additionally, the multiple *dq* approach exposes the magnetic coupling between the different three-phase systems, so this should be borne in mind when using it for controlling purposes. For machines with phase number higher than six, the VSD transformation does not provide means to easily operate the machine with different load sharing amongst its three-phase windings. This is so because its auxiliary subspaces do not have a clear physical interpretation. To overcome this difficulty, a novel transformation has been introduced that facilitates the load sharing between the different three-phase systems for any multiple three-phase winding machine. Generalization of the novel transformation to any *n*-phase machine (with *n* being an integer multiple of three) is obtained with the script provided in the Appendix 2. The novel

transformation presented in this work allows to easily operate a multiple three-phase winding machine with different load sharing between them by means of a simple method to calculate fundamental frequency current references in the auxiliary subspaces.

In Chapter 4, detailed modelling of two and three three-phase winding permanent magnet machines following the different available approaches has been performed. The models for each of the approaches in both stationary and synchronous frames are derived, showing a great impact, in the form of cross-couplings and time-dependant terms, of rotor saliency in the former frame. This makes it very complex to implement a control strategy in the stationary frame when high saliency machines are used (as might be the case of certain permanent magnet machines types). In order to obtain control loops that could be used for any type of machine, the synchronous frame was chosen as the preferred option. The state space representation of the machines have been developed showing different structures depending on the modelling approach. The modelling following the multiple *dq* approach may seem to yield a more complex model since a lot of cross-couplings are exposed. These cross-couplings would negatively affect the performance of the control introducing oscillations, overshoots, etc. On the contrary, following VSD (and novel) approaches, the resulting model is much simpler since the cross-couplings are not exposed by means of the mathematics involved in the transformations. These latter approaches leave a resultant model very similar to the classic three-phase machine's one with only a cross-coupling between the *dq* axes. Further, a decoupling strategy has been proposed for the multiple *dq* approach that yields $2k$ (with k being the number of three-phase windings) fully decoupled first order systems. With the state space representation in the synchronous frame, a machine model for SimPower has been developed and validated with experimental results.

In Chapter 5, the FOC for the multiple three-phase permanent magnets machines is introduced. As FOC relies on the control of machine's variables (flux and torque) by means of the control of the currents, the current regulators play a central role. The modelling of a real control loop is presented taking into consideration all the non-idealities of it (*dq* transformations, complex filters, delays, etc.). An important result from the modelling phase is that the dynamic response of the loops degrades as the rotating speed of the machine increases. This led to analyse its behaviour across the entire rotational speed range of the machine. The control loop model has been validated against simulation firstly and experimentally afterwards yielding a very good correlation in both cases. With the control loop mathematically represented, a tuning procedure for it has been proposed. It calculates the regulator parameters that optimize the dynamic response under certain criteria, such as minimum settling time, minimum quadratic error, constant overshoot, etc. This tuning procedure has been validated by simulations and also against the experimental results obtained from Ingeteam's offshore wind testbench. As the experimental rig machine was especially acquired for this research, the manufacturer given parameters were used first. After some experiments, a dynamic response mismatch was detected and was associated to a machine parameter deviation. In order to obtain a precise match between simulation and experimental data, an identification procedure was developed yielding the machine inductance values that best fit the experimental results.

Finally in Chapter 6, the operation of the machines with different power sharings is presented. The power sharing in double and triple three-phase machines is analysed following the multiple *dq*, VSD and novel modelling approaches. Even though the former approach yields a more complex control loop, with the appropriate decoupling strategy, the power sharing becomes extremely intuitive as it transforms the original machine into a set of virtually independent three-phase machines. The VSD and novel approaches differ in the interpretation of non-flux/torque producing subspaces. This leads to the necessity of different current references on said subspaces to obtain certain power sharing. As the novel approach is specifically designed to facilitate the power sharing, the references for non-flux/torque producing subspaces can be easily calculated once the desired scenario is known. On the other hand, VSD approach requires some more mathematics to obtain the current references. A current limiting technique is proposed to avoid overloading the windings when following VSD and novel approaches. It especially applies when the power sharing is continuously varied and avoids the overloading of the three-phase windings operated at maximum power. Experimental results show that, independently of the modelling approach followed, any power sharing can be obtained. The power sharing can even allow to operate some of the three-phase windings in motor mode and the others in

generator mode. With this mode of operation, a simplified machine testbench is proposed that allows to test the machine at full rated power without the need of driving machine (and all its ancillary systems).

To sum up, the mathematical models of multiple three-phase permanent magnet machines are presented in this thesis. This includes the models following the two main modelling approaches already described in the literature plus an additional approach proposed focusing on power sharing in multiple three-phase machines. The models showed certain cross-couplings that adversely affect the response of the control (especially in the multiple *dq* approach); so a decoupling strategy has been proposed yielding excellent results in terms of minimization of the interactions between the different three-phase systems in the machine. Next, a detailed representation of the current loops including said decoupling strategy, and focusing on low switching to fundamental frequency ratios, has also been presented. The implementation of said current loops in C has also been developed in order to make it run in a real DSP. The limitation in the switching frequency imposed by the MV converters amplifies the effect of certain non-idealities of the control such as delays, frame transformations, filtering stages, etc. and special care in the modelling needs to be taken in order to reproduce the real behaviour. Both of these models (machine and current control loops) have been correlated and validated obtaining excellent match with the experimental results from Ingeteam's offshore wind testbench. With the control and machine correctly modelled, a tuning algorithm for the current regulators is developed in order to obtain regulator parameters that guarantee certain dynamic response across the entire speed operational range of the machine. For the cases in which the machine parameters are not correctly known, an identification algorithm has also been developed. With experimental records from the dynamic response of the current loops, it can obtain the machine parameters that best match the experimental results in simulation.

From the industrial point of view, a directly applicable current control for multiple three-phase machines has been developed. With the tuning algorithm, the knowledge in advance of the precise operation of the current loops across the entire operational range is obtained. Additionally, when machine parameters are not perfectly known, the parameter identification procedure provides invaluable help. With all this, a reduction in the commissioning time is to be obtained, usually leading to lower costs, and increased customer satisfaction.

7.2   Future work

This thesis has mainly focused on the modelling and control of multiple three-phase machines with sinusoidally distributed windings. The constraint of the low switching to fundamental frequency ratio has introduced additional complications when it comes to control modelling, and has shown the implications of all the non-idealities that are seldom considered due to high switching frequencies. With the current trend in industry of reducing the switching frequency, the work performed in this thesis gains importance and applicability to other scenarios. Therefore, the following additional research work may be carried out using and broadening the outputs of this research:
- Perform the experimental validation of the current control on an industrial scale model (8-10 MW)
- Investigate the possibility of optimizing the machine parameter identification algorithm so that it can be integrated in a CCU to perform online parameter estimations.
- Investigate the possibility of including stationary frame regulators, such as resonant PI, in the control modelling.
- Generalize the machine and control models to include concentrated winding machines.
- Develop the current control model for the grid side converter following the approach developed in this research.
- Develop the corresponding tuning algorithm for the grid side control.
- Investigate the possibility to modify the parameter identification algorithm to estimate grid side parameters and change the regulator parameters accordingly.

CHAPTER 8

References

ABB. 2011. *"Technical guide No. 1 Direct torque control - the world's most advanced ac drive technology"*. [online]. [Accessed 12 Nov 2014]. Available from World Wide Web: <http://www05.abb.com/global/scot/scot201.nsf/veritydisplay/14f3a3ad8f3362bac12578a70041e728/$file/ABB_Technical_guide_No_1_REVC.pdf>

ABB. 2013. *"ABB wind turbine converters. Increased turbine output for creating the perfect wind economy"*. [online]. [Accessed 26 Sep 2014]. Available from World Wide Web: <http://www05.abb.com/global/scot/scot232.nsf/veritydisplay/719ad05cf280d0bbc1257bf60022ccdb/$file/ABB%20wind%20turbine%20converters_lowres.pdf>

ABB. 2013. *"Model predictive DTC: Computational control methods for MV motor drives"*. [online]. [Accessed 25 Oct 2014]. Available from World Wide Web: <http://control.ee.ethz.ch/~stdavid/invited_speaker_talks_2013/George_Papafotiou/MPDTC_MPC_Course_2013_v1.pdf>

Abbas, M. A., R. Christen, and T.M. Jahns, 1984. "Six-phase voltage source inverter driven induction motor". *IEEE Trans. on Industry Applications,* **IA-20(5)**, pp. 1251-1259.

Agarlita, S., C. Coman, G. Andreescu, and I. Boldea, 2013. "Stable V/f control system with controlled power factor angle for permanent magnet synchronous motor drives". *IET Electric Power Applications,* **7(4)**, pp. 278-286.

Alonso, O., 2005. *"Análisis, diseño y control de convertidores multinivel de tipo NPC"*. Universidad Pública de Navarra, Pamplona, Spain. PhD Dissertation.

Anjar, B., M. Dalberg, and M Uppsäll. 2011. *"Elforsk"*. [online]. [Accessed 15 Jan 2015]. Available from World Wide Web: <http://www.elforsk.se/Programomraden/El--Varme/Rapporter/?download=report&rid=11_19_onyUPa-hPgD&usg=AFQjCNETo4ztq2woiI_F9Er47-K8lWTdTw&bvm=b>

Barcaro, M., N. Bianchi, and F. Magnussen, 2010. "Analysis and Tests of a Dual Three-Phase 12-Slot 10-Pole Permanent-Magnet Motor". *IEEE Trans. on Industry Applications,* **46(6)**, pp. 2355-2362.

Barrero, F., M.R. Arahal, R. Gregor, S. Toral, and M.J. Duran, 2009a. "A proof of concept study of predictive current control for VSI-driven asymmetrical dual three-phase ac machines". *IEEE Trans on Industrial Electronics,* **56(6)**, pp. 1937-1954.

Barrero, F., M.R. Arahal, R. Gregor, S. Toral, and M.J. Duran, 2009b. "One-step modulation predictive current control method for the asymmetrical dual three-phase induction machine". *IEEE Trans. on Industrial Electronics,* **56(6)**, pp. 1974-1983.

Barrero, F., J. Prieto, E. Levi, R. Gregor, S. Toral, M.J. Duran, and M. Jones, 2011. "An enhanced predictive current control method for asymmetrical six-phase motor drives". *IEEE Trans. on Industrial Electronics,* **58(8)**, pp. 3242-3252.

Bauer, J.G., M. Wissen, T. Gutt, J. Biermann, C. Schäffer, G. Schmidt, and F. Pfirsch, 2014. "New 4.5 kV IGBT and diode chip set for HVDC transmission applications". *Proc. Power Conversion Intelligent Motion (PCIM),* Nuremberg, Germany, pp. 60-67.

Bausch, H., K. Kanelis, B. Lange, and W. Zeng, 1994. "Torque control of synchronous and asynchronous drives without mechanical sensors". *Proc. Int. Conference on Electrical Machines (ICEM),* Paris, France, pp. 324-328.

Ben Ammar, F. and G. Sami, 2008. "The improvement avalability of a double star asynchronous machine supplied by redundant voltage source inverters". *Journal of electrical systems (JES),* **4(4)**.

Betin, F., G.A. Capolino, D. Casadei, B. Kawkabani, R. I. Bojoi, L. Harnefors, E. Levi, L. Parsa, and B. Fahimi, 2014. "Samples for classical, sensorless, and fault-tolerant techniques". *IEEE Industrial Electronics Magazine,* **June**, pp. 43-55.

Bianchi, N. and M. Dai Pre, 2006. "Use of the star of slots in designing fractional-slot single-layer synchronous motors". *IEE Proc.- Electric Power Applications,* **153(3)**, pp. 459-466.

Birk, J. and B. Andresen, 2007. "Parallel-connected converters for optimizing efficiency, reliability and grid harmonics in a wind turbine". *Proc. European Conference on Power Electronics and Applications (EPE),* Aalborg, Denmark, pp. 1-7.

Bojoi, I.R., 2002. *"Analysis, design and implementation of a dual three-phase vector controlled induction motor drive".* Politecnico di Torino. Torino, Italy. PhD Dissertation

Bojoi, R., F. Farina, G. Griva, F. Profumo, and A. Tenconi, 2005. "Direct torque control for dual three-phase induction motor drives". *IEEE Trans. on Industry Applications,* **41(6)**, pp. 1627-1636.

Bojoi, Radu, Francesco Farina, Francesco Profumo, and Alberto Tenconi, 2006. "Dual-three phase induction machine drives control - A survey". *IEEJ Trans. on Industry Applications,* **126(4)**, pp. 420-429.

Bojoi, R., M. Lazzari, F. Profumo, and A. Tenconi, 2002. "Digital field oriented control for dual three-phase induction motor drives". *Proc. IEEE Industry Applications Society Annual Meeting (IAS),* Pittsburgh, USA, pp. 818-825.

Bojoi, R., E. Levi, F. Farina, A. Tenconi, and F. Profumo, 2006. "Dual three-phase induction motor drive with digital current control in the stationary reference frame". *IEE Proc. - Electric Power Applications,* **153(1)**, pp. 129-139.

Bojoi, R., F. Profumo, and A. Tenconi, 2003. "Digital synchronous frame current regulation for dual three-phase induction motor drives". *Proc. IEEE Power Electronics Specialist Conference (PESC),* Acapulco, Mexico, pp. 1475-1480.

Bojoi, R., A. Tenconi, G. Griva, and F. Profumo, 2005. "Vector control of dual-three phase induction motor drives using two current sensors". *Proc. IEEE Industry Applications Conference,* Kowloon, Hong Kong, pp. 1805-1812.

Bojoi, R., A. Tenconi, F. Profumo, and F. Farina, 2005. "Dual-source fed multi-phase induction motor drive for fuel cell vehicles: Topology and control". *Proc. IEEE Power Electronics Specialists Conference (PESC),* Recife, Brazil, pp. 2676-2683.

Bojoi, R., A. Tenconi, and S. Vaschetto, 2010. "Direct stator flux and torque control for asymmetrical six-phase induction motor drives". *Proc. IEEE Int. Conference on Industrial Technology (ICIT),* Viña del Mar, Chile, pp. 1507-1512.

Briz, F., M.W. Degner, and R.D. Lorenz, 1999. "Dynamic analysis of current regulators for AC motors using complex vectors". *IEEE Trans. on Industry Applications,* **35(6)**, pp. 1424-1432.

Briz, F., M.W. Degner, and R.D. Lorenz, 2000. "Analysis and design of current regulators using complex vectors". *IEEE Trans. on Industry Applications,* **36(3)**, pp. 817-825.

Brock, S. and T. Pajchrowski, 2011. "Energy-optimal V/f control of permanent magnet synchronous motors for fan applications". *Zeszyty Problemowe - Maszyny Elektryczne,* pp. 169-174.

Buso, S., S. Fasolo, L. Malesani, and P. Mattavelli, 2000. "A dead-beat adaptive hysteresis current control". *IEEE Trans. on Industry Applications,* **36(4)**, pp. 1174-1180.

Buso, S. and P. Mattavelli, 2006. "Digital control in power electronics". *Synthesis Lectures on Power Electronics,* **1(1)**, pp. 1-158.

Casadei, D., G. Grandi, G. Serra, and A. Tani, 1994. "Effects of flux and torque hysteresis band amplitude in direct torque control of induction machines". *Proc. Int. Conference on Industrial Electronics, Control and Instrumentation (IECON),* Bologna, Italy, pp. 299-304.

Casadei, D., G. Serra, A. Tani, and L. Zarri, 2013. "Direct torque control for induction machines: A technology status review". *Proc. IEEE Workshop on Electrical Machines Design Control and Diagnosis (WEMDCD),* Paris, France, pp. 117-129.

Che, H.S., M.J. Duran, E. Levi, M. Jones, Wooi-Ping Hew, and N. Abd Rahim, 2014b. "Postfault operation of an asymmetrical six-phase induction machine with single and two isolated neutral points". *IEEE Trans. on Power Electronics,* **29(10)**, pp. 5406-5416.

Che, H.S., M. Duran, E. Levi, M. Jones, W.P. Hew, and N.A. Rahim, 2013. "Post-fault operation of an asymmetrical six-phase induction machine with single and two isolated neutral points". *Proc. IEEE Energy Conversion Congress and Exposition (ECCE),* Denver, USA, pp. 1131-1138.

Che, H. S., E. Levi, M. Jones, W. Hew, and N. Rahim, 2014a. "Current control methods for an asymmetrical six-phase induction motor drive". *IEEE Trans. on Power Electronics,* **29(1)**, pp. 407-417.

Chikhi, A., M. Djarallah, and K. Chikhi, 2010. "A comparative study of field-oriented control and direct-torque control of induction motors using an adaptative flux observer". *Serbian Journal of Electrical Engineering,* **7(1)**, pp. 41-55.

Chouhan, H. and D Chandra Jain, 2011. "Modeling and simulation of speed and flux estimator based on current & voltage model". *Int. Journal of Engineering and Technology,* **3(5)**, pp. 313-317.

Clarke, E., 1943. In: *"Circuit analysis of ac power systems".* New York: Wiley and sons, pp. 281-307.

Corley, M.J. and R.D. Lorenz, 1998. "Rotor position and velocity estimation for a salient-pole permanent magnet synchronous machine at standstill and high speeds". *IEEE Trans. on Industry Applications,* **34(4)**, pp. 784-789.

De Camillis, L., M. Matuonto, A Monti, and A Vignati, 2001. "Optimizing current control performance in double winding asynchronous motors in large power inverter drives". *IEEE Trans. on Power Electronics,* **16(5)**, pp. 676-685.

Depenbrock, M., 1988. "Direct self-control (DSC) of inverter-fed induction machine". *IEEE Trans. on Power Electronics,* **3(4)**, pp. 420-429.

Di Gerlando, A, G. Foglia, M.F. Iacchetti, and R. Perini, 2012. "Analysis and test of diode rectifier solutions in grid-connected wind energy conversion systems employing modular permanent-magnet synchronous generators". *IEEE Trans. on Industrial Electronics,* **59(5)**, pp. 2135-2146.

Dujic, D., M. Jones, and E. Levi, 2007. "Space vector PWM for nine-phase VSI with sinusoidal output voltage generation: Analysis and implementation". *Proc. IEEE Conference of Industrial Electronics Society (IECON),* Taipei, Taiwan, pp. 1524-1529.

Dujic, D., E. Levi, and M. Jones, 2010. "Dc bus utilisation in multiphase VSI supplied drives with a composite stator phase number". *Proc. IEEE Int. Conference on Industrial Technology (ICIT),* Viña del Mar, Chile, pp. 1495-1500.

Duran, M. J., F. Barrero, and S. Toral, 2007. "Multi-phase space vector pulse width modulation: Applications and strategies". *Proc. Int. Conference on Renewable Energies and Power Quality,* Sevilla, Spain, pp. 341.

Duran, M.J., S. Kouro, B. Wu, E. Levi, F. Barrero, and S. Alepuz, 2011. "Six-phase PMSG wind energy conversion system based on medium-voltage multilevel converter". *Proc. European Conference on Power Electronics and Applications (EPE),* Birmingham, UK, CD-ROM.

Duran, M.J. and E. Levi, 2006. "Multi-Dimensional Approach to Multi-Phase Space Vector Pulse Width Modulation". *Proc. IEEE Industrial Electronics (IECON),* Paris, France, pp. 2013-2108.

Escobar, G., A.M. Stankovic, J.M. Carrasco, E. Galvan, and R. Ortega, 2003. "Analysis and design of direct power control (DPC) for a three phase synchronous rectifier via output regulation subspaces". *IEEE Trans. on Power Electronics,* **18(3)**, pp. 823-830.

Estay, G., L. Vattuone, S. Kouro, M. Duran, and B. Wu, 2012. "Dual-boost-NPC converter for a dual three-phase PMSG wind energy conversion system". *Proc. IEEE Int. Conference on Drives and Energy Systems (PEDES),* Bangalore, India, pp. 1-6.

Figueroa, J., J. Cros, and P. Viarouge, 2006. "Generalized transformations for polyphase phase-modulation motors". *IEEE Trans. on Energy Conversion,* **21(2)**, pp. 332-341.

Filsecker, F., R. Alvarez, and S. Bernet, 2013. "Comparison of 4.5-kV press-pack IGBTs and IGCTs for medium-voltage converters". *IEEE Trans. on Industrial Electronics,* **60(2)**, pp. 440-449.

Fnaiech, M.A., F. Betin, G.-A. Capolino, and F. Fnaiech, 2010. "Fuzzy logic and sliding-mode controls applied to six-phase induction machine with open phases". *IEEE Trans. on Industrial Electronics,* **57(1)**, pp. 354-364.

Fu, J. and T.A. Lipo, 1994. "Disturbance-free operation of a multiphase current-regulated motor drive with an opened phase". *IEEE Trans. on Industry Applications,* **30(5)**, pp. 1267-1274.

Gao, L., J.E. Fletcher, and L. Zheng, 2010. "Low speed control improvements for classic Direct Torque Control of a 2-level 5-phase inverter-fed induction machine". *Proc. IEEE Int. Symposium on Industrial Electronics (ISIE),* Bari, Italy, pp. 2172-2177.

Gao, Y. and L. Parsa, 2007. "Modified direct torque control of five-phase permanent magnet synchronous motor drives". *Proc. IEEE Applied Power Electronics Conference (APEC),* Anaheim, U.S.A., pp. 1428-1433.

Garcia, X. T., B. Zigmund, A. Terlizzi, R. Pavlanin, and L. Salvatore, 2006. "Comparison between FOC and DTC strategies for permanent magnet synchronous motors". *Advances in Electrical and Electronic Engineering,* **5(1)**, pp. 76-81.

Gataric, S., 2000. "A polyphase cartesian vector approach to control of polyphase ac machines". *Proc. IEEE Industry Applications Conference,* pp. 1648-1654.

Germanischer Lloyd. 2012. "Guideline for the certification of offshore wind turbines" *Germanischer Lloyd Wind Energy.*

Geyer, T., 2010. "A comparison of control and modulation schemes for medium-voltage drives: Emerging predictive control concepts versus Field Oriented Control". *Proc. IEEE Energy Conversion Congress and Exposition (ECCE),* Atlanta, USA, pp. 2836-2843.

Geyer, T., 2011. "A comparison of control and modulation schemes for medium-voltage drives: Emerging predictive control concepts versus PWM-based schemes". *IEEE Trans. on Industry Applications,* **47(3)**, pp. 1380-1389.

Geyer, T., G. Papafotiou, and M. Morari, 2009. "Model predictive direct torque control—Part I: concept, algorithm, and analysis". *IEEE Trans. on Industrial Electronics,* **56(6)**, pp. 1894-1905.

Geyer, T. and S. Schröder, 2010. "Reliability considerations and fault-handling strategies for multi-MW modular drive systems". *IEEE Trans. on Industry Aplications,* **46(6)**, pp. 2442-2451.

Gonzalez, I., M.J. Duran, H.S. Che, E. Levi, and J. Aguado, 2014. "Fault-tolerant efficient control of six-phase induction generators in wind energy conversion systems with series-parallel machine-side converters". *Proc. IET Int. Conference on Power Electronics, Machines and Drives (PEMD),* Manchester, UK, pp. 1-6.

Grandi, G., D. Casadei, and P Sanjeevikumar, 2011. "Preliminary hardware implementation of a six-phase quad-inverter induction motor drive". *Proc. European Conference on Power Electronics and Applications (EPE),* Birmingham, UK, pp. 1815-1824.

Gregor, R., F. Barrero, S.L. Toral, M.J. Duran, M.R. Arahal, J. Prieto, and J.L. Mora, 2010. "Predictive-space vector PWM current control method for asymmetrical dual three-phase induction motor drives". *IET Electric Power Applications,* **4(1)**, pp. 26-34.

Guillaud, X., P. Degobert, and R. Teodorescu, 2007. "Use of resonant controller for grid-connected converters in case of large frequency fluctuations". *Proc. European Conference on Power Electronics and Applications,* Aalborg, Denmark, pp. 1-8.

Guzman, H., M.J. Duran, and F. Barrero, 2012. "A comprehensive fault analysis of a five-phase induction motor drive with an open phase". *Proc. Power Electronics and Motion Control Conference (PEMC),* Novi Sad, Serbia, pp. LS5b.3-1 LS5b.3-6.

Hadiouche, D., H. Razik, and A. Rezzoug, 2000. "Study and simulation of space vector PWM control of double-star induction motors". *Proc. IEEE Int. Power Electronics Congress (CIEP),* Acapulco, Mexico, pp. 42-47.

Hadiouche, D., H. Razik, and A. Rezzoug, 2004. "On the modeling and design of dual-stator windings to minimize circulating harmonic currents for VSI fed AC machines". *IEEE Trans. on Industry Applications,* **40(2)**, pp. 506-515.

Harnefors, L., 2007. "Modeling of three-phase dynamic systems using complex transfer functions and transfer matrices". *IEEE Trans. on Industrial Electronics,* **54(4)**, pp. 2239-2248.

Harnefors, L. and H-P Nee, 1998. "Model-based current control of ac machines using the internal model control method". *IEEE Trans. on Industry Applications,* **34(1)**, pp. 133-141.

Harnefors, L., A.G. Yepes, A. Vidal, and J. Doval-Gandoy, 2015. "Passivity-based controller design of grid-connected VSCs for prevention of electrical resonance instability". *IEEE Trans. on Industrial Electronics,* **62(2)**, pp. 702-710.

Ha, Jung-Ik and Seung-Kil Sul, 1999. "Sensorless field-orientation control of an induction machine by high-frequency signal injection". *IEEE Trans. on Industry Applications,* **35(1)**, pp. 45-51.

Hatua, K. and V.T. Ranganathan, 2005. "Direct torque control schemes for split-phase induction machine". *IEEE Trans. on Industry Applications,* **41(5)**, pp. 1243-1254.

Hoang, K. D., Y. Ren, Z.-Q. Zhu, and M. Foster, 2015. "Modified switching-table strategy for reduction of current harmonics in direct torque controlled dual-three-phase permanent magnet synchronous machine drives". *IET Electric Power Applications,* **9(1)**, pp. 10-19.

Ho, W.K., O.P. Gan, E.B. Tay, and E.L. Ang, 1996. "Performance and gain and phase margins of well-known PID tuning formulas". *IEEE Trans. on Control Systems Technology,* **4(4)**, pp. 473-477.

Holmes, D.G., T.A Lipo, B.P. McGrath, and W.Y. Kong, 2009. "Optimized design of stationary frame three phase ac current regulators". *IEEE Trans. on Power Electronics,* **24(11)**, pp. 2417-2426.

Holtz, J. and J. Quan, 2003. "Drift- and parameter-compensated flux estimator for persistent zero-stator-frequency operation of sensorless-controlled induction motors". *IEEE Trans. on Industry Applications,* **39(4)**, pp. 1052-1060.

Holtz, J., J. Quan, J. Pontt, J. Rodriguez, P. Newman, and H. Miranda, 2004. "Design of fast and robust current regulators for high-power drives based on complex state variables". *IEEE Trans. on Industry Applications,* **40(5)**, pp. 1388-1397.

Hua, L., Z. Yunping, and H. Bi, 2006. "The vector control strategies for multiphase synchronous motor drive systems". *Proc. IEEE Int. Symposium on Industrial Electronics,* Montreal, Canada, pp. 2205-2210.

Hu, J. and B. Wu, 1998. "New integration algorithms for estimating motor flux over a wide speed range". *IEEE Trans. on Power Electronics,* **13(5)**, pp. 969-977.

Hu, Y., Z Zhu, and K. Liu, 2014. "Current control for dual three-phase permanent magnet synchronous motors accounting for current unbalance and harmonics". *IEEE Journal of Emerging and Selected Topics in Power Electronics,* **2(2)**, pp. 272-284.

Iqbal, A. and E. Levi, 2006. "Space vector PWM techniques for sinusoidal output voltage generation with a five-phase voltage source inverter". *Electric Power Components and Systems,* **34**, pp. 119-140.

Irena. 2012. *"International Renewable Energy Agency".* [online]. [Accessed 30 Mar 2015]. Available from World Wide Web: <https://www.irena.org/DocumentDownloads/Publications/RE_Technologies_Cost_Analysis-WIND_POWER.pdf>

Jansen, P.L. and R.D. Lorenz, 1994. "Transducerless position and velocity estimation in induction and salient ac machines". *Proc. IEEE Industry Applications Society (IAS),* Denver, USA, pp. 488-495.

Jones, M., O. Dordevic, N. Bodo, and E. Levi, 2012. "PWM algorithms for multilevel inverter supplied multiphase variable-speed drives". *Proc. Int. Symposium Power Electronics,* Novi Sad, Serbia, pp. 22-31.

Jones, M., S.N. Vukosavic, E. Levi, and A Iqbal, 2005. "A six-phase series-connected two-motor drive with decoupled dynamic control". *IEEE Trans. on Industry Applications,* **41(4)**, pp. 1056-1066.

Jordan, S., 2013. *"Multiphase synchronous generators for dc aircraft power systems".* University of Manchester, Manchester, U.K. PhD Dissertation.

Jordan, S. and J. Apsley, 2011. "Diode rectification of multiphase synchronous generators for aircraft applications". *Proc. IEEE Energy Conversion Congress and Exposition (ECCE),* Phoenix, USA, pp. 3208-3215.

Kale, M. and E. Ozdemir. 2004. *"An adaptative hysteresis band current controller for shunt active power filter".* [online]. [Accessed 23 Oct 2014]. Available from World Wide Web: <http://akademikpersonel.kocaeli.edu.tr/eozdemir/sci/eozdemir19.04.2010_09.03.31sci.pdf>

Kallio, S., M. Andriollo, A. Tortella, and J. Karttunen, 2013. "Decoupled d-q model of double-star interior-permanent-magnet synchronous machines". *IEEE Trans. on Industrial Electronics,* **60(6)**, pp. 2486-2494.

Karttunen, J., S. Kallio, P. Peltoniemi, P. Silventoinen, and O. Pyrhonen, 2012. "Dual three-phase permanent magnet synchronous machine supplied by two independent voltage source inverters". *Proc. IEEE Int. Symposium on Power Electronics, Electrical Drives, Automation and Motion (SPEEDAM),* Sorrento, Italy, pp. 741-747.

Kestelyn, X., E. Semail, and JP. Hautier. 2009. *"Vectorial multi-machine modeling for a five-phase machine".* [online]. [Accessed 06 Nov 2014]. Available from World Wide Web: <http://eric.semail.free.fr/>

Kestelyn, X., E. Semail, and D. Loroil, 2005. "Direct torque control of multi-phase permanent magnet synchronous motor drive: application to a five-phase". *Proc. IEEE Int. Electric Machines and Drives Conference (IEMDC),* San Antonio, USA, pp. 137-143.

Khan, K.S., W.M. Arshad, and S. Kanerva, 2008. "On performance figures of multiphase machines". *Proc. IEEE Int. Conference on Electrical Machines (ICEM),* Vilamoura, Portugal, pp. 1-5.

Kianinezhad, R., B. Nahid-Mobarakeh, L. Baghli, F. Betin, and G.-A. Capolino, 2008. "Modeling and control of six-phase symmetrical induction machine under fault condition due to open phases". *IEEE Trans. on Industrial Electronics,* **55(5)**, pp. 1966-1977.

Kim, H., M.W. Degner, J.M. Guerrero, F. Briz, and R.D. Lorenz, 2010. "Discrete-time current regulator design for ac machine drives". *IEEE Trans. on Industry Applications,* **46(4)**, pp. 1425-1435.

Kolar, J.W. and F.C. Zach, 1994. "A novel three-phase utility interface minimizing line current harmonics of high-power telecommunications rectifier modules". *Proc. IEEE Int. Telecommunications Energy Conference,* Vancouver, Canada, pp. 367-374.

Kouro, S., P. Cortes, R. Vargas, U. Ammann, and J. Rodriguez, 2009. "Model Predictive Control—A Simple and Powerful Method to Control Power Converters". *IEEE Trans. on Industrial Electronics,* **56(6)**, pp. 1826-1838.

Kubota, K. and K. Matsuse, 1994. "Speed sensorless field-oriented control of induction motor with rotor resistance adaptation". *IEEE Trans. on Industry Applications,* **30(5)**, pp. 1219-1224.

Kukrer, O., 1996. "Discrete-time current control of voltage-fed three-phase PWM inverters". *IEEE Trans. on Power Electronics,* **11(2)**, pp. 260-269.

Kulkarni, A.B. and M. Ehsani, 1992. "A novel position sensor elimination technique for the interior permanent-magnet synchronous motor drive". *IEEE Trans. on Industry Applications,* **28(1)**, pp. 144-150.

Lang, B., W. Liu, X. Zhou, and R. Li, 2006. "Research on direct torque control of permanent magnet synchronous motor based on optimized state selector". *Proc. IEEE Int. Symposium on Industrial Electronics (ISIE),* Montreal, Canada, pp. 2105-2109.

Lawson, J. 2012. "Renewable Energy World.com". *[online]. [Accessed 28 Nov 2014]. Available from World Wide Web: <http://www.renewableenergyworld.com/rea/news/article/2012/10/which-wind-turbine-generator-will-win>*

Le-Huy, H., K. Slimani, and P. Viarouge, 1991. "Analysis and implementation of a real-time predictive current controller for permanent-magnet synchronous servo drives". *Proc. IEEE Industry Applications Society Annual Meeting,* Dearborn, U.S.A., pp. 996-1002.

Levi, E., 2008. "Multiphase electric machines for variable-speed applications". *IEEE Trans. on Industrial Electronics,* **55(5)**, pp. 1893-1909.

Levi, E., 2011a. Chapter: *"Multiphase AC Machines".* In: *"The Industrial Electronics Handbook: Power Electronics and Motor Drives".* B. M. Wilamowski. CRC Press.

Levi, E., 2011b. Chapter: *"FOC: Field-Oriented Control".* In: *"The Industrial Electronics Handbook: Power Electronics and Motor Drives".* B. M. Wilamowski. CRC Press.

Levi, E., R. Bojoi, F. Profumo, H.A. Toliyat, and S. Williamson, 2007. "Multiphase induction motor drives - a technology status review". *IET Electric Power Applications,* **1(4)**, pp. 489-516.

Levi, E., M. Jones, S.N. Vikosavic, and H.A. Toliyat, 2004a. "A five-phase two-machine vector controlled induction motor drive supplied from a single inverter". *EPE Journal,* **14(3)**, pp. 38-48.

Levi, E., M. Jones, S.N. Vukosavic, and H.A. Toliyat, 2004b. "Operating principles of a novel multiphase multimotor vector-controlled drive". *IEEE Trans. on Energy Conversion,* **19(3)**, pp. 508-517.

Limei, W. and G. Yanping, 2007. "A novel strategy of direct torque control for PMSM drive reducing ripple in torque and flux". *Proc. IEEE Int. Electric Machines & Drives Conference (IEMDC),* Antalya, Turkey, pp. 403-406.

Lim, C.S., E. Levi, M. Jones, N.A. Rahim, and W.P. Hew, 2014. "FCS-MPC-Based current control of a five-phase induction motor and its comparison with PI-PWM control". *IEEE Trans. on Industrial Electronics,* **61(1)**, pp. 149-163.

Limongi, L., R. Bojoi, G. Griva, and A. Tenconi, 2009. "Digital current-control schemes". *IEEE Industrial Electronics Magazine,* **3(1)**, pp. 20-31.

Lipo, T.A., 1980. "A d-q model for six phase induction machines". *Proc. Int. Conf. Electric Machines,* Athens, Greece, pp. 860-867.

Lipo, T.A. and Feng X. Wang, 1984. "Design and performance of a converter optimized ac machine". *IEEE Trans. on Industry Applications,* **IA-20(4)**, pp. 834-844.

Li, L., X. Wang, and H. Sun, 2002. "A variable-voltage direct torque control based on DSP in PM synchronous motor drive". *Proc. IEEE Region 10 Conference on Computers, Communications, Control and Power Engineering,* Beijing, China, pp. 2065-2068.

Luenberger, D.G., 1979. *"Introduction to Dynamic Systems".* USA. John Wiley & Sons

Luukko, J., 2000. *"Direct torque control of permanent magnet synchronous machines - analysis and implementation".* Lappeeranta University of Technology. Stockholm, Sweden. PhD Dissertation.

Malvar, J., O. Lopez, AG. Yepes, A Vidal, F.D. Freijedo, P. Fernandez-Comesana, and J. Doval-Gandoy, 2014. "Graphical diagram for subspace and sequence identification of time harmonics in symmetrical multiphase machines". *IEEE Trans. on Industrial Electronics,* **61(1)**, pp. 29-42.

Mantero, S., E. De Paola, and G. Marina, 1999. "An optimised control strategy for double star motors configuration in redundancy operation mode". *Proc. European Power Electronics Applications Conference (EPE),* Lausanne, Switzerland.

Martin, K.W., 2004. "Complex signal processing is not complex". *IEEE Trans. on Circuits and Systems I: Regular Papers,* **51(9)**, pp. 1823-1836.

Meinguet, F., P. Sandulescu, B. Aslan, Li Lu, Ngac-Ky Nguyen, X. Kestelyn, and E. Semail, 2012. "A signal-based technique for fault detection and isolation of inverter faults in multi-phase drives". *Proc. IEEE Conference on Power Electronics, Drives and Energy Systems (PEDES),* Bangalore, India, pp. 1-6.

Mese, E., M. Tezcan, M. Ayaz, Y. Yasa, and K. Yilmaz, 2012. "Design considerations for dual winding permanent magnet synchronous machines". *Proc. Energy Conversion Congress and Exposition (ECCE),* Raleigh, USA, pp. 1894-1901.

Mohammadpour, A., 2014. *"Universal control techniques for fault-tolerant multi-phase permanent magnet motor drives".* Rensselaer Polytechnic Institute, New York, USA. PhD Dissertation.

Monajemy, R., 2000. *"Control strategies and parameter compensation for permanent magnet synchronous motor drives".* Virginia Polytechnic Institute and State University. Blacksburg, USA. PhD Dissertation

Morimoto, S., M. Sanada, and Y. Takeda, 1994. "Wide-speed operation of interior permanent magnet synchronous motors with high-performance current regulator". *IEEE Transactions on Industry Applications,* **30(4)**, pp. 920-926.

Mythili, S. and K. Thyagarajah, 2005. "Direct torque control (DTC) of multi-phase induction motor using TMS320F2407 digital signal processor". *Proc. Int. Conference on Power Electronics and Drives Systems (PEDS),* Kuala Lumpur, Malaysia, pp. 1024-1029.

Nabi, H. P., P. Dadashi, and A. Shoulaie, 2011. "A novel structure for vector control of symmetrical six-phase induction machines with three current sensors". *Engineering, Technology & Applied Science Research (ETASR),* **1(2)**, pp. 23-29.

Nelson, R.H. and P.C. Krause, 1974. "Induction machine analysis for arbitrary displacement between multiple winding sets". *IEEE Trans. on Power Apparatus and Systems,* **PAS-93(3)**, pp. 841-848.

Nikouei, M., 2013. *"Design and evaluation of the vienna rectifier for a 5MW wind turbine system".* Chalmers University of Technology, Gothenburg, Sweden. MSc Dissertation.

Novotny, D. and T. Lipo, 2000. *"Vector control and dynamics of AC drives"*. Oxford. Clarendon Press

Ozcira, S. and N. Bekiroglu, 2011. Chapter: *"Direct Torque Control of Permanent Magnet Synchronous Motors"*. In: *"Torque Control"*. Moulay Tahar Lamchich. , pp. 129-154.

Papafotiou, G., T. Geyer, and M. Morari, 2004. "Optimal direct torque control of three-phase symmetric induction motors". *Proc. IEEE Conference on Decision and Control,* Atlantis, Bahamas, pp. 1860-1865.

Park, R. H., 1929. "Two-reaction theory of synchronous machines: generalized method of analysis - Part I". *Proc. Winter Convention of the A.I.E.E.,* New York, USA, pp. 716-730.

Parsa, L. and H.A. Toliyat, 2005. "Five-phase permanent-magnet motor drives". *IEEE Trans. on Industry Applications,* **41(1)**, pp. 30-37.

Peterson, B., 1996. *"Induction machine speed estimation: Observations on observers"*. Lund Institute of Technology (LTH), Lund, Sweden. PhD Dissertation.

Radomski, G., 2005. "Analysis of vienna rectifier". *Electrical power quality and utilisation,* **XI(1)**, pp. 49-56.

Ramirez, J. C., R.M. Kennel, and T. Geyer, 2010. "Model predictive direct current control". *Proc. IEEE Int. Conference on Industrial Technology (ICIT),* Viña del Mar, Chile, pp. 1808-1813.

Rashed, M., P.F.A. MacConnell, A.F. Stronach, and P. Acarnley, 2007. "Sensorless indirect-rotor-field-orientation speed control of a permanent-magnet synchronous motor with stator-resistance estimation". *IEEE Trans. on Industrial Electronics,* **54(3)**, pp. 1664-1675.

ReliaWind, EU FP7. 2013. *"EU FP7 Reliawind Project"*. [online]. [Accessed 2014]. Available from World Wide Web: <http://www.reliawind.eu>

Rockhill, A. and T.A. Lipo, 2009. "A simplified model of a nine-phase synchronous machine using vector space decomposition". *Proc. IEEE Power Electronics and Machines in Wind Applications (PEMWA),* Lincoln, USA, pp. 1-5.

Rodriguez, A., M. Moranchel, E. J. Bueno, and F. J. Rodriguez, 2012. "Tuning of resonant controllers applied to the current control of voltage-source converters". *Proc. IEEE Industrial Electronics Society Annual Conference (IECON),* Montreal, Canada.

Rodriguez, J., J. Pontt, C.A. Silva, P. Correa, P. Lezana, P. Cortes, and U. Ammann, 2007. "Predictive current control of a voltage source inverter". *IEEE Trans. on Industrial Electronics,* **54(1)**, pp. 495-503.

Shen, L. C., 2013. *"Model predictive control of multi-leg inverter supplied drives"*. University of Malaya. Kuala Lumpur, Malaya. PhD. Dissertation

Sheng-Nian, Y., H. Jonq-Chin, H. Ming-Chih, and C. Li-Hsiu. 2011. *"Development of wind power control system for six-phase permanent-magnet synchronous generators"*. [online]. [Accessed 15 Aug 2014]. Available from World Wide Web: <http://www.docin.com/p-75673236.html>

Shen, J., S. Schroder, H. Stagge, and R.W. De Doncker, 2012. "Precise modeling and analysis of DQ-frame current controller for high power converters with low pulse ratio". *Proc. IEEE Energy Conversion Congress and Exposition (ECCE),* Raleigh, USA, pp. 61-68.

Siemens. 2012. "Siemens industry presents new gearless direct drive wind generator". *[online]. [Accessed 28 Nov 2014]. Available from World Wide Web: <http://www.siemens.com/press/en/pressrelease/?press=/en/pressrelease/2012/industry/drive-technologies/idt2012094045.htm>*

Spinato, F., P.J. Tavner, G.J.W. van Bussel, and E. Koutoulakos, 2009. "Reliability of wind turbine subassemblies". *IET Renewable Power Generation,* **3(4)**, pp. 387-401.

Stojic, D., 2012. "An algorithm for induction motor stator flux estimation". *Advances in Electrical and Computer engineering,* **12(3)**, pp. 47-52.

Stulrajter, M., V. Hrabovcová, and M. Franko, 2007. "Permanent magnets synchronous motor control theory". *Journal of Electrical Engineering,* **58(2)**, pp. 79-84.

Sudhoff, S.D., K.A. Corzine, and H.J. Hegner, 1995. "A flux-weakening strategy for current-regulated surface-mounted permanent-magnet machine drives". *IEEE Transactions on Energy Conversion,* **10(3)**, pp. 431-437.

Sutikno, T., N. Rumzi Nik Idris, and A. Jidin, 2011. "A new fixed switching frequency direct torque controlled PMSM drives with low ripple in flux and torque". *Journal of Engineering and Technological Sciences , ***43(3)**, pp. 173-190.

Swierczynski, D. and M.P. Kazmierkowski, 2002. "Direct torque control of permanent magnet synchronous motor (PMSM) using space vector modulation (DTC-SVM)-simulation and experimental results". *Proc. IEEE Conference of the Industrial Electronics Society (IECON),* Sevilla, Spain, pp. 751-755.

Tajima, H. and Y. Hori, 1993. "Speed sensorless field-orientation control of the induction machine". *IEEE Trans. on Industry Applications,* **29(1)**, pp. 175-180.

Takahashi, I. and T. Noguchi, 1986. "A new quick-response and high-efficiency control strategy of an induction motor". *IEEE Trans. on Industry Applications,* **IA-22(5)**, pp. 820-827.

Tani, A., G. Serra, M. Mengoni, L. Zarri, G. Rini, and D. Casadei, 2013. "Dynamic stator current sharing in quadruple three-phase induction motor drives". *Proc. IEEE 39th Annual Conference of the Industrial Electronics Society (IECON),* Vienna, Austria, pp. 5173-5178.

Tavner, P. 2011. *"Wind-watch".* [online]. [Accessed 01 Apr 2015]. Available from World Wide Web: <http://docs.wind-watch.org/2011-04-20_7_SUPERGEN-Wind2011GA_ReliableOffshoreWindFarms_PJT.pdf>

Teodorescu, R., M. Liserre, and P. Rodriguez, 2011. Chapter: *"Grid converter structures for wind turbine systems".* In: *"Grid converters for photovoltaic and wind power systems".* ISBN: 978-0-470-05751-3: John Wiley & Sons, Ltd, pp. 123-143.

Terrien, F. and M-F Benkhoris, 1999. "Analysis of double star motor drives for electrical propulsion". *Proc. IEE Int. Conference on Electrical Machines and Drives,* Canterbury, UK, pp. 90-94.

Tessarolo, A., 2009. "On the modeling of poly-phase electric machines through Vector-Space Decomposition: Theoretical considerations". *Proc. IEEE Int. Conference on Power Engineering, Energy and Electrical Drives (POWERENG),* Lisbon, Portugal, pp. 519-523.

Tessarolo, A., 2011. Chapter: *"Modeling and simulation of multiphase machines in the Matlab/Simulink environment".* In: *"Engineering education and research using MATLAB".* Ali H. Assi. http://www.intechopen.com, pp. 1-24.

Tessarolo, A., M. Bortolozzi, and A. Contin, 2013a. "Modeling of split-phase machines in Park's coordinates. Part I: Theoretical foundations". *Proc. IEEE EuroCon,* Zagreb, Croatia, pp. 1308-1313.

Tessarolo, A., M. Bortolozzi, and A. Contin, 2013b. "Modeling of split-phase machines in Park's coordinates. Part II: Equivalent circuit representation". *Proc. IEEE EuroCon,* Zagreb, Croatia, pp. 1314-1319.

Toliyat, H.A., T.A. Lipo, and J.C. White, 1991a. "Analysis of a concentrated winding induction machine for adjustable speed drive applications. I. Motor analysis". *IEEE Trans. on Energy Conversion,* **6(4)**, pp. 679-683.

Toliyat, H.A., M.M. Rahimian, and T.A. Lipo, 1991b. "dq modeling of five phase synchronous reluctance machines including third harmonic of air-gap MMF". *Proc. IEEE Industry Applications Society Annual Meeting,* Dearborn, USA, pp. 231-237.

Toliyat, H.A. and H. Xu, 2000. "A novel direct torque control (DTC) method for five-phase induction machines". *Proc. IEEE Applied Power Electronics Conference and Exposition (APEC),* New Orleans, USA, pp. 162-168.

Umeno, T., Y. Hori, and H. Suzuki, 1990. "Design of the flux-observer-based vector control system of induction machines taking into consideration robust stability". *Electrical Engineering in Japan,* **110(6)**, pp. 53-65.

Vizireanu, D., X. Kestelyn, S. Brisset, P. Brochet, Y. Milet, and D. Laloy, 2005. "Polyphased modular direct-drive wind turbine generator". *Proc. European Conference on Power Electronics and Applications (EPE),* Dresden, Germany, CD-ROM.

Vukosavic, S. N., M. Jones, E. Levi, and J. Varga, 2005. "Rotor flux oriented control of a symmetrical six-phase induction machine". *Electric Power Systems Research,* **75(2-3)**, pp. 142-152.

Vyncke, T. J., R. K. Boel, and J. A. Melkebeek, 2006. "Direct torque control of permanent magnet synchronous motors - An overview". *Proc. IEEE Benelux young Researchers Symposium in Electrical Engineering,* Ghent, Belgium.

Wallmark, O., Lennart Harnefors, and O. Carlson, 2007. "Control algorithms for a fault-tolerant PMSM drive". *IEEE Trans. on Industrial Electronics,* **54(4)**, pp. 1973-1980.

Wang, T., F. Fang, X Wu, and X. Jiang, 2013. "Novel filter for stator harmonic currents reduction in six-step converter fed multiphase induction motor drives". *IEEE Trans. on Power Electronics,* **28(1)**, pp. 498-506.

Ward, E. E. and H. Härer, 1969. "Preliminary investigation of an invertor-fed 5-phase induction motor". *Proc. of the Institution of Electrical Engineers,* **116(6)**, pp. 980-984.

Watson, N. and J. Arrillaga, 2003. *"Power Systems Electromagnetic Transients Simulation".* Institution of Electrical Engineers.

White, D.C. and H.H. Woodson, 1959. Chapter: *"Electromechanical Energy Conversion".* New York: John Wiley & sons, pp. 545-637.

Widmer, J., R. Martin, and M. Kimiabeigi, 2015. "Electric vehicle traction motors without rare earth magnets". *Sustainable Materials and Technologies,* **3**, pp. 7-13.

Wilkinson, M., 2011. "Measuring wind turbine reliability, results of the Reliawind Project". *Proc. European Wind Energy Conference & Exhibition (EWEA),* Brussels, Belgium.

Wolf, G. 2012. "Transmission and distribution world". *[online]. [Accessed 08 Oct 2014]. Available from World Wide Web: <http://tdworld.com/transmission/war-currents-update>*

Wu, R. and G.R. Slemon, 1990. "A permanent magnet motor drive without a shaft sensor". *Proc. IEEE Industry Applications Society Annual Meeting (IAS),* Seattle, USA, pp. 553-558.

Xiang-Jun, Z., Y. Yongbing, Z. Hongtao, L. Ying, F. Luguang, and Y. Xu, 2012. "Modelling and control of a multi-phase permanent magnet synchronous generator and efficient hybrid 3L-converters for large direct-drive wind turbines". *IET Electric Power Applications,* **6(6)**, pp. 322-331.

Xu, H., H.A. Toliyat, and L.J. Petersen, 2001. "Rotor field oriented control of five-phase induction motor with the combined fundamental and third harmonic currents". *Proc. IEEE Annual Applied Power Electronics Conference and Exposition (APEC),* Shanghai, China, pp. 392-398.

Xu, L. and L. Ye, 1995. "Analysis of a novel winding structure minimizing harmonic current and torque ripple for dual six-step converter-fed high power AC machines". *IEEE Trans. on Industry Applications,* **31(1)**, pp. 84-90.

Yang, S., A. Bryant, P. Mawby, Dawei Xiang, L. Ran, and P. Tavner, 2011. "An industry-based survey of reliability in power electronic converters". *IEEE Trans. on Industry Applications,* **47(3)**, pp. 1441-1451.

Yepes, A. G., 2011. *"Digital resonant current controllers for voltage source converters".* University of Vigo. Vigo, Spain. PhD. Dissertation

Yepes, A. G., A. Vidal, F. D. Freijedo, J. Malvar, O. Lopez, and J. Doval-Gandoy, 2012. "Transient response evaluation of resonant controllers for AC drives". *Proc. IEEE Energy Conversion Congress and Exposition (ECCE),* Raleigh, USA, pp. 471-478.

Yepes, A., A Vidal, J. Malvar, O. Lopez, and J. Doval-Gandoy, 2014. "Tuning method aimed at optimized settling time and overshoot for synchronous proportional-integral current control in electric machines". *IEEE Trans. on Power Electronics,* **29(6)**, pp. 3041-3054.

Zabaleta, M., 2014. "Benefits of modular power converters for wind turbine applications". *FuturEnergy,* **Nov-Dec**, pp. 17-20.

Zabaleta, M., E. Burguete, D. Madariaga, I. Zubimendi, and M. Zubiaga and I. Larrazabal, 2016. "LCL Grid Filter Design of a Multimegawatt Medium-Voltage Converter for Offshore Wind Turbine Using SHEPWM Modulation". *IEEE Trans. on Power Electronics,* **31(3)**, pp. 1993-2001.

Zabaleta, M., M. Jones, and E. Levi, 2017a. "A tuning procedure for the current regulator loops in multiple three phase permanent magnet machines with low switching to fundamental frequency ratio". *Proc. 19th European Conference on Power Electronics and Applications (EPE),* Warsaw, Poland.

Zabaleta, M., E. Levi, and M. Jones, 2016a. "Modelling approaches for an asymmetrical six-phase machine". *Proc. IEEE 25th International Symposium on Industrial Electronics (ISIE),* Santa Clara, USA, pp. 173-178.

Zabaleta, M., E. Levi, and M. Jones, 2016b. "Modelling approaches for triple three-phase permanent magnet machines". *Proc. XXII International Conference on Electrical Machines (ICEM),* Lausanne, Swiss, pp. 466-472.

Zabaleta, M., E. Levi, and M. Jones, 2017b. "Dual three-phase PM generator parameter identification using experimental and simulated system responses". *Proc. 19th International Symposium Power Electronics,* Novi Sad, Serbia.

Zabaleta, M., E. Levi, and M. Jones, 2018a. "Regenerative testing of multiphase machines with multiple three-phase windings". *International Conference on Power Electronics and Motion Control (PEMC),* Budapest, Hungary, accepted for publication.

Zabaleta, M., E. Levi, and M. Jones, 2018b. "A novel synthetic loading method for multiple three-phase winding electric machines". *IEEE Trans. on Energy Conversion,* accepted for publication.

Zarri, L., M. Mengoni, Y. Gritli, A. Tani, F. Filippetti, G. Serra, and D. Casadei, 2011. "Behavior of multiphase induction machines with unbalanced stator windings". *Proc. IEEE Int. Symposium on Diagnostics for Electric Machines, Power Electronics & Drives (SDEMPED),* Bologna, Italy, pp. 84-91.

Zhang, Z., R. Nilssen, A. Nysveen, A. Chen, and A. Matveev. 2013. *"Sintef".* [online]. [Accessed 28 May 2018]. Available from World Wide Web: <https://www.sintef.no/globalassets/project/deepwind-2013/deepwind-presentations-2013/a2/zhangz._ntnu.pdf>

Zhao, Y. and T. Lipo, 1995. "Space vector PWM control of dual three-phase induction machine using vector space decomposition". *Proc. IEEE Industry Applications Society Annual Meeting,* Denver, USA.

Zhao, Y. and T. Lipo, 1996. "Modelling and control of a multi-phase induction machine with structural unbalance". *IEEE Trans. on Energy Conversion,* **11(3)**, pp. 570-577.

Zhen, L. and Longya Xu, 1998. "Sensorless field orientation control of induction machines based on a mutual MRAS scheme". *IEEE Trans. on Industrial Electronics,* **45(5)**, pp. 824-831.

Zhong, L. and M. F. Rahman, 1997. "Analysis of direct torque control in permanent magnet synchronous motor drives". *IEEE Trans. on Power Electronics,* **12(3)**, pp. 528-536.

Zmood, D.N., D.G. Holmes, and G.H. Bode, 2001. "Frequency-domain analysis of three-phase linear current regulators". *IEEE Trans. on Industry Applications,* **37(2)**, pp. 601-610.

Zoric, I., M. Zabaleta, M. Jones, and E. Levi, 2017. "Techniques for power sharing between winding sets of multiple three-phase machines". *Proc. IEEE Workshop on Electrical Machines Design, Control and Diagnosis (WEMDCD),* Nottingham, UK, pp. 208-2015.

APPENDIX 1

Inductance matrix

The following script constructs the inductance matrix of an *n*-phase machine in the phase variables domain.

```matlab
%% CONSTRUCTION OF THE STATOR INDUCTANCES MATRIX

% Parameter input
n=9;              % number of phases
sigma=pi/n;       % phase shift between the three-phase systems

La=sym('La','real');    % equals (Lmd+Lmq)/2
L2=sym('L2','real');    % equals (Lmd-Lmq)/2
Th=sym('Th','real');    % it is the angle of the rotor
L=sym(zeros(n,n));

for i=1:n
    statori=floor((i-1)/3)+1;
    for j=1:n
        statorj=floor((j-1)/3)+1;
        if i==j          % self inductances
            if mod(i,3)==1           % its a phase ai
                L(i,j)=La+L2*cos(2*Th-2*(statori-1)*sigma);
            elseif mod(i,3)==2       % its a phase bi
                L(i,j)=La+L2*cos(2*Th-4*pi/3-2*(statori-1)*sigma);
            else                     % its a phase ci
                L(i,j)=La+L2*cos(2*Th-2*pi/3-2*(statori-1)*sigma);
            end
        else             % mutual inductances
            if (mod(i,3)==1 && mod(j,3)==1)            % its a phase ai vs a phase aj
                L(i,j)=La*cos((statori-statorj)*sigma)+ ...
                        L2*cos(2*Th-(statori+statorj-2)*sigma);
            elseif (mod(i,3)==2 && mod(j,3)==2)        % its a phase bi vs a phase bj
                L(i,j)=La*cos((statori-statorj)*sigma)+ ...
                        L2*cos(2*Th-4*pi/3-(statori+statorj-2)*sigma);
            elseif (mod(i,3)==0 && mod(j,3)==0)        % its a phase ci vs a phase cj
                L(i,j)=La*cos((statori-statorj)*sigma)+ ...
                        L2*cos(2*Th-2*pi/3-(statori+statorj-2)*sigma);
            elseif (mod(i,3)==1 && mod(j,3)==2)        % its a phase ai vs a phase bj
                L(i,j)=La*cos(2*pi/3-(statori-statorj)*sigma)+ ...
                        L2*cos(2*Th-2*pi/3-(statori+statorj-2)*sigma);
            elseif  (mod(i,3)==2 && mod(j,3)==1)       % its a phase bi vs a phase aj
                L(i,j)=La*cos(2*pi/3+(statori-statorj)*sigma)+ ...
                        L2*cos(2*Th-2*pi/3-(statori+statorj-2)*sigma);
            elseif (mod(i,3)==1 && mod(j,3)==0)        % its a phase ai vs a phase cj
                L(i,j)=La*cos(2*pi/3+(statori-statorj)*sigma)+ ...
                        L2*cos(2*Th-4*pi/3-(statori+statorj-2)*sigma);
            elseif (mod(i,3)==0 && mod(j,3)==1)        % its a phase ci vs a phase aj
                L(i,j)=La*cos(2*pi/3-(statori-statorj)*sigma)+ ...
                        L2*cos(2*Th-4*pi/3-(statori+statorj-2)*sigma);
            elseif (mod(i,3)==2 && mod(j,3)==0)        % its a phase bi vs a phase cj
                L(i,j)=La*cos(2*pi/3-(statori-statorj)*sigma)+ ...
                        L2*cos(2*Th-(statori+statorj-2)*sigma);
            elseif (mod(i,3)==0 && mod(j,3)==2)        % its a phase ci vs a phase bj
                L(i,j)=La*cos(2*pi/3+(statori-statorj)*sigma)+ ...
                        L2*cos(2*Th-(statori+statorj-2)*sigma);
            end
        end
    end
end
```

APPENDIX 2

Novel transformation matrix

The following code obtains the transformation matrix according the novel transformation for any *n*-phase number machine (with *n* being an integer multiple of 3). This script can be executed under any Matlab ® version as no special functions are used.

```
%% FILE TO BUILD UP THE TRANSFORMATION MATRIX C FOR AN n-PHASE MACHINE
% WITH n AN INTEGER MULTIPLE OF 3 (MULTIPLE THREE-PHASE WINDING MACHINE)

% Parameter input
n=9;            % number of phases
sigma=pi/n;     % phase shift between the three-phase systems

C=zeros(n,n);
TWOPI_3=2*pi/3;

% Two first rows for Alpha-Beta subspace
for k=1:n/3
    for j=1:3
        C(1,3*(k-1)+j)=cos(TWOPI_3*(j-1)+sigma*(k-1));
        C(2,3*(k-1)+j)=sin(TWOPI_3*(j-1)+sigma*(k-1));
    end
end

% (n-4)/2 subsequent rows for xi-yi subspaces
for i=3:2:n-n/3
    for k=1:n/3
        for j=1:3
            if k==1 % fills the first three-phase system columns
                C(i,3*(k-1)+j)=cos(TWOPI_3*(j-1)+sigma*(k-1));
                C(i+1,3*(k-1)+j)=sin(TWOPI_3*(j-1)+sigma*(k-1));
            elseif 2*k-1==i %fills the correspondent three-phase system
                C(i,3*(k-1)+j)=-cos(TWOPI_3*(j-1)+sigma*(k-1));
                C(i+1,3*(k-1)+j)=-sin(TWOPI_3*(j-1)+sigma*(k-1));
            else
                C(i,3*(k-1)+j)=0;
                C(i+1,3*(k-1)+j)=0;
            end
        end
    end
end

% (n-k) last rows for the zi subspaces
stator=2;
for i=n-n/3+1:n
    for j=1:3        % fills the first 3 columns
        C(i,j)=1;
    end

    for j=3*stator-2:3*stator % fills the correspondent three-phase system cols
        C(i,j)=-1;
    end

    if i==n      % fills the last row with 1s
        for j=1:n
            C(i,j)=1;
        end
    end
    if stator<n/3
        stator=stator+1;
    end
end
% Output of the result
C
```

With this transformation matrix, an easy current sharing amongst the different three-phase systems in the stator can be obtained by means of introducing certain currents in the auxiliary subspaces. These currents have been calculated for the case of six- and nine-phase machines in sections 3.6.1 and 3.6.2 respectively and here the extension for twelve- and fifteen-phase machines is provided.

For the case of a twelve-phase machine:

$$i_{d12} = |k_{d1} - k_{d2}| \cdot i_d$$
$$i_{q12} = |k_{q1} - k_{q2}| \cdot i_q$$
$$i_{d13} = |k_{d1} - k_{d3}| \cdot i_d$$
$$i_{q13} = |k_{q1} - k_{q3}| \cdot i_q \tag{A2.1}$$
$$i_{d14} = |2 \cdot k_{d1} + k_{d2} + k_{d3} - 1| \cdot i_d$$
$$i_{q14} = |2 \cdot k_{q1} + k_{q2} + k_{q3} - 1| \cdot i_q$$

Equation (A2.1) shows the reference currents in the auxiliary subspaces that produce the required current sharing governed by current sharing coefficients k_{di} and k_{qi}. For a fifteen-phase machine, the following applies:

$$i_{d12} = |k_{d1} - k_{d2}| \cdot i_d$$
$$i_{q12} = |k_{q1} - k_{q2}| \cdot i_q$$
$$i_{d13} = |k_{d1} - k_{d3}| \cdot i_d$$
$$i_{q13} = |k_{q1} - k_{q3}| \cdot i_q$$
$$i_{d14} = |k_{d1} - k_{d4}| \cdot i_d \tag{A2.2}$$
$$i_{q14} = |k_{q1} - k_{q4}| \cdot i_q$$
$$i_{d15} = |2 \cdot k_{d1} + k_{d2} + k_{d3} + k_{d4} - 1| \cdot i_d$$
$$i_{q15} = |2 \cdot k_{q1} + k_{q2} + k_{q3} + k_{q4} - 1| \cdot i_q$$

APPENDIX 3

Decoupling terms in multiple *dq* approach

In this appendix, the expressions of the different decoupling terms, in the case of multiple *dq* approach, are written in a DSP-legible C-code style so that they can be easily introduced in the control software. It has to be noted that the following changes in the parameter names have been introduced:

$g_{\alpha\beta}$	gab
$g_{\alpha 1 \alpha 1}$	ga1a1
$g_{\alpha 1 \alpha 2}$	ga1a2
$g_{\beta 1 \beta 1}$	gb1b1
$g_{\beta 1 \beta 2}$	gb1b2
θ_r	Th
ω_r	wr

Six-phase machine in stationary frame

g_{a1a1}	(4*Lls*Lls+9*Lls*Lmd+9*Lls*Lmq+18*Lmd*Lmq-3*Lls*Lmd*cos(2*Th)+3*Lls*Lmq*cos(2*Th))/(4*Lls*(Lls+3*Lmd)*(Lls+3*Lmq))
g_{a1a2}	-(3*(Lls*Lmd+Lls*Lmq+6*Lmd*Lmq+Lls*Lmd*cos(2*Th)-Lls*Lmq*cos(2*Th)))/(4*Lls*(Lls+3*Lmq)*(Lls+3*Lmd))
g_{ab}	-(3*sin(2*Th)*(Lmd-Lmq))/(4*(Lls+3*Lmd)*(Lls+3*Lmq))
g_{b1b1}	(4*Lls*Lls+9*Lls*Lmd+9*Lls*Lmq+18*Lmd*Lmq+3*Lls*Lmd*cos(2*Th)-3*Lls*Lmq*cos(2*Th))/(4*Lls*(Lls+3*Lmd)*(Lls+3*Lmq))
g_{b1b2}	(3*(Lls*Lmd*cos(2*Th)-Lls*Lmq-6*Lmd*Lmq-Lls*Lmd-Lls*Lmq*cos(2*Th)))/(4*Lls*(Lls+3*Lmq)*(Lls+3*Lmd))
$k_{\alpha\alpha}$	(gab*(3*Lmq*gb1b1*cos(2*Th)-3*Lmd*gb1b1*cos(2*Th)-3*Lmd*gb1b2*cos(2*Th)-2*gab*rs+3*Lmq*gb1b2*cos(2*Th)+6*Lmd*gab*sin(2*Th)-6*Lmq*gab*sin(2*Th)))/(-4*gab*gab+ga1a1*gb1b1+ga1a1*gb1b2+ga1a2*gb1b1+ga1a2*gb1b2)
$k_{\alpha\beta}$	((gb1b1+gb1b2)*(2*gab*rs+3*Lmd*ga1a1*cos(2*Th)+3*Lmd*ga1a2*cos(2*Th)-3*Lmq*ga1a1*cos(2*Th)-3*Lmq*ga1a2*cos(2*Th)+6*Lmd*gab*sin(2*Th)-6*Lmq*gab*sin(2*Th)))/(2*(-4*gab*gab+ga1a1*gb1b1+ga1a1*gb1b2+ga1a2*gb1b1+ga1a2*gb1b2))
$k_{\beta\alpha}$	((ga1a1+ga1a2)*(2*gab*rs+3*Lmd*gb1b1*cos(2*Th)+3*Lmd*gb1b2*cos(2*Th)-3*Lmq*gb1b1*cos(2*Th)-3*Lmq*gb1b2*cos(2*Th)-6*Lmd*gab*sin(2*Th)+6*Lmq*gab*sin(2*Th)))/(2*(-4*gab*gab+ga1a1*gb1b1+ga1a1*gb1b2+ga1a2*gb1b1+ga1a2*gb1b2))
$k_{\beta\beta}$	-(2*gab*(gab*(rs+3*sin(2*Th)*(Lmd-Lmq))+ga1a1*cos(2*Th)*((3*Lmd)/2-(3*Lmq)/2)+ga1a2*cos(2*Th)*((3*Lmd)/2-(3*Lmq)/2)))/(-4*gab*gab+ga1a1*gb1b1+ga1a1*gb1b2+ga1a2*gb1b1+ga1a2*gb1b2)
k_{st1}	-((ga1a2*(rs-(3*sin(2*Th)*(Lmd-Lmq))/2)-(3*ga1a1*sin(2*Th)*(Lmd-Lmq))/2+2*gab*cos(2*Th)*((3*Lmd)/2-(3*Lmq)/2))*(-2*gab*gab+ga1a2*gb1b1+ga1a2*gb1b2))/((ga1a1-ga1a2)*(-4*gab*gab+ga1a1*gb1b1+ga1a1*gb1b2+ga1a2*gb1b1+ga1a2*gb1b2))
k_{st2}	-(gab*(gb1b2*(rs+(3*sin(2*Th)*(Lmd-Lmq))/2)+(3*gb1b1*sin(2*Th)*(Lmd-

	Lmq))/2+2*gab*cos(2*Th)*((3*Lmd)/2-(3*Lmq)/2)))/(-4*gab*gab+ga1a1*gb1b1+ga1a1*gb1b2+ga1a2*gb1b1+ga1a2*gb1b2)
k_{st3}	((ga1a2*(rs-(3*sin(2*Th)*(Lmd-Lmq))/2)-(3*ga1a1*sin(2*Th)*(Lmd-Lmq))/2+2*gab*cos(2*Th)*((3*Lmd)/2-(3*Lmq)/2))*(-2*gab*gab+ga1a1*gb1b1+ga1a1*gb1b2))/((ga1a1-ga1a2)*(-4*gab*gab+ga1a1*gb1b1+ga1a1*gb1b2+ga1a2*gb1b1+ga1a2*gb1b2))
k_{st4}	-(gab*(ga1a2*(rs-(3*sin(2*Th)*(Lmd-Lmq))/2)-(3*ga1a1*sin(2*Th)*(Lmd-Lmq))/2+2*gab*cos(2*Th)*((3*Lmd)/2-(3*Lmq)/2)))/(-4*gab*gab+ga1a1*gb1b1+ga1a1*gb1b2+ga1a2*gb1b1+ga1a2*gb1b2)
k_{st5}	-((gb1b2*(rs+(3*sin(2*Th)*(Lmd-Lmq))/2)+(3*gb1b1*sin(2*Th)*(Lmd-Lmq))/2+2*gab*cos(2*Th)*((3*Lmd)/2-(3*Lmq)/2))*(-2*gab*gab+ga1a1*gb1b2+ga1a2*gb1b2))/((gb1b1-gb1b2)*(-4*gab*gab+ga1a1*gb1b1+ga1a1*gb1b2+ga1a2*gb1b1+ga1a2*gb1b2))
k_{st6}	((gb1b2*(rs+(3*sin(2*Th)*(Lmd-Lmq))/2)+(3*gb1b1*sin(2*Th)*(Lmd-Lmq))/2+2*gab*cos(2*Th)*((3*Lmd)/2-(3*Lmq)/2))*(-2*gab*gab+ga1a1*gb1b1+ga1a2*gb1b1))/((gb1b1-gb1b2)*(-4*gab*gab+ga1a1*gb1b1+ga1a1*gb1b2+ga1a2*gb1b1+ga1a2*gb1b2))
k_{in1}	-(2*gab*gab-ga1a1*(gb1b1+gb1b2))/((ga1a1-ga1a2)*(-4*gab*gab+ga1a1*gb1b1+ga1a1*gb1b2+ga1a2*gb1b1+ga1a2*gb1b2))
k_{in2}	-gab/(-4*gab*gab+ga1a1*gb1b1+ga1a1*gb1b2+ga1a2*gb1b1+ga1a2*gb1b2)
k_{in3}	(2*gab*gab-ga1a2*(gb1b1+gb1b2))/((ga1a1-ga1a2)*(-4*gab*gab+ga1a1*gb1b1+ga1a1*gb1b2+ga1a2*gb1b1+ga1a2*gb1b2))
k_{in4}	-(2*gab*gab-gb1b1*(ga1a1+ga1a2))/((gb1b1-gb1b2)*(-4*gab*gab+ga1a1*gb1b1+ga1a1*gb1b2+ga1a2*gb1b1+ga1a2*gb1b2))
k_{in5}	(2*gab*gab-gb1b2*(ga1a1+ga1a2))/((gb1b1-gb1b2)*(-4*gab*gab+ga1a1*gb1b1+ga1a1*gb1b2+ga1a2*gb1b1+ga1a2*gb1b2))

Six-phase machine in synchronous frame

g_{d11}	1/(2*Lls)+1/(2*Lls+6*Lmd))
g_{d12}	1/(2*Lls+6*Lmd)-1/(2*Lls)
g_{q11}	1/(2*Lls)+1/(2*Lls+6*Lmq))
g_{q12}	1/(2*Lls+6*Lmq)-1/(2*Lls)
k_{d1}	-(Lls+3*Lmq/2)*wr
k_{d2}	-(3*Lmq*wr)/2
k_{q1}	(Lls+3*Lmd/2)*wr
k_{q2}	(3*Lmd*wr)/2
k_{st1}	-(gd12*gd12*rs)/(gd11*gd11-gd12*gd12)
k_{st2}	(gd11*gd12*rs)/(gd11*gd11-gd12*gd12)
k_{st3}	-(gq12*gq12*rs)/(gq11*gq11-gq12*gq12)
k_{st4}	(gq11*gq12*rs)/(gq11*gq11-gq12*gq12)

Nine-phase machine in stationary frame

g_{a1a1}	(4*Lls*Lls+15*Lls*Lmd+15*Lls*Lmq+54*Lmd*Lmq-3*Lls*Lmd*cos(2*Th)+3*Lls*Lmq*cos(2*Th))/(Lls*(2*Lls+9*Lmd)*(2*Lls+9*Lmq))
g_{a1a2}	-(3*(Lls*Lmd+Lls*Lmq+9*Lmd*Lmq+Lls*Lmd*cos(2*Th)-Lls*Lmq*cos(2*Th)))/(Lls*(2*Lls+9*Lmq)*(2*Lls+9*Lmd))
g_{ab}	-(3*sin(2*Th)*(Lmd-Lmq))/((2*Lls+9*Lmd)*(2*Lls+9*Lmq))
g_{b1b1}	(4*Lls*Lls+15*Lls*Lmd+15*Lls*Lmq+54*Lmd*Lmq+3*Lls*Lmd*cos(2*Th)-3*Lls*Lmq*cos(2*Th))/(Lls*(2*Lls+9*Lmd)*(2*Lls+9*Lmq))
g_{b1b2}	(3*(Lls*Lmd*cos(2*Th) -Lls*Lmq-9*Lmd*Lmq -Lls*Lmd-Lls*Lmq*cos(2*Th)))/(Lls*(2*Lls+9*Lmq)*(2*Lls+9*Lmd))
$k_{\alpha\alpha}$	(3*gab*(3*Lmq*gb1b1*cos(2*Th)-3*Lmd*gb1b1*cos(2*Th)-6*Lmd*gb1b2*cos(2*Th)-2*gab*rs+6*Lmq*gb1b2*cos(2*Th)+9*Lmd*gab*sin(2*Th)-9*Lmq*gab*sin(2*Th)))/(2*(-9*gab*gab+ga1a1*gb1b1+2*ga1a1*gb1b2+2*ga1a2*gb1b1+4*ga1a2*gb1b2))
$k_{\alpha\beta}$	((gb1b1+2*gb1b2)*(2*gab*rs+3*Lmd*ga1a1*cos(2*Th)+6*Lmd*ga1a2*cos(2*Th)-3*Lmq*ga1a1*cos(2*Th)-6*Lmq*ga1a2*cos(2*Th)+9*Lmd*gab*sin(2*Th)-9*Lmq*gab*sin(2*Th)))/(2*(-9*gab*gab+ga1a1*gb1b1+2*ga1a1*gb1b2+2*ga1a2*gb1b1+4*ga1a2*gb1b2))
$k_{\beta\alpha}$	((ga1a1+2*ga1a2)*(2*gab*rs+3*Lmd*gb1b1*cos(2*Th)+6*Lmd*gb1b2*cos(2*Th)-3*Lmq*gb1b1*cos(2*Th)-6*Lmq*gb1b2*cos(2*Th)-9*Lmd*gab*sin(2*Th)+9*Lmq*gab*sin(2*Th)))/(2*(-9*gab*gab+ga1a1*gb1b1+2*ga1a1*gb1b2+2*ga1a2*gb1b1+4*ga1a2*gb1b2))
$k_{\beta\beta}$	-(3*gab*(2*gab*rs+3*Lmd*ga1a1*cos(2*Th)+6*Lmd*ga1a2*cos(2*Th)-3*Lmq*ga1a1*cos(2*Th)-6*Lmq*ga1a2*cos(2*Th)+9*Lmd*gab*sin(2*Th)-9*Lmq*gab*sin(2*Th)))/(2*(-9*gab*gab+ga1a1*gb1b1+2*ga1a1*gb1b2+2*ga1a2*gb1b1+4*ga1a2*gb1b2))
k_{st1}	((-3*gab*gab+ga1a2*gb1b1+2*ga1a2*gb1b2)*(9*Lmq*gab*cos(2*Th)-9*Lmd*gab*cos(2*Th)-2*ga1a2*rs+3*Lmd*ga1a1*sin(2*Th)+6*Lmd*ga1a2*sin(2*Th)-3*Lmq*ga1a1*sin(2*Th)-6*Lmq*ga1a2*sin(2*Th)))/((ga1a1-ga1a2)*(-9*gab*gab+ga1a1*gb1b1+2*ga1a1*gb1b2+2*ga1a2*gb1b1+4*ga1a2*gb1b2))
k_{st2}	(gab*(2*gb1b2*rs+9*Lmd*gab*cos(2*Th)-9*Lmq*gab*cos(2*Th)+3*Lmd*gb1b1*sin(2*Th)+6*Lmd*gb1b2*sin(2*Th)-3*Lmq*gb1b1*sin(2*Th)-6*Lmq*gb1b2*sin(2*Th)))/(9*gab*gab-ga1a1*gb1b1-2*ga1a1*gb1b2-2*ga1a2*gb1b1-4*ga1a2*gb1b2)
k_{st3}	((-3*gab*gab+ga1a1*gb1b1+2*ga1a1*gb1b2)*(2*ga1a2*rs+9*Lmd*gab*cos(2*Th)-9*Lmq*gab*cos(2*Th)-3*Lmd*ga1a1*sin(2*Th)-6*Lmd*ga1a2*sin(2*Th)+3*Lmq*ga1a1*sin(2*Th)+6*Lmq*ga1a2*sin(2*Th)))/(2*(ga1a1-ga1a2)*(-9*gab*gab+ga1a1*gb1b1+2*ga1a1*gb1b2+2*ga1a2*gb1b1+4*ga1a2*gb1b2))
k_{st4}	(gab*(9*Lmq*gab*cos(2*Th)-9*Lmd*gab*cos(2*Th)-2*ga1a2*rs+3*Lmd*ga1a1*sin(2*Th)+6*Lmd*ga1a2*sin(2*Th)-3*Lmq*ga1a1*sin(2*Th)-6*Lmq*ga1a2*sin(2*Th)))/(-9*gab*gab+ga1a1*gb1b1+2*ga1a1*gb1b2+2*ga1a2*gb1b1+4*ga1a2*gb1b2)
k_{st5}	((3*gab*gab-ga1a1*gb1b2-2*ga1a2*gb1b2)*(2*gb1b2*rs+9*Lmd*gab*cos(2*Th)-9*Lmq*gab*cos(2*Th)+3*Lmd*gb1b1*sin(2*Th)+6*Lmd*gb1b2*sin(2*Th)-3*Lmq*gb1b1*sin(2*Th)-6*Lmq*gb1b2*sin(2*Th)))/((gb1b1-gb1b2)*(-9*gab*gab+ga1a1*gb1b1+2*ga1a1*gb1b2+2*ga1a2*gb1b1+4*ga1a2*gb1b2))
k_{st6}	((-3*gab*gab+ga1a1*gb1b1+2*ga1a2*gb1b1)*(2*gb1b2*rs+9*Lmd*gab*cos(2*Th)-9*Lmq*gab*cos(2*Th)+3*Lmd*gb1b1*sin(2*Th)+6*Lmd*gb1b2*sin(2*Th)-3*Lmq*gb1b1*sin(2*Th)-6*Lmq*gb1b2*sin(2*Th)))/(2*(gb1b1-gb1b2)*(-9*gab*gab+ga1a1*gb1b1+2*ga1a1*gb1b2+2*ga1a2*gb1b1+4*ga1a2*gb1b2))
k_{in1}	(-6*gab*gab+ga1a1*(gb1b1+2*gb1b2)+ga1a2*(gb1b1+2*gb1b2))/((ga1a1-ga1a2)*(-9*gab*gab+ga1a1*gb1b1+2*ga1a1*gb1b2+2*ga1a2*gb1b1+4*ga1a2*gb1b2))
k_{in2}	-gab/(-9*gab*gab+2*ga1a2*gb1b1+4*ga1a2*gb1b2+ga1a1*(gb1b1+2*gb1b2))
k_{in3}	-(ga1a2*(gb1b1+2*gb1b2)-3*gab*gab)/((ga1a1-ga1a2)*(-

	9*gab*gab+ga1a1*gb1b1+2*ga1a1*gb1b2+2*ga1a2*gb1b1+4*ga1a2*gb1b2))
k_{in4}	(-6*gab*gab+gb1b1*(ga1a1+2*ga1a2)+gb1b2*(ga1a1+2*ga1a2))/((gb1b1-gb1b2)*(-9*gab*gab+ga1a1*gb1b1+2*ga1a1*gb1b2+2*ga1a2*gb1b1+4*ga1a2*gb1b2))
k_{in5}	-(gb1b2*(ga1a1+2*ga1a2)-3*gab*gab)/((gb1b1-gb1b2)*(-9*gab*gab+ga1a1*gb1b1+2*ga1a1*gb1b2+2*ga1a2*gb1b1+4*ga1a2*gb1b2))

Nine-phase machine in synchronous frame

g_{d11}	(2*Lls+6*Lmd)/(Lls*(2*Lls+9*Lmd))
g_{d12}	-(3*Lmd)/(Lls*(2*Lls+9*Lmd))
g_{q11}	(2*Lls+6*Lmq)/(Lls*(2*Lls+9*Lmq))
g_{q12}	-(3*Lmq)/(Lls*(2*Lls+9*Lmq))
k_{d1}	-(Lls+3*Lmq/2)*wr
k_{d2}	-(3*Lmq*wr)/2
k_{q1}	(Lls+3*Lmd/2)*wr
k_{q2}	(3*Lmd*wr)/2
k_{st1}	-(2*gd12*gd12*rs)/(gd11*gd11+gd11*gd12-2*gd12*gd12)
k_{st2}	(gd11*gd12*rs)/(gd11*gd11+gd11*gd12-2*gd12*gd12)
k_{st3}	-(2*gq12*gq12*rs)/(gq11*gq11+gq11*gq12-2*gq12*gq12)
k_{st4}	(gq11*gq12*rs)/(gq11*gq11+gq11*gq12-2*gq12*gq12)

Twelve-phase machine in stationary frame

g_{a1a1}	(4*Lls*Lls+21*Lls*Lmd+21*Lls*Lmq+108*Lmd*Lmq-3*Lls*Lmd*cos(2*Th)+3*Lls*Lmq*cos(2*Th))/(4*Lls*(Lls+6*Lmq)*(Lls+6*Lmd))
g_{a1a2}	-(3*(Lls*Lmd+Lls*Lmq+12*Lmd*Lmq+Lls*Lmd*cos(2*Th)-Lls*Lmq*cos(2*Th)))/(4*Lls*(Lls+6*Lmq)*(Lls+6*Lmd))
g_{ab}	-(3*sin(2*Th)*(Lmd-Lmq))/(4*(Lls+6*Lmd)*(Lls+6*Lmq))
g_{b1b1}	(4*Lls*Lls+21*Lls*Lmd+21*Lls*Lmq+108*Lmd*Lmq+3*Lls*Lmd*cos(2*Th)-3*Lls*Lmq*cos(2*Th))/(4*Lls*(Lls+6*Lmq)*(Lls+6*Lmd))
g_{b1b2}	(3*(Lls*Lmd*cos(2*Th)-Lls*Lmq-12*Lmd*Lmq-Lls*Lmd-Lls*Lmq*cos(2*Th)))/(4*Lls*(Lls+6*Lmq)*(Lls+6*Lmd))
$k_{\alpha\alpha}$	(2*gab*(3*Lmq*gb1b1*cos(2*Th)-3*Lmd*gb1b1*cos(2*Th)-9*Lmd*gb1b2*cos(2*Th)-2*gab*rs+9*Lmq*gb1b2*cos(2*Th)+12*Lmd*gab*sin(2*Th)-12*Lmq*gab*sin(2*Th)))/(-16*gab*gab+ga1a1*gb1b1+3*ga1a1*gb1b2+3*ga1a2*gb1b1+9*ga1a2*gb1b2)
$k_{\alpha\beta}$	((gb1b1+3*gb1b2)*(2*gab*rs+3*Lmd*ga1a1*cos(2*Th)+9*Lmd*ga1a2*cos(2*Th)-3*Lmq*ga1a1*cos(2*Th)-9*Lmq*ga1a2*cos(2*Th)+12*Lmd*gab*sin(2*Th)-12*Lmq*gab*sin(2*Th)))/(2*(-16*gab*gab+ga1a1*gb1b1+3*ga1a1*gb1b2+3*ga1a2*gb1b1+9*ga1a2*gb1b2))
$k_{\beta\alpha}$	((ga1a1+3*ga1a2)*(2*gab*rs+3*Lmd*gb1b1*cos(2*Th)+9*Lmd*gb1b2*cos(2*Th)-3*Lmq*gb1b1*cos(2*Th)-9*Lmq*gb1b2*cos(2*Th)-12*Lmd*gab*sin(2*Th)+12*Lmq*gab*sin(2*Th)))/(2*(-16*gab*gab+ga1a1*gb1b1+3*ga1a1*gb1b2+3*ga1a2*gb1b1+9*ga1a2*gb1b2))

$k_{\beta\beta}$	-(2*gab*(2*gab*rs+3*Lmd*ga1a1*cos(2*Th)+9*Lmd*ga1a2*cos(2*Th)-3*Lmq*ga1a1*cos(2*Th)-9*Lmq*ga1a2*cos(2*Th)+12*Lmd*gab*sin(2*Th)-12*Lmq*gab*sin(2*Th)))/(-16*gab*gab+ga1a1*gb1b1+3*ga1a1*gb1b2+3*ga1a2*gb1b1+9*ga1a2*gb1b2)
k_{st1}	-(3*(-4*gab*gab+ga1a2*gb1b1+3*ga1a2*gb1b2)*(ga1a2*(rs-(3*sin(2*Th)*(Lmd-Lmq))/2)-(3*ga1a1*sin(2*Th)*(Lmd-Lmq))/2-3*ga1a2*sin(2*Th)*(Lmd-Lmq)+4*gab*cos(2*Th)*((3*Lmd)/2-(3*Lmq)/2)))/((ga1a1-ga1a2)*(-16*gab*gab+ga1a1*gb1b1+3*ga1a1*gb1b2+3*ga1a2*gb1b1+9*ga1a2*gb1b2))
k_{st2}	-(3*gab*(gb1b2*(rs+(3*sin(2*Th)*(Lmd-Lmq))/2)+(3*gb1b1*sin(2*Th)*(Lmd-Lmq))/2+3*gb1b2*sin(2*Th)*(Lmd-Lmq)+4*gab*cos(2*Th)*((3*Lmd)/2-(3*Lmq)/2)))/(-16*gab*gab+ga1a1*gb1b1+3*ga1a1*gb1b2+3*ga1a2*gb1b1+9*ga1a2*gb1b2)
k_{st3}	((-4*gab*gab+ga1a1*gb1b1+3*ga1a1*gb1b2)*(2*ga1a2*rs+12*Lmd*gab*cos(2*Th)-12*Lmq*gab*cos(2*Th)-3*Lmd*ga1a1*sin(2*Th)-9*Lmd*ga1a2*sin(2*Th)+3*Lmq*ga1a1*sin(2*Th)+9*Lmq*ga1a2*sin(2*Th)))/(2*(ga1a1-ga1a2)*(-16*gab*gab+ga1a1*gb1b1+3*ga1a1*gb1b2+3*ga1a2*gb1b1+9*ga1a2*gb1b2))
k_{st4}	-(3*gab*(ga1a2*(rs-(3*sin(2*Th)*(Lmd-Lmq))/2)-(3*ga1a1*sin(2*Th)*(Lmd-Lmq))/2-3*ga1a2*sin(2*Th)*(Lmd-Lmq)+4*gab*cos(2*Th)*((3*Lmd)/2-(3*Lmq)/2)))/(-16*gab*gab+ga1a1*gb1b1+3*ga1a1*gb1b2+3*ga1a2*gb1b1+9*ga1a2*gb1b2)
k_{st5}	-(3*(-4*gab*gab+ga1a1*gb1b2+3*ga1a2*gb1b2)*(gb1b2*(rs+(3*sin(2*Th)*(Lmd-Lmq))/2)+(3*gb1b1*sin(2*Th)*(Lmd-Lmq))/2+3*gb1b2*sin(2*Th)*(Lmd-Lmq)+4*gab*cos(2*Th)*((3*Lmd)/2-(3*Lmq)/2)))/((gb1b1-gb1b2)*(-16*gab*gab+ga1a1*gb1b1+3*ga1a1*gb1b2+3*ga1a2*gb1b1+9*ga1a2*gb1b2))
k_{st6}	((-4*gab*gab+ga1a1*gb1b1+3*ga1a2*gb1b1)*(2*gb1b2*rs+12*Lmd*gab*cos(2*Th)-12*Lmq*gab*cos(2*Th)+3*Lmd*gb1b1*sin(2*Th)+9*Lmd*gb1b2*sin(2*Th)-3*Lmq*gb1b1*sin(2*Th)-9*Lmq*gb1b2*sin(2*Th)))/(2*(gb1b1-gb1b2)*(-16*gab*gab+ga1a1*gb1b1+3*ga1a1*gb1b2+3*ga1a2*gb1b1+9*ga1a2*gb1b2))
k_{in1}	(-12*gab*gab+ga1a1*(gb1b1+3*gb1b2)+ga1a2*(2*gb1b1+6*gb1b2))/((ga1a1-ga1a2)*(-16*gab*gab+ga1a1*gb1b1+3*ga1a1*gb1b2+3*ga1a2*gb1b1+9*ga1a2*gb1b2))
k_{in2}	-gab/(-16*gab*gab+3*ga1a2*gb1b1+9*ga1a2*gb1b2+ga1a1*(gb1b1+3*gb1b2))
k_{in3}	-(ga1a2*(gb1b1+3*gb1b2)-4*gab*gab)/((ga1a1-ga1a2)*(-16*gab*gab+ga1a1*gb1b1+3*ga1a1*gb1b2+3*ga1a2*gb1b1+9*ga1a2*gb1b2))
k_{in4}	(-12*gab*gab+gb1b1*(ga1a1+3*ga1a2)+gb1b2*(2*ga1a1+6*ga1a2))/((gb1b1-gb1b2)*(-16*gab*gab+ga1a1*gb1b1+3*ga1a1*gb1b2+3*ga1a2*gb1b1+9*ga1a2*gb1b2))
k_{in5}	-(gb1b2*(ga1a1+3*ga1a2)-4*gab*gab)/((gb1b1-gb1b2)*(-16*gab*gab+ga1a1*gb1b1+3*ga1a1*gb1b2+3*ga1a2*gb1b1+9*ga1a2*gb1b2))

Twelve-phase machine in synchronous frame

g_{d11}	(2*Lls+9*Lmd)/(Lls*(2*Lls+12*Lmd))
g_{d12}	-(3*Lmd)/(Lls*(2*Lls+12*Lmd))
g_{q11}	(2*Lls+9*Lmq)/(Lls*(2*Lls+12*Lmq))
g_{q12}	-(3*Lmq)/(Lls*(2*Lls+12*Lmq))
k_{d1}	-(Lls+3*Lmq/2)*wr
k_{d2}	-(3*Lmq*wr)/2
k_{q1}	(Lls+3*Lmd/2)*wr
k_{q2}	(3*Lmd*wr)/2
k_{st1}	-(3*gd12*gd12*rs)/(gd11*gd11+2*gd11*gd12-3*gd12*gd12)

k_{st2}	(gd11*gd12*rs)/(gd11*gd11+2*gd11*gd12-3*gd12*gd12)
k_{st3}	-(3*gq12*gq12*rs)/(gq11*gq11+2*gq11*gq12-3*gq12*gq12)
k_{st4}	(gq11*gq12*rs)/(gq11*gq11+2*gq11*gq12-3*gq12*gq12)

APPENDIX 4

PI tuning procedure

Considering the following transfer function in the Laplace domain for a PI regulator,

$$\frac{OUT}{IN} = k_p \cdot \left(\frac{T_n \cdot s + 1}{T_n \cdot s}\right) \qquad\qquad \textbf{(A4.1)}$$

the calculation of the controller parameters (k_p and T_n), following the bandwidth (BW) and phase margin (PM) procedure for a closed loop similar to the one shown in Fig. A4.1, consists of the following steps:

- Select the desired BW of the control loop. A general rule of thumb for selecting it is to use a BW at least ten times higher than the maximum frequency that the closed loop should follow.
- Select an appropriate PM to control the overshoot (and guarantee the stability) when sudden changes in the reference may occur (step inputs). This is usually chosen between 45 and 70°.
- Open the feedback loop and obtain the transfer function of the direct path. This includes the controller, the plant and the filter.
- Calculate the phase of the direct path transfer function at the desired BW frequency. This phase depends only on the T_n parameter of the PI.
- To achieve the desired PM at the desired BW, equate the phase of the direct path calculated in the previous step to -180°+PM and solve for T_n (the only unknown term).
- The final step is to select the controller gain (k_p) to obtain the desired BW. This is done by calculating the magnitude of the direct path transfer function at the desired BW frequency and equating it to 1. From this equality, the value for the controller gain can be obtained as it is the only unknown term.
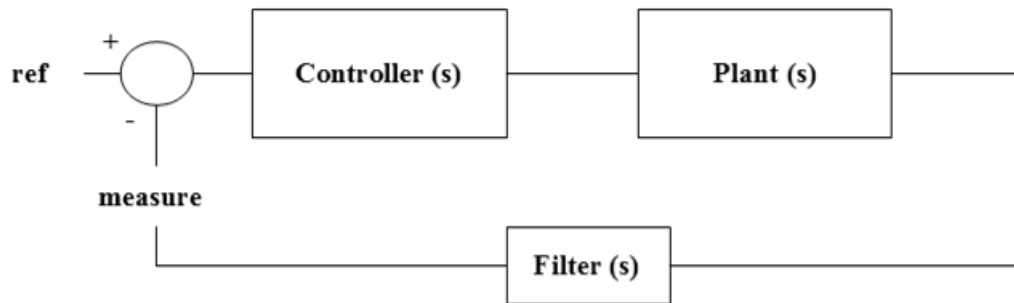

Fig. A4.1 Block diagram of a typical closed control loop.

Once the controller parameters have been obtained, the Bode plot of the open loop transfer function (the direct path) should look like the one in Fig. A4.2. In it, it can be seen how the magnitude plot crosses the 0 dB (1 p.u.) line at the desired BW frequency and, furthermore, the phase of the open loop at said frequency is above the -180° line by the desired PM degrees.
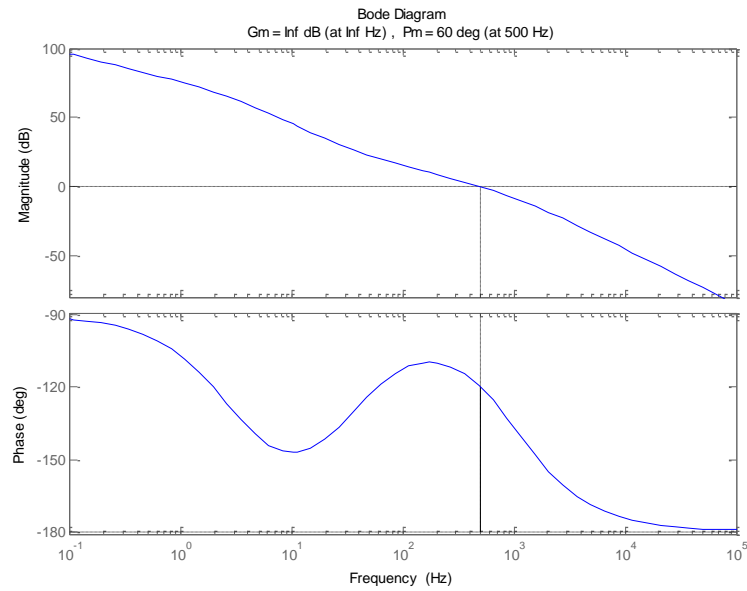
Fig. A4.2 Open loop Bode diagram of a controlled loop for a BW of 500 Hz and a PM of 60°.

When the feedback loop is closed and its transfer function is calculated, its Bode plot may look like the one shown in Fig. A4.3. It can be seen how the closed loop will follow the reference changes at frequencies below one tenth of the BW (50 Hz) with neither phase nor amplitude errors. Above such frequency, the closed loop will start introducing primarily a phase delay between the reference and its output; this may produce undesired effects such as resonances, so the introduction of reference changes at such frequencies should be avoided.
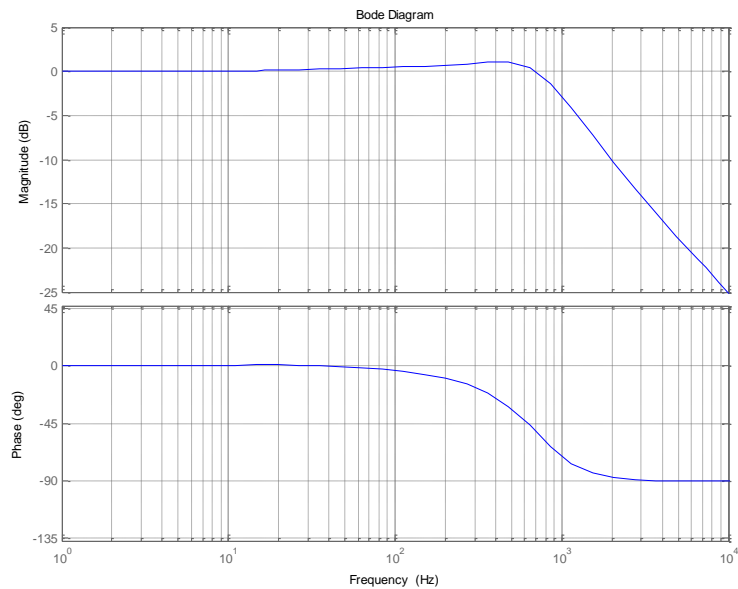

Fig. A4.3 Closed loop Bode diagram of a controlled loop for a BW of 500 Hz and a PM of 60°.

APPENDIX 5

Current regulators tuning procedure output file

The following text shows the output file of the current regulator tuning for the case of the test bench machine with the inductance values theoretically identified as described in 5.5. The rotational speed range is set from 30 to 80 Hz.

CURRENT REGULATOR TUNING FOR Multiple dq WITH MINIMIZATION OF THE QUADRATIC ERRORS
SAMPLE TIME DSP Ts= 625 us
Results for We=30 [Hz] BW=40 [Hz] PM=60 [º]
Kp_id is 326.698
Tn_id is 0.011
Kp_iq is 326.698
Tn_iq is 0.011
Overshoot d-axis is 1.06
Overshoot q-axis is 1.06
PM d-axis is 60
Error min in d-axis is 4.66
Error min in q-axis is 4.66
Results for We=40 [Hz] BW=35 [Hz] PM=64 [º]
Kp_id is 323.717
Tn_id is 0.013
Kp_iq is 323.717
Tn_iq is 0.013
Overshoot d-axis is 1.63
Overshoot q-axis is 1.63
Error min in d-axis is 4.92
Error min in q-axis is 4.92
Results for We=50 [Hz] BW=30 [Hz] PM=64 [º]
Kp_id is 302.353
Tn_id is 0.013
Kp_iq is 302.353
Tn_iq is 0.013
Overshoot d-axis is 1.26
Overshoot q-axis is 1.26
Error min in d-axis is 5.34
Error min in q-axis is 5.34
Results for We=60 [Hz] BW=25 [Hz] PM=64 [º]
Kp_id is 265.275
Tn_id is 0.013
Kp_iq is 265.275
Tn_iq is 0.013
Overshoot d-axis is 1.59
Overshoot q-axis is 1.59
Error min in d-axis is 6.02
Error min in q-axis is 6.02
Results for We=70 [Hz] BW=20 [Hz] PM=66 [º]
Kp_id is 214.556

Tn_id is 0.014
Kp_iq is 214.556
Tn_iq is 0.014
Overshoot d-axis is 1.52
Overshoot q-axis is 1.52
Error min in d-axis is 7.29
Error min in q-axis is 7.29
Results for We=80 [Hz] BW=20 [Hz] PM=60 [º]
Kp_id is 237.161
Tn_id is 0.013
Kp_iq is 237.161
Tn_iq is 0.013
Overshoot d-axis is 1.35
Overshoot q-axis is 1.35
Error min in d-axis is 9.29
Error min in q-axis is 9.29
double Wx[6]={2.*PI*30,2.*PI*40,2.*PI*50,2.*PI*60,2.*PI*70,2.*PI*80};
double KpId[6]={326.698,323.717,302.353,265.275,214.556,237.161};
double KpIq[6]={326.698,323.717,302.353,265.275,214.556,237.161};
double TnId[6]={0.011,0.013,0.013,0.013,0.014,0.013};
double TnIq[6]={0.011,0.013,0.013,0.013,0.014,0.013};

APPENDIX 6

Publications from the thesis

CONFERENCE PAPERS

Zabaleta, M., E. Levi, and M. Jones, (2016), Modelling approaches for an asymmetrical six-phase machine, *Proc. IEEE 25th International Symposium on Industrial Electronics (ISIE),* Santa Clara, USA, pp. 173-178.

Zabaleta, M., E. Levi, and M. Jones, (2016), Modelling approaches for triple three-phase permanent magnet machines, *Proc. XXII International Conference on Electrical Machines (ICEM),* Lausanne, Swiss, pp. 466-472.

Zabaleta, M., M. Jones, and E. Levi, (2017), A tuning procedure for the current regulator loops in multiple three phase permanent magnet machines with low switching to fundamental frequency ratio, *Proc. 19th European Conference on Power Electronics and Applications (EPE),* Warsaw, Poland.

Zabaleta, M., E. Levi, and M. Jones, (2017), Dual three-phase PM generator parameter identification using experimental and simulated system responses, *Proc. 19th International Symposium Power Electronics*, Novi Sad, Serbia.

Zabaleta, M., E. Levi, and M. Jones, 2018b. Regenerative testing of multiphase machines with multiple three-phase windings. *International Conference on Power Electronics and Motion Control (PEMC),* Budapest, Hungary, accepted for publication.

JOURNAL PAPERS

Zabaleta, M., E. Levi, and M. Jones, 2018a. A novel synthetic loading method for multiple three-phase winding electric machines. *IEEE Trans. on Energy Conversion,* accepted for publication.